Karlsruher Institut für Technologie

Fakultät für Physik
Institut für theoretische Festkörperphysik

Modeling Optical Metamaterials with Strong Spatial Dispersion

M. Sc. Karim Mnasri

von der KIT-Fakultät für Physik
des Karlsruher Instituts für Technologie (KIT)
genehmigte Dissertation zur Erlangung des akademischen Grades eines
DOKTORS DER NATURWISSENSCHAFTEN
(Dr. rer. nat.)

Tag der mündlichen Prüfung: 29. November 2019
Referent: Prof. Dr. Carsten Rockstuhl (Institut für theoretische Festkörperphysik)
Korreferent: Prof. Dr. Michael Plum (Institut für Analysis)

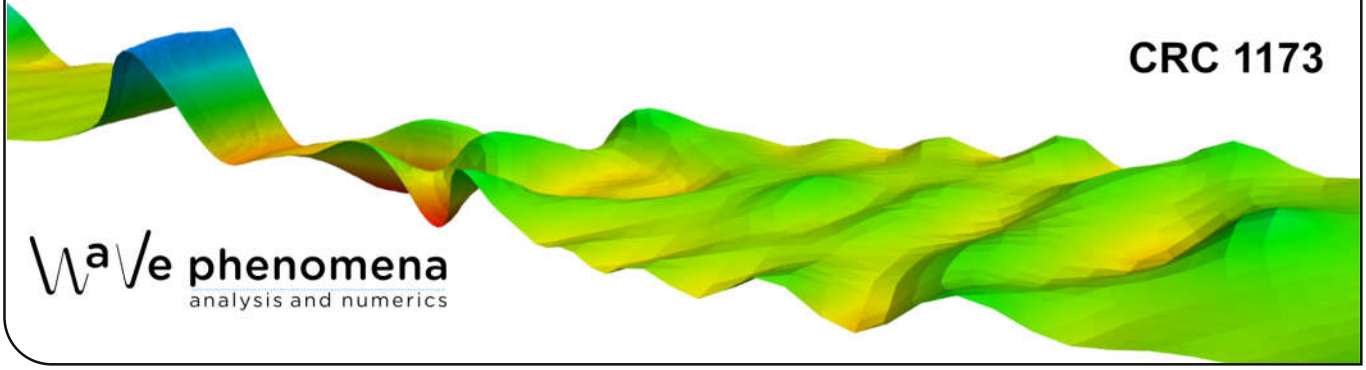

Erklärung zur Selbstständigkeit

Ich versichere, dass ich diese Arbeit selbstständig verfasst habe und keine anderen als die angegebenen Quellen und Hilfsmittel benutzt habe, die wörtlich oder inhaltlich übernommenen Stellen als solche kenntlich gemacht und die Satzung des KIT zur Sicherung guter wissenschaftlicher Praxis in der gültigen Fassung vom 24. Mai 2018 beachtet habe.

Karlsruhe, den 21. Oktober 2019, _____

Karim Mnasri

Als Prüfungsexemplar genehmigt von

Karlsruhe, den 28. Oktober 2019, _____

Prof. Dr. Carsten Rockstuhl

To Ouiem and Adam

Thesis abstract

Optical metamaterials are artificial media made from subwavelength inclusions with unconventional properties at optical frequencies. While a response to the magnetic field of light in natural material is absent, metamaterials prompt to lift this limitation and to exhibit a response to both electric and magnetic fields at optical frequencies. Due to the interplay of both the actual shape of the inclusions and the material from which they are made, but also from the specific details of their arrangement, the response can be driven to one or multiple resonances within a desired frequency band. With such a high number of degrees of freedom, tedious trial-and-error simulations and costly experimental essays are inefficient when considering optical metamaterials in the design of specific applications. Therefore, to be able to discuss metamaterials on equal footing as natural materials and to consider them in the design of functional applications, the homogenization of optical materials is of utmost importance. Such effective description consists of mapping the optical response of an actual metamaterial to a set of spatially averaged, effective material parameters of a continuum. This step requires that the building blocks from which the metamaterials are made of are small and arranged with sufficient density in space in comparison to the operating wavelength.

Often, local material laws have been considered in this mapping process, i.e., metamaterials are frequently modelled at the effective, i.e. the homogeneous level, by an electric permittivity, magnetic permeability, and in case of optical activity, terms that express magneto-electric coupling. Such description is borrowed from natural materials at optical frequencies, where the characteristic length scale is in the subnanometer range. Metamaterials, however, possess a characteristic length that is only slightly smaller than the wavelength of light. Thus, the spatial variations of the fields begin to become important and a local description is not enough to adequately describe the metamaterial at the effective level.

In this thesis, we lift this limitation and consider nonlocal constitutive relations in the homogenization process for a realistic modelling of optical metamaterials. Nonlocality means that the effective response of a material at every point depends on the fields of light at some distant points or, alternatively, on spatial derivatives of the fields at the same point, or both. We focus on periodic metamaterials with centrosymmetric unit cells with a non-negligible period-to-wavelength ratio and show the importance of retaining nonlocality in the effective description of metamaterials.

After introducing the necessary mathematical background, we discuss the physical origin of nonlocality, which in the spatial Fourier domain translates to spatial dispersion, i.e., to a generalized permittivity that depends on the wave vector of light. This can lead to an artificial magnetic response and ultimately to a negative effective index of refraction, and even beyond. Then, the aforementioned generalized permittivity is expanded into a Taylor polynomial of the wave vector up to the fourth order. Dispersion relations describing light propagation in bulk metamaterials that are characterized by such constitutive relations are derived. We discuss the additional mode that emerges with nonlocality. We further, derive the appropriate interface conditions from first principles, in order to study how light couples from one media to another. With the interface conditions at hand, the Fresnel matrices, which ultimately allow us to analytically derive the reflection and transmission coefficients from a slab, are derived.

Finally, we apply this formalism to three metamaterial examples. We show that a nonlocal description captures the properties of actual metamaterials much more accurate than the ordinary local description. Based on the scattering parameter retrieval, the effective material parameters are retrieved from different structures, where the referential reflection and transmission coefficients are numerically calculated with a very high precision. In the first example, we studied an all-dielectric and isotropic material made of an array of spheres arranged in a cubic lattice. We find that the optical features such as the presence of the Brewster angle are better captured with a nonlocal description, especially at frequencies close to the first photonic band gap. In the second example, we investigated the fishnet metamaterial. It has a negative effective refractive index in the studied frequency range. We find that a nonlocal description allows to predict the optical properties at oblique incidence, where a local description failed to do so. Further, in the retrieved effective material parameters within the local approach, an unphysical anti-Lorentzian in the permittivity arises. This could be lifted when a nonlocal description is considered. In the third and last example, we studied a wire medium structure, that is a prototypical metamaterial that supports a nonlocal optical response. For this material, a phenomenological approach with nonlocality already exists. We first show that the existing model fundamentally differs from the nonlocal model we have been proposing in this thesis, which suggests that homogenization is not unique and multiple models for an effective description may be used to explain the optical response of a specific metamaterial.

We finalize this work by showing the limits of homogenization, and the drawbacks of the proposed retrieval method.

In summary, we demonstrate that the nonlocal constitutive relations can describe the optical response much better than local constitutive relations would do. The general formulation we choose here can be extended to other kinds of nonlocal constitutive relations and renders our approach applicable to a wide class of centrosymmetric metamaterials.

Table of Contents

List of Figures

List of Symbols

$\boldsymbol{\mathcal{M}}$	Magnetic polarization density
$\boldsymbol{\mathcal{P}}$	Electric polarization density
χ_{el}	Electric susceptibility
χ_{magn}	Magnetic susceptibility
$\delta(k_0)$	Objective function
$\underline{\underline{\mathbf{F}}}$	Fresnel matrix
d_{slab}	Slab thickness
η	Nonlocality parameter of the wire medium model
Γ	Interface between two half-spaces
$\Gamma_{\pm}$	First $(-)$ and second $(+)$ interface of a slab material
Γ_L	Loss parameter
$\hat{\beta}^j$	Nonlocal material parameter (SYM)
$\hat{\epsilon}$	Electric permittivity tensor
$\hat{\gamma}$	Nonlocal material parameter (SSD)
$\hat{\mu}$	Magnetic permeability tensor
$\hat{\xi}$, $\hat{\zeta}$	Magneto-electric coupling terms
$\hat{\mathbf{e}}_x$	Unit vector in spatial direction x
$\hat{\mathbf{R}}$	Effective electric response tensor
$\hat{\mathbf{R}}_{\text{magn}}$	Effective magnetic response tensor
$\Im u$	Imaginary part of u
Λ	lateral periodicity of the metamaterial
λ	Wavelength of light
λ_0	Wavelength of light in free-space
$\mathcal{D}'(\Omega)$, $\mathcal{S}'(\Omega)$, and $\mathcal{E}'(\Omega)$	Different spaces of distributions in Ω
$\mathcal{D}(\Omega)$, $\mathcal{S}(\Omega)$, and $\mathcal{E}(\Omega)$	Different spaces of infinitely differentiable functions in Ω
$\mathcal{F}$	Fourier transform operator
$\mathcal{F}^{-1}$	Inverse Fourier transform operator

$\mathcal{H}_{\mathrm{loc}}(\mathrm{curl}, \Omega)$ Sobolev space of functions and their curl in $\mathcal{L}^2_{\mathrm{loc}}(\Omega)$

$\mathcal{H}_{\mathrm{loc}}(\mathrm{div}, \Omega)$ Sobolev space of functions and their divergence in $\mathcal{L}^2_{\mathrm{loc}}(\Omega)$

$\mathcal{L}^p$ Space of p-integrable functions

$\mathcal{L}^p_{\mathrm{loc}}$ Space of locally p-integrable functions

$\mathbf{a}$ (or a) characteristic length scale of the structure

$\mathbf{B}$ Macroscopic magnetic flux

$\mathbf{b}$ Microscopic magnetic flux

$\mathbf{D}$ Macroscopic displacement field

$\mathbf{E}$ Macroscopic electric field

$\mathbf{e}$ Microscopic electric field

$\mathbf{H}$ Macroscopic magnetic field

$\mathbf{k} = (k_x, k_y, k_z)$ Spatial frequency of light

$\mathbf{n}$ Normal unit vector of the interface

$\mathbf{Q}$ Gauge vector field

$\mathbf{r} = (x, y, z)$ Spatial coordinate in three-dimensional real space

Ω Space occupied by the metamaterial

ω Frequency of light

Ω_+ Space occupied by the substrate (transmission half-space)

Ω_- Space occupied by the cladding (incidence half-space)

Ω_0 Resonance amplitude

ω_0 Resonance frequency

ω_p Plasma frequency

$\Re u$ Real part of u

ρ Reflection coefficient

ρ^{HS} Reflection coefficient from a half-space

$\sigma = \pm$ Mode index in the homogeneous medium

τ Transmission coefficient

$\tilde{\mathbf{u}}(\mathbf{k})$ Spatial Fourier transform of $\mathbf{u}(\mathbf{r})$

$\underline{\mathbf{E}}$ Electric field amplitudes at the interfaces of a slab

$\underline{\mathbf{I}}$	Input vector of the incident wave
c	Speed of light in vacuum
f	Filling factor
k_0	Normalized frequency of light $k_0 = \frac{\omega}{c}$
M_{ij}	Macroscopic magnetic quadrupole moment
M_i	Macroscopic magnetic dipole moment
O_{ijk}	Macroscopic electric octupole moment
P_i	Macroscopic electric dipole moment density
p_i	Electric dipole moment
Q_{ij}	Macroscopic electric quadrupole moment density
t	Time coordinate
V	Macroscopic averaging volume
v_0	Mesoscopic averaging volume
$w(k_t)$	weight function as a function of the transverse wave vector
EMP	Effective Material Parameter
FMM	Fourier Modal Method
KKR	Korringa-Kohn-Rostoker method
p.v.	Cauchy principal value
SSD	Strong Spatial Dispersion
SYM	Symmetry Model
WM	Wire Medium
WSD	Weak Spatial Dispersion

1 | Introduction

I am acutely aware of the fact that the marriage between mathematics and physics, which was so enormously fruitful in past centuries, has recently ended in divorce.

Freeman John Dyson

Among other findings, this thesis proves the quote above wrong.

Metamaterials consist of a suitable arrangement of scattering inclusions that are structured on a length scale that is mostly much smaller than the wavelength [1]. Research endeavors in the context of metamaterials are driven by the ability to control the propagation of light in a way inaccessible with natural materials [1]–[3]. By virtues of the ability to respond to both electric and magnetic fields of light, metamaterials can be employed for many groundbreaking applications at optical frequencies. For instance, we may mention perfect lenses [4]–[6], structures that conceal objects from external observers [7]–[9], broadband anti-reflection coatings [10]–[12], or the generation of electromagnetic black holes [13], or applications such as information processing devices, that solve Fredholm's integral equations of the second kind [14], just for a few examples. That list could go on.

The peculiar properties of metamaterials arise from the sophisticated interplay of both the actual shape of the inclusions and the material from which they are made, but also from the specific details of their arrangement. The building blocks forming the metamaterial are called meta-atoms, and their arrangement can be either periodic or amorphous. Periodic metamaterials usually form planar materials with a well-defined geometry. The periodic arrangement allows to detect a far-field signal that is rather a collective response of the entire lattice and not of a single unit cell. On the other hand, amorphous metamaterials which may consist of either long-range or short-range ordered meta-atoms, consist mostly of self-assembled structures. Due to the random orientation of the meta-atoms, self-assembled metamaterials allow of an isotropic response that is affected by the resonance of a single meta-atom [15]. Even though fundamentally different, both periodic and amorphous metamaterials allow for a unique response to light by changing their geometrical arrangements and the materials therein.

This versatile tunability renders the manipulation of wave properties manifold. For instance, it was experimentally demonstrated that broadband anomalous dispersion, leading to superluminal group velocity [16], is possible with metamaterials. Furthermore, around fifty years ago, V. Veselago predicted that when the real valued material parameters ϵ and μ are negative, the index of refraction is negative too and, hence, phase velocity is opposite to the energy velocity [17]. In the early research of metamaterials, the possibility to attain simultaneously negative permittivity ϵ and permeability μ, by means of microwave scattering experiments on an array of split-ring resonators combined with metallic wires was experimentally demonstrated by Smith *et al.* [18] . Split-ring resonators, responsible for providing the magnetic response, are made of a pair of concentric conducting metallic rings, with slits on opposite sides. When excited by an external electromagnetic field, the induced currents in the loops generate a resonant magnetic dipole moment. The slit size and the ring radius can be rationally engineered to tune the resonance position to a desired frequency. The design idea of split-ring structures was first evoked by Pendry *et*

al. [19]. The wire medium in this example provided the necessary electric response as it basically constituted a diluted metal.

These promising features, that were easily feasible in the microwave regime, raised the interest of enabling metamaterials to operate at optical or near-infrared wavelengths. With nowadays nanofabrication techniques [20], it is indeed possible to manufacture metamaterials that allow for controlling wave propagation in the visible and telecommunication wavelengths. To this end, different meta-atoms have been suggested with different geometries with nanometer features, which are supposed to provide the desired optical response [21]. We mainly distinguish between two fabrication methods, the bottom-up and the top-down approaches. A particular example for a bottom-up meta-atom is the self-assembled core-shell nanoparticles with magnetic resonances in the visible wavelengths [22], or with negative index in the near-infrared wavelengths [23]. On the other hand, examples for top-down metamaterials that are of central importance to this thesis, are the fishnet metamaterial [24] and the wire medium [25]. The fishnet is a multilayer material with periodically arranged rectangular holes with nanometer size, and it specifically draws attention due to its negative index behaviour in the near infrared band. The wire medium is an array of conducting wires, which allows for the possibility to achieve epsilon-near-zero behaviour at the infrared and optical frequencies [26]. Here, we focus on the of study of periodic top-down metamaterials, and in particular on the fishnet and wire medium structures.

Even though the considered metamaterials are periodic, the concept shall not be confused with that of a photonic crystal. The definition of photonic crystals is *"Photonic crystals are regular arrays of materials with different refractive indices."* (*cf.* Sakoda [27]). Whereas metamaterials shall here be understood as *"Metamaterials are rationally designed composites aiming at effective material parameters that go beyond those of the ingredient materials."* (*cf.* Kadic *et al.* [28]). This definition, however, evokes a term of major importance, namely the effective material parameters. These are spatially averaged parameters of a hypothetical, homogeneous material, that shall substitute the original, heterogeneous metamaterial, with the condition that light propagation in both materials is identical, but they must also show the same reflection and transmission coefficients at the interfaces that delimit the materials. The mapping of the properties of a metamaterial to effective material parameters is called homogenization. Of course, full-wave numerical simulations allow for an accurate computation of both propagation and scattering aspects of a certain metamaterial, but they barely explain the underlying physics. Besides, numerical solvers such as the Fourier Modal Method (FMM) [29], the finite Element Method (FEM) [30], or the finite-difference time-domain (FDTD) method [31] share the heavy request on computational resources, since the exact description of the detailed unit cells is quite demanding. Further, the numerical computation of the same material must be re-performed at each time, when the geometry of the material is changed. Homogenization, however, allows the discussion of metamaterials, composed of a large system of different components, on the same physical level as natural materials. The, the mesoscopic details of the unit cell are no longer required to be considered, and instead, the metamaterial is described by a few numbers of effective material parameters. Commonly assigned effective material parameters are the permittivity ϵ and the permeability μ. Moreover, if homogenization is valid, it needs to be done only once for predicting the electromagnetic response from materials with the same geometry and with different thicknesses, inclusions, or inclusion densities.

The transition from the discrete picture to an averaged continuum, usually requires

that the characteristic lengthscale of the unit cell of the metamaterial, let it be a, is much smaller than the wavelength λ of the external light. If this condition is met, a sane averaging may take place. For periodic metamaterials, the fields of light, should vary on much longer lengthscales than the size of the unit cell. It is, therefore, necessary but not sufficient [32] that the critical parameter $(a/\lambda) \ll 1$. To our knowledge, one of the first work on the homogenization of composite media dates back to the work of Maxwell Garnett [33], that is over one hundred years old. This approach is in particular applicable to systems when operated in the quasi-static regime [34], where the spatial variation of the fields across a are neglected.

In the cause of time, tremendous further efforts were made to develop homogenization techniques. For instance, by assuming certain material laws, i.e. assuming that homogenization holds, the material parameters are obtained by averaging of the numerically calculated fields [35]–[37]. Unfortunately, the method suffers from unphysical effects such as anisotropic dispersion, even if the metamaterial was isotropic. Alternatively, the effective material parameters can be retrieved from inversion of the scattering parameters [38] obtained from metamaterials, that are periodic in two dimensions, and have a finite finite thickness is in the third direction. Such materials are termed as bi-periodic slabs. In this thesis, we consider such slab metamaterials from which the scattering parameters are numerically calculated and used to retrieve the effective material parameters from different homogenization models. This approach is called S-parameter retrieval and will be discussed in detail in Ch. 5.

A part of the asymptotic analysis in mathematics, also deals with the homogenization of composite media. This homogenization method is called asymptotic homogenization, where the modeling of phenomena occurring in composite materials leads to partial differential equations with strongly oscillating coefficients, that can generate numerical problems. In the context of electrodynamics of composite media, the problem consists of the wave equation with a highly oscillating permittivity. The asymptotic homogenization theory in the mathematical literature [39]–[42] serves to overcome this difficulty by replacing problems with fast oscillating coefficients by approximate problems whose coefficients are rather constant, and therefore much simpler to process numerically. In general, the small parameter a, that refers to the period of the oscillating coefficients, is scaled towards 0. Homogenizing this problem consists in studying the asymptotic behavior of the solution u_a when $a \to 0$ (cf. Ref. [43]). If u is a limit, one asks the question whether u can be characterized as a solution of a limiting problem, which naturally does not contain any fast oscillations that are compensated by a high-valued coefficient [44]. If this is the case, it has to be shown that the function u_a is sufficiently close to the limit function u, which can be considered as a good approximation of u_a.

However, such scaling is not applicable for metamaterials, as their unit cells have fixed size and are designed in a way, to exhibit unconventional spectral features at a specific wavelength range. This means that, even if a downscaling to an infinitesimal small unit cell was possible, the desired spectral feature would smear out and shift to a different wavelength [45]. This usually occurs when the meta-atoms are made of metallic or dispersive materials, i.e., are frequency-dependent. Nonetheless, this is not desirable as we wish to study the response of a real metamaterial. In fact, to get access to features that are inaccessible with natural materials at optical wavelengths, metamaterials must have a finite size of the unit cell, and in particular $(a/\lambda) \nrightarrow 0$. Yet, the approaches discussed above mostly work within the quasi-static approximations, while the theory of homogenization is usually applied in a frequency range, where the spatial dynamics

of the fields across a are important. In this case, the techniques discussed above have limited applicability in the homogenization of mesoscopic metamaterials, and hence, a more general approach is in order.

When the (a/λ) is not negligible, but is still smaller than one, the spatial dynamics of the wave become important and the fields of light start to probe the heterogeneities of the unit cell [46]. Thus, the response of matter towards excitation by an electromagnetic field, i.e., the polarization field $\boldsymbol{\mathcal{P}}(r,t)$, is at each given point in space determined by the field values not only at that point, but also by the field values in the vicinity of that point. A response of such kind is called nonlocal. Nonlocality is of utmost importance in this thesis. The physical origin of the nonlocal response is the inertial motion of the charge carriers of the medium. While moving through the medium, they also carry the response of that external influence, i.e. of the field, to which they were subjected at past times, while being at other points in space. Hence, the resulting response at a given point in space is given by the change of the field, which is averaged over the vicinity with dimensions of the order of a. Accordingly, nonlocality is negligibly small for fields that may be regarded as homogeneous within such a region, i.e., whose wavelengths are much larger than a, e.g. in the quasi-static regime. For these reasons, it important to keep the critical parameter (a/λ) in mind. Typical examples where a nonlocal response takes place are in Plasma [47], in certain metals with anomalous skin effect [48], [49], or in dielectrics close to a resonance line [50].

A nonlocal response in the real space of the spatial domain amounts to a $\mathbf{k}$-dependent generalized permittivity in the Fourier space of the spatial domain (also called momentum or impulse space), where $\mathbf{k}$ is the wave vector, sometimes also called the spatial frequency. This is somewhat in analogy to the temporal delay of a material's response, i.e., the dependence of the polarization field on the current fields of light and also on the current fields at preceding moments of time. A retardation in the response in the time domain corresponds to a frequency (ω, or k_0) dependent response in the frequency domain. This is called (temporal) dispersion. A $\mathbf{k}$-dependent response, that is a consequence of nonlocality, is called spatial dispersion. The strength of spatial dispersion in a material is given by the critical parameter (a/λ), or alternatively by $(a|\mathbf{k}|)$. Composite media such as metamaterials with a non-negligible (a/λ) have a nonlocal response and, hence, show spatial dispersion [51]. A first-order spatial dispersion effect, i.e. of order $(a/\lambda)^1$, is the chirality at optical frequencies. This effect occurs when the unit cell has no spatial inversion symmetry, even in the case when the materials are intrinsically non-chiral [52]. For structures with central symmetry, particularly important are the effects of order $(a/\lambda)^2$, as under certain conditions, that we will discuss throughout the thesis, the metamaterial at the effective level begins to respond to the magnetic field, i.e., an artificial magnetization occurs. In other terms, we obtain a dispersive magnetic permeability $\mu(\omega) \neq 1$, at optical frequencies. For natural materials at optical frequencies, the characteristic length a is of atomic or molecular scale and, therefore, $(a/\lambda)^2$ is negligibly small. This also explains the absence of the magnetic response of natural materials at optical frequencies.

The homogenization with spatial dispersion can be bifurcated into two main branches. When a model or a set of constitutive relations is assumed that can be described with effective material parameters and simultaneously without any spatial derivatives of the fields, we call it a local model or local constitutive relations, e.g., $\mathbf{D}(\mathbf{r},\omega) = \hat{\epsilon}(\omega)\mathbf{E}(\mathbf{r},\omega)$ and $\mathbf{H}(\mathbf{r},\omega) = \hat{\mu}^{-1}(\omega)\mathbf{B}(\mathbf{r},\omega)$. However, if, and only if, the model or the constitutive relations contain spatial derivatives of the fields that are equivalent, in terms of dispersion relation and interface conditions, to a different set of constitutive relations without

any spatial derivatives, we refer to this model to be the weak spatial dispersion (WSD) approximation. The model is called *weak* because, by means of a suitable gauge transformation, one can rewrite the macroscopic fields **D** and **H** such that no spatial derivatives appear in the constitutive relations. However, if a model or some constitutive relations that have spatially independent parameters but spatial derivatives of the fields and that cannot be reduced to a local model or is not equivalent to a local model, we call this to be a strong spatial dispersion (SSD) model. According to the aforementioned definitions, the constitutive relations with artificial magnetization, that turns out to be a second-order nonlocal effect in the electric field, is part of the WSD approximation. However, it was previously shown [53], and we will also show in the current thesis, that WSD is not always sufficient to adequately describe the response of a mesoscopic metamaterial.

The homogenization with strong spatial dispersion is in this thesis of central importance and we will present the significance of retaining nonlocality in the effective description of metamaterials with mesoscopic features. Of course, nonlocality is not a new topic by itself. There are other research groups that work with strong spatial dispersion as well. For instance, we mention the non-asymptotic homogenization technique [54]–[56] that provides an effective medium description without taking the limit $a \to 0$. Further, the authors in Refs. [57]–[61] did a considerable amount of work to homogenize wire media with strong spatial dispersion. Their approach, however, applies only to metamaterials with specific geometry. In the current thesis, we propose a homogenization approach, based on a phenomenological ansatz, that can be applied to any periodic metamaterial made of centrosymmetric and subwavelength unit cells.

A peculiar signature of spatial dispersion is the presence of additional modes [50]. This is in contrast to the WSD, or the local limit, where an illumination by a single plane wave generates in the metamaterial slab only one forward and one backward propagating plane wave. An experimental evidence of spatial dispersion in the near infrared range was found in GaAs semiconductor arrays [62]. When an electromagnetic wave is incident to semiconductors, it creates electron-hole pairs. These are bound states and the elementary excitation is called an exciton, when spatial dispersion occurs, the excitons can propagate in the semiconductor [63]). The material's response near such an excitonic transition may be modeled by a **k**-dependent Lorentz permittivity, which in frequency domain reads

$$\epsilon(\omega, \mathbf{k}) = 1 + \frac{\Omega_0^2}{\omega_0^2 - \omega^2 - \mathrm{i}\omega\Gamma_L + D(c\mathbf{k})^2}\,, \tag{1.1}$$

where Ω_0 denotes the oscillator strength, ω_0 the (resonance) transition frequency, Γ_L the relaxation factor. The coefficient D is of particular importance and is a measure for the kinetic energy of the exciton, and hence, of spatial dispersion. The dispersion relations, i.e., the solutions of Maxwell's equations with the response from Eq. (1.1) are depicted in Fig. 1.1 with (right) and without (left) spatial dispersion. We only show the solutions of transverse waves and if spatial dispersion is taken into account, a substantially new feature arises at frequencies above $\omega_l = \sqrt{\omega_0^2 + \Omega_0^2}$, namely the emergence of two solutions (branches) with different **k** values. The solution with the larger value of $\Re(\mathbf{k})$ is the additional mode that is a manifestation of spatial dispersion. We shortly want to note that an additional mode also exists at frequencies below ω_l, but with purely imaginary **k**. In Fig. 1.1 we only show the modes with simultaneously real ω and real **k**. In the effective medium picture, the additional mode shall be an additional propagating plane wave that contributes to the total field in the medium. Identifying this, requires the introduction of an additional interface condition, which is part of this thesis. The usual

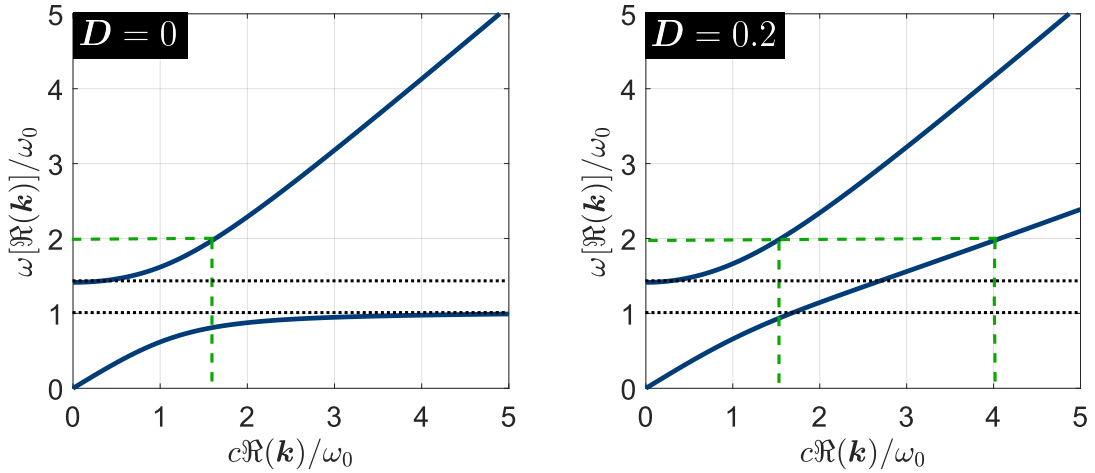

Figure 1.1: Dispersion relations $\omega[\Re(k)]$ of propagating polaritons without (left) and with (right) spatial dispersion. In the presence of spatial dispersion, two modes with different propagation constants k exist with the same frequency ω when larger than ω_l (green dashed lines). The mode with the larger $\Re(k)$ represents the additional mode. The lower black dotted line represents the resonance frequency ω_0 and the higher one represents the frequency ω_l at which the permittivity $\epsilon(\omega_l, 0) = 0$. For simplicity, we chose the loss parameter $\Gamma_L = 0$ and $\omega_0/\Omega_0 = 1$.

interface conditions are insufficient to serve the purpose. We will discuss this aspect in depth and derive from first principles the required interface conditions for two effective medium models with nonlocality in Chapter 4.

Structure of the thesis In this thesis, we develop an effective medium approach with nonlocal constitutive relations, that can be generally applied to any centrosymmetric subwavelength metamaterial. The analysis consists of three main steps. First, assuming constitutive relations that take spatial dispersion into account, we calculate the bulk dispersion relation to understand how an electromagnetic field propagates in the infinitely extended homogeneous metamaterial. Second, to unambiguously find the field amplitudes, the interface conditions must be derived, that further allow for an analytical calculation of reflection and transmission coefficients form a bi-periodic slab upon illumination with a plane wave. The derivation of the interface conditions was done in a collaboration with Prof. Dr. Michael Plum and Dr. Andrii Khrabustovskyi [64] from the Institute of Analysis (IANA) at the Karlsruhe Institute of Technology (KIT), where the credits to the mathematical rigour go to them. In the third and last part, we apply the derived reflection and transmission coefficients form step two together with the dispersion relations from step one to retrieve the effective material parameters that accurately reconstruct the optical coefficients of the original metamaterial subject to homogenization. The retrieval is based on an S-parameter optimization approach which relies on fitting the analytically calculated reflection and transmission coefficients of the homogeneous material to the simulated, or the experimentally measured, coefficients of slabs of metamaterials.

As the work presented here, especially at the level of deriving interface conditions, requires some mathematical analysis that are not commonly known in the physics community, we start in Chapter 2 by introducing the necessary mathematical background for understanding the approach applied here. It consists of selected topics from distribution theory and functional analysis from Refs. [65]–[67]. Most importantly, we highlight the

important steps of the weak formulation of partial differential equations, which shall serve as the main tool for deriving the interface conditions by evaluating the traces that arise at the interface between two different materials. Finally, since we work with plane waves, that are not (globally) integrable functions and treated as distributions, we discuss the Fourier transforms of such (generalized) functions. The analysis of the dispersion relation requires to go to the spatial Fourier space, i.e. to the **k**-domain. Therefore, we wish to clarify this mathematically.

Chapter 3 contains the core physics of the thesis. Here, we give the theoretical background behind the nonlocality in metamaterials. We start with the transition from microscopic to macroscopic Maxwell's equations and discuss the impossibility to distinguish the physical origin of the polarization current $\partial_t \boldsymbol{\mathcal{P}}(\mathbf{r}, t)$ and the magnetization current $\nabla \times \boldsymbol{\mathcal{M}}(\mathbf{r}, t)$ with the presence of spatial dispersion. We show that this ambiguity leads to the nonuniqueness of the auxiliary fields $\mathbf{D}(\mathbf{r}, t)$ and $\mathbf{H}(\mathbf{r}, t)$. Finally, we discuss the properties of the nonlocal response function and the physical implications of the assumption of the WSD approximation.

In Chapter 4 we propose two nonlocal models that take strong spatial dispersion into account. Side by side with the local WSD approach, we derive the dispersion relations to study the propagation of an electromagnetic field in the bulk of a homogenized metamaterial. Then, we derive for each model the necessary interface conditions, which allow for the reconstruction of the Fresnel matrix and, thus, the calculation of the reflection and transmission coefficient from a slab. Finally, we present two already existing homogenization approaches for subsequent comparison. Once, the local Maxwell-Garnett mixing rule, and second, the nonlocal homogenization model for wire media.

In Chapter 5 we apply the results from the previous chapter and construct a retrieval approach for metamaterials characterized by nonlocal constitutive relations. We apply this methodology to three different metamaterials. Once for a quick tutorial an array of dielectric spheres, then the fishnet metamaterial that has a negative index in the studied frequency range, and finally, a wire medium model that shows strong nonlocality. We conclude the chapter by demonstrating the importance of nonlocality in the effective description of metamaterials, and that homogenization by itself is not unique. We, further, show the limits of homogenization, in general, and the drawbacks of the used retrieval method.

Ultimately, in Chapter 6, we summarize the analytical and numerical work of this thesis and discuss possible future research, which can benefit from the methods developed in this thesis.

2 | Mathematical Background

Just by studying mathematics we can hope to make a guess at the kind of mathematics that will come into the physics of the future.

Paul Adrien Maurice Dirac

This Chapter is an introduction to distribution theory, weak formulation, and generalized Fourier-transform. The aim is to introduce the basic mathematical concepts and notions we will encounter throughout the thesis. First, we recap the principles and main properties of generalized functions, as our models of the effective response of light have to be defined in a generalized sense. Second, the characteristics of partial differential equations (PDEs) will be shortly discussed. We put emphasis on the hyperbolic wave equation (operator), describing light propagation in continuous media. At this point, we also introduce specific spaces of finite energy solutions to the PDEs that are required to fully identify the function space of the solutions, namely Sobolev spaces. Third, the concept of a weak formulation will be sketched and enriched with a physical example, where the Poisson equation for the electric potential will be solved. In this part of the chapter, we will also introduce the concept of traces that arise at the boundary of a domain or at the interface between two domains. Finally, we review the generalized Fourier transform of generalized functions, as we deal with non-integrable functions in both real- and Fourier-spaces, where the *classic* Fourier-Transform in its integral representation breaks down (recall, e.g., plane waves). Reading this chapter is recommended to understand the underlying math behind the derivations elaborated throughout this thesis. This chapter assumes some basic knowledge concerning functional analysis. Physics will be a tangent topic here and will be only touched in examples for further clarifications. We would further like to note that none of the definitions, theorems, lemmas, or remarks that we state are *redundant*. They were well selected and should provide a good mathematical background of the tools used throughout the derivations in the thesis. For a more comprehensive mathematical discussion of the topics below, we would like to refer to the books of H. Bremermann [65] and of E. J. Beltrami [66] for an introduction to generalized functions and Fourier transforms and to the book of L. Hörmander [68] for the topics of differential operators.

Preliminaries

Let Ω be an open set in $\mathbb{R}^n$ and $\overline{\Omega}$ its closure. In our applications, Ω is usually $\mathbb{R}^3_+$, $\mathbb{R}^3_-$ or Γ which are defined as follows:

- $\mathbb{R}^3_+ = \{(x, y, z) \in \mathbb{R}^3 | z > 0\}$
- $\mathbb{R}^3_- = \{(x, y, z) \in \mathbb{R}^3 | z < 0\}$
- $\Gamma = \overline{\mathbb{R}^3_-} \cap \overline{\mathbb{R}^3_+} = \{(x, y, z) \in \mathbb{R}^3 | z = 0\}$

Definition 2.0.1. *Let f be a function defined on Ω. The support of a function is the closure of the set of all points for which the function is nonzero, i.e.,*

$$\mathrm{supp}(f) := \overline{\{\mathbf{x} \in \Omega \,\big|\, f(\mathbf{x}) \neq 0\}}\,.$$

Definition 2.0.2. *Let V be a linear space over the field $\mathbb{C}$. We define its dual space V' as the set of all linear continuous functionals $u : V \to \mathbb{C}$, i.e.,*

1. $\langle \alpha u_1 + \beta u_2, \phi\rangle = \alpha\langle u_1, \phi\rangle + \beta\langle u_2, \phi\rangle$, $\forall u_1, u_2 \in V'$, $\phi \in V$ *and* $\alpha, \beta \in \mathbb{C}$ *(linearity),*
2. *and* $\lim_{n\to\infty}\langle u, \phi_n\rangle = \langle u, \lim_{n\to\infty}\phi_n\rangle$ *(continuity),*

where $\langle\cdot,\cdot\rangle$ represents the duality pair for the spaces V and V'.

2.1 Generalized Functions (Distributions)

Already in the early courses of theoretical physics, generalized functions (also called distributions) are handled in the same way as classical functions for solving differential equations of idealized systems. In classical mechanics one investigates for example, a body with a finite mass that is connected to a wall with a spring that is characterized by a spring constant. This is the canonical implementation of a classical harmonic oscillator. To study the impulse response of the system, comprising the mass and the spring, upon a pointwise excitation (an external force acting on it using Newton's laws of mechanics), an infinitely strong and infinitely short force applied on the mass in the direction of the spring has been exerted - the idealization of a hit with a hammer. Such excitation at $t = t_0$ is usually modeled with a "function" called Dirac's δ-distribution defined as

$$\delta(t - t_0) = \begin{cases} 0\,, & \text{for } t \neq t_0\,, \\ \infty\,, & \text{for } t = t_0\,, \end{cases}$$

with $\int_{-\infty}^{\infty}\delta(t-t_0)\mathrm{d}t = 1$. Even though the physical problem seems to be quite straightforward and fully understood, the introduction of Dirac's δ-distribution led to mathematical controversies. Simply, because the δ-distribution is not a function in the ordinary sense, which has a well-defined value at every point in its domain of definition. The same "function" has also been used to describe the charge density of a point-charge. There, a particle with a total electric charge Q that is localized at a position $\mathbf{r}_0 = (x_0, y_0, z_0)$ has an electric charge density

$$\rho_e(\mathbf{r}) = Q\delta(\mathbf{r} - \mathbf{r}_0)\,,$$

such that the integral of $\rho_e(\mathbf{r})$ over a Volume Ω gives 0 if $\mathbf{r}_0 \notin \Omega$ or Q if $\mathbf{r}_0 \in \Omega$. A further elementary physical setup that caused mathematical dilemmas is the RLC-circuit - the electric analogue of the damped mechanical harmonic oscillator - with a constant voltage source V_0. Suppose that the circuit is open for times $t < 0$, is closed at $t = 0$, and remains closed for $t > 0$. The external voltage that generates the current in the circuit as a function of time is then the step function

$$V(t) = \begin{cases} 0\,, & \text{for } t < 0\,, \\ V_0\,, & \text{for } t \geq 0\,. \end{cases}$$

Using Kirchhoff's laws, which are a consequence of Maxwell's equations, one can derive the ordinary differential equation for the electric current $I(t)$ in the circuit that reads for all times $t \in (-\infty, \infty)$

$$\frac{\mathrm{d}^2 I(t)}{\mathrm{d}t^2} + \frac{R}{L}\frac{\mathrm{d}I(t)}{\mathrm{d}t} + \frac{1}{LC}I(t) = \frac{\mathrm{d}V(t)}{\mathrm{d}t}\,. \tag{2.1}$$

Obviously, $V(t)$ is not continuous, and therefore not differentiable, at $t = 0$, as the jump from 0 to a strictly positive value $V_0 > 0$ represents an infinite slope, and is zero elsewhere, thereupon a δ-distribution. The quantity on the RHS of Eq. (2.1) is, therefore, not well-defined at $t = 0$, but it would be fortunate to be able to somehow evaluate the LHS of Eq. (2.1) for all times ranging from $-\infty$ to ∞.

The application of such "functions" seems to be diverse and gives rise to good physical understanding to simple as well as not-so-simple systems, but these functions are not educated in a rigorous way. A not-so-simple physical system is the main topic of this thesis. In the context of nonlocal effective response, which will be defined as a generalized response function of metamaterials towards excitation with light, which by themselves generate generalized functions (see Sec. 2.1.2 for proof). It is, therefore, worthwhile to extend the concept of classical functions to generalized functions and treat them with mathematical rigor.

2.1.1 The spaces $\mathcal{D}$ of test functions and $\mathcal{D}'$ of distributions

Let us introduce some important function spaces, for $k < \infty$ and $\Omega \subset \mathbb{R}^n$:
$\mathcal{C}^k(\Omega)$, is the space of k-times continuously differentiable functions on Ω.
$\mathcal{C}_0^k(\Omega)$, is the space of functions in $\mathcal{C}^k(\Omega)$ with compact support.
$\mathcal{C}^k(\overline{\Omega})$, is the space of all restrictions of $\mathcal{C}^k(\mathbb{R}^n)$ to $\overline{\Omega}$.
$\mathcal{C}^\infty(\Omega)$, is the space of infinitely differentiable functions, also called smooth functions. This space is sometimes noted as $\mathcal{E}$.
$\mathcal{C}_0^\infty(\Omega)$, is the space of infinitely differentiable functions with compact support. Usually it is considered as the space of test functions in Ω. In the literature, is is also denoted by the space $\mathcal{D}(\Omega)$. A practical example of a function defined on $\mathbb{R}$ with $\mathcal{D}$-regularity is

$$g(x) = \begin{cases} N\mathrm{e}^{-\frac{1}{1-x^2}}\,, & |x| < 1\,, \\ 0\,, & |x| \geq 1\,, \end{cases} \tag{2.2}$$

where the constant N ensures normalization such that $\int_{\mathbb{R}} g(x)dx = 1$. Clearly, $g(x)$ is infinitely differentiable where g and all its derivatives are zero for $|x| = 1$. Moreover, the support of g is the set $\{x \in \mathbb{R} | \, |x| \leq 1\}$. Hence, $g \in \mathcal{D}(\mathbb{R})$. For practical usage, we define the sequence $(g_j)_{j\in\mathbb{N}}$ by $g_j(x) = jg(jx)$. Hence, $\mathrm{supp}(g_j) = \{x \in \mathbb{R} | \, |x| \leq 1/j\}$ and $\int_{\mathbb{R}} g_j(x)dx = 1$, for all $j \geq 1$. In the limit $j \to \infty$, the support of g_j converges to $\{0\}$, but the integral of g_j over $\mathbb{R}$ remains equal to 1. We say that the sequence $(g_j)_{j\in\mathbb{N}}$ converges pointwise towards the Dirac δ-function (distribution). Such sequences are called regularizing sequences and have practical applications in many fields. They are mostly used as an approximation of the delta-function in numerical applications. They are also often employed to approximate continuous functions by their regularization. In other terms the convolution $f * g_j$ uniformly converges to f, where f is continuous. The notion of convergence in $\mathcal{D}(\Omega)$ is the following.

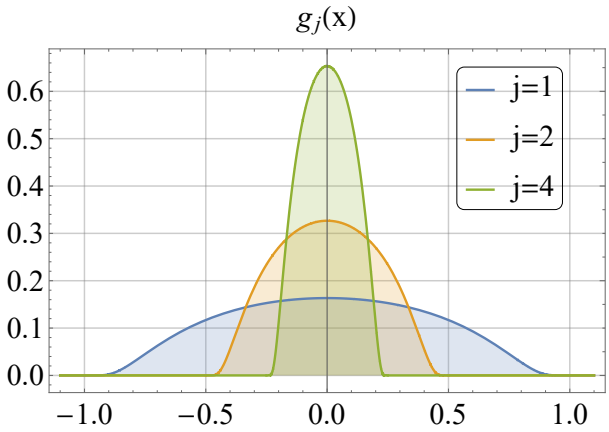

Figure 2.1: Illustration of $g_j(x)$ for $j = 1, 2, 4$. While the support of g_j scales with $1/j$, the supremum scales with j, such that the surface delimited by the function and the axis $y = 0$ remains constant.

Definition 2.1.1. *Let $(\phi_j)_{j\in\mathbb{N}}$ be a sequence in $\mathcal{D}(\Omega)$ and $\phi \in \mathcal{D}(\Omega)$. Then we say that $(\phi_j)_{j\in\mathbb{N}}$ converges to ϕ and write $\phi_j \xrightarrow[j\to\infty]{} \phi$ if:*

1. *$\forall j \in \mathbb{N} : \mathrm{supp}(\phi_j) \subset K$ with $K \subset \Omega$ compact.*
2. *$(D^\alpha \phi_j) \xrightarrow[j\to\infty]{} D^\alpha \phi$ uniformly for every $\alpha \in \mathbb{N}^n$ with $D^\alpha := \frac{\partial^{\alpha_1}}{\partial x_1^{\alpha_1}} \frac{\partial^{\alpha_2}}{\partial x_2^{\alpha_2}} \cdots \frac{\partial^{\alpha_n}}{\partial x_n^{\alpha_n}}$. Here, α is an n-dimensional multi-index $\alpha = (\alpha_1, \alpha_2, \cdots, \alpha_n)$ with $|\alpha| = \alpha_1 + \alpha_2 + \cdots + \alpha_n$.*

Definition 2.1.2. *$\mathcal{D}'(\Omega)$ is the space of distributions on Ω. It is the space of linear continuous functionals acting on $\mathcal{D}(\Omega)$, i.e., the dual space of $\mathcal{D}(\Omega)$. Hence, for $T \in \mathcal{D}'(\Omega)$ and $\phi \in \mathcal{D}(\Omega)$ we have the linear continuous mapping $F_T[\phi]$ such that*

$$F_T[\phi] := \langle T, \phi \rangle_\Omega \,. \tag{2.3}$$

Example: The δ-distribution is a generalized function defined on[1] $\mathcal{D}(\mathbb{R})$ by $\langle \delta_{x_0}, \phi(x) \rangle = \phi(x_0)$ for all $\phi \in \mathcal{D}(\mathbb{R})$. For locally integrable functions, Def. 2.1.2 may be further extended and written as

$$F_T[\phi] := \int_\Omega T\phi d\mathbf{x} \,. \tag{2.4}$$

This convenient expression will be used in several occasions in this thesis. We prove it in Lemma 2.1.1.

The derivative of a distribution $T \in \mathcal{D}'(\Omega)$ is defined in a weak sense as the functional on $\mathcal{D}(\Omega)$ for which

$$\langle D^\alpha T, \phi \rangle_\Omega = (-1)^{|\alpha|} \langle T, D^\alpha \phi \rangle_\Omega \,, \qquad \text{for all} \qquad \phi \in \mathcal{D}(\Omega) \,. \tag{2.5}$$

The derivative is said weak, because it requires the introduction of a test function ϕ. The concept of weak differentiation was first introduced by Sobolev [69]. Since ϕ is infinitely differentiable, generalized functions, in contrast to *classical* functions, are infinitely, but

[1] Please note the grammatical use of **on** and of **in** here: A function defined **on** a vector space V means it acts on V by means of Eq. (2.3) while it is defined **in** the dual space V'.

only weakly, differentiable. As one might guess, the origin behind Eq. (2.5) is roughly speaking, because it is just true for integrable functions, $|\alpha|$-times integration by parts and shifting all the derivatives on T to the test function ϕ. Because ϕ has compact support, the restrictions involving ϕ on the boundary of Ω (the traces) vanish.
Example: Let f be a $\mathcal{C}^1$-function, then $\langle \delta', f\rangle = -\langle \delta, f'\rangle$.
Another space of test functions that is frequently used in many fields in physics, but is less restrictive than $\mathcal{D}$, is the space of rapidly decreasing $\mathcal{C}^\infty$-functions.

Definition 2.1.3. *A function ϕ is said to be rapidly decreasing, if for all $k, \alpha \in \mathbb{N}_0^n$*

$$\lim_{|\mathbf{x}|\to\infty} |\mathbf{x}|^k D^\alpha \phi(\mathbf{x}) = 0\,.$$

The function space $\mathcal{S}$ of all rapidly decreasing $\mathcal{C}^\infty$-functions is called Schwartz space.

Example: The Gauss-function $\phi(x) = \mathrm{e}^{-ax^2}$, with $\Re(a) > 0$ is an element of $\mathcal{S}(\mathbb{R})\backslash\mathcal{D}(\mathbb{R})$.
The space $\mathcal{S}$ is less restrictive than $\mathcal{D}$ and all functions in $\mathcal{D}$ are contained in $\mathcal{S}$. Then, by duality, the space $\mathcal{S}'$ of tempered distributions is more restrictive than $\mathcal{D}'$ (the space of all distributions). In other terms, the quantity $\langle T, \phi\rangle$ with $\phi \in \mathcal{S}$ and for some fixed $N \geq 1$, $\phi \in \mathcal{O}\left(|\mathbf{x}|^{-N-2}\right)$ at infinity, is only finite, if $T \in \mathcal{O}\left(|\mathbf{x}|^N\right)$ as $|\mathbf{x}| \to \infty$. We define

Definition 2.1.4. *We define the space $\mathcal{S}'$ as the space of linear functionals on $\mathcal{S}$. It is the set of tempered distributions. These are distributions of slow growth, meaning that each derivative of grows at most as fast as some polynomial.*

Examples of tempered distributions are all distributions with compact support such as Dirac's δ-distribution and its derivatives to an arbitrary order, and Cauchy's principal value integral of $\frac{1}{x}$, i.e, p.v.$\frac{1}{x}$. Functions with slow growth (tempered functions), e.g., plane waves or polynomials generate (regular) tempered distributions.

Finally, we would like to introduce another important space larger than $\mathcal{D}$, namely, the space of $\mathcal{E} = \mathcal{C}^\infty$ of "only" infinitely differentiable test functions. It's dual space $\mathcal{E}'$ is the most restrictive space of distributions, i.e., the distributions with compact support, which also contains Dirac's δ-distribution and all its partial derivatives. In particular, the following ordering holds [65]:

Spaces of test functions:	$\mathcal{D}$	$\subset$	$\mathcal{S}$	$\subset$	$\mathcal{E}$
	$\mathcal{C}^\infty$-compact support functions		$\mathcal{C}^\infty$-rapidly decreasing functions		$\mathcal{C}^\infty$-functions
Spaces of distributions:	$\mathcal{D}'$	$\supset$	$\mathcal{S}'$	$\supset$	$\mathcal{E}'$
	all distributions		polynomially increasing distributions		compactly supported distributions

Remark 2.1.1. *This space $\mathcal{E}'$ is particularly interesting for the study of nonlocality, where the nonlocal kernel is a series of Dirac's δ-distributions and their partial derivatives, which are all elements of $\mathcal{E}'(\mathbb{R}^3)$.*

2.1.2 Lebesgue spaces

Throughout the thesis, we will often encounter $\mathcal{L}^p$-spaces. These are complete normed linear spaces, hence Banach spaces, of functions whose p-th power of their absolute value is Lebesgue integrable.

Definition 2.1.5. *Let* $\Omega \subset \mathbb{R}^n$ *and* $1 \leq p < \infty$

$$\mathcal{L}^p(\Omega) := \{f : \Omega \to \mathbb{C} \Big| \, \|f\|_{\mathcal{L}^p} < \infty\}\,, \tag{2.6}$$

with the p-norm $\|f\|_{\mathcal{L}^p} := \left(\int_\Omega |f|^p\right)^{\frac{1}{p}}$.

The dual space of $\mathcal{L}^p(\Omega)$ is the space $(\mathcal{L}^p(\Omega))' = \mathcal{L}^q(\Omega)$ where q is given by $\frac{1}{p} + \frac{1}{q} = 1$. Then, for $f \in \mathcal{L}^p(\Omega)$ and for $g \in \mathcal{L}^q(\Omega)$ the dual pairing

$$|\langle f, g\rangle_\Omega| = \left|\int_\Omega f g \mathrm{d}\mathbf{x}\right| \leq \|f\|_{\mathcal{L}^p}\|g\|_{\mathcal{L}^q} < \infty\,,$$

exists for $p > 1$. For $p = 1$, $(\mathcal{L}^1(\Omega))' = \mathcal{L}^\infty(\Omega)$ is its dual that is defined as the space of essentially bounded measurable functions, i.e., functions that are bounded up to a set of Lebesgue-measure zero. The norm of $\mathcal{L}^\infty(\Omega)$ is given by

$$\|f\|_{\mathcal{L}^\infty} := \operatorname*{ess\,sup}_{x\in\Omega} |f(x)| = \inf\{C \geq 0 \Big| |f(x)| \leq C \text{ a.e.}\}.$$

Example: Plane waves are bounded everywhere with $C = 1$ and are therefore elements of $\mathcal{L}^\infty(\mathbb{R}^4)$.
To prove the duality, let $f \in \mathcal{L}^1(\Omega)$ and $g \in \mathcal{L}^\infty(\Omega)$. Then, $\exists C > 0$ such that $\|g\|_{\mathcal{L}^\infty} = C$. It follows that

$$|\langle f, g\rangle_\Omega| = \left|\int_\Omega f g \mathrm{d}\mathbf{x}\right| \leq \int_\Omega |f||g|\mathrm{d}\mathbf{x} < C\int_\Omega |f|\mathrm{d}\mathbf{x} < \infty\,,$$

while the latter inequality holds because $f \in \mathcal{L}^1(\Omega)$.

Remark 2.1.2. *For* $1 \leq p \leq q$*, the space* $\mathcal{L}^q(\Omega)$ *is more restrictive than the space* $\mathcal{L}^p(\Omega)$*. Hence, the following embedding holds* $\mathcal{L}^q(\Omega) \subseteq \mathcal{L}^p(\Omega)$*, for bounded* Ω*. Such ordering does not exist for* $\Omega = \mathbb{R}^n$*.*
Example: Let $\Omega = [1, \infty)$ *and* $f\colon \Omega \to (0, 1]$, $x \mapsto \frac{1}{x}$*. Clearly* $\|f\|_{\mathcal{L}^2} = 1 < \infty$ *but* $\|f\|_{\mathcal{L}^1} = \infty$*, whereas* $f \in \mathcal{L}^2([1, \infty))$ *but* $f \notin \mathcal{L}^1([1, \infty))$*.*

In what follows, we shall discuss some special cases that play a significant role in physics.

$\mathcal{L}^1$-space: The space $\mathcal{L}^1$ is the space of (Lebesgue-)integrable functions, i.e., $\exists C > 0$ such that $\|f\|_{\mathcal{L}^1} \leq C$. A physical example of such quantity is the electric charge density $\rho_e(\mathbf{r})$ of a body occupying the volume $\Omega \subseteq \mathbb{R}^3$. The norm $\|\rho_e\|_{\mathcal{L}^1} = |Q|$ yields the total charge $\pm Q$ of the body.

$\mathcal{L}^2$-space: The space $\mathcal{L}^2$ defines the space of square integrable functions and deserves special attention for many reasons. First, the space is self-dual, i.e., $(\mathcal{L}^2)' = (\mathcal{L}^2)$, because $\frac{1}{2} + \frac{1}{2} = 1$. As a consequence, the dual pairing is a scalar product and the space is then a Hilbert space. Second, functions in $\mathcal{L}^2$ play an important role in physics. All observable, physical quantities have to be elements of $\mathcal{L}^2$. For instance, the electric and magnetic fields need to be at least square integrable such that the energy (intensity) of light can be meaningfully defined and measured.

Very frequently in optics, we deal with interfaces between different media, where the material parameters emerging in the wave-equation become only locally continuous. Hence, it is favorable to introduce the class of locally p-integrable functions.

Definition 2.1.6. *Let Ω be an open set and $1 \leq p < \infty$. A function f is called locally p-integrable, if for all compact subsets K of Ω it holds*

$$\int_K |f|^p \mathrm{d}\mathbf{x} < \infty \,.$$

The set of locally p-integrable functions is denoted by $\mathcal{L}^p_{\mathrm{loc}}(\Omega)$.

Remark 2.1.3. *The space $\mathcal{L}^p_{\mathrm{loc}}(\Omega)$ does not require that the functions are integrable in their domain of definition and does also not require that the functions vanish at infinity. It is, therefore, less restrictive than $\mathcal{L}^p(\Omega)$. Hence, every integrable function is locally integrable, but not conversely, i.e., $\mathcal{L}^p(\Omega) \subset \mathcal{L}^p_{\mathrm{loc}}(\Omega)$ for $1 \leq p < \infty$.*
Example: Let $\Omega = \mathbb{R}$ and the plane wave defined as $f\colon \mathbb{R} \to \{z \in \mathbb{C} \,\big|\, |z| = 1\}$, $x \mapsto \mathrm{e}^{\mathrm{i}kx}$, with $k \in \mathbb{R}$. It is easy to show that $\|f\|_{\mathcal{L}^1_{\mathrm{loc}}} \leq \sup\{x, y \in K \,\big|\, |x - y|\}$, where K is compact in $\mathbb{R}$, but $\|f\|_{\mathcal{L}^1} = \infty$. Hence, $f \in \mathcal{L}^1_{\mathrm{loc}}(\mathbb{R})$ but $f \notin \mathcal{L}^1(\mathbb{R})$.

$\mathcal{L}^1_{\mathrm{loc}}$−space: Again, we shall discuss a specific $\mathcal{L}^p_{\mathrm{loc}}(\Omega)$-space that is particularly interesting in this thesis, namely the $\mathcal{L}^1_{\mathrm{loc}}$-space. It denotes the set of locally integrable functions and is of special importance, particularly in distribution theory.

Lemma 2.1.1. *Every locally integrable function f on Ω generates a distribution $F_f \in \mathcal{D}'(\mathbb{R})$, i.e., $\exists \phi \in \mathcal{D}(\mathbb{R})$, by means of Eq.* (2.3).

Proof: Suppose $K \subset \Omega$ is the compact support of ϕ. Then

$$|F_f[\phi]| = \left| \int_\Omega f\phi \mathrm{d}\mathbf{x} \right| = \left| \int_K f\phi \mathrm{d}\mathbf{x} \right| \leq \int_K |f\phi| \, \mathrm{d}\mathbf{x} \leq \|\phi\|_{\mathcal{L}^\infty} \int_K |f| \, \mathrm{d}\mathbf{x} < \infty \,.$$

So far for the existence. The proof of the continuity requires the usage of the notion of convergence in $\mathcal{D}(\Omega)$ as defined in Def. 2.1.1. Let $\phi_j \xrightarrow[j\to\infty]{} \phi$ in $\mathcal{D}(\Omega)$, with $\mathrm{supp}(\phi_j) \subset K \subseteq \Omega$, then we obtain

$$|F_f(\phi) - F_f(\phi_j)| \leq \int_\Omega |f\phi - f\phi_j| \, \mathrm{d}\mathbf{x} \leq \underbrace{||\phi - \phi_j||_\infty}_{\xrightarrow[j\to\infty]{} 0} \int_K |f| \, \mathrm{d}\mathbf{x} \to 0 \,.$$

Distributions generated by $\mathcal{L}^1_{\mathrm{loc}}$-functions are called regular distributions. Common regular distributions in physics are plane waves and Heaviside step-functions. Distributions that cannot be written in form of F_f with f being locally integrable, are called singular. For instance, the Dirac δ-distribution is a singular distribution.

Remark 2.1.4. *By means of Eq.* (2.5)*, and in contrast to classical functions, distributions are infinitely differentiable. However, the derivative of regular distributions are not necessarily regular as well. For instance, consider the Heaviside step-function $\Theta(x)$ that has a discontinuity at zero and is therefore not differentiable in the classical sense. Since, $\Theta \in L^1_{\mathrm{loc}}(\mathbb{R})$, it can be considered as a regular distribution and its weak derivative is defined according to Eq.* (2.5)*. Let $\phi \in \mathcal{D}(\mathbb{R})$, then*

$$\langle H', \phi \rangle \overset{p.i.}{=} H(x)\phi(x)|_{-\infty}^{\infty} - \langle H, \phi' \rangle = \phi(0) = \langle \delta, \phi \rangle \,.$$

Hence $H' = \delta$ is a singular distribution.

Remark 2.1.5. *Let $\Omega = \mathbb{R}^n$ and $1 \leq p < \infty$. It must not hold [70] that for functions $f \in \mathcal{L}^p(\mathbb{R}^n)$ to vanish as $|\mathbf{x}| \to \infty$ and $\mathcal{D}(\mathbb{R}^n) \subset \mathcal{S}(\mathbb{R}^n) \subset \mathcal{L}^p(\mathbb{R}^n) \subset \mathcal{D}'(\mathbb{R}^n)$.*

Notation: For every function space $\mathcal{X}$, we notate by $\boldsymbol{\mathcal{X}}$ the space of vector-functions $\boldsymbol{\phi} : \Omega \to \mathbb{C}^3$ whose components are contained in $\mathcal{X}$. For example, the electric field $\mathbf{E}$ is in $\boldsymbol{\mathcal{L}}^2(\Omega)$ if, and only if its three components E_x, E_y and $E_z \in \mathcal{L}^2(\Omega)$.

2.2 Sobolev spaces and weak formulation

In theoretical electrodynamics, and in theoretical physics in general, the encounter of partial differential equations (PDEs) is unavoidable when it comes to the study of dynamic processes, and in particular wave phenomena. Eventually, one seeks for solving these PDEs and identifying the spaces in where the solutions exist. Linear PDEs can be understood as differential operators acting linearly on functions, that satisfy enough regularity and measurability.

Definition 2.2.1. *A linear differential operator A of order m is defined as the linear application from a function space $\mathcal{X}$ (the solution space) to function space $\mathcal{Y}$, where $u \in \mathcal{X}$ and $Au \in \mathcal{Y}$,*

$$A := \sum_{|\alpha| \leq m} c_\alpha D^\alpha \,, \tag{2.7}$$

where $\alpha = (\alpha_1, \alpha_2, ..., \alpha_n)$ is a multi-index with $|\alpha| = \alpha_1 + \alpha + ... + \alpha_n$.

Remark 2.2.1. *For $Au \in \mathcal{Y}$, it is not required that every single term in Au is an element of $\mathcal{Y}$. It is therefore possible, and no issue, that some terms of Au do not exist in $\mathcal{Y}$, given that they may cancel each other in their linear combination.*

For a second-order partial differential operator A, depending on the characteristics of A, the operator can be classified as either hyperbolic, elliptic, or parabolic. Hyperbolic PDEs have oscillatory solutions and describe wave phenomena. The wave-equation for instance, is of hyperbolic type. For divergence-free and time-harmonic fields however, the wave equation (operator) turns out to be the Helmholtz equation, which is classified as quasi-elliptic. These two classes are of utmost relevance in this work. Parabolic PDEs, such as the heat equation, describe diffusion processes and the elliptic PDEs, such as the Poisson equation in the static regime, will not be discussed here.

In our applications, we look for finite-energy solutions (of any PDEs we encounter). As a consequence, the inhomogeneity f is required to be (at least) an element of $\mathcal{L}^2(\Omega)$, and the functions u, which represent the field components must be (at least) in $\mathcal{L}^2(\Omega)$ as well. Hence, we end up with handling functions as well as their weak derivatives being (at least) in the Hilbert space $\mathcal{L}(\Omega)^2$. Hence, we define the special Sobolev space $\mathcal{H}^k(\Omega)$ which will be the topic of the next subsection.

2.2.1 The Sobolev Spaces $\mathcal{H}^k$, $\mathcal{H}(\mathrm{div})$, and $\mathcal{H}(\mathrm{curl})$

Sobolev spaces are indispensable in the variational theory of Maxwell's equations and are also called spaces of finite-energy solutions. There, partial integrations will be used for calculating weak derivatives of distributions, which will be the main tool for deriving the interface conditions at the interface between two distinct media. The finite element method (FEM) as well is based on the weak formulation of partial differential equations and thus on Sobolev space theory.

Definition 2.2.2. *Let $\Omega \subset \mathbb{R}^n$ and $k \in \mathbb{N}$. The Sobolev space $\mathcal{H}^k(\Omega)$ is the Hilbert space of functions $f \in \mathcal{L}^2(\Omega)$ and all their weak partial derivatives up to the order k being elements of $\mathcal{L}^2(\Omega)$ as well. Formally:*

$$\mathcal{H}^k(\Omega) := \{f \in \mathcal{L}^2(\Omega) \Big| \forall \alpha \in \mathbb{N}^n, \text{ with } |\alpha| \leq k : \ D^\alpha f \in \mathcal{L}^2(\Omega)\}, \tag{2.8}$$

which is by itself a Hilbert space as well, equipped with the norm

$$\|f\|_{\mathcal{H}^k(\Omega)} := \left(\sum_{|\alpha| \leq k} \|D^\alpha f\|^2_{\mathcal{L}^2} \right)^{\frac{1}{2}}. \tag{2.9}$$

We also define the Sobolov space $\mathcal{H}^k_0(\Omega)$ of functions in $\mathcal{H}^k(\Omega)$ that vanish at the boundary, i.e.,

$$\mathcal{H}^k_0(\Omega) := \{f \in \mathcal{H}^k(\Omega) \Big| f|_{\partial\Omega} = 0\}. \tag{2.10}$$

Analogously to the Lebesgue spaces (and all other Bannach spaces), for practical uses one can also define the localized version of Sobolev spaces.

Definition 2.2.3. *Let $\Omega \subset \mathbb{R}^n$. The function space $\mathcal{H}^k_{\text{loc}}(\Omega)$ is the space of functions which together with their partial derivatives up to the order k are locally square integrable, i.e.,*

$$\mathcal{H}^k_{\text{loc}}(\Omega) := \{f \in \mathcal{L}^2_{\text{loc}}(\Omega) \Big| \forall \alpha \in \mathbb{N}^n, \text{ with } |\alpha| \leq k : \ D^\alpha f \in \mathcal{L}^2_{\text{loc}}(\Omega)\}. \tag{2.11}$$

In the following, we introduce two additional function (Sobolev) spaces that play an important role in the macroscopic theory of Maxwell's equations, and specifically for the equations of time harmonic electromagnetic waves. This situation will be considered throughout the manuscript, where time derivatives simplify to algebraic multiplication proportional to the temporal frequency ω. These (Maxwell Eqs.) turn into four coupled PDEs of the fields $\mathbf{D}$, $\mathbf{B}$, $\mathbf{E}$, and $\mathbf{H}$ and their spatial derivatives. Since, we look for solutions in which an energy can be well defined, all four vector functions $(\mathbf{D}, \mathbf{B}, \mathbf{E}, \mathbf{H})$ must be elements of $\boldsymbol{\mathcal{L}}^2(\Omega)$. Consequently, from Gauss's law (in the absence of external charges) it must hold that $\nabla \cdot \mathbf{D} \in \mathcal{L}^2(\Omega)$ and $\nabla \cdot \mathbf{B} \in \mathcal{L}^2(\Omega)$, since $0 \in \mathcal{L}^2(\Omega)$. Furthermore, we can deduce from Faraday's law that $\nabla \times \mathbf{E} \in \boldsymbol{\mathcal{L}}^2(\Omega)$ and from Ampère's law that $\nabla \times \mathbf{H} \in \boldsymbol{\mathcal{L}}^2(\Omega)$. The vector functions $\mathbf{D}, \mathbf{B}$ and $\mathbf{E}, \mathbf{H}$ are, respectively, elements of the Sobolev spaces $\boldsymbol{\mathcal{H}}(\text{div}, \Omega)$ and $\boldsymbol{\mathcal{H}}(\text{curl}, \Omega)$, which are defined as follows.

Definition 2.2.4. *Let $\Omega \subset \mathbb{R}^3$ bounded Lipschitz domain[2] and $\mathbf{f} \in (\mathcal{L}^2(\Omega))^3$. Then we define*

1. $\boldsymbol{\mathcal{H}}(\text{div}, \Omega) := \{\mathbf{f} \in \boldsymbol{\mathcal{L}}^2(\Omega) \Big| \nabla \cdot \mathbf{f} \in \mathcal{L}^2(\Omega)\}$,
   with the norm $\|f\|_{\boldsymbol{\mathcal{H}}(\text{div},\Omega)} := \left(\|\mathbf{f}\|^2_{\mathcal{L}^2} + \|\nabla \cdot \mathbf{f}\|^2_{\mathcal{L}^2}\right)^{\frac{1}{2}}$.
2. $\boldsymbol{\mathcal{H}}(\text{curl}, \Omega) := \{\mathbf{f} \in \boldsymbol{\mathcal{L}}^2(\Omega) \Big| \nabla \times \mathbf{f} \in \boldsymbol{\mathcal{L}}^2(\Omega)\}$,
   with the norm $\|f\|_{\boldsymbol{\mathcal{H}}(\text{curl},\Omega)} := \left(\|\mathbf{f}\|^2_{\mathcal{L}^2} + \|\nabla \times \mathbf{f}\|^2_{\mathcal{L}^2}\right)^{\frac{1}{2}}$.

[2]**Def.:** A bounded Lipschitz domain is a bounded domain whose boundary can be locally parametrized with a Lipschitz continuous function γ, i.e., $\exists L > 0 : \forall, x, y \in B : |\gamma(x) - \gamma(y)| \leq L|x - y|$, where $\gamma(B) = \partial\Omega$. Examples: $x \mapsto |x|$ is Lipschitz continuous but $x \mapsto \sqrt{|x|}$ is not Lipschitz-continuous.

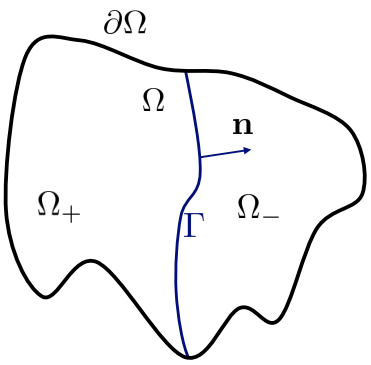

Figure 2.2: The domain Ω (Island of Djerba) with Lipschitz Boundary is decomposed into subdomains Ω_+ and Ω_-, whose closure meet at the interface $\Gamma = \overline{\Omega_+} \cap \overline{\Omega_-}$. The unit-vector $\mathbf{n}$ is the normal vector and pointing outwards of Ω_+.

Alternatively, i.e., by incorporating test functions, the spaces above may be also defined as follows [71]:

1. $\mathbf{f} \in \boldsymbol{\mathcal{H}}(\mathrm{div}, \Omega) \Leftrightarrow \exists v \in \boldsymbol{\mathcal{L}}^2(\Omega) : \forall \phi \in \mathcal{D}(\Omega)$, *it holds*

$$(\nabla \cdot \mathbf{f})[\phi] = \int_\Omega v\phi \, \mathrm{d}\mathbf{x} \,.$$

As $(\nabla \cdot \mathbf{f})$ *is understood as a distribution acting on* ϕ*, it further holds*

$$(\nabla \cdot \mathbf{f})[\phi] = -\int_\Omega \mathbf{f} \cdot (\nabla\phi) \, \mathrm{d}\mathbf{x} \,.$$

2. $\mathbf{f} \in \boldsymbol{\mathcal{H}}(\mathrm{curl}, \Omega) \Leftrightarrow \exists \mathbf{v} \in \boldsymbol{\mathcal{L}}^2(\Omega) : \forall \boldsymbol{\phi} \in \boldsymbol{\mathcal{D}}(\Omega)$, *it holds*

$$(\nabla \times \mathbf{f})[\boldsymbol{\phi}] = \int_\Omega \mathbf{v} \cdot \boldsymbol{\phi} \, \mathrm{d}\mathbf{x} \,,$$

As $(\nabla \times \mathbf{f})$ *is understood as a distribution acting on* $\boldsymbol{\phi}$*, it further holds*

$$(\nabla \times \mathbf{f})[\boldsymbol{\phi}] = \int_\Omega \mathbf{f} \cdot (\nabla \times \boldsymbol{\phi}) \, \mathrm{d}\mathbf{x} \,.$$

Functions that reside in $\boldsymbol{\mathcal{H}}(\mathrm{div}, \Omega)$ and in $\boldsymbol{\mathcal{H}}(\mathrm{curl}, \Omega)$ have special properties concerning their normal and their tangential components at the boundary $\partial\Omega$, respectively. Before we state the next lemma, let us first decompose the vector field $\mathbf{f}$ into components tangential and normal to the boundary Ω. Let $\mathbf{n}$ be the normal unit vector of $\partial\Omega$ and pointing outside Ω. Then, every vector on Ω can be decomposed into a tangential $\mathbf{f}_t$ and a normal $\mathbf{f}_n$ components:

$$\mathbf{f} := \mathbf{f}_t + \mathbf{f}_n = (\mathbf{n} \times \mathbf{f}) \times \mathbf{n} + (\mathbf{n} \cdot \mathbf{f})\mathbf{n} \,.$$

Theorem 2.2.1. *Let* $\Omega \subset \mathbb{R}^3$ *and* $\Omega_\pm$ *be bounded Lipschitz domains with* $\Omega = \Omega_+ \cup \Omega_- \cup \Gamma$*, where* $\Gamma = \overline{\Omega_+} \cap \overline{\Omega_-}$ *is the interface between the sub-domains* Ω_+ *and* Ω_-*, with an oriented normal* $\mathbf{n}$*. And let* $\mathbf{f} \in \boldsymbol{\mathcal{L}}^2(\Omega)$ *with* $\mathbf{f} = \mathbf{f}_+$ *for* $\mathbf{x} \in \Omega_+$ *and* $\mathbf{f} = \mathbf{f}_-$ *for* $\mathbf{x} \in \Omega_-$*, such that* $\nabla \cdot \mathbf{f}_\pm \in \boldsymbol{\mathcal{L}}^2(\Omega_\pm)$ *or* $\nabla \times \mathbf{f}_\pm \in \boldsymbol{\mathcal{L}}^2(\Omega_\pm)$*. Then*

$$\mathbf{f} \in \boldsymbol{\mathcal{H}}(\mathrm{div}, \Omega) \Leftrightarrow \mathbf{f}_{+,n}|_\Gamma = \mathbf{f}_{-,n}|_\Gamma \,. \tag{2.12}$$

$$\mathbf{f} \in \boldsymbol{\mathcal{H}}(\mathrm{curl}, \Omega) \Leftrightarrow \mathbf{f}_{+,t}|_\Gamma = \mathbf{f}_{-,t}|_\Gamma \,. \tag{2.13}$$

Proof: The proof of this theorem for both curl and div operators resemble in their augmentations. Since, we will mostly apply Eq. (2.13), we only show the proof for the curl operator.
⇒-part: Let $\mathbf{f} \in \boldsymbol{\mathcal{H}}(\mathrm{curl}, \Omega)$, i.e., $\mathbf{f} \in \boldsymbol{\mathcal{L}}^2(\Omega)$ and $\nabla \times \mathbf{f} \in \boldsymbol{\mathcal{L}}^2(\Omega)$. Then for any $\boldsymbol{\phi} \in \boldsymbol{\mathcal{D}}(\Omega)$, it holds using Green's first identity

$$\int_\Omega \mathbf{f} \cdot (\nabla \times \boldsymbol{\phi}) \, \mathrm{d}\mathbf{x} = \int_\Omega (\nabla \times \mathbf{f}) \cdot \boldsymbol{\phi} \, \mathrm{d}\mathbf{x} \,. \tag{2.14}$$

With the hypothesis $\mathbf{f}_\pm \in \boldsymbol{\mathcal{H}}(\mathrm{curl}, \Omega_\pm)$, we obtain

$$\begin{aligned}\int_\Omega \mathbf{f} \cdot (\nabla \times \boldsymbol{\phi}) \, \mathrm{d}\mathbf{x} &= \int_{\Omega_+} \mathbf{f}_+ \cdot (\nabla \times \boldsymbol{\phi}) \, \mathrm{d}\mathbf{x} + \int_{\Omega_-} \mathbf{f}_- \cdot (\nabla \times \boldsymbol{\phi}) \, \mathrm{d}\mathbf{x} \\ &= \int_{\Omega_+} (\nabla \times \mathbf{f}_+) \cdot \boldsymbol{\phi} \, \mathrm{d}\mathbf{x} + \int_\Gamma \mathbf{f}_+ \cdot (\mathbf{n} \times \phi) \, \mathrm{d}\mathbf{x} \\ &+ \int_{\Omega_-} (\nabla \times \mathbf{f}_-) \cdot \boldsymbol{\phi} \, \mathrm{d}\mathbf{x} - \int_\Gamma \mathbf{f}_- \cdot (\mathbf{n} \times \phi) \, \mathrm{d}\mathbf{x}\end{aligned}$$

By virtue of the property of the mixed product, we have $\mathbf{f}_\pm \cdot (\mathbf{n} \times \phi) = -(\mathbf{f}_\pm \times \mathbf{n}) \cdot \phi$. Hence, by merging both volume integrals over $\Omega_\pm$, we get after sorting the terms

$$\int_\Omega \mathbf{f} \cdot (\nabla \times \boldsymbol{\phi}) \, \mathrm{d}\mathbf{x} - \int_\Omega (\nabla \times \mathbf{f}) \cdot \boldsymbol{\phi} \, \mathrm{d}\mathbf{x} = \int_\Gamma ((\mathbf{f}_+ - \mathbf{f}_-) \times \mathbf{n}) \cdot \boldsymbol{\phi} \, \mathrm{d}\mathbf{x} \tag{2.15}$$

According to Green's first identity (2.14), LHS of Eq. (2.15) vanishes and for all $\boldsymbol{\phi} \in \boldsymbol{\mathcal{D}}(\Omega)$

$$\int_\Gamma ((\mathbf{f}_+ - \mathbf{f}_-) \times \mathbf{n}) \cdot \boldsymbol{\phi} \, \mathrm{d}\mathbf{x} = 0 \Rightarrow (\mathbf{f}_+ - \mathbf{f}_-) \times \mathbf{n} = 0 \,, \text{ a.e. on } \Gamma \tag{2.16}$$

⇐-part: Let $\mathbf{f} \in \boldsymbol{\mathcal{L}}^2(\Omega)$ and $\nabla \times \mathbf{f}_\pm \in \boldsymbol{\mathcal{L}}^2(\Omega_\pm)$ (note that this still not imply that f is in $\boldsymbol{\mathcal{H}}(\mathrm{curl}, \Omega)$, which has to be shown here). Then for $\boldsymbol{\phi} \in \boldsymbol{\mathcal{D}}(\Omega)$, $\nabla \times \mathbf{f}$ may be defined as distribution acting on $\boldsymbol{\phi}$

$$(\nabla \times \mathbf{f})[\boldsymbol{\phi}] = \int_\Omega \mathbf{f} \cdot (\nabla \times \boldsymbol{\phi}) \, \mathrm{d}\mathbf{x} \,. \tag{2.17}$$

Separating the integration domain into $\Omega_\pm$ gives

$$\int_\Omega \mathbf{f} \cdot (\nabla \times \boldsymbol{\phi}) \, \mathrm{d}\mathbf{x} = \int_{\Omega_+} \mathbf{f}_+ \cdot (\nabla \times \boldsymbol{\phi}) \, \mathrm{d}\mathbf{x} + \int_{\Omega_-} \mathbf{f}_- \cdot (\nabla \times \boldsymbol{\phi}) \, \mathrm{d}\mathbf{x} \,. \tag{2.18}$$

With $\nabla \times \mathbf{f}_\pm \in \boldsymbol{\mathcal{L}}^2(\Omega_\pm)$ we may integrate by parts the equation above and obtain

$$\int_\Omega \mathbf{f} \cdot (\nabla \times \boldsymbol{\phi}) \, \mathrm{d}\mathbf{x} = \int_{\Omega_+} (\nabla \times \mathbf{f}_+) \cdot \boldsymbol{\phi} \, \mathrm{d}\mathbf{x} + \int_\Gamma \mathbf{f}_+ \cdot (\mathbf{n} \times \phi) \, \mathrm{d}\mathbf{x} \tag{2.19}$$

$$+ \int_{\Omega_-} (\nabla \times \mathbf{f}_-) \cdot \boldsymbol{\phi} \, \mathrm{d}\mathbf{x} - \int_\Gamma \mathbf{f}_- \cdot (\mathbf{n} \times \phi) \, \mathrm{d}\mathbf{x} \tag{2.20}$$

$$= \int_{\Omega_+} (\nabla \times \mathbf{f}_+) \cdot \boldsymbol{\phi} \, \mathrm{d}\mathbf{x} + \int_{\Omega_-} (\nabla \times \mathbf{f}_-) \cdot \boldsymbol{\phi} \, \mathrm{d}\mathbf{x} + \int_\Gamma \mathbf{n} \times (\mathbf{f}_+ - \mathbf{f}_-) \cdot \boldsymbol{\phi} \, \mathrm{d}\mathbf{x} \tag{2.21}$$

From the assumption $\mathbf{f}_{+,t}|_\Gamma = \mathbf{f}_{-,t}|_\Gamma$, the last integrand drops and we obtain

$$\int_\Omega \mathbf{f} \cdot (\nabla \times \boldsymbol{\phi})\, \mathrm{d}\mathbf{x} = \int_{\Omega_+} (\nabla \times \mathbf{f}_+) \cdot \boldsymbol{\phi}\, \mathrm{d}\mathbf{x} + \int_{\Omega_-} (\nabla \times \mathbf{f}_-) \cdot \boldsymbol{\phi}\, \mathrm{d}\mathbf{x} = \int_\Omega \mathbf{v} \cdot \boldsymbol{\phi}\, \mathrm{d}\mathbf{x}\,, \quad (2.22)$$

where $\mathbf{v} \in \boldsymbol{\mathcal{L}}^2(\Omega)$ with $\mathbf{v} := \nabla \times \mathbf{f}_\pm$ on $\Omega_\pm$. This theorem has crucial implications in optics and the FEM of Maxwell's equations is based on Eqs. (2.12, 2.13). When we consider an interface Γ between two distinct media occupying the half-spaces $\mathbb{R}^3_\pm$, then we can deduce the classical interface conditions for the electromagnetic fields. Since the fields $\mathbf{D}$ and $\mathbf{B}$ are elements of $\boldsymbol{\mathcal{H}}(\mathrm{div}, \mathbb{R}^3)$ it follows that the normal components of $\mathbf{D}$ and of $\mathbf{B}$ are continuous at the interface Γ. Similarly, since fields $\mathbf{E}$ and $\mathbf{H}$ are elements of $\boldsymbol{\mathcal{H}}(\mathrm{curl}, \mathbb{R}^3)$, we obtain the continuity of the tangential components of $\mathbf{E}$ and of $\mathbf{H}$ at the interface Γ between the two media. These interface conditions are considered as fundamental. However, it should be mentioned that it is possible to break the continuity of the quantities above by introducing some external charges (currents) or surface charges (surface currents) at the interface. The proof of this theorem requires a basic understanding of the weak formulation as well as the introduction of trace operators, the key tools for deriving the additional interface conditions in this work.

2.2.2 Essence of weak formulation

Weak solutions

Solving the strong form, i.e., finding u that satisfies

$$Au = f\,, \quad (2.23)$$

is not always the most efficient way, since the latter equation requires strong regularity, i.e., smoothness of the data in A and of u and of its partial derivatives to a certain order. However, if the source field f has discontinuities or if the operator A has piecewise continuous coefficients, the required smoothness of u is not guaranteed, but is still necessary to calculate its partial derivatives (up to a certain order). This especially holds for composed domains or in the presence of different material interfaces. In addition, the inclusion of boundary (or interface) conditions is always a difficult task, since strong forms must be solved with a function with strong regularity. The requirement for the continuity of field variables is much stronger. This scenario appears very frequently in optics and arises whenever two distinct media with different material parameters meet at an interface. This is a central aspect in this thesis . Our main tool to circumvent this issue is by formulating the problem such that there exist solutions that do not need to satisfy the regularities required in Eq. (2.23), but still solve the strong form in a weaker sense. This formulation is called the weak formulation and the solutions are called weak solutions. The term weak comes because the strong requirements imposed for the solutions u become *relaxed*, or simply *weakened*. The weak form is obtained by going through these steps:

1. first, multiplying the strong form with a suitable test function ϕ with enough regularity and integrate over Ω. For safety reasons, it is usually recommended to take $\phi \in \mathcal{D}(\Omega)$, then partial integrations can be done arbitrarily often and all the terms evaluated at the boundary vanish since we require that it holds $\phi|_{\partial\Omega} = 0$. Hence, Au can be considered as a distribution and can be treated in that sense.

2. Next, by integration by parts, one shifts the derivatives on u to the test function ϕ. In a distributional sense, the derivatives on u are interpreted in the sense of Eq. (2.5).

In the following, we wish to clarify this abstract formalism on an example of physical interest. Assume we have a charge distribution with an electric charge density $\rho_e(\mathbf{r})$ that generates a scalar electric potential $\Phi(\mathbf{r})$. The strong form of the Poisson equation with Dirichlet boundary condition is then

$$\begin{cases} \Delta\Phi(\mathbf{r}) = -\rho_e(\mathbf{r})\,, \text{ in } \Omega \subset \mathbb{R}^3\,, \\ \Phi(\mathbf{r})|_{\partial\Omega} = 0\,, \end{cases} \tag{2.24}$$

with $\Phi \in \mathcal{C}^2(\Omega)$. In the weak formulation, we multiply the strong form of the Poisson-equation, i.e., Eq. (2.24), by a test function $\phi \in \mathcal{D}(\Omega)$ and integrate over Ω which gives

$$\int_\Omega (\Delta\Phi)\,\phi \;\mathrm{d}\mathbf{r} = -\int_\Omega \rho_e\phi \;\mathrm{d}\mathbf{r}. \tag{2.25}$$

Since Φ has to satisfy Eq. (2.24) it also has to satisfy Eq. (2.25). Integrating the LHS by parts using Green's first identity, yields

$$\int_\Omega (\Delta\Phi)\,\phi \;\mathrm{d}\mathbf{r} = -\int_\Omega (\nabla\Phi)\cdot(\nabla\phi)\;\mathrm{d}\mathbf{r} + \int_{\partial\Omega} (\nabla\Phi\cdot\mathbf{n})\,\phi \mathrm{d}\mathbf{s}\,, \tag{2.26}$$

where $\mathrm{d}\mathbf{s}$ refers to the surface element on the boundary $\partial\Omega$. With ϕ being compactly supported in Ω, we have $\phi|_{\partial\Omega} = 0$, thus the second term on the RHS vanishes and the weak formulation of the Poisson equation simplifies to

$$\int_\Omega (\nabla\Phi)\cdot(\nabla\phi)\;\mathrm{d}\mathbf{r} = \int_\Omega \rho_e\phi \;\mathrm{d}\mathbf{r}\,, \tag{2.27}$$

where now Φ is only required to be an element of $\mathcal{C}^1(\Omega)$ but still solves Eq. (2.24).

Since the total charge $Q = \int_{\mathbb{R}^3} \rho_e(\mathbf{r})\;\mathrm{d}\mathbf{r} < \infty$ exists, $\rho_e(\mathbf{r}) \in \mathcal{L}^2(\Omega)$, with $\Omega \subset \mathbb{R}^3$. We will use the $\mathcal{L}^2$-space instead of the $\mathcal{L}^1$-space for convenience, because it is self-dual and thus, the weak formulation becomes the scalar product. The solution space is then the space of functions and their partial derivatives being in $\mathcal{L}^2(\Omega)$ that vanish at the boundary $\partial\Omega$, hence the weak solutions are now elements of $\mathcal{H}_0^1(\Omega)$. With the usage of the Lax-Milgram thoerem [67], one can prove that there exists a unique weak solution $\Phi \in \mathcal{H}_0^1(\Omega)$ to Eq. (2.27), i.e., the strong from (2.24) has exactly one weak solution. It is sufficient to show that the bilinear functional $a(\Phi,\phi) := \int_\Omega (\nabla\Phi)\cdot(\nabla\phi)\;\mathrm{d}\mathbf{r}$ is continuous and coercive. The finite element method is based on the weak formulation and numerically determines the approximate weak solutions to the original problem. The uniqueness here is a huge advantage in numerical applications, as it is desirable to have a deterministic numerical approach to solve a specific problem. The Lax-Milgram thoerem is, however, not a universal tool. For a whole class of differential operators, e.g., for hyperbolic operators, the bilinear functional lacks of coercivity and the uniqueness of the weak formulation is not guaranteed by the Lax-Milgram thoerem. Under certain conditions, the Fredholm alternative [72] can be used to show the existence and the uniqueness of weak solutions. This matter is based on the very advanced Fredholm theory and is beyond the scope of this thesis. However, this theory finds application when considering the system of Maxwell equations that can be rewritten to the wave-equation, a hyperbolic second-order PDE. Under the assumption of time-harmonic waves (in fact we assume this throughout the thesis), Fredholm's alternative serves as the tool to give an answer to the question of existence of a unique weak solution to Maxwell's equations [73]–[75].

Traces in $\mathcal{H}(\mathrm{div},\Omega)$, and $\mathcal{H}(\mathrm{curl},\Omega)$ in a distributional sense

In contrast to the easy example above, in our applications, the differential operator A has piecewise continuous coefficients, later they will be identified as the effective material parameters arising in the wave equation. Then, one has to decompose Ω into domains with Lipschitz boundary, in which the respective restriction of A has continuous coefficients, i.e., adapted to the decomposition $\Omega = \Omega_+ \cup \Omega_- \cup \Gamma$ with the interface $\Gamma = \overline{\Omega_+} \cap \overline{\Omega_-}$. In this case, the weak solutions u will also be defined piecewisely in the corresponding subdomains. However, weak solutions are, in general, not always continuous and their restriction on the interface Γ, that has a Lebesgue measure zero, cannot be defined in a classical sense. Besides, boundary conditions appear after integration by parts in the weak formulation and they have to be somehow evaluated. To this end, the concept of traces gains special importance and the weak solutions $u \in \mathcal{L}^2(\Omega)$ are defined as $u = u_+$ for $\mathbf{x} \in \Omega_+$ and $u = u_-$ for $\mathbf{x} \in \Omega_-$, with $u_\pm \in \mathcal{H}^k(\Omega_\pm)$. Recall that the derivatives of functions residing in Sobolev spaces are solely weak derivatives and are defined in a distributional sense as in Eq. (2.5). The restrictions of u and its partial derivatives at the interface Γ, are called traces. They strongly depend on the differential operators that act on u. One way to study the traces is the weak formulation, since by partial integrations, boundary terms arise (cf. Eqs. (2.30, 2.31)). In Maxwell's theory, we usually deal with div and curl operators and functions residing in $\mathcal{H}(\mathrm{div},\Omega)$ or in $\mathcal{H}(\mathrm{curl},\Omega)$. We will, therefore, specifically study the traces of such functions. To evaluate these traces, we use Green's identities for all $\phi \in \mathcal{C}^1(\Omega)$ and $\boldsymbol{\phi} \in \boldsymbol{\mathcal{C}}^1(\Omega)$:

$$\int_{\partial\Omega} (\mathbf{n}\cdot\mathbf{u})\phi \,\mathrm{d}\mathbf{s} := \int_\Omega (\nabla\cdot\mathbf{u})\phi \,\mathrm{d}\mathbf{x} + \int_\Omega \mathbf{u}\cdot(\nabla\phi)\,\mathrm{d}\mathbf{x}\,,\ \text{for } \mathbf{u}\in\boldsymbol{\mathcal{H}}(\mathrm{div},\Omega)\,, \tag{2.28}$$

$$\int_{\partial\Omega} (\mathbf{n}\times\mathbf{u})\cdot\boldsymbol{\phi} \,\mathrm{d}\mathbf{s} := \int_\Omega (\nabla\times\mathbf{u})\cdot\boldsymbol{\phi}_t \,\mathrm{d}\mathbf{x} - \int_\Omega \mathbf{u}\cdot(\nabla\times\boldsymbol{\phi})\,\mathrm{d}\mathbf{x}\,,\ \text{for } \mathbf{u}\in\boldsymbol{\mathcal{H}}(\mathrm{curl},\Omega)\,. \tag{2.29}$$

Using the notation introduced in Eq. (2.3), the traces (2.28, 2.29) read as

$$\langle \mathbf{n}\cdot\mathbf{u},\phi\rangle_{\partial\Omega} = \langle\nabla\cdot\mathbf{u},\phi\rangle_\Omega + \langle\,\mathbf{u},\nabla\phi\rangle_\Omega\,,\ \text{for } \mathbf{u}\in\boldsymbol{\mathcal{H}}(\mathrm{div},\Omega)\,, \tag{2.30}$$

$$\langle \mathbf{n}\times\mathbf{u},\boldsymbol{\phi}_t\rangle_{\partial\Omega} = \langle\nabla\times\mathbf{u},\boldsymbol{\phi}\rangle_\Omega - \langle\mathbf{u},\nabla\times\boldsymbol{\phi}\rangle_\Omega\,,\ \text{for } \mathbf{u}\in\boldsymbol{\mathcal{H}}(\mathrm{curl},\Omega)\,, \tag{2.31}$$

where $\Omega \subset \mathbb{R}^3$ is a bounded Lipschitz domain with an oriented boundary $\partial\Omega$ and an outward pointing unit vector $\mathbf{n}$. Equations (2.30, 2.31) shall serve as the basis of the weak formulation involving div and curl operators, that are the main operators in Maxwell's theory of light.

This is an informal way for defining the traces of functions in $\boldsymbol{\mathcal{H}}(\mathrm{div},\Omega)$ and $\boldsymbol{\mathcal{H}}(\mathrm{curl},\Omega)$. The formal construction of trace operators requires a deeper understanding of Sobolev theory, as their introduction involves Sobolev spaces $\mathcal{H}^s(\Omega)$ with rational and/or negative order s. Their analysis is much more complicated than the Sobolev spaces with positive integers k and are not of much intellectual interest in this thesis. Nonetheless, the notion of traces is in general important in studying PDEs, but in this study we will not focus on that. They also do not affect the main results in this work and will, therefore, not be discussed here.

Let us study the traces arising with the divergence operator in the situation where the domain Ω is separated into Ω_+ and Ω_-. With $\mathbf{u} \in \boldsymbol{\mathcal{L}}^2(\Omega)$ decomposed into $\mathbf{u}_\pm \in \boldsymbol{\mathcal{H}}(\mathrm{div},\Omega_\pm)$

and for all $\phi \in \mathcal{D}(\Omega)$, it holds

$$\begin{aligned}\langle \nabla \cdot \mathbf{u}, \phi \rangle_\Omega &= \langle \nabla \cdot \mathbf{u}_+, \phi \rangle_{\Omega_+} + \langle \nabla \cdot \mathbf{u}_-, \phi \rangle_{\Omega_-} \\ &\overset{Eq.\ (2.30)}{=} \langle \mathbf{n} \cdot \mathbf{u}_+, \phi \rangle_{\partial\Omega_+} - \langle \mathbf{u}_+, \nabla\phi \rangle_{\Omega_+} - \langle \mathbf{n} \cdot \mathbf{u}_-, \phi \rangle_{\partial\Omega_-} - \langle \mathbf{u}_-, \nabla\phi \rangle_{\Omega_-} .\end{aligned}$$

Note the minus sign in front of the third term on the RHS, which occurs from the fact that the normal vector $\mathbf{n}$ is pointing inside the domain Ω_-. Since $\phi \in \mathcal{D}(\Omega)$, we have $\phi = 0$ in $\partial\Omega_+ \backslash \Gamma$ and in $\partial\Omega_- \backslash \Gamma$. Hence, the restrictions on the boundary reduce to the restrictions on the interface Γ. Together with $\mathbf{u} \in \boldsymbol{\mathcal{L}}^2(\Omega)$:

$$\begin{aligned}\langle \nabla \cdot \mathbf{u}, \phi \rangle_\Omega &= \langle \mathbf{n} \cdot \mathbf{u}_+, \phi \rangle_\Gamma - \langle \mathbf{u}_+, \nabla\phi \rangle_{\Omega_+} - \langle \mathbf{n} \cdot \mathbf{u}_-, \phi \rangle_\Gamma - \langle \mathbf{u}_-, \nabla\phi \rangle_{\Omega_-} \\ &= \langle \mathbf{n} \cdot (\mathbf{u}_+ - \mathbf{u}_-), \phi \rangle_\Gamma - \langle \mathbf{u}, \nabla\phi \rangle_\Omega\end{aligned}$$

Finally, we have for $\mathbf{u}_\pm \in \boldsymbol{\mathcal{H}}(\mathrm{div}, \Omega_\pm)$, $\mathbf{u} \in \boldsymbol{\mathcal{L}}^2(\Omega)$ and for all $\phi \in \mathcal{D}(\Omega)$:

$$\langle \mathbf{n} \cdot (\mathbf{u}_+ - \mathbf{u}_-), \phi \rangle_\Gamma = \langle \nabla \cdot \mathbf{u}, \phi \rangle_\Omega + \langle \mathbf{u}, \nabla\phi \rangle_\Omega . \tag{2.32}$$

Equation (2.32) is of utmost importance and deserves some physical interpretation. It represents the continuity condition of the normal component of the field $\mathbf{u}$ at the interface Γ. It can be, therefore, interpreted as an interface condition for fields being in $\boldsymbol{\mathcal{L}}^2(\Omega) \cup \boldsymbol{\mathcal{H}}(\mathrm{div}, \Omega_+ \cup \Omega_-)$. If $\mathbf{u}$ is additionally in $\boldsymbol{\mathcal{H}}(\mathrm{div}, \Omega)$, then for all $\phi \in \mathcal{D}(\Omega)$, the trace in Eq. (2.30) vanishes as $\phi = 0$ at the boundary $\partial\Omega$ (due to the compact support of ϕ in Ω) and $\langle \nabla \cdot \mathbf{u}, \phi \rangle_\Omega = -\langle\ \mathbf{u}, \nabla\phi \rangle_\Omega$. Thus RHS of Eq. (2.32) vanishes and finally we obtain $(\mathbf{u}_+ - \mathbf{u}_-) \cdot \mathbf{n} = 0$ at the interface Γ, i.e., the continuity of the normal component of $\mathbf{u}$.

Now, for the case of the curl operator, we impose that $\mathbf{u} \in \boldsymbol{\mathcal{L}}^2(\Omega)$ with $\mathbf{u}_\pm \in \boldsymbol{\mathcal{H}}(\mathrm{curl}, \Omega_\pm)$. After following the same steps as for the divergence operator, for all $\boldsymbol{\phi} \in \boldsymbol{\mathcal{D}}(\Omega)$ it holds

$$\langle \mathbf{n} \times (\mathbf{u}_+ - \mathbf{u}_-), \boldsymbol{\phi}_t \rangle_\Gamma = \langle \nabla \times \mathbf{u}, \boldsymbol{\phi} \rangle_\Omega - \langle \mathbf{u}, \nabla \times \boldsymbol{\phi} \rangle_\Omega . \tag{2.33}$$

Following the same arguments as above, we find that Eq. (2.33) refers to a continuity condition for the components of the field $\mathbf{u}$ that are tangential to the interface Γ, where $\mathbf{u}$ is in $\boldsymbol{\mathcal{L}}^2(\Omega) \cup \boldsymbol{\mathcal{H}}(\mathrm{curl}, \Omega_+ \cup \Omega_-)$. If we additionally impose $\mathbf{u} \in \boldsymbol{\mathcal{H}}(\mathrm{curl}, \Omega)$ with $\boldsymbol{\phi} \in \boldsymbol{\mathcal{D}}(\Omega)$, the RHS of Eq. (2.33) becomes zero, and consequently, $(\mathbf{u}_+ - \mathbf{u}_-) \times \mathbf{n} = 0$, i.e., the continuity of the tangential component of $\mathbf{u}$ follows.

This is how we derive interface conditions for the electromagnetic fields. First formulating the weak formulation, second by separating the domains into two subdomains, domain Ω_+ occupied by material 1 and domain Ω_- occupied by material 2, that meet at an interface Γ. Third evaluating the traces that arise after partial integration.

The traces act differently on normal and tangential components depending on the Sobolev spaces in which the functions exist, since the curl and div operators act on different components of a vector field. Details on concrete models may be found in Ch. 4.

2.3 Generalized Fourier transforms

2.3.1 Fourier transform of functions and the desire for an extended definition

Our reference for these and other facts about Fourier transforms are the books of Bremermann [65] and of Stein [76].

The Fourier transform is one of the most used tools in optics in particular, and in physics in general, essentially due to the very useful convolution theorem and to the transformation of derivatives into algebraic products with polynomials. However, it is often misused and important details about existence and applicability are very often neglected. For instance, the well-known formula, i.e., the integral representation, of the Fourier transform and its inverse are used for all functions. However, this only holds for integrable functions. For $f \in \mathcal{L}^1(\mathbb{R}^n)$, the Fourier transform $\tilde{f}$ is defined as

$$\mathcal{F}[f](\boldsymbol{\xi}) = \tilde{f}(\boldsymbol{\xi}) := \int_{\mathbb{R}^n} f(\mathbf{x}) \mathrm{e}^{-\mathrm{i}\boldsymbol{\xi}\cdot\mathbf{x}} \mathrm{d}\mathbf{x}\,. \tag{2.34}$$

While it holds that $|\tilde{f}(\boldsymbol{\xi})| \leq \|f(\mathbf{x})\|_{\mathcal{L}^1}$, it is not guaranteed that $\tilde{f}$ is integrable as well[3]. However, for $\tilde{f} \in \mathcal{L}^1(\mathbb{R}^n)$ we define its inverse Fourier transform as

$$\mathcal{F}^{-1}[\tilde{f}](\boldsymbol{x}) = f(\mathbf{x}) := \frac{1}{(2\pi)^n} \int_{\mathbb{R}^n} \tilde{f}(\boldsymbol{\xi}) \mathrm{e}^{\mathrm{i}\boldsymbol{\xi}\cdot\mathbf{x}} \mathrm{d}\boldsymbol{\xi}\,, \tag{2.35}$$

where the factor $(2\pi)^{-n}$ ensures normalization.

Despite of that, most physically measurable quantities must be elements of $\mathcal{L}^2$ and we wish to know their Fourier transforms to solve Maxwell's equations algebraically. Note that Eq. (2.34), a priori, does only hold for functions in $\mathcal{L}^1(\mathbb{R}^n)$ and that $\mathcal{L}^2(\mathbb{R}^n) \not\subset \mathcal{L}^1(\mathbb{R}^n)$. We will not go into the details of constructing the Fourier transform of $\mathcal{L}^2$-functions, but only sketch the idea how it is developed in the following theorem (Plancharel) that states:

Theorem 2.3.1. *Let $f \in \mathcal{L}^2(\mathbb{R}^n)$. Then*

$$g(\boldsymbol{\xi}) = \lim_{R\to\infty} \int_{|\mathbf{x}|\leq R} f(\mathbf{x}) \mathrm{e}^{-\mathrm{i}\boldsymbol{\xi}\cdot\mathbf{r}} \mathrm{d}\mathbf{x} \tag{2.36}$$

exists and belongs to $\mathcal{L}^2(\mathbb{R}^n)$ and

$$\lim_{R\to\infty} \int_{|\boldsymbol{\xi}|\leq R} g(\boldsymbol{\xi}) \mathrm{e}^{\mathrm{i}\boldsymbol{\xi}\cdot\mathbf{r}} \mathrm{d}\boldsymbol{\xi} = f(\mathbf{x})\,. \tag{2.37}$$

For the proof we refer to Appendix 3.8 and 3.9 of Ref. [65]. Consequently, we write for $\mathcal{L}^2(\mathbb{R}^d)$-functions $\mathcal{F}[f](\boldsymbol{\xi}) = \tilde{f}(\boldsymbol{\xi})$ and $\mathcal{F}^{-1}[\tilde{f}](\boldsymbol{x}) = f(\mathbf{x})$. Hence $\mathcal{F} : \mathcal{L}^2(\mathbb{R}^n) \to \mathcal{L}^2(\mathbb{R}^n)$. An important relation between a function and its (inverse) Fourier transform that we require for defining the Fourier transform for regular distributions is Parseval's formula that reads

Theorem 2.3.2. *Let f_1, f_2 be both in $\mathcal{L}^1(\mathbb{R}^n)$ or both in $\mathcal{L}^2(\mathbb{R}^n)$. Then*

$$\int_{\mathbb{R}^n} \mathcal{F}[f_1](\mathbf{x}) f_2(\mathbf{x}) \mathrm{d}\mathbf{x} = \int_{\mathbb{R}^n} f_1(\mathbf{x}) \mathcal{F}[f_2](\mathbf{x}) \mathrm{d}\mathbf{x}\,, \tag{2.38}$$

and

$$\int_{\mathbb{R}^n} \mathcal{F}^{-1}[f_1](\mathbf{x}) f_2(\mathbf{x}) \mathrm{d}\mathbf{x} = \int_{\mathbb{R}^n} f_1(\mathbf{x}) \mathcal{F}^{-1}[f_2](\mathbf{x}) \mathrm{d}\mathbf{x}\,. \tag{2.39}$$

While for $\mathcal{L}^1$ the identities follow directly from Fubini's theorem, the treatment for $\mathcal{L}^2$ is done by using Eqs. (2.36, 2.37), respectively, and by the fact that the product of two $\mathcal{L}^2$-functions is an $\mathcal{L}^1$-function. As a matter of fact, for future purposes we only need the Parseval's formula for $\mathcal{L}^1$-functions. The case for $\mathcal{L}^2$-functions is only presented for completeness.

[3]Example: $f(x) = \frac{1}{2a}$ for $|x| \leq a$, zero for $|x| > a$, is in $\mathcal{L}^1(\mathbb{R})$, but $\tilde{f}(\xi) = \mathrm{sinc}(a\xi) \notin \mathcal{L}^1(\mathbb{R})$.

2.3.2 Fourier transform of test functions and of distributions

Plane waves, polynomials, and Dirac's δ-distribution are neither $\mathcal{L}^1$-, nor $\mathcal{L}^2$-functions. Then, the definition of $\mathcal{F}$ above cannot be blindly used to calculate Fourier transform of such functions. However, we wish to define their Fourier transforms and, therefore, need to discuss the extension of the notion of Fourier transforms to distributions.

While the space $\mathcal{D}$ is very convenient to use in the weak formulation, mainly due to the compact support, the usage of $\mathcal{D}$ and its dual space $\mathcal{D}'$ is not handy in Fourier transforms. Essentially, because $\mathcal{F}(\mathcal{D}) \nrightarrow \mathcal{D}$. In the following we shall clarify this statement on test functions in $\mathcal{D}$. An explanation for $\mathcal{F}(\mathcal{D}') \neq \mathcal{D}'$ may be found in Sec. 8.29 of Ref. [65].

Let f be a locally integrable function and F_f its associated (regular) distribution (bear in mind that $\mathcal{L}^1_{\text{loc}}(\mathbb{R}^n) \supset \mathcal{D}(\mathbb{R}^n)$). The question is, what is the distribution associated to $\tilde{f}$? Let's consider a test function $\phi \in \mathcal{D}(\mathbb{R}^n) \subset \mathcal{L}^1_{\text{loc}}(\mathbb{R}^n)$. Then, by Parseval's identity (2.38) we have

$$\begin{aligned}
\langle F_{\tilde{f}}, \phi \rangle &= \int_{\mathbb{R}^n} \tilde{f}(\mathbf{y})\phi(\mathbf{y})\mathrm{d}\mathbf{y} = \int_{\mathbb{R}^n} \left(\int_{\mathbb{R}^n} f(\mathbf{x}) \mathrm{e}^{-\mathrm{i}\mathbf{y}\cdot\mathbf{x}} \mathrm{d}\mathbf{x} \right) \phi(\mathbf{y})\mathrm{d}\mathbf{y} \\
&\overset{\text{Fubini}}{=} \int_{\Omega} f(\mathbf{x}) \left(\int_{\mathbb{R}^n} \mathrm{e}^{-\mathrm{i}\mathbf{y}\cdot\mathbf{x}} \phi(\mathbf{y})\mathrm{d}\mathbf{y} \right) \mathrm{d}\mathbf{x} = \int_{\mathbb{R}^n} f(\mathbf{x})\tilde{\phi}(\mathbf{x})\mathrm{d}\mathbf{x} \\
&= \langle F_f, \tilde{\phi} \rangle \,. \qquad (2.40)
\end{aligned}$$

However, $\phi \in \mathcal{D}(\mathbb{R}^n)$ does not imply that $\tilde{\phi} \in \mathcal{D}(\mathbb{R}^n)$ as well. Now the problem that arises for $\phi \in \mathcal{D}(\mathbb{R}^n)$, is that it cannot be guaranteed that $\tilde{\phi}$ is compactly supported, except if $\phi \equiv 0$. Hence, $\mathcal{F}(\mathcal{D}) \not\subset \mathcal{D}$, but is rather a mapping into a function space that is larger than $\mathcal{D}$, and similarly we may show that $\mathcal{F}(\mathcal{D}')$ maps into a space different from $\mathcal{D}'$.

To overcome this issue, it is best to consider the Fourier transform of functions and of distributions in $\mathcal{S}$ and $\mathcal{S}'$, respectively. There, the statements are much simpler as the corresponding (inverse) Fourier transforms are isometric automorphisms [65]:

Theorem 2.3.3. *Let $\phi \in \mathcal{S}$ and $\tilde{\phi} := \mathcal{F}[\phi]$. Then $\tilde{\phi} \in \mathcal{S}$.*
The inverse Fourier transform $\mathcal{F}^{-1}[\tilde{\phi}](\mathbf{x}) = \mathcal{F}[\tilde{\phi}](-\mathbf{x})$ and $\mathcal{F}^{-1}[\mathcal{F}[\phi]] = \phi$.
Further [77], (by using Plancharel's identity) it holds $\|\phi\|_{\mathcal{L}^2} = \|\tilde{\phi}\|_{\mathcal{L}^2}$, i.e., the Fourier transform is an isometric automorphism on $\mathcal{S}(\mathbb{R}^n)$.

By duality, one may define the (inverse) Fourier transform of $\mathcal{S}'$, i.e., of tempered distributions.

Definition 2.3.1. *Let $T \in \mathcal{S}'$. We define the Fourier transform $\mathcal{F}[T]$ of T using Parseval's identity* (2.38) *as*

$$\langle \mathcal{F}[T], \phi \rangle := \langle T, \mathcal{F}[\phi] \rangle \,, \qquad (2.41)$$

and $\mathcal{F}[T] \in \mathcal{S}'$.

Using the definitions of Fourier transform for distributions in $\mathcal{S}'$, we show that the Fourier transform of the delta distribution $\mathcal{F}[\delta] \equiv 1$. In fact $\forall \phi \in \mathcal{S}$:

$$\begin{aligned}
\langle \mathcal{F}[\delta], \phi \rangle &\overset{\text{Def. (2.41)}}{=} \langle \delta, \mathcal{F}[\phi] \rangle = \tilde{\phi}(0) = \int_{\mathbb{R}^n} \phi(x)\mathrm{d}\mathbf{x} \\
&= \langle 1, \phi \rangle \,. \qquad (2.42)
\end{aligned}$$

Theorem 2.3.4. *Let $T \in \mathcal{S}'$. Then $\mathcal{F}^{-1}[T] \in \mathcal{S}'$.*
Further, it holds $\langle \mathcal{F}\left[\mathcal{F}^{-1}[T]\right], \phi\rangle = \langle \mathcal{F}^{-1}\left[\mathcal{F}[T]\right], \phi\rangle = \langle T, \phi\rangle$ which makes the Fourier transform also an isometric automorphism on $\mathcal{S}'$.

Remark 2.3.1. *For test functions ϕ in $\mathcal{D}$, the Fourier transform maps into a subspace of $\mathcal{S}$ of real analytic functions in $\mathbb{C}$ (see Ref. [65], Sec. 8.28). For now, let us call this space $\mathcal{Z}$ and its dual space $\mathcal{Z}'$. Further, the Fourier transforms of distributions in $\mathcal{D}'$ are distributions in $\mathcal{Z}'$ (see Ref. [65], Sec. 8.29).*

2.3.3 Important Properties of Fourier transforms

Now that we have defined the Fourier transforms for test functions and for distributions of different classes, we would like to state some properties that are necessary for our studies. Most importantly, we wish to simplify PDEs and reduce them to algebraic equations, where Fourier transforms of derivatives cut down to polynomials. Another important aspect of Fourier transform is the convolution theorem. While it is often hard to compute convolutions analytically, but by using Fourier transforms the convolution becomes a simple product of the Fourier-transformed functions.

Fourier of derivatives and derivatives of Fourier transforms

First we start with the Fourier transform of derivatives. For all functions in $\mathcal{L}^1(\mathbb{R}^n)$ or $\mathcal{L}^2(\mathbb{R}^n)$ $|f(\mathbf{x})| \to 0$ as $|\mathbf{x}| \to \infty$, as well as for all test functions $\phi \in \mathcal{S}$ (that is a dense subset of $\mathcal{L}^1$), $|\phi(\mathbf{x})| \to 0$ as $|\mathbf{x}| \to \infty$. By $|\alpha|$-times integrations by parts, one can show (also for functions f) that

$$\mathcal{F}[D^\alpha \phi](\boldsymbol{\xi}) = \mathrm{i}^{|\alpha|}\boldsymbol{\xi}^\alpha \mathcal{F}[\phi](\boldsymbol{\xi})\,. \tag{2.43}$$

Analogously, one can show that

$$\mathcal{F}[x^\alpha \phi](\boldsymbol{\xi}) = (-\mathrm{i})^{|\alpha|} D^\alpha \mathcal{F}[\phi](\boldsymbol{\xi})\,, \tag{2.44}$$

where the derivatives in Eq. (2.44) are w.r.t. the variable $\boldsymbol{\xi}$. The same relation also holds for the Fourier transforms of distributions. This, however, requires using the derivative of distributions, namely Eq. (2.5), and Theorem 2.3.3. Let $T \in \mathcal{S}'$. To avoid confusion we write the variables explicitly. Thus, we have

$$\begin{aligned}
\langle \mathcal{F}[D^\alpha T](\boldsymbol{\xi}), \phi(\boldsymbol{\xi})\rangle &\overset{\text{Def. (2.41)}}{=} \langle D^\alpha T(\mathbf{x}), \mathcal{F}[\phi](\mathbf{x})\rangle \overset{\text{Eq. (2.5)}}{=} (-1)^{|\alpha|}\langle T(\mathbf{x}), D^\alpha \mathcal{F}[\phi](\mathbf{x})\rangle \\
&\overset{Eq.\ (2.44)}{=} \langle T(\mathbf{x}), \mathrm{i}^{|\alpha|}\mathcal{F}[\boldsymbol{\xi}^\alpha \phi](\mathbf{x})\rangle \overset{\text{Def. (2.41)}}{=} \mathrm{i}^{|\alpha|}\langle \mathcal{F}[T](\boldsymbol{\xi}), \boldsymbol{\xi}^\alpha \phi(\boldsymbol{\xi})\rangle \\
&= \mathrm{i}^{|\alpha|}\langle \xi^\alpha \mathcal{F}[T](\boldsymbol{\xi}), \phi(\boldsymbol{\xi})\rangle\,.
\end{aligned} \tag{2.45}$$

Similarly, one can show that

$$\langle \mathcal{F}[x^\alpha T](\boldsymbol{\xi}), \phi(\boldsymbol{\xi})\rangle = (-\mathrm{i})^{|\alpha|}\langle D^\alpha \mathcal{F}[x^\alpha T](\boldsymbol{\xi}), \phi(\boldsymbol{\xi})\rangle\,. \tag{2.46}$$

With this, we have shown that Fourier transform of derivatives reduce to algebraic products with the variable $\boldsymbol{\xi}$. Thus, differential operators of order $|\alpha|$ become polynomials of $|\alpha|^{\text{th}}$ degree, and can be replaced by their principal symbol

$$D^\alpha \underset{\mathcal{F}^{-1}}{\overset{\mathcal{F}}{\rightleftarrows}} \mathrm{i}^{|\alpha|}\boldsymbol{\xi}^\alpha\,. \tag{2.47}$$

Consequently, we find the Fourier transform of the derivatives of Dirac's δ-distribution, that read

$$\langle \mathcal{F}[\delta^{(n)}], \phi \rangle = \mathrm{i}^n \langle \boldsymbol{\xi}^\alpha \mathcal{F}[\delta], \phi \rangle \,, \text{ with } |\alpha| = n \,. \tag{2.48}$$

Particularly interesting are the Fourier transforms in the $3+1$-dimensional space-time domain. Spatial derivatives are represented by the nabla operator, which becomes

$$\nabla = (\partial_x, \partial_y, \partial_z)^{\mathrm{T}} \underset{\mathcal{F}^{-1}}{\overset{\mathcal{F}}{\rightleftarrows}} \mathrm{i}\mathbf{k} = \mathrm{i}(k_x, k_y, k_z)^{\mathrm{T}} \,, \tag{2.49}$$

where (x, y, z) are defined in the real space and represent the spatial coordinates and (k_x, k_y, k_z) are defined in Fourier (reciprocal or momentum) space, that represent the momentum coordinates. The curl operator amounts to the skew-symmetric matrix

$$\nabla\times \underset{\mathcal{F}^{-1}}{\overset{\mathcal{F}}{\rightleftarrows}} \mathrm{i}\mathbf{k}\times = \mathrm{i} \begin{pmatrix} 0 & k_z & -k_y \\ -k_z & 0 & k_x \\ k_y & -k_x & 0 \end{pmatrix} . \tag{2.50}$$

Concerning the temporal derivative, we use the convention with the minus sign

$$\partial_t \underset{\mathcal{F}^{-1}}{\overset{\mathcal{F}}{\rightleftarrows}} -\mathrm{i}\omega \,, \tag{2.51}$$

where t represents the time and ω the frequency. An example of a differential operator of actual interest that considers space and time dynamics is the wave operator. Let $\mathbf{E}(\mathbf{r}, t) \in \mathcal{C}^2(\mathbb{R}^{3+1})$, with $\tilde{\mathbf{E}}(\mathbf{k}, \omega)$ its Fourier transform, and similarly for the displacement field $\mathbf{D}(\mathbf{r}, t)$. Then the following equations are equivalent

$$\nabla \times \nabla \times \mathbf{E}(\mathbf{r}, t) + \frac{1}{c^2} \partial_t^2 \mathbf{D}(\mathbf{r}, t) = 0 \Leftrightarrow \mathbf{k} \times \mathbf{k} \times \tilde{\mathbf{E}}(\mathbf{k}, \omega) + \left(\frac{\omega}{c}\right)^2 \tilde{\mathbf{D}}(\mathbf{k}, \omega) = 0 \,. \tag{2.52}$$

While the former equation represents three coupled second-order PDEs, the latter equation is simply a system of three coupled algebraic equations, than can be easily solved by calculating the determinant of a 3×3 complex matrix.

Convolution theorem for distributions

The next crucial aspects of Fourier transform is the convolution theorem. For $\mathcal{L}^1(\mathbb{R}^n)$-functions it is possible to state the following theorem

Definition and Theorem 2.3.1. *Let $f, g \in \mathcal{L}^1(\mathbb{R}^n)$. Then*

$$\mathcal{F}[f * g] = \mathcal{F}[f]\mathcal{F}[g] \,, \tag{2.53}$$

where the $*$ product denotes the convolution

$$(f * g)(\mathbf{x}) := \int f(\mathbf{x}') g(\mathbf{x} - \mathbf{x}') \mathrm{d}\mathbf{x}' \,. \tag{2.54}$$

Proof: For f and g being in $\mathcal{L}^1$, the convolution theorem follows directly using Fubini's theorem and by a subsequent change of variables.

For $\mathcal{L}^2$-functions, however, the situation is more subtle as, according to Young's convolution inequality [78], their convolution is in $\mathcal{L}^\infty(\mathbb{R}^n)$. In fact, for $f \in \mathcal{L}^p(\mathbb{R}^n)$ and $g \in \mathcal{L}^q(\mathbb{R}^n)$, it holds that $(f * g) \in \mathcal{L}^r(\mathbb{R}^n)$, with $\frac{1}{p} + \frac{1}{q} = \frac{1}{r} + 1$. Particularly, for $p = q = 2$, it follows $r = \infty$.

In Ch. 3, we will deal with convolutions between a plane wave and Dirac's δ-distribution and its partial derivatives. A plane wave is not integrable, but locally integrable, i.e., an element of $\mathcal{L}^1_{loc}(\subset \mathcal{D}')$. Dirac's δ-distributions and their partial derivatives are distributions with compact support, i.e., elements of $\mathcal{E}'$. The convolution between distributions is defined as

Definition 2.3.2. *Let $T \in \mathcal{D}'$ or in $\mathcal{S}'$ and $V \in \mathcal{E}'$. We define the convolution $T * V$ as*

$$T * V = \mathcal{F}^{-1}(\mathcal{F}[T] \cdot \mathcal{F}[V])\,. \tag{2.55}$$

Here, we did not properly define of the Fourier transform of $\mathcal{E}'$-distributions. Nevertheless, the interested reader may refer to Sec. 9.10 of Ref. [65] for a proper definition. Next, we state the last important theorem of this chapter, that makes statements on the convolution of distributions in $\mathcal{S}'$ or in $\mathcal{D}'$ and $V \in \mathcal{E}'$.

Theorem 2.3.5. *Let $T_S \in \mathcal{S}'$, $T_D \in \mathcal{D}'$ and $V \in \mathcal{E}'$. Then*

(a) $T_S * V \in \mathcal{S}'$.

(b) $T_D * V \in \mathcal{D}'$.

Note that $T_S \in \mathcal{S}'$ implies $T_S \in \mathcal{D}'$.

Proof: The proof requires to know that $\mathcal{F}(V)$ is a multiplier in $\mathcal{S}$ or $\mathcal{Z}$ for (a) and (b), respectively. Together with $\mathcal{F}(\mathcal{S}') = \mathcal{S}'$ or $\mathcal{F}(\mathcal{D}') = \mathcal{Z}'$. This proves the theorem.

This theorem has a central application in our work. In the following chapters, we will model the nonlocal response of an optical metamaterial by the following convolution integral

$$\mathbf{D}(\mathbf{r}, k_0) = \int_{\mathbb{R}^3} \hat{\mathbf{R}}(\mathbf{r} - \mathbf{r}', k_0)\mathbf{E}(\mathbf{r}', k_0)\mathrm{d}\mathbf{r}'\,, \tag{2.56}$$

where for a fixed k_0, $\hat{\mathbf{R}}(\mathbf{x}, k_0)$ is a linear combination of δ-distributions and of its partial derivatives, i.e., distributions of compact support $\boldsymbol{\mathcal{E}}'(\mathbb{R}^3)$ and $\mathbf{E}(\mathbf{x}, k_0)$ being a plane wave, i.e., can be regarded as a distribution in $\boldsymbol{\mathcal{S}}'(\mathbb{R}^3)$. Then, according to Theo. 2.3.5(a), the displacement field $\mathbf{D}(\mathbf{x}, k_0)$ belongs to $\boldsymbol{\mathcal{S}}'$ as well. Alternatively, we could have assumed that $\mathbf{E}(\mathbf{x}, k_0) \in \boldsymbol{\mathcal{D}}'$, which would imply, according to Theo. 2.3.5(b), that $\mathbf{D}(\mathbf{x}, k_0) \in \boldsymbol{\mathcal{D}}'$. However, this can be unhandy as it's Fourier transform is in $\boldsymbol{\mathcal{Z}}'$, while $\mathcal{F}(\boldsymbol{\mathcal{S}}') = \boldsymbol{\mathcal{S}}'$. Considering the space $\boldsymbol{\mathcal{S}}'$ renders the analysis a bit more convenient, without the necessity to introduce any further spaces, as discussed in remark 2.3.1.

2.4 Chapter summary and discussion

In this chapter, we gave a mathematical introduction into selected topics of functional analysis that are relevant for the research we did in the rest of this thesis. We first

recapitulated Schwartz's distribution theory and essentially studied the properties of $\mathcal{D}'$-distributions. We gave a proof that plane waves, that are basically elements of $\mathcal{L}^1_{\text{loc}}(\mathbb{R}^{3+1})$, generate continuous distributions on $\mathcal{D}$. Emphasis was put on the concept of weak formulation. This formalism will be the main tool of this thesis for deriving the additional interface conditions between a metamaterial described by nonlocal constitutive relations and ordinary homogeneous material. Finally, we studied the Fourier transforms of different classes of functions. We have seen the Fourier transform in its integral representation for $\mathcal{L}^1$-functions, its extension to $\mathcal{L}^2$-functions, and its generalized definition for distributions. Because the electromagnetic fields, depending on the application, are either considered as square-integrable functions or as generalized functions, it is important to extend the notion of Fourier transforms beyond that of integrable functions only. Particularly, we wish to consider the fields as distributions in $\boldsymbol{\mathcal{S}}'$, due to the automorphism property of the Fourier transform on $\boldsymbol{\mathcal{S}}'$.

In the next chapter, we will introduce the relevant physical background for deriving an effective medium theory of optical metamaterials with nonlocal response. Very often, we will refer to definitions, theorems, and lemmas stated in this chapter, justifying the validity of some assumptions and the mathematical steps made in the derivation and in the analysis.

3 | Theoretical Background: Spatial dispersion

These (Maxwell's) equations are, however, largely useless until the relations between the quantities **D**, **B**, **E** *and* **H** *which appear in them have been established.*

Lew D. Landau and Jewgeni M. Lifschitz

In this chapter, we give the necessary physical background of electrodynamics in (supposedly) continuous media. The focus here will be on elaborating on the passage from the microscopic theory of multipoles, through mesoscopic physics of structures with permittivity distributions, to macroscopic field equations and material laws, i.e., constitutive relations that link the macroscopic fields **D** and **H** to the physical fields **E** and **B** with spatially independent material parameters. We will pinpoint on the effective description of light propagation in complex media with spatial dispersion. Some basic properties of (effective) material parameters that are usually disregarded in some related works in optics will be discussed as well. Many parts of this section are based on Chapters 1-4 and 7-8 from the book of R. E. Raab and O. L. De Lange [79]. Starting from a general multipole perspective towards constitutive relations requires the introduction of Maxwell's equations in the microscopic regime. In a medium with a microscopic charge distribution $\rho_{\text{micro}}(\mathbf{r},t)$ and a microscopic current density $\mathbf{j}_{\text{micro}}(\mathbf{r},t)$, Maxwell's equations in time and (real-)space domain and in CGS units read as

$$\begin{aligned} \nabla\times\mathbf{e}(\mathbf{r},t) &= -\frac{1}{c}\partial_t\mathbf{b}(\mathbf{r},t)\,, \quad \nabla\cdot\mathbf{e}(\mathbf{r},t) = 4\pi\rho_{\text{micro}}(\mathbf{r},t)\,,\\ \nabla\times\mathbf{b}(\mathbf{r},t) &= \frac{1}{c}\partial_t\mathbf{e}(\mathbf{r},t) + \frac{4\pi}{c}\mathbf{j}_{\text{micro}}(\mathbf{r},t)\,, \qquad \nabla\cdot\mathbf{b}(\mathbf{r},t) = 0\,, \end{aligned} \tag{3.1}$$

where $\mathbf{e}(\mathbf{r},t)$ and $\mathbf{b}(\mathbf{r},t)$ denote the microscopic electric and magnetic fields, respectively. As the number of charge carriers described by the microscopic quantities $\rho_{\text{micro}}(\mathbf{r},t)$ and their motion by $\mathbf{j}_{\text{micro}}(\mathbf{r},t)$ is conserved, these quantities obey the continuity equation $\nabla\cdot\mathbf{j}_{\text{micro}}(\mathbf{r},t) + \partial_t\rho_{\text{micro}}(\mathbf{r},t) = 0$.

In optics, we are interested in investigating phenomena in light-matter interaction scenarios. By the introduction of the microscopic electric displacement density **d** and the microscopic magnetic field **h**, such that

$$\mathbf{d}(\mathbf{r},t) = \mathbf{e}(\mathbf{r},t)\,, \qquad \mathbf{h}(\mathbf{r},t) = \mathbf{b}(\mathbf{r},t)\,, \tag{3.2}$$

the microscopic Maxwell equations can be (only marginally) simplified to

$$\begin{aligned} \nabla\times\mathbf{e}(\mathbf{r},t) &= -\frac{1}{c}\partial_t\mathbf{b}(\mathbf{r},t)\,, \quad \nabla\cdot\mathbf{d}(\mathbf{r},t) = 4\pi\rho_{\text{micro}}(\mathbf{r},t)\,,\\ \nabla\times\mathbf{h}(\mathbf{r},t) &= \frac{1}{c}\left(\partial_t\mathbf{e}(\mathbf{r},t) + 4\pi\mathbf{j}_{\text{micro}}(\mathbf{r},t)\right)\,, \qquad \nabla\cdot\mathbf{b}(\mathbf{r},t) = 0\,. \end{aligned} \tag{3.3}$$

At this level, the introduction of **d** and **h** seem to be futile, but we will see that this new form will be preserved when we average the discrete charge distributions and study the

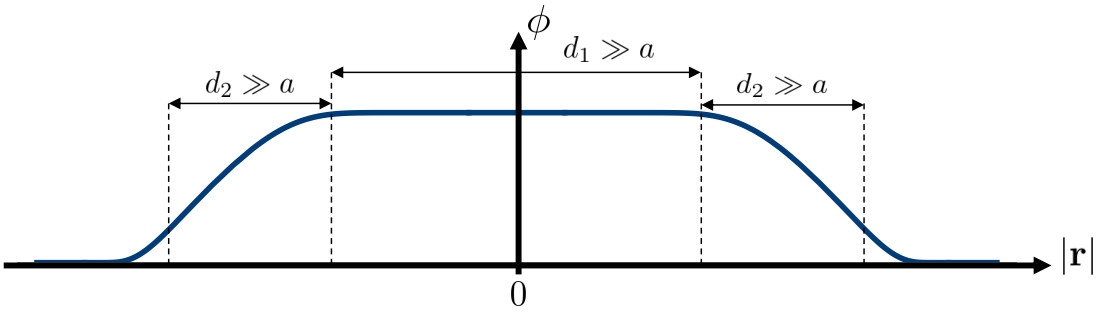

Figure 3.1: Illustration of a test function with compact support for spatial averaging. The function is constant over a region of extent $d_1 \gg a$ and adiabatically goes to zero over a distance $d_2 \gg a$, where a is a length in microscopic length scales. Furthermore, the wavelength λ must be longer than both d_1 and d_2 as well.

electrodynamics of continuous media. Nonetheless, Eqs. (3.1) or Eqs. (3.3) are impractical to apply on a bulk problem. Per cm^3 there exist about 10^{23} charge carriers and each of them contributes individually to $\rho_{\text{micro}}(\mathbf{r},t)$ and $\mathbf{j}_{\text{micro}}(\mathbf{r},t)$, which is usually not feasible to be handled either analytically nor numerically. In the latter case, one must store the field information of approx 10^{23} charges. Moreover, it has to be noted that features that arise on a microscopic scale, such as the vibration of the charges, are not resolved on the much larger scales of optical wavelengths. It is, therefore, legit and even recommended to smear out these effects by averaging over length scales (or a volume v_0) that contain many atoms (molecules) as their individual effects at optical frequencies are too small to be measurable in any way and their treatment, both analytical and numerical, is too cumbersome. As a matter of fact, the averaging volume v_0 should contain a large numbers of particles, but it should still be small relative to the wavelength of interest. Hence, the averaged fields have to be slowly varying, or shall be preferably approximately constant. Therefore, v_0 must be large compared to atomic scales but small compared to macroscopic scales, thus of mesoscopic size, e.g. volume V. Following the averaging method used in Refs. [80] and [81], we define the following averaged quantities.

Definition 3.0.1. *Let* $\phi \in \mathcal{D}(\mathbb{R}^3)$ *with* $\int_{\mathbb{R}^3}\phi(\mathbf{r})\mathrm{d}\mathbf{r} = 1$ *(e.g. see Fig. 3.1) and* $\mathrm{supp}(\phi) \subset v_0$ *and* $\forall \mathbf{r}_0 \in \mathbb{R}^3 : |\phi(\mathbf{r}_0) - \phi(\mathbf{r}_0 + \mathbf{a})|/|\mathbf{a}| > |\phi'(\mathbf{r}_0)|$*, where* $|\mathbf{a}|$ *is of molecular dimension. Let* $\mathbf{f} \in \boldsymbol{\mathcal{L}}^1_{\text{loc}}(\mathbb{R}^3)$*, then the spatial average* $\mathbf{F}(\mathbf{r})$ *of a vector field* $\mathbf{f}$ *over a volume* v_0 *is defined as the convolution*

$$\mathbf{F}(\mathbf{r}) := \langle \mathbf{f}(\mathbf{r}) \rangle_V := (\mathbf{f} * \phi)(\mathbf{r}). \tag{3.4}$$

According to this definition, we obtain the macroscopic quantities

$$\mathbf{E}(\mathbf{r},t) = \langle \mathbf{e}(\mathbf{r},t) \rangle_V \ , \qquad \mathbf{B}(\mathbf{r},t) = \langle \mathbf{b}(\mathbf{r},t) \rangle_V \ ,$$
$$\rho(\mathbf{r},t) = \langle \rho_{\text{micro}} \rangle_V \ , \qquad \mathbf{J}(\mathbf{r},t) = \langle \mathbf{J}_{\text{micro}} \rangle_V \ .$$

After performing such averaging, it is natural that the charge density ρ can contain both free charges ρ_{free}, i.e., charges highly dislocated beyond the microscopic scale, and charges that are bounded ρ_{bound} to the atoms or molecules due to a restoring force, i.e., mobile only on the microscopic scale. Freely moving charges are, for example, the conduction electrons in metals, and bounded charges are the ones confined to the neighborhood of an ionic core, due to the effective restoring force that comes form the nuclei, and will experience only a local perturbation leading to an electric polarization $\boldsymbol{\mathcal{P}}$ or magnetization $\boldsymbol{\mathcal{M}}$ of the medium. The total current density can be also separated into a current $\mathbf{J}_{\text{free}}$ linked to the

motion of the free charges and into a current $\mathbf{J}_{\text{bound}}$ associated to the bounded charges, that either describe displacements inducing an electric field, or to charges that describe closed loops and generate some magnetization, respectively. In fact, the total charge density $\rho(\mathbf{r},t)$ is preserved and, thus, obeys the continuity equation

$$\partial_t \rho(\mathbf{r},t) + \nabla \cdot \mathbf{J}(\mathbf{r},t) = 0\,. \tag{3.5}$$

The same relationships hold for the bound and free charges and currents independently. Along these lines, Maxwell's equation in the macroscopic domain become

$$\begin{aligned} \nabla \times \mathbf{E}(\mathbf{r},t) = -\frac{1}{c}\partial_t \mathbf{B}(\mathbf{r},t)\,, \nabla \cdot \mathbf{E}(\mathbf{r},t) = 4\pi(\rho_{\text{free}}(\mathbf{r},t) + \rho_{\text{bound}}(\mathbf{r},t))\,, \\ \nabla \times \mathbf{B}(\mathbf{r},t) = \frac{1}{c}\partial_t \mathbf{E}(\mathbf{r},t) + \frac{4\pi}{c}\left[\mathbf{J}_{\text{free}}(\mathbf{r},t) + \mathbf{J}_{\text{bound}}(\mathbf{r},t)\right]\,, \nabla \cdot \mathbf{B}(\mathbf{r},t) = 0\,. \end{aligned} \tag{3.6}$$

The above definitions, Eqs. (3.2), of the microscopic auxiliary fields $\mathbf{d}$ and $\mathbf{h}$ do, in general, not hold for the averaged quantities. The functional dependency of the material fields $\mathbf{D}[\mathbf{E},\mathbf{B}]$ and $\mathbf{H}[\mathbf{E},\mathbf{B}]$ as well as their derivation will be the core subject of the thesis, where emphasis is put to provide the link to optical metamaterials.

In the following sections, we will construct the material fields $\mathbf{D}[\mathbf{E},\mathbf{B}]$ and $\mathbf{H}[\mathbf{E},\mathbf{B}]$ based on two approaches. First on the general multipole approach, second on a more abstract phenomenological level. We will discuss the differences and similarities between both approaches especially under the consideration of spatial nonlocality. Temporal nonlocality must be always assumed as the response of the material can never be instantaneous. The response to light will also always depend on the polarization of the material and is determined only by the present field and the field at previous times. This is causality and leads to (temporal) dispersion, i.e., to a frequency dependent response to the electromagnetic fields of light. We will prove that the emerging artificial magnetization in mesoscopic media at optical frequencies is nothing else, but a second-order nonlocal phenomena in the electric field. The proof is based on the fact that the material fields $\mathbf{D}$ and $\mathbf{H}$ are not unique, i.e., there exits a transformation field, that we will call $\mathbf{Q}$, that redefines $\mathbf{D}$ and $\mathbf{H}$ without changing Maxwell's equation or light propagation in an infinitely extended medium.

3.1 Multi pole theory - From microscopic to macroscopic equations

From a multipolar perspective, the homogenization of optical metamaterials amounts to their description with the spatially independent, macroscopic multipole moment densities [82]. In the quasi-static regime, usually only the electric dipole order is considered as the spatial variation of the electric field across a unit cell of volume V, even larger than v_0, is neglected. However, this turned out to lead to some inconsistencies in terms of material's response to light [83]. The reason is that for metamaterials with finite structure size, the assumption of a constant electric field is an oversimplification of the problem. The spatial variation of the field will distort the charge distributions, where higher-order multipoles become relevant. At the end of this section, we will show that also corrections to the induced dipole moment become relevant and have to be introduced when a nonlocal response is manifested.

The passage from microscopic to mesoscopic quantities is reflected by assigning multipole moments to the metamaterial's building blocks (metamolecules). Considering a charge distribution $\rho_{\text{micro}}(\mathbf{r},t)$ in a metamaterial's unit cell, the mesoscopic description in a good approximation is given by the dipole moments of the metamolecules

$$p_i(t) = \int_{v_0} r_i \rho_{\text{micro}}(\mathbf{r},t)\mathrm{d}\mathbf{r}\,, \tag{3.7}$$

where p_i represents the electric dipole moment, a mesoscopic quantity. Thereby, we simplified the original problem consisting of microscopic charges and currents and substituted them by a dipole moment, defined by the averaging over a volume v_0 of mesoscopic size. However, in general, multipole moments of a finite charge distribution depend on the origin of the coordinate system within the charge distribution. For example, a translation of the coordinate system by a vector $\mathbf{r}_0$ changes the electric dipole $p_i' \to p_i - qr_{0,i}$, where q is the electric charge in volume v_0. With the propose of homogenization, the description of a metamaterial with quantities that depend on the coordinate system is inappropriate, considering the translation invariance in a homogeneous space. Further, the unit cell of a periodic metamaterial consists of many building blocks (metamolecules). Each metamolecule is described by a dipole moment $\mathbf{p}$, and a collective description of the whole unit cell by a single quantity is desired. That is why a further averaging over a macroscopic volume V is essential for the homogenization process, where macroscopic moment densities come into play. These quantities do not depend on the origin but only on the local field and on its partial derivatives.

In metamaterials possess a characteristic length that is only slightly smaller than the wavelength of light, spatially non-uniform electromagnetic fields across its unit cell have to be taken into consideration. Hence, the gradients of the electric field, will distort the charge distribution in the bulk material [84], rendering the bound charge density up to the octupole-moment order in volume V taking the following form

$$\rho_{\text{bound}}(\mathbf{r},t) = -\nabla_i P_i(\mathbf{r},t) + \frac{1}{2}\nabla_i\nabla_j Q_{ij}(\mathbf{r},t) - \frac{1}{6}\nabla_k\nabla_j\nabla_i O_{ijk}(\mathbf{r},t) + \cdots \tag{3.8}$$

and the bound current density up to electric-octupole magnetic-quadrupole moments in a volume $\mathrm{d}V$

$$\begin{aligned} J_{\text{bound},i}(\mathbf{r},t) = {} & \epsilon_{ijk}\nabla_j M_k(\mathbf{r},t) + \varepsilon_{ijl}\nabla_k\nabla_j M_{lk}(\mathbf{r},t) + \cdots \\ & + \partial_t\left(P_i(\mathbf{r},t) - \frac{1}{2}\nabla_j Q_{ij}(\mathbf{r},t) + \frac{1}{6}\nabla_k\nabla_j O_{ijk}(\mathbf{r},t) + \cdots\right). \end{aligned} \tag{3.9}$$

Here, the quantities P_i, Q_{ij}, and O_{ijk} represent the electric dipole, quadrupole, octupole moment densities, while M_k, and M_{lk}, refer to the magnetic dipole and quadrupole densities, respectively. These quantities are the macroscopic densities that are obtained by averaging over the volume V, which corresponds to the volume of the unit cell. Consequently, the inhomogeneous Maxwell Eqs. (3.6) in the macroscopic picture read

$$\nabla_i\left(\frac{E_i(\mathbf{r},t)}{4\pi} + P_i(\mathbf{r},t) - \frac{1}{2}\nabla_j Q_{ij}(\mathbf{r},t) + \frac{1}{6}\nabla_k\nabla_j O_{ijk}(\mathbf{r},t) + \cdots\right) = \rho_{\text{free}}(\mathbf{r},t)\,, \tag{3.10}$$

and

$$\varepsilon_{ijk}\nabla_j\left(\frac{B_k(\mathbf{r},t)}{4\pi} - M_k(\mathbf{r},t) + \frac{1}{2}\nabla_l M_{kl}(\mathbf{r},t) + \cdots\right)$$
$$= \frac{1}{c}J_{\text{free},i}(\mathbf{r},t) + \frac{1}{c}\partial_t\left(\frac{E_i(\mathbf{r},t)}{4\pi} + P_i(\mathbf{r},t) - \frac{1}{2}\nabla_j Q_{ij}(\mathbf{r},t) + \frac{1}{6}\nabla_k\nabla_j O_{ijk}(\mathbf{r},t) + \cdots\right). \tag{3.11}$$

In contrast to the microscopic Maxwell Eqs. (3.1), at this occasion it actually makes sense to define the macroscopic response fields $\mathbf{D}$ and $\mathbf{H}$ and to plug them into the inhomogeneous Eqs.(3.10-3.11) such that we obtain

$$\nabla\cdot\mathbf{D}(\mathbf{r},t) = \rho_{\text{free}}(\mathbf{r},t)\,, \qquad \nabla\times\mathbf{H}(\mathbf{r},t) = \frac{1}{c}\left(\mathbf{J}_{\text{free}}(\mathbf{r},t) + \partial_t\mathbf{D}(\mathbf{r},t)\right), \tag{3.12}$$

where up to the electric-octupole magnetic-quadrupole order we have

$$D_i(\mathbf{r},t) = E_i(\mathbf{r},t) + 4\pi\left(P_i - \frac{1}{2}\nabla_j Q_{ij}(\mathbf{r},t) + \frac{1}{6}\nabla_k\nabla_j O_{ijk}(\mathbf{r},t) + \cdots\right), \tag{3.13}$$

$$H_i(\mathbf{r},t) = B_i(\mathbf{r},t) - 4\pi\left(M_i(\mathbf{r},t) + \frac{1}{2}\nabla_j M_{ij}(\mathbf{r},t)\right) + \cdots. \tag{3.14}$$

In general, the definitions of $\mathbf{D}$ and $\mathbf{H}$ are not unique. The version we show in Eqs.(3.13-3.14) clearly separates the electric moments from the magnetic moments, where the electric displacement field $\mathbf{D}$ only contains electric multipole moment densities and the magnetic field $\mathbf{H}$ only the magnetic moment densities. On the other hand, by virtue of the continuity equation (3.5) for the macroscopic charge and current densities, the terms appearing on the LHS of Eq. (3.11) can be rearranged, such that all multipole moment densities, both electric and magnetic, can be associated to the displacement fields $\mathbf{D}$ only. To this end, let's assume the external electromagnetic fields being weak and time-harmonic. According to the Lorentz force, the charges in the bulk matter couple to the fields $\mathbf{E}$ and $\mathbf{B}$ of the wave and will experience some displacement. The weakness of the fields ensures the applicability of the linear response theory, where induced moments only linearly depend on $\mathbf{E}$ and $\mathbf{B}$. Next, for a time harmonic wave, i.e. $\mathbf{E}(\mathbf{r},t) \propto \mathrm{e}^{-\mathrm{i}\omega t}$, derivatives w.r.t. time coordinates that appear in Eq. (3.9) become simple algebraic multiplications by $-\mathrm{i}\omega$ such that, for example on the electric dipole moment, $\partial_t P_i(\mathbf{r},t)$ becomes $-\mathrm{i}\omega P_i(\mathbf{r},\omega)$ in the frequency domain. Physically, this can be made clear by the fact that a temporally oscillating field will cause that the induced charges will oscillate as well, with exactly the same frequency.

Finally, Maxwell's Eq. (3.11) with shuffled multipole moments in frequency domain can be written as

$$\varepsilon_{ijk}\nabla_j\frac{B_k(\mathbf{r},\omega)}{4\pi} = \frac{1}{c}J_{\text{free},i}(\mathbf{r},\omega)$$
$$+\frac{-\mathrm{i}\omega}{c}\left[\frac{E_i(\mathbf{r},\omega)}{4\pi} + P_i(\mathbf{r},\omega) - \frac{1}{2}\nabla_j Q_{ij}(\mathbf{r},\omega) + \frac{1}{6}\nabla_k\nabla_j O_{ijk}(\mathbf{r},\omega) + \cdots\right.$$
$$\left.+\frac{\mathrm{i}c}{\omega}\epsilon_{ijk}\nabla_j\left(M_k(\mathbf{r},\omega) + \frac{1}{2}\nabla_l M_{kl}(\mathbf{r},\omega) + \cdots\right)\right]. \tag{3.15}$$

In connection with the inhomogeneous Maxwell Eqs. (3.12), we readout that the response fields should take the following form:

$$D_i(\mathbf{r},\omega) = E_i(\mathbf{r},\omega) + 4\pi\left(P_i(\mathbf{r},\omega) - \frac{1}{2}\nabla_j Q_{ij}(\mathbf{r},\omega) + \frac{1}{6}\nabla_k\nabla_j O_{ijk}(\mathbf{r},\omega) + \cdots\right) + \frac{\mathrm{i}4\pi c}{\omega}\epsilon_{ijk}\nabla_j\left(M_k(\mathbf{r},\omega) + \frac{1}{2}\nabla_l M_{kl}(\mathbf{r},\omega) + \cdots\right), \tag{3.16}$$

$$H_i(\mathbf{r},\omega) = B_i(\mathbf{r},\omega)\,. \tag{3.17}$$

Here, the macroscopic medium is said to be intrinsically nonmagnetic, as the magnetic response field $\mathbf{H}(\mathbf{r},t)$ is identical to the magnetic induction $\mathbf{B}(\mathbf{r},t)$. Both electric and magnetic multipole moment densities seem to be directly linked to the electric displacement field $\mathbf{D}(\mathbf{r},t)$, which also satisfies Maxwell's Eqs. (3.12), as the magnetic moment densities arising in $\mathbf{D}$ are divergence-free and do not affect $\nabla\cdot\mathbf{D}(\mathbf{r},t) = 4\pi\rho_{\text{free}}(\mathbf{r},t)$. With that said, there is no physical difference between the set of Eqs. (3.13-3.14) and Eqs. (3.16-3.17). The only reason why one could possibly consider shuffling between the multipole contributions is to facilitate the analytical treatment of a certain problem. More details concerning this matter can be found on Chapter 7 in Ref. [79]. Specifically this kind of ambiguity for the auxiliary fields $\mathbf{D}(\mathbf{r},t)$ and $\mathbf{H}(\mathbf{r},t)$ will be used in the next section to motivate the nature of the artificial magnetization in metamaterials at optical frequencies as a nonlocal electric response of second-order.

3.2 Linear constitutive relations and spatial dispersion

In this section, we will investigate the nonlocal response of optical metamaterials on phenomenological grounds. In contrast to the multipole approach, where the variation of the electric field arises from different multipole contributions, here nonlocality rather means that the electric polarization $\boldsymbol{\mathcal{P}}$ and the magnetization $\boldsymbol{\mathcal{M}}$ of the homogenized material at every point depend on the fields $\mathbf{E}$ and $\mathbf{B}$ of light at some distant points or, alternatively, on spatial derivatives of the fields at the same point, or both. In general, the homogenized material is described by effective macroscopic parameters. The latter ones have to be spatially independent, otherwise they contradict with the homogeneity and the material cannot be regarded as homogeneous.

3.2.1 Field equations and linear constitutive relations

As a starting point, we will use the macroscopic Maxwell Eqs. (3.12), where the response fields are defined as the functionals

$$\mathbf{D}[\mathbf{E},\mathbf{B}] = \mathbf{E}(\mathbf{r},t) + 4\pi\boldsymbol{\mathcal{P}}[\mathbf{E},\mathbf{B}]\,, \qquad \mathbf{H}[\mathbf{E},\mathbf{B}] = \mathbf{B}(\mathbf{r},t) - 4\pi\boldsymbol{\mathcal{M}}[\mathbf{E},\mathbf{B}]\,, \tag{3.18}$$

where the linear functionals $\boldsymbol{\mathcal{P}}[\mathbf{E},\mathbf{B}]$ and $\boldsymbol{\mathcal{M}}[\mathbf{E},\mathbf{B}]$ denote the electric polarization and the magnetization densities, respectively, and are both elements of $\boldsymbol{\mathcal{L}}^2_{\text{loc}}(\mathbb{R}^3)$. Note that $\boldsymbol{\mathcal{P}}[\mathbf{E},\mathbf{B}]$ is more than the electric dipole density $\mathbf{P}(\mathbf{r},t)$ and that $\boldsymbol{\mathcal{M}}[\mathbf{E},\mathbf{B}]$ not always contain only the magnetic dipole density $\mathbf{M}(\mathbf{r},t)$, as higher multipole moment densities can, in general, be induced as well [cf. Eqs. (3.13)-(3.14)]. These quantities contain

actually the response of the material. The source of the electric polarization density $\boldsymbol{\mathcal{P}}(\mathbf{r},t)$ is phenomenologically set to be the bound charges, i.e, $\nabla\cdot\boldsymbol{\mathcal{P}}(\mathbf{r},t)=-\rho_{\text{bound}}(\mathbf{r},t)$. Being discussed in the previous section, the motion of induced bounded charge density can be decomposed into two physically independent current densities. The first part amounts to the distorted charges that experience some translational motion, that can be fully linked to $\boldsymbol{\mathcal{P}}(\mathbf{r},t)$ such that, technically, we can write

$$\rho_{\text{ind}}(\mathbf{r},t)=-\nabla\cdot\boldsymbol{\mathcal{P}}(\mathbf{r},t)\,, \tag{3.19}$$

obeying the continuity equation

$$\nabla\cdot(\mathbf{J}_{\text{ind}}(\mathbf{r},t)-\partial_t\boldsymbol{\mathcal{P}}(\mathbf{r},t))=0\,, \tag{3.20}$$

where $\mathbf{J}_{\text{ind}}$ denotes the polarization current density. On the other hand, there exist also charges that experience motions over closed loops, generating some magnetization field perpendicular to the loop, where the corresponding current density $\mathbf{J}_{\text{magn}}$ is by its very nature divergence free. Hence, we have

$$\nabla\cdot\mathbf{J}_{\text{magn}}(\mathbf{r},t)=0\Leftrightarrow\mathbf{J}_{\text{magn}}(\mathbf{r},t)=c\nabla\times\boldsymbol{\mathcal{M}}(\mathbf{r},t)\,. \tag{3.21}$$

As a matter of fact, the bounded current is the sum of both currents and can be written as

$$\mathbf{J}_{\text{bound}}(\mathbf{r},t)=\partial_t\boldsymbol{\mathcal{P}}(\mathbf{r},t)+c\nabla\times\boldsymbol{\mathcal{M}}(\mathbf{r},t)\,, \tag{3.22}$$

while the first term usually appears for electrically polarizable media and the second for magnetizable media.

The magnetization $\boldsymbol{\mathcal{M}}(\mathbf{r},t)=(\mathbf{B}(\mathbf{r},t)-\mathbf{H}(\mathbf{r},t))/(4\pi)$ is only different from zero for intrinsically magnetizable media, such as ferromagnets at low frequencies [85]. However, at optical frequencies, the term $|c\nabla\times\boldsymbol{\mathcal{M}}(\mathbf{r},t)|$ is usually much smaller than $|\partial_t\boldsymbol{\mathcal{P}}(\mathbf{r},t)|$, as the corresponding charge carriers cannot respond to the fast oscillating wave. Based on the argumentation from Ref. [86], §79, one can estimate the magnitudes of the polarizabilities as follows. Let us consider a body with size a under the time harmonic electromagnetic field with frequency $k_0=\omega/c$. From the Maxwell equation $\nabla\times\mathbf{E}(\mathbf{r},k_0)=\mathrm{i}k_0\mathbf{B}(\mathbf{r},k_0)$, we get the spatial variation of the electric field in the body with size a to be in the order of $|\mathbf{E}(\mathbf{r},k_0)|/a\sim k_0\mathbf{H}(\mathbf{r},k_0)$. Under the assumption of a linear response, i.e., $\boldsymbol{\mathcal{P}}(\mathbf{r},k_0)=\chi_{\text{el}}(k_0)\mathbf{E}(\mathbf{r},k_0)$ and $\boldsymbol{\mathcal{M}}(\mathbf{r},k_0)=\chi_{\text{magn}}(k_0)\mathbf{H}(\mathbf{r},k_0)$, where the coefficients $\chi_{\text{el}}(k_0)$ and $\chi_{\text{magn}}(k_0)$ denote the electric and magnetic susceptibilities, we have in frequency domain

$$|-\mathrm{i}\omega\boldsymbol{\mathcal{P}}(\mathbf{r},k_0)/c|=k_0|\chi_{\text{el}}\mathbf{E}(\mathbf{r},k_0)|\sim ak_0^2|\chi_{\text{el}}\mathbf{H}(\mathbf{r},k_0)|\,, \tag{3.23}$$

$$|\nabla\times\boldsymbol{\mathcal{M}}(\mathbf{r},k_0)|=|\chi_{\text{magn}}(k_0)\nabla\times\mathbf{H}(\mathbf{r},k_0)|\sim|\chi_{\text{magn}}(k_0)\mathbf{H}(\mathbf{r},k_0)|/a\,. \tag{3.24}$$

Now, assuming that both electric and magnetic responses are of comparable strength, i.e., if $|\partial_t\boldsymbol{\mathcal{P}}(\mathbf{r},t)/c|\approx|\nabla\times\boldsymbol{\mathcal{M}}(\mathbf{r},t)|$ then:

$$k_0^2a|\chi_{\text{el}}(k_0)|\approx|\chi_{\text{magn}}(k_0)|/a\Leftrightarrow\left(\frac{a}{\lambda}\right)^2\approx\left|\frac{\chi_{\text{magn}}(k_0)}{\chi_{\text{el}}(k_0)}\right|\,. \tag{3.25}$$

The critical parameter here is the ratio a/λ or equivalently k_0a. In the optical range, the parameter a/λ is very small if a is of molecular dimensions and of the order $a/\lambda\sim10^{-3}$. Hence, similarity (3.25) yields $1\gg10^{-6}>\left|\frac{\chi_{\text{magn}}}{\chi_{\text{el}}}\right|$ which means that the magnetic response

at optical frequencies is actually much smaller than the electric response. Consequently, at optical wavelengths the assumption $\boldsymbol{\mathcal{M}} = 0$ can be safely done, which in particular leads to $\mu = 1$. However, for optical metamaterials with a characteristic dimension of mesoscopic size, $a/\lambda \lesssim 1$ it becomes evident that the (effective) magnetic and electric contributions become comparable. Nonetheless, one can still assume that $\boldsymbol{\mathcal{M}} = 0$ if the metamaterial is made of constituents that are intrinsically nonmagnetic, i.e., no magnetic response even for lower frequencies. We show in Sec. 3.2.3 that the effective magnetic response in such structures, i.e, the artificial magnetization in optical metamaterials, is an effect caused by spatial dispersion and specifically of order $(a/\lambda)^2$. Moreover, if the metamaterial is made from unit cells without central symmetry, effects of optical activity of order a/λ such as gyrotropy occur as well.

As motivated in the previous section on the basis of multipole expansion, the definition of the response fields $\mathbf{D}(\mathbf{r}, t)$ and $\mathbf{H}(\mathbf{r}, t)$ is not unique. In fact, in the transition from microscopic to macroscopic Maxwell equations, the separation of the induced current into electric polarization and magnetization parts is not unique, i.e., it is physically impossible to distinguish between $\partial_t \boldsymbol{\mathcal{P}}$ and $\nabla \times \boldsymbol{\mathcal{M}}$ [87]. Undeniably, the vector fields $\boldsymbol{\mathcal{P}}$ and $\boldsymbol{\mathcal{M}}$ in Eqs. (3.19) and (3.22) are invariant under the following gauge transformation:

$$\boldsymbol{\mathcal{P}}'[\mathbf{E}, \mathbf{B}] = \boldsymbol{\mathcal{P}}[\mathbf{E}, \mathbf{B}] + \nabla \times \mathbf{Q}[\mathbf{E}, \mathbf{B}], \qquad \boldsymbol{\mathcal{M}}'[\mathbf{E}, \mathbf{B}] = \boldsymbol{\mathcal{M}}[\mathbf{E}, \mathbf{B}] - \partial_t \mathbf{Q}[\mathbf{E}, \mathbf{B}], \quad (3.26)$$

where $\mathbf{Q} \in \boldsymbol{\mathcal{L}}^2_{\mathrm{loc}}(\mathbb{R}^3)$ is a linear functional acting on the fields $\mathbf{E}$ and $\mathbf{B}$. Consequently, the response fields $\mathbf{D}$ and $\mathbf{H}$ are, as well, not unique and obey the following transformation:

$$\mathbf{D}'[\mathbf{E}, \mathbf{B}] = \mathbf{D}[\mathbf{E}, \mathbf{B}] + \nabla \times \mathbf{Q}[\mathbf{E}, \mathbf{B}], \qquad \mathbf{H}'[\mathbf{E}, \mathbf{B}] = \mathbf{H}[\mathbf{E}, \mathbf{B}] + \partial_t \mathbf{Q}[\mathbf{E}, \mathbf{B}] \quad (3.27)$$

Such transformation, does not change the Maxwell Eqs. (3.12), nor light propagation in the infinitely extended bulk material. However, at the presence of interfaces, the introduction of $\mathbf{Q}$ might change the interface conditions for the fields [88]. This discrepancy can be regarded as a feature as one might simplify the derivation of interface condition by properly introducing such vector field $\mathbf{Q}$.

3.2.2 Effective medium theory with spatial dispersion

Prior discussing electrodynamics with spatial dispersion, we would like to review one important fact about temporal dispersion. This will give a brief analogy and ease the understanding of the less commonly employed spatial dispersion. The response of a polarizable medium to an electromagnetic field can never be instantaneous as the polarization of the material has finite relaxation frequency ω_r. Hence, the polarization $\boldsymbol{\mathcal{P}}$ at at time t depends on the electric field at that instant and as well as at the field at previous times t'. Such functional dependency can be written in the following integral form

$$\boldsymbol{\mathcal{P}}(\mathbf{r}, t) = \int_\Omega \int_0^\infty \hat{\chi}_{\mathrm{el}}(\mathbf{r}, \mathbf{r}', t') \mathbf{E}(\mathbf{r}', t - t') \mathrm{d}t' \mathrm{d}\mathbf{r}' = \int_\Omega \int_0^\infty \hat{\chi}_{\mathrm{el}}(\mathbf{r}, \mathbf{r}', t - t') \mathbf{E}(\mathbf{r}', t) \mathrm{d}t' \mathrm{d}\mathbf{r}' \,, \quad (3.28)$$

where $\Omega \subset \mathbb{R}^3$ represents the volume of the medium. Equation (3.28) represents the most general electromagnetic response to light[1] [89]. Here, χ_{el} denotes the spatially dependent response function. Due to time invariance (the material does not get deformed or heats

[1] The fact that the polarization can depend on the magnetic induction $\mathbf{B}$ is included in the definition above too, as χ_{el} can contain curl operators that act on $\mathbf{E}$ such that $\nabla \times \mathbf{E} = -\frac{1}{c}\partial_t \mathbf{B}$.

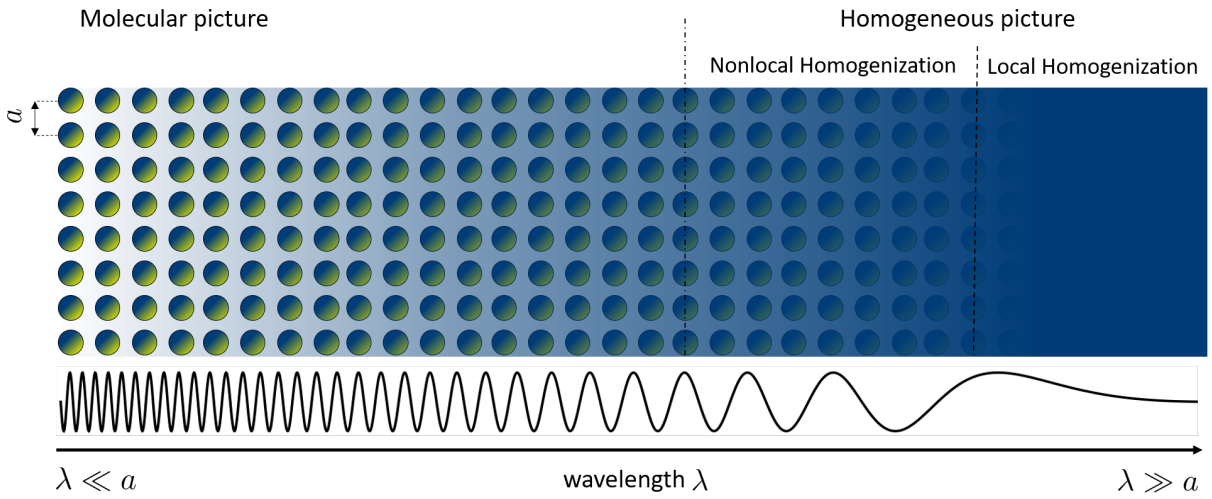

Figure 3.2: Illustration of different homogenization regimes, as a function of the critical parameter a/λ. In the regime where $a/\lambda > 1$, the details of the structure are spatially resolved and the fields oscillate too fast to be meaningfully averaged over a distance a. On the other hand, in the long-wavelength limit, i.e. $a/\lambda \ll 1$, the fields can be assumed to be constant and the material can be homogenized by the introduction of effective material parameters. Particularly interesting is crossover regime where $a/\lambda \lesssim 1/2$, dynamics of the field start to become important, where a nonlocal description must be considered.

up, etc.), $\chi_{\rm el}$ cannot be a function of absolute times but only on the time difference $t - t'$. Temporal convolutions[2] as in Eq. (3.28) are appealing, because one can use the convolution theorem (2.53) and writes down

$$\boldsymbol{\mathcal{P}}(\mathbf{r}, k_0) = \int_\Omega \hat{\chi}_{\rm el}(\mathbf{r}, \mathbf{r}', k_0)\mathbf{E}(\mathbf{r}', k_0)\mathrm{d}\mathbf{r}' \,. \tag{3.29}$$

Hence, temporal nonlocality ($t-t' \neq 0$) amounts to a temporal dispersion, i.e., a frequency-dependent material response. Since for most media the relaxation frequency happen to be within the optical frequency range, temporal dispersion is generally necessary to be taken into account. The critical parameter indicating the strength of the frequency dispersion is the ratio ω/ω_r. In the limit $\omega/\omega_r \to 0$, temporal dispersion vanishes.

In accordance with the Casimir-Onsager relations for reciprocal media, a generalized principle to the symmetry of $\hat{\chi}_{\rm el}(\mathbf{r}, \mathbf{r}', k_0)$ can be stated. In the theory of electromagnetism, this translates the processes with of time-reversal symmetry. In fact, it holds that the displacement field $\mathbf{D}$ and the electric field $\mathbf{E}$ are polar vectors, i.e., symmetric under time inversion and the magnetic flux $\mathbf{B}$ and the magnetic field $\mathbf{H}$ are axial vectors, i.e., anti-symmetric under time inversion [81]. These symmetries of the fields have consequences on the symmetry of the nonlocal response function. The components of the tensor $\chi_{{\rm el},ij}(\mathbf{r}, \mathbf{r}', k_0)$ satisfy the symmetry relations [90]

$$\chi_{{\rm el},ij}(\mathbf{r}, \mathbf{r}', k_0) = \chi_{{\rm el},ji}(\mathbf{r}', \mathbf{r}, k_0) \,. \tag{3.30}$$

This principle is sometimes regarded as the fourth law of thermodynamics. The proof of this principle purely bases on thermodynamic considerations for physical states out of

[2]The integral can be extended over $(-\infty, \infty)$ with the extension of $\chi_{\rm el}(\mathbf{r}, \mathbf{r}', t) = 0$ for $t < 0$ (causality).

thermodynamic equilibrium (but not too far from the equilibrium) and can be found in Ref. [91], §125.

Spatial nonlocality, from now on simply nonlocality, is reflected by the explicit dependence of the response function on both positions $\mathbf{r}$ and $\mathbf{r}'$, where the polarization at a position $\mathbf{r}$ is induced by the external electric field at distant position $\mathbf{r}'$. In contrast, if the medium experiences a polarization at a fixed position that depends only on the actual value of the electric field at that same position, the response is called local. A local response does not incorporate the effect of the environment or multipoles beyond the dipole approximation. Such responses can be modeled by Dirac's delta-distribution, that gives a contribution if, and only if $\mathbf{r} = \mathbf{r}'$. Accordingly, the (local) response $\hat{\chi}_{\mathrm{el}}(\mathbf{r}, \mathbf{r}', k_0) = \hat{\chi}_{\mathrm{loc}}(\mathbf{r}, k_0)\delta(\mathbf{r} - \mathbf{r}')$ is a distribution that acts on the electric field in a way the polarization field becomes $\boldsymbol{\mathcal{P}}(\mathbf{r}, k_0) = \chi_{\mathrm{loc}}(\mathbf{r}, k_0)\mathbf{E}(\mathbf{r}, k_0)$. This relationship is usually employed in numerical Maxwell-solvers, where a permittivity distribution in space is given and the local field is calculated, where the classical interface conditions (2.12-2.13) for the fields $\mathbf{D}$, $\mathbf{B}$ and $\mathbf{E}$, $\mathbf{H}$, respectively, are sufficient. However, this is an oversimplification for a metamaterial, since the characteristic distance over which the field within the length scale corresponding to one unit cell of the metamaterial varies, is of the order of the wavelength and must, therefore, be considered in the full study. In such situation, to properly calculate the fields with a numerical solver for Maxwell's equations with a high resolution is necessary. See, e.g., Sec. 5.2 and in particular Fig. 5.3. Either way, this is in some sense unsatisfactory, as the numerical computation is either inaccurate and cannot resolve the mesoscopic features of the structure, or too cumbersome and resource demanding.

To overcome this issue, we assume that the periodic metamaterial is homogenizable. This assumption is fine if the period of the structure is smaller than half of the wavelength [92], which is usually the case for optical metamaterials. This assumption simplifies the analytical treatment of complex materials leading to effective medium properties beyond what nature can possibly offer. In some cases however, effective continuum descriptions are not perfect. Usually, because only a local response is assumed, which might work fine in the quasi-static approximation but is not sufficient if the dynamics of the wave becomes prominent, which is the case in optics [53], [93]. For the purpose of a nonlocal homogenization theory, let's assume that the volume Ω of the infinitely extended metamaterial is $\mathbb{R}^3$, thereupon the absence of interfaces. In the analogy to temporal nonlocality, the spatially nonlocal response can be approximated by a function of $\mathbf{r} - \mathbf{r}'$, as in a homogeneous space the response does not depend on the actual positions $\mathbf{r}$ and $\mathbf{r}'$ but rather on the relative Euclidean distance $\mathbf{r} - \mathbf{r}'$. Following these considerations, the constitutive relation (3.18) in (temporal-)frequency domain becomes

$$\mathbf{D}(\mathbf{r}, k_0) = \int_{\mathbb{R}^3} \hat{\mathbf{R}}(\mathbf{r} - \mathbf{r}', k_0)\mathbf{E}(\mathbf{r}', k_0)\mathrm{d}\mathbf{r}' \,, \tag{3.31}$$

with the nonlocal response kernel

$$\hat{\mathbf{R}}(\mathbf{r} - \mathbf{r}', k_0) = \mathbb{1}\delta(\mathbf{r} - \mathbf{r}') + 4\pi\hat{\chi}_{\mathrm{el}}(\mathbf{r} - \mathbf{r}', k_0) \,. \tag{3.32}$$

Additionally, under the assumption of the material being intrinsically nonmagnetic, we have $\mathbf{H}(\mathbf{r}, k_0) = \mathbf{B}(\mathbf{r}, k_0)$. These material equations are the key equations in this thesis and represent the most general nonlocal electromagnetic response for homogeneous media. By performing the spatial Fourier transforms, the convolution above translates to an algebraic product such that

$$\tilde{\mathbf{D}}(\mathbf{k}, k_0) = \hat{\tilde{\mathbf{R}}}(\mathbf{k}, k_0)\tilde{\mathbf{E}}(\mathbf{k}, k_0) \,, \tag{3.33}$$

where the $\tilde{\cdot}$ denotes the corresponding quantities in spatial Fourier space. The wave vector $\mathbf{k}$ refers to the spatial frequency and its modulus is not forcibly a multiple of the wave number $k_0 = \frac{\omega}{c}$. The latter quantity is simply the reduced temporal frequency with the same unit as the wave vector $\mathbf{k}$, namely inverse length. The fact that the nonlocal response kernel $\mathbf{R}(\mathbf{r}-\mathbf{r}', k_0)$ is a function of the Euclidean difference $\mathbf{r}-\mathbf{r}'$ in real space, its Fourier transform $\hat{\tilde{\mathbf{R}}}$ translates to a $\mathbf{k}$-dependent function. Consequently, spatial nonlocality amounts to spatial dispersion. At this point, it is natural to state that spatial dispersion expresses the dependence of the effective medium property of the homogeneous metamaterial on the spatial heterogeneity of the wave, i.e., spatial dynamics of the fields. This is in complete analogy to the temporal dispersion that is a consequence of temporal dynamics of the fields. For arbitrary $\mathbf{k} = (k_x, k_y, k_z)$ and k_0, Casimir-Onsager reciprocity relations (3.30) in Fourier space read

$$\hat{\tilde{R}}_{ij}(\mathbf{k}, k_0) = \hat{\tilde{R}}_{ji}(-\mathbf{k}, k_0)\,. \tag{3.34}$$

If the unit cell of the metamaterial has a center of symmetry, then the material is called nongyrotropic. In such crystals there exist three independent mirror planes such that any transformations of $\mathbf{k} \to (\pm k_x, \pm k_y, \pm k_z)$ do not change the properties of the metamaterial. Then, we have

$$\hat{\tilde{R}}_{ij}(\mathbf{k}, k_0) = \hat{\tilde{R}}_{ji}(\mathbf{k}, k_0)\,, \tag{3.35}$$

for any arbitrary $\mathbf{k}$ and k_0. The local limit $|\mathbf{k}| \to 0$, i.e. $\lambda \to \infty$, is equivalent to the assumption that field is uniform. In that case $\hat{\tilde{\mathbf{R}}}(\mathbf{k}, k_0)$ simplifies to

$$\lim_{|\mathbf{k}|\to 0} \hat{\tilde{\mathbf{R}}}(\mathbf{k}, k_0) = \hat{\epsilon}(k_0)\,, \tag{3.36}$$

where $\hat{\epsilon}(k_0) \in \mathbb{C}^{3\times 3}$ is the classical electric permittivity matrix. By virtue of Eq. (3.34), $\hat{\epsilon}(k_0)$ is symmetric.

Some mathematical remarks concerning the concepts above are necessary. By latest in Eq. (3.32) it is clear that $\hat{\mathbf{R}}$ is a distribution, specifically an element of $\boldsymbol{\mathcal{E}}'$. Furthermore, in a homogeneous space, the eigenmodes (as we will prove in Ch. 4) are plane waves. Therefore, $\mathbf{E}$ is only locally integrable and as discussed in Sec. 2.3.3, its Fourier transform cannot be defined by the ordinary integral representation as in Eq. (2.34) and care has to be taken. Since $\mathbf{E}$ is locally integrable with at most polynomial growth at infinity (both properties are guaranteed from plane waves), the relevant subject here is the Fourier transform of tempered distributions $\boldsymbol{\mathcal{S}}'$. The Fourier transform of such distributions was defined in Def. 2.3.3. According to the convolution theorem 2.3.5, the convolution between distributions in $\boldsymbol{\mathcal{E}}'$ and $\boldsymbol{\mathcal{S}}'$ maps into $\boldsymbol{\mathcal{S}}'$. Therefore, $\mathbf{D}$ and $\tilde{\mathbf{D}}$ can be regarded as a tempered distribution, i.e., an element of $\boldsymbol{\mathcal{S}}'$, just as $\mathbf{E}$ and $\tilde{\mathbf{E}}$. According to property (2.45), Maxwell's equation in Fourier space $(\mathbf{k}, k_0)$ read

$$\mathbf{k}\cdot\tilde{\mathbf{D}}(\mathbf{k}, k_0) = 0\,, \qquad \mathbf{k}\times\tilde{\mathbf{H}}(\mathbf{k}, k_0) = -k_0\tilde{\mathbf{D}}(\mathbf{k}, k_0)\,, \tag{3.37}$$

$$\mathbf{k}\cdot\tilde{\mathbf{B}}(\mathbf{k}, k_0) = 0\,, \qquad \mathbf{k}\times\tilde{\mathbf{E}}(\mathbf{k}, k_0) = k_0\tilde{\mathbf{B}}(\mathbf{k}, k_0)\,. \tag{3.38}$$

An essential part of this thesis is the study of ways to reconstruct the response kernel for specific metamaterials and discuss the nature of various approximations. Expression (3.33) is too general for practical purposes, as in general, interface conditions have to be derived as well. To this end, it is unavoidable to reformulate the problem in real space by

inverse Fourier transform and derive the necessary continuity conditions for the fields at the interface. This is more delicate as it seems to be on the first glance. First of all, it is not clear how to evaluate the convolution integral (3.31) at the interface if the support of $\hat{\mathbf{R}}(\mathbf{r}, k_0)$ overlaps with the interface. In the literature, interface conditions were derived by the introduction of Drude transition layers, where $\hat{\mathbf{R}}(\mathbf{r}, k_0)$ is regularized across the interface to adequately describe both materials that occupy the two half-spaces [94]–[96]. Unfortunately, this is not always satisfying, as the interface conditions depend on the phenomenologically introduced thickness of the Drude layers [97].

A more subtle way to avoid both issues is to define $\hat{\mathbf{R}}(\mathbf{r}, k_0)$ by a distribution of compact support, i.e., an element of $\boldsymbol{\mathcal{E}}'$. We propose to define $\hat{\mathbf{R}}(\mathbf{r}, k_0)$ as a linear combination of Dirac's delta distribution and of it's partial derivatives. In terms of equations we propose

$$\hat{\mathbf{R}}(\mathbf{r}-\mathbf{r}', k_0) = \sum_{\alpha \in \mathbb{N}_0^3, |\alpha| \leq N} \mathbf{C}_\alpha(k_0) D^\alpha \delta(\mathbf{r}-\mathbf{r}')\,, \tag{3.39}$$

with $N \in \mathbb{N}$ the truncation order, the matrices $\mathbf{C}_\alpha \in \mathbb{C}^{3\times 3}$ the spatially independent effective material parameters, and $D^\alpha = \nabla_{\alpha_1}\nabla_{\alpha_2}\nabla_{\alpha_3}$, where $|\alpha| = \alpha_1 + \alpha_2 + \alpha_3$. The fact that the material parameters $\mathbf{C}_\alpha$ are spatially independent is due to the homogenization. The nonlocality is encrypted in the derivatives of the delta distributions. From the mathematical perspective, Eq. (3.31) is well defined as a dual mapping in which the distribution $\hat{\mathbf{R}} \in \boldsymbol{\mathcal{E}}'$ linearly acts on the electric field $\mathbf{E} \in \boldsymbol{\mathcal{S}}'$. Following the definition of the weak derivatives of distributions (2.5) and theorem 2.3.5, the constitutive relation (3.31) becomes

$$\mathbf{D}(\mathbf{r}, k_0) = \sum_{\alpha \in \mathbb{N}_0^3, |\alpha| \leq N} \mathbf{C}_\alpha(k_0) D^\alpha \mathbf{E}(\mathbf{r}, k_0)\,. \tag{3.40}$$

The first term $\mathbf{C}_0(k_0)$ in the expansion corresponds to the usual permittivity matrix of a local material and $\mathbf{C}_{\alpha\neq 0}(k_0)$ give the corrections including the nonlocal responses. Following this logic, nonlocality reflects to the dependency of the response at a position $\mathbf{r}$ on the electric field as well as on its partial derivatives at that point. This is physically equivalent to the case where the response at $\mathbf{r}$ depends on the environment, simply because the eclectic field as well as its partial derivatives are determined by the surroundings. A consideration of nonlocality is of paramount importance if one these situations are met:

(a) The size of the unit cell and the averaging volume are not negligibly small compared to the wavelength.

(b) The building blocks forming the unit cell have strong higher order multipole moments.

In the first case, the unit cell is only slightly smaller than the wavelength and the response must depend on the environment, as the mesoscopic features of the structure can only be resolved by retaining the spatial derivatives of the field. In the second case, and as discussed in Sec. 3.1, the contribution of higher order multipole moments causes the dependence of the response on spatial derivatives of the field. Either way, a nonlocal response has to be taken into account to adequately homogenize the metamaterial.

It is important here to emphasize that, now, the displacement field $\mathbf{D}$ depends on the derivatives of the electric field $\mathbf{E}$. This will definitely have consequences on the interface conditions for the fields, that will depend on the coefficients $\mathbf{C}_\alpha$ and on the truncation order N. The mathematical reason for this subtlety is that we cannot imply from $\nabla \times$

$\mathbf{H}(\mathbf{r}, k_0) = -\mathrm{i}k_0\mathbf{D}(\mathbf{r}, k_0)$ that $\mathbf{H}$ is an element of $\boldsymbol{\mathcal{H}}_{\mathrm{loc}}(\mathrm{curl}, \mathbb{R}^3)$, which is only guaranteed in the local approach, or for a specific choice of $\mathbf{C}_\alpha$ and N. According to theorem 2.2.1, $\mathbf{H} \in \boldsymbol{\mathcal{H}}_{\mathrm{loc}}(\mathrm{curl}, \mathbb{R}^3)$, is equivalent to the continuity of the tangential component of $\mathbf{H}$. A fact of life is that when nonlocality is taking place, additional interface conditions are always required [98]. However, in some situations, these can be circumvented by a proper choice of the gauge field $\mathbf{Q}$ in Eq. (3.27).

The response in Eq. (3.40) is still too general and impracticable. To be able to derive the interface conditions and to calculate the dispersion relations, some assumptions on the matrix-valued coefficients $\mathbf{C}_\alpha$ and on the truncation order N have to be taken into account. There is no doubt that a high approximation quality can be obtained for a high truncation order N. However, the expansion is not very convenient to handle. In most previous works [53], [93] metamaterials are mostly modeled with material equations up to second-order derivatives, i.e., $N = 2$. However, this assumption is, in most cases, justified only for sufficiently diluted metamaterials (but still dense on the level of the wavelength) made from isolated inclusions with a negligible scattering strength. This simplification is in accordance with a regime where the building blocks of the metamaterial are negligibly small compared to the wavelength. Unfortunately, this leads to the observation of very weak resonances, if there are any. However, notable scattering phenomena require that these inclusions have mesoscopic sizes which cannot be simply homogenized by a local permittivity and a local permeability only. A refined homogenization requires the consideration of higher order terms that lead to strong spatial dispersion. This is what we do in this work and will be discussed in depth in Ch. 4, where we consider more general second-order terms and more importantly increase the truncation order up to fourth-order derivatives.

In the interest of providing a brief preface on spatial dispersion and its consequences, let us in this section focus on a specific form of constitutive relations up to the second-order. This will provide the reader an instructive introduction into the effect of spatial dispersion in optical metamaterials. In the following, we will show the origin of extrinsic chirality and of artificial magnetization at optical wavelengths.

To see the physical significance of spatial nonlocality, let us return to our response ansatz in Eq. (3.40) and study the problem in the spatial Fourier space. According to property (2.45) of Fourier transforms of derivatives, the constitutive relation reads

$$\tilde{\mathbf{D}}(\mathbf{k}, k_0) = \hat{\tilde{\mathbf{R}}}(\mathbf{k}, k_0)\tilde{\mathbf{E}}(\mathbf{k}, k_0) = \sum_{\alpha \in \mathbb{N}_0^3, |\alpha| \leq N} \tilde{\mathbf{C}}_\alpha(k_0)\mathbf{k}^\alpha \tilde{\mathbf{E}}(\mathbf{k}, k_0)\,. \tag{3.41}$$

In fact, spatial derivatives on the electric field in real space translate into simple multiplications by polynomials of $\mathbf{k}$. In CGS units, the displacement field and electric field have the same dimensions and $\mathbf{k}$ is an inverse length $[\mathrm{m}^{-1}]$. Therefore, the material parameter of order $|\alpha|$ have the dimension of $\mathrm{m}^{|\alpha|}$.

3.2.3 Weak spatial dispersion approximation

Let a be a characteristic length of the homogenized metamaterial. Only on the assumption that $(a|\mathbf{k}|)^2 \ll 1$, an expansion up to the second order is justified. Then, the i-th component $\tilde{D}_i$ of the displacement field is

$$\tilde{D}_i(\mathbf{k}, k_0) = a_{ij} + b_{ijk}k_k\tilde{E}_j(\mathbf{k}, k_0) + c_{ijkl}k_k k_l \tilde{E}_j(\mathbf{k}, k_0) \tag{3.42}$$

where the tensorial coefficients a_{ij}, b_{ijk} and c_{ijkl} refer to the frequency dependent effective material parameters. For the sake of readability, we drop the explicit frequency dependence of the coefficients above, but the reader shall consistently bear in mind that they always depend on the frequency k_0. In connection with the Casimir-Onsager relations (3.34), the number of independent coefficients can be dramatically reduced. The general symmetry properties for each coefficient of $\hat{\tilde{\mathbf{R}}}(\mathbf{k},\omega)$ are

$$a_{ij} = a_{ji} \quad b_{ijk} = -b_{jik} \quad c_{ijkl} = c_{jikl}\,, \tag{3.43}$$

and analogously for higher order terms. Furthermore, we require that the electric field $\mathbf{E}$ is at least a $\boldsymbol{\mathcal{C}}^2(\mathbb{R}^3)$-function. Consequently, according to the equality of mixed partials (Schwartz's theorem), the second-order derivatives can be interchanged which renders $c_{ijkl} = c_{ijlk}$. These are the fundamental symmetry conditions for the fourth-rank tensor c_{ijkl}. These symmetries reduce the number of nonzero components from 81 to only 36. If we consider a concrete crystal with specific geometrical symmetries, the number of independent components can be further reduced. A comprehensive summary of the symmetry properties of the tensors b_{ijk} and c_{ijkl} for different symmetry classes can be found the book of Agranovich and Ginzburg [50], Ch. 3.

At this point, let us focus on the terms linear on $\mathbf{k}$ in Eq. (3.42), i.e., on the first-order spatial dispersion. These terms, and also all terms with odd exponents of $\mathbf{k}$, lead to optical activity, i.e., materials with such properties tend to change the polarization of the incident light. Such materials are usually called chiral media with the chirality parameters b_{ijk}, and if spatial dispersion is strong, other odd higher-order terms may contribute to chirality. Now, if b_{ijk} resembles a combination of a matrix $\hat{\xi}$ multiplied with a Levi-Civita tensor ε_{ilm}, we get for $\mathbf{D}$

$$\tilde{D}_i(\mathbf{k},k_0) = \epsilon_{ij}\tilde{E}_j(\mathbf{k},k_0) + \frac{2}{k_0}\xi_{ij}\varepsilon_{jlm}k_l\tilde{E}_m(\mathbf{k},k_0)\,, \tag{3.44}$$

where the zeroth-order terms a_{ij} represent the usual electric permittivity matrix $\hat{\epsilon}$. This is in accordance with the limit (3.36), which is the only term surviving the quasi-static approximation. According to Maxwell's Equation $\varepsilon_{jlm}k_l\tilde{E}_m(\mathbf{k},k_0) = k_0\tilde{B}_j(\mathbf{k},k_0)$, we can get rid of the explicit $\mathbf{k}$ dependence in $\tilde{\mathbf{D}}(\mathbf{k},k_0)$. In real space, this would mean we would eliminate the explicit spatial derivatives on $\mathbf{E}(\mathbf{r},k_0)$ appearing in $\mathbf{D}(\mathbf{r},k_0)$. Accordingly, in spatial Fourier space we obtain

$$\tilde{D}_i(\mathbf{k},k_0) = \epsilon_{ij}\tilde{E}_j(\mathbf{k},k_0) + 2\xi_{ij}\tilde{B}_j(\mathbf{k},k_0)\,, \tag{3.45}$$

and $\tilde{\mathbf{H}}(\mathbf{k},k_0) = \tilde{\mathbf{B}}(\mathbf{k},k_0)$. The interface conditions emerging for such non-reciprocal systems are rather complicated. By a proper choice of $\mathbf{Q}(\mathbf{r},k_0)$, the constitutive relations can be further simplified and the classical interface conditions, i.e., the continuity of the tangential components of $\mathbf{E}(\mathbf{r},k_0)$ and $\mathbf{H}(\mathbf{r},k_0)$ and the normal components of $\mathbf{D}(\mathbf{r},k_0)$ and $\mathbf{B}(\mathbf{r},k_0)$ at the interface, can be reached. In fact, by choosing in Fourier space $\tilde{Q}_i(\mathbf{k},k_0) = -\xi_{ij}\varepsilon_{jlm}k_l\tilde{E}_m(\mathbf{k},k_0)$ we obtain

$$\begin{aligned}\tilde{D}_i(\mathbf{k},k_0) &= \epsilon_{ij}\tilde{E}_j(\mathbf{k},k_0) + \xi_{ij}\tilde{B}_j(\mathbf{k},k_0)\,,\\ \tilde{H}_i(\mathbf{k},k_0) &= \tilde{B}_i(\mathbf{k},k_0) - \xi_{ji}\tilde{E}_j(\mathbf{k},k_0)\,,\end{aligned} \tag{3.46}$$

which constitute the very common material laws for bi-anisotropic media (without a magnetic response yet). Optical activity turns out to be an effect of order $a|\mathbf{k}|$, or alternatively

a/λ. On the optical activity in spatially dispersive media, maybe one of the first work mentioning this is by J. W. Gibbs in the end of 19th century [99]. Nowadays, this effect can be easily engineered in optical wavelengths using specially designed metamaterials. All it requires is to have an array of unit cells that has at most two orthogonal mirror planes such as structures with Helices or Split-Ring Resonators [100]–[102]. There, a linearly polarized electric field generates a magnetic moment, perpendicular to the split-rings, inducing a magnetic response $\mathbf{H} \neq \mathbf{B}$, that is directly proportional to $\mathbf{E}$. Such phenomena is often called magneto-electric coupling. Optical activity, or chirality, can be also reached in isotropic systems, if the inclusions are intrinsically chiral and randomly oriented [103]. If the unit cell of the metamaterial is made of achiral building blocks and has a center of symmetry, the term proportional to $\hat{\xi}$ cannot exist, as $\mathbf{D}(\mathbf{r}, k_0)$ is symmetric under parity transformation while $\mathbf{B}(\mathbf{r}, k_0)$ is not. Hence, $\hat{\xi}$ must be zero. This is in compliance with condition (3.35). Consequently, the non-vanishing contributions leading to spatial dispersion are of the order $(a|\mathbf{k}|)^2$. Here effects such as artificial magnetization and birefringence induced by spatial dispersion in cubic crystals can be found. The latter effect was seemingly originally predicted by H. A. Lorentz in the end of the 19th century as well [104]. This can be easily understood by looking at the second-order terms for an isotropic system with a center of symmetry. Even under these assumptions, the nonlocal response tensor is not a scalar, but rather a dense 3×3 matrix which can be decomposed into a part transverse to $\mathbf{k}$ and into a part longitudinal to $\mathbf{k}$:

$$\tilde{\mathbf{R}}_{ij}(\mathbf{k}, k_0) = \epsilon_t(|\mathbf{k}|, k_0)\left(\delta_{ij} - \frac{k_i k_j}{|\mathbf{k}|^2}\right) + \epsilon_l(|\mathbf{k}|, k_0)\frac{k_i k_j}{|\mathbf{k}|^2}\,, \tag{3.47}$$

where ϵ_t and ϵ_l are, respectively, the transverse and longitudinal permittivities, and depend only on the magnitude of the wave vector and not on its direction. First of all, it is clear that $\tilde{\mathbf{R}}_{ij}(\mathbf{k}, k_0)$ can have off-diagonal elements proportional to $|\mathbf{k}|^2$. Second, for different directions of $\mathbf{k}$, the diagonal elements are in general different, leading to different responses for different illumination directions, even though, the metamaterial was assumed to be isotropic. This feature is proportional to $|\mathbf{k}|^2$ as well and is actually the birefringence that is induced by spatial dispersion. At optical frequencies, it was first observed around ninety years after it's first invocation by H. A. Lorentz in cubic crystals of silicon [105] and in gallium arsenide [62], and recently measured in metamaterials with cubic symmetry [106], [107].

In the remaining part of this section, we will discuss the origin of artificial magnetization at optical frequencies. In general, for the second-order coefficients c_{ijkl} it is always proposed [90] that

$$\tilde{\mathbf{D}}(\mathbf{k}, k_0) = \hat{\epsilon}\tilde{\mathbf{E}}(\mathbf{k}, k_0) + \mathbf{k} \times \left[\hat{\alpha}\mathbf{k} \times \tilde{\mathbf{E}}(\mathbf{k}, k_0)\right] + \mathbf{k} \cdot \left[\hat{\beta}\mathbf{k} \cdot \tilde{\mathbf{E}}(\mathbf{k}, k_0)\right]\,, \tag{3.48}$$

where $\hat{\alpha}$, $\hat{\beta} \in \mathbb{C}^{3\times3}$ are diagonal matrices that, again, implicitly depend on k_0. However, the $\hat{\beta}$-term was only introduced on the level of the constitutive relations. When it came to the derivation of the additional interface conditions, $\hat{\beta}$ was usually set to zero and only $\hat{\alpha}$ was discussed. The reason behind this negligence is that $\hat{\beta}$ requires an additional interface condition which was not easy to formulate. Meanwhile, as we will show soon, the $\hat{\alpha}$-term can be reinterpreted as a local permittivity, without changing the classical interface conditions. The positions of $\hat{\alpha}$ and $\hat{\beta}$ have to be exactly between the two $\mathbf{k}$ vectors, because otherwise the coefficients c_{ijkl} would violate Casimir-Onsager reciprocity principle, i.e., would not satisfy the general symmetry condition (3.35). We exemplary

prove this on the $\hat{\alpha}$-term in App. A. The term proportional to $\hat{\alpha}$ is of special importance. It arises by enforcing (with $\hat{\beta} = 0$) that

$$c_{ijkl} k_k k_l \tilde{E}_j(\mathbf{k}, k_0) \stackrel{!}{=} \left[\mathbf{k} \times \left(\hat{\alpha}\mathbf{k} \times \tilde{\mathbf{E}}(\mathbf{k}, k_0)\right)\right]_i , \tag{3.49}$$

which is clearly a restriction in general. How exactly α_{ij} relate to c_{ijkl}, is summarized in Eq. (A.1) of App. A. However, assumption (3.49) is very appealing for multiple reasons. Such term characterizes a current in which the induced charges describe a closed-loop trajectory. Such currents can be induced in specially designed structures such as split-ring resonators [108], cut-plate pairs [109], or the fishnet metamaterial [110]. By taking advantage of the non-uniqueness of the displacement field $\tilde{\mathbf{D}}(\mathbf{k}, k_0)$, we can show that this nonlocal term literally translates into an effective local magnetic permeability. By choosing

$$\tilde{\mathbf{Q}}(\mathbf{k}, k_0) = -\hat{\alpha}(k_0)\mathbf{k} \times \tilde{\mathbf{E}}(\mathbf{k}, k_0) = -\mathrm{i}k_0 \hat{\alpha}(k_0)\tilde{\mathbf{B}}(\mathbf{k}, k_0) , \tag{3.50}$$

we eliminate the nonlocal contribution $\propto \hat{\alpha}$ in $\tilde{\mathbf{D}}$ and simultaneously obtain

$$\tilde{\mathbf{H}}(\mathbf{k}, k_0) = \tilde{\mathbf{B}}(\mathbf{k}, k_0) - \mathrm{i}k_0 \tilde{\mathbf{Q}}(\mathbf{k}, k_0) = \left(1 - k_0^2 \hat{\alpha}(k_0)\right) \tilde{\mathbf{B}}(\mathbf{k}, k_0) . \tag{3.51}$$

With this, we define the local, temporally dispersive, magnetic permeability $\hat{\mu}$ that reads

$$\hat{\mu}^{-1}(k_0) = \mathbb{1} - k_0^2 \hat{\alpha}(k_0) , \tag{3.52}$$

and specifically we have $\hat{\mu}(k_0) \neq \mathbb{1}$ for $\hat{\alpha}(k_0) \neq 0$.

From the considerations above, we can conclude that the artificial magnetization in metamaterials at optical frequencies is nothing else, but a second-order spatial dispersion effect on the electric field. In real space, this translates into a specific second-order nonlocal effect. However, it has to be stated that the gauge field $\mathbf{Q}(\mathbf{r}, k_0)$ in real space changes the interface conditions for $\nabla \times \mathbf{E}(\mathbf{r}, k_0)$ and $\mathbf{H}(\mathbf{r}, k_0)$, but conveniently, in a subtle way where the reflection and transmission coefficients do not change, in other words, the actually measurable quantities remain invariant, which is advantageous. Details concerning the interface conditions will be elaborated in depth in Ch. 4.

Furthermore, we would like to note that the origin of $\hat{\mu} \neq 1$ and the definition of $\hat{\mu}$ by itself at optical frequencies are versatile and their interpretation as well. In the book of Landau and Lifshitz [89], §103, the difference of $\hat{\mu}$ from 1 is defined by the difference of the longitudinal and transverse permittivities defined in Eq. (3.47) in the limit $|\mathbf{k}| \to 0$. This issue is controversially discussed in literature [111], [112].

The second term proportional to $\hat{\beta}$ represents a nonlocal material parameter, in which the nonlocality couples longitudinally to the electric field. With $\hat{\beta}$ being diagonal, equating the coefficients between Eq. (3.42) and Eq. (3.48) leads to the constraint

$$c_{ijkl} k_k k_l \stackrel{!}{=} \beta_{jj} k_j^2 \Rightarrow c_{jjjj} \stackrel{!}{=} \beta_{jj} , \tag{3.53}$$

and zero else wise. Such nonlocal effects have been only studied in a uniaxially polarizable bulk material such as the wire media [113]. In contrast to the preceding term, this term cannot be transformed to a local material property. I.e., in real space, there exists no $\mathbf{Q}(\mathbf{r}, k_0)$ that can possibly simultaneously eliminate the explicit derivatives proportional to $\hat{\beta}$ in both expressions for $\mathbf{D}(\mathbf{r}, k_0)$ and $\mathbf{H}(\mathbf{r}, k_0)$. In Fourier space, this translates to an explicit $\mathbf{k}$-dependence in the constitutive relations. When this term is considered, a new wave propagating in the bulk appears which leads to the request for an additional

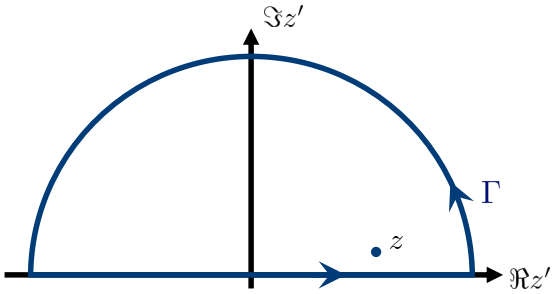

Figure 3.3: Contour integral enclosing the singularity at z.

interface condition. The latter is essential to unambiguously determine the amplitudes of the fields at the interface, and was to our knowledge never introduced. Hence, it was always assumed that $\hat{\beta} = 0$. This oversimplification is not always justified, as this assumption is equivalent to enforcing that simultaneously $c_{xxxx} = c_{yyyy} = c_{zzzz} = 0$ holds. From a general symmetry perspective, there is no reason, why this conjecture is applicable. Even for a cubic system with least number of independent coefficients c_{ijkl}, only four independent nonzero components remain and the three above are among these four nonzero ones. In the next chapter, we discuss the effect of this specific term on the dispersion relations and derive the corresponding interface conditions.

Throughout this thesis, we will encounter the terminology of the weak spatial dispersion (WSD) approximation. A WSD approximation is a set of constitutive relations in which the spatially dispersive contributions can be eliminated via suitable gauge transformations. "Spatial dispersion" because it originates form nonlocal material laws and "weak" because there exists a gauge field $\mathbf{Q}(\mathbf{r}, k_0)$ that gives local constitutive relations, with a local magnetoelectric coupling $\hat{\xi}$ and a local permeability $\hat{\mu}$, hence a local bi-anisotropic medium:

$$\mathbf{D}(\mathbf{r}, k_0) = \hat{\epsilon}(k_0)\mathbf{E}(\mathbf{r}, k_0) + \hat{\xi}(k_0)\mathbf{B}(\mathbf{r}, k_0)\,, \tag{3.54}$$

$$\mathbf{H}(\mathbf{r}, k_0) = \hat{\mu}^{-1}(k_0)\mathbf{B}(\mathbf{r}, k_0) + \hat{\xi}^{\mathrm{T}}(k_0)\mathbf{E}(\mathbf{r}, k_0)\,. \tag{3.55}$$

For metamaterials that possess a centre of symmetry we have $\hat{\xi} = 0$, such that the magnetoelectric coupling terms vanish.

3.3 Causality and Passivity with spatial dispersion

As already discussed in the beginning of Sec. 3.2.2, the response of the medium cannot depend on the electromagnetic field of light at future times, namely $\hat{\tilde{\chi}}(\mathbf{k}, t) = 0$ for $t < 0$. This is the causality condition. It implies that for $z = k_0 + \mathrm{i}\eta$, $\eta > 0$

$$\hat{\tilde{\chi}}(\mathbf{k}, z) = \int_0^\infty \hat{\tilde{\chi}}(\mathbf{k}, t)\mathrm{e}^{\mathrm{i}k_0 ct - \eta t}\mathrm{d}t \tag{3.56}$$

exists and is a holomorphic function in the upper half-plane for $\eta > 0$ and for fixed $\mathbf{k}$. For such functions, Cauchy's integral formula holds

$$\hat{\tilde{\chi}}(\mathbf{k}, z) = \frac{1}{2\pi\mathrm{i}} \oint_\Gamma \frac{\hat{\tilde{\chi}}(\mathbf{k}, z')}{z' - z}\mathrm{d}z'\,, \tag{3.57}$$

where Γ is a closed contour that includes the point $z = k_0 + \mathrm{i}\eta$ in it's interior. As shown in Fig. 3.3, it consists of a line integration over the real axis and of a semicircle in the upper half-plane. We expect that the polarization vanishes at extremely high frequencies, as the induced electrons can no longer collectively follow the rapidly oscillating field of light. Hence, $\hat{\tilde{\chi}}(\mathbf{k}, |z|) \to 0$, as $|z| \to \infty$. By exploiting this asymptotic behaviour, the contour integral reduces to a line integral over $\mathbb{R}$ and we obtain

$$\hat{\tilde{\chi}}(\mathbf{k}, z) = \frac{1}{2\pi\mathrm{i}} \int_{\mathbb{R}} \frac{\hat{\tilde{\chi}}(\mathbf{k}, z')}{k_0' - k_0 - \mathrm{i}\eta} \mathrm{d}k_0' \,. \tag{3.58}$$

For real frequencies, i.e., in the limit $\eta \to 0$, it is a well-known fact [80] that the denominator in Eq. (3.58) becomes the distribution

$$\lim_{\eta \to 0} \frac{1}{k_0' - k_0 - \mathrm{i}\eta} = \mathrm{p.v.} \frac{1}{k_0' - k_0} + \mathrm{i}\pi\delta(k_0' - k_0) \in \mathcal{S}'(\mathbb{R}) \,, \tag{3.59}$$

acting on $\hat{\tilde{\chi}}(\mathbf{k}, z')$, which can be regarded as the test function in the dual space $\mathcal{S}(\mathbb{R})$. The latter inclusion is guaranteed as $\hat{\tilde{\chi}}(\mathbf{k}, t)\mathrm{e}^{-\eta t} \in \mathcal{S}(\mathbb{R})$ and the Fourier Transform $\mathcal{F}(\mathcal{S}) = \mathcal{S}$ (cf. Def. (2.3.3)). Following these considerations, the integral Eq. (3.58) in the limit $\eta \to 0$ becomes the dual mapping

$$\hat{\tilde{\chi}}(\mathbf{k}, k_0) = \langle \hat{\tilde{\chi}}(\mathbf{k}, k_0'), \delta(k_0 - k_0') \rangle_{\mathbb{R}} + \frac{1}{\mathrm{i}\pi} \langle \hat{\tilde{\chi}}(\mathbf{k}, k_0'), \mathrm{p.v.} \frac{1}{k_0' - k_0} \rangle_{\mathbb{R}} \,, \tag{3.60}$$

where the integration variable is k_0'. Finally, by separating real and imaginary parts of $\hat{\tilde{\chi}}(\mathbf{k}, k_0)$, we obtain the Kramers-Kronig relations for the $\mathbf{k}$-dependent nonlocal response tensor $\hat{\tilde{\mathbf{R}}}(\mathbf{k}, k_0) = \mathbb{1} + 4\pi\hat{\tilde{\chi}}(\mathbf{k}, k_0)$ that read

$$\begin{aligned} \Re\hat{\tilde{\mathbf{R}}}(\mathbf{k}, k_0) &= \mathbb{1} + \frac{1}{\pi} \langle \Im\hat{\tilde{\mathbf{R}}}(\mathbf{k}, k_0), \mathrm{p.v.} \frac{1}{k_0' - k_0} \rangle_{\mathbb{R}} \\ \Im\hat{\tilde{\mathbf{R}}}(\mathbf{k}, k_0) &= \frac{1}{\pi} \langle \Re\hat{\tilde{\mathbf{R}}}(\mathbf{k}, k_0), \mathrm{p.v.} \frac{1}{k_0' - k_0} \rangle_{\mathbb{R}} \,. \end{aligned} \tag{3.61}$$

A very important statement can be drawn from these relations, is that real and imaginary parts are mutually coupled and cannot be chosen arbitrarily. The real parts describe the displacements from the resting positions and the imaginary parts the losses due to frictions and collisions with the nuclei. Hence, a huge real part come with a huge imaginary part. To some extent, this mimics the fluctuation-dissipation theorem in thermodynamics.

It is natural to ask whether Kramers-Kronig type relations for the spatial frequency $\mathbf{k}$ exist as well. The answer is no, because these relations follow from causality that does not hold in spatial domain. In the time domain, the response of the material does not depend on the source at future times. However, in the spatial domain, the response depends on the electric field in the surroundings as well as on its spatial derivatives in all directions.

A further restriction on $\hat{\tilde{\mathbf{R}}}(\mathbf{k}, k_0)$ is that the material can only absorb energy and not generate it. This reflects to the fact that the imaginary parts of $\hat{\tilde{\mathbf{R}}}(\mathbf{k}, k_0)$ cannot be negative. In other words, the matrix $\Im\hat{\tilde{\mathbf{R}}}(\mathbf{k}, k_0)$ must be positive semi-definite for all $\mathbf{k}$ and k_0. This is the passivity condition. The derivation is quite tedious and requires the introduction of concepts that are beyond the scope of this thesis. The interested reader can refer to Ch. 2 of Ref. [50] and Appendix C of Ref. [112].

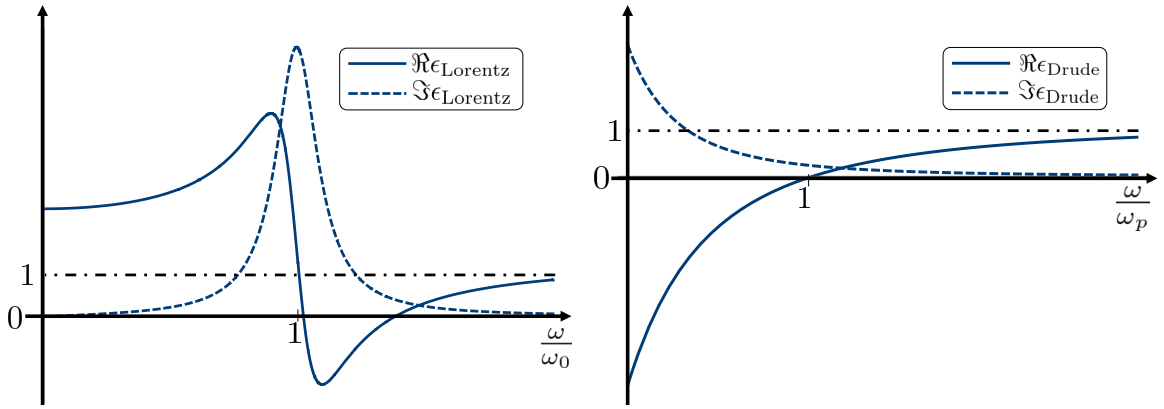

Figure 3.4: Sketch of the real and imaginary parts of Lorentz (left) and Drude (right) permittivities as function of the frequency. Due to the losses, the resonance frequencies are shifted.

Basic examples of optical responses

How exactly the effective material parameters depend on the frequency, varies strongly from material to material. To find these dependencies in the macroscopic picture, a phenomenological description has to be found. The identification of this effective description with parameters while not having to explicitly pay attention to the microscopic behaviour is part of the homogenization process. To this end, let us describe the collective motion of elections in the bulk material. To simplify the discussion, let us assume a local isotropic response, but temporally dispersive response, in a homogeneous material. Under the assumption that the charges move in the same direction as the electric field $E(t)$, the polarization $\mathcal{P}(t)$ in the dipole approximation obeys the following equation of motion:

$$\partial_t^2 \mathcal{P}(t) + \Gamma_L \partial_t \mathcal{P}(t) + \omega_0^2 \mathcal{P}(t) = \Omega_0^2 E(t) \tag{3.62}$$

On the L.H.S., the first term corresponds to the acceleration of the charges, the second term proportional to Γ_L accounts for the damping due to the collisions of the electrons with the cores, and the third term describes the restoring forces for an oscillator with the characteristic frequency ω_0 due to the binding of the electrons with the cores. On the R.H.S., we have the driving force due to the external field with a coupling coefficient $\Omega_0^2 = \frac{N_c f_0 e^2}{m}$, where m and e are the (effective) mass and the charge of the electron, N_c the atomic concentration, and f_0 the oscillator strength. In temporal frequency domain, temporal derivatives ∂_t become multiplications by $(-\mathrm{i}\omega)$ such that the second-order ODE becomes

$$\tilde{\mathcal{P}}(\omega) = \frac{\Omega_0^2}{\omega_0^2 - \omega^2 - \mathrm{i}\Gamma_L \omega} \tilde{E}(\omega)\,. \tag{3.63}$$

Assuming a linear response, namely $\tilde{\mathcal{P}}(\omega) = \chi_{el}(\omega)\tilde{E}(\omega)$, we deduce from the susceptibility the dielectric function $\epsilon(\omega) = 1 + 4\pi\chi_{el}(\omega)$ that reads

$$\epsilon_{\text{Lorentz}}(\omega) = 1 - \frac{4\pi\Omega_0^2}{\omega^2 - \omega_0^2 + \mathrm{i}\Gamma_L \omega}\,. \tag{3.64}$$

This is the response function of the damped harmonic oscillator, called the Lorentz model (see Fig. 3.4, left). This model is in good approximation when the induced currents

describe closed paths, or rather charges that are bounded to the cores, i.e, a good description of most dielectrics. In metals, however, the restoring force is negligible such that the electrons are free. Under this approximation, we obtain the Drude model

$$\epsilon_{\text{Drude}}(\omega) = 1 - \frac{\omega_p^2}{\omega^2 + \mathrm{i}\Gamma_L\omega}\,, \tag{3.65}$$

where $\omega_p^2 = 4\pi\Omega_0^2$ represents the plasma frequency, in which the real part of the permittivity changes sign (see Fig. 3.4, right). For the Fishnet metamaterial considered later in this thesis, the permittivity will be of Drude type, due to the metallic nano wires. At the same time the magnetic permeability of Lorentz type, that arises from the anti-symmetric coupling between the metallic layers.

In fact, both Lorentz and Drude models satisfy both Causality (3.61) and passivity conditions. The consequences of Kramers-Kronig relations become clearly visible in the Lorentz model, cf. Fig. 3.4, left. Whenever there is a fluctuation, i.e., $\Re\partial_\omega\epsilon(\omega) \neq 0$ (dynamics), a dissipation, i.e., $\Im\epsilon(\omega) > 0$ arises, particularly around the resonance frequency ω_0. Under specific circumstances both permittivity and permeability can have negative real parts, simultaneously, resulting to the negative index behaviour in optical metamaterials, which is inaccessible with ordinary materials. In this case, the direction of the energy flux is opposite to the direction of the propagation.

3.4 Chapter Summary and concluding remarks

In this chapter, we derived the macroscopic Maxwell equations using a suitable averaging technique. In both multipole and phenomenological approaches, we have discussed the non-uniqueness of the material fields $\mathbf{D}(\mathbf{r}, k_0)$ and $\mathbf{H}(\mathbf{r}, k_0)$, leading to the freedom of choice of the nonlocal response tensor $\hat{\mathbf{R}}(\mathbf{r}-\mathbf{r}', k_0)$ and discussed its general properties for both gyrotropic and nongyrotropic media. In the multipolar analysis, we concluded that the discussion of spatial dispersion in this framework is helpful to recognize a physical origin of spatial dispersion, but is inappropriate for the purpose of homogenization. In the phenomenological approach, we prove why intrinsic magnetization is absent at optical frequencies and its emergence requires that the characteristic length scale of a metamaterial must be comparable to the wavelength λ. By virtue of the gauge transformation (3.27) we have shown that optical activity and artificial magnetization are, respectively, effects of first-order and second-order spatial dispersion.

Now the true question is whether the introduction of effective material parameters to homogenize a given metamaterial is meaningful or not. This can only be answered by comparing the electromagnetic response of both the heterogeneous metamaterial and its homogeneous substitute. Hence, each metamaterial has to be studied individually. In the past, it was shown that the weak spatial dispersion approximation, i.e., the local constitutive relations as given in Eqs. (3.54) and (3.55) are insufficient to adequately predict the response of an actual material [53].

This is particularly true when the electromagnetic response of a material is studied near absorption lines, i.e., resonances. There, the modulus of the refractive index $|\mathbf{n}| := |\mathbf{k}|/k_0$ increases, and so does the parameter $a/\lambda = a|\mathbf{n}|/\lambda_0$, where λ and λ_0 are, respectively, the wavelengths in the material and in free-space. Consequently, the isofrequency surfaces change dramatically [114]–[116] and will deviate from the ordinary ellipsoids and hyperboloids known from the classical courses of theoretical optics. As well as

the number of modes sustained at the interface of a nonlocal material increases by the strength of the spatial dispersion. Evidently, the reflection and transmission coefficients from a finite slab will experience some changes as well.

In the next chapter, a study of different models for homogenization will be performed. Specifically, we will discuss the dispersion relations of a bulk medium and the interface conditions at the interface between a homogenized metamaterial described with a specific nonlocal response kernel and an ordinary material with a local permittivity. For benchmark reasons, we will shortly elaborate on the consequences of the weak spatial dispersion approximation. Emphasize will be put on the more sophisticated nonlocal model in the strong spatial dispersion approximation. We will discuss the dispersion of the additional modes and derive the corresponding additional interface conditions by means of a weak formulation of the wave equation.

4 | Homogenization of centrosymmetric metamaterials

The permeability μ has no meaning at optical frequencies. In that range, the effects due to the difference of μ from unity are in general indistinguishable from those of spatial dispersion of the permittivity.

Lew D. Landau and Jewgeni M. Lifschitz

In the previous chapter, we discussed the possible origins of nonlocality in mesoscopic, optical metamaterials and some peculiar effects that are not present in natural materials. Emphasis was put on the general properties of the nonlocal response tensor $\hat{\mathbf{R}}(\mathbf{r}-\mathbf{r}', k_0)$ and on the non-uniqueness of the auxiliary fields $\mathbf{D}(\mathbf{r}, k_0)$ and $\mathbf{H}(\mathbf{r}, k_0)$. However, Eq. (3.40) is as general as impracticable. In order to proceed, we need to calculate the dispersion relations and the interface conditions. To this end, for centrosymmetric metamaterials, we assume specific coefficients $\mathbf{C}_\alpha(k_0)$. First of all, with centrosymmetry, all coefficients followed by a $\mathbf{k}$-polynomial of odd power vanish. Further, departing from the WSD approximation from Sec. 3.2.3 and extend it with specific nonlocal terms up to the fourth order, for which we have derived dispersion relations and interface conditions in our publications [64], [117]. Ultimately, the constitutive relations in real space of the spatial domain are assumed to read

$$\begin{aligned}\mathbf{D}(\mathbf{r}, k_0) =& \hat{\epsilon}(k_0)\mathbf{E}(\mathbf{r}, k_0) + \nabla \times (\hat{\alpha}(k_0)\nabla \times \mathbf{E}(\mathbf{r}, k_0)) + \sum_{j\in(x,y,z)} \nabla_j(\hat{\beta}^j(k_0)\nabla_j \mathbf{E}(\mathbf{r}, k_0)) \\ &+ \nabla \times \nabla \times (\hat{\gamma}(k_0)\nabla \times \nabla \times \mathbf{E}(\mathbf{r}, k_0))\,,\end{aligned} \tag{4.1}$$

and $\mathbf{H}(\mathbf{r}, k_0) = \mathbf{B}(\mathbf{r}, k_0)$, where $\hat{\epsilon}(k_0)$, $\hat{\alpha}(k_0)$, $\hat{\beta}^j(k_0)$ and $\hat{\gamma}(k_0)$ are $[0, \infty) \to \mathbb{C}^{3\times 3}$, bounded with $\boldsymbol{\mathcal{E}}$-regularity. The first two terms, respectively, amount to the local permittivity and to the so-called reluctivity [118], where the latter can be transformed to a local magnetic permeability $\hat{\mu}(k_0)$. The model with only $\hat{\epsilon}(k_0)$ and $\hat{\alpha}(k_0)$ (or equivalently $\hat{\mu}(k_0)$) is called the local model or the weak spatial dispersion (WSD) model. However, it got more and more evident that such a local assumption is limited for at least two reasons. In the first place, there is no physical justification why the second-order term can only contain the term with $\hat{\alpha}(k_0)$. For metamaterials that possess a centre of symmetry, terms proportional to $\hat{\beta}^j(k_0)$ are, in general, allowed to exist (cf. Ch 3.2 in Ref. [50]). Only if the local description is valid, these terms are negligibly small and vanish. Nonetheless, for metamaterials with mesoscopic features, this cannot be guaranteed beforehand. In the second place, a truncation of the Taylor approximation up to the second order in the material laws are is not justified as well. A refined analysis of nonlocal responses to light requires the consideration of higher order spatial derivatives of the exciting field of light $\mathbf{E}(\mathbf{r}, k_0)$. Note that there are neither first-order nor third-order terms in the expansion (4.1). This is a consequence from the Casimir-Onsager symmetries for centrosymmetric crystals.

In contrast, the last two terms in Eq. (4.1) are truly nonlocal terms. There exists no gauge field $\mathbf{Q}(\mathbf{r}, k_0)$ that can possibly eliminate the spatial derivatives in the constitutive

relations. The term proportional to $\beta^j(k_0)$ with $\beta^j(k_0) = \beta_{jj}(k_0)\hat{\mathbf{e}}_j\hat{\mathbf{e}}_j$, where $\beta_{jj}(k_0) = c_{jjjj}(k_0)$ is a scalar and $\hat{\mathbf{e}}_j$ is a unit vector in j direction, is usually neglected due to the cumbersome analysis of the arising additional modes that request additional interface conditions. Here, the consequences of this term will be studied in depth. Regarding the fourth order term, we require the expression to be comparable to the assumption of the second order term proportional to $\hat{\alpha}(k_0)$. Namely, we enforce that

$$e_{ijklmn}(k_0)\nabla_k\nabla_l\nabla_m\nabla_n E_j(\mathbf{r},k_0) \stackrel{!}{=} \left[\nabla\times\nabla\times(\hat{\gamma}(k_0)\nabla\times\nabla\times\mathbf{E}(\mathbf{r},k_0))\right]_i\,. \tag{4.2}$$

With such an assumption, we are able to derive the required interface conditions from first principles by using the generalized weak formulation that we introduced in Sec. 2.2. Furthermore, the position of $\hat{\gamma}(k_0)$ cannot be chosen freely for both mathematical and physical reasons.

In the following sections, we will fully analyze three effective medium models for homogenization. First in the bulk problem, i.e., analyzing the dispersion relations. Second, the half-space problem, i.e., deriving the interface conditions. Prior studying the complicated models leading to strong spatial dispersion (SSD), we shortly study the WSD model. This state-of-the-art model shall serve for a comparative analysis and for giving an introduction to the homogenization procedure.

Remark 4.0.1. *The analysis of the dispersion relation in the infinitely extended homogeneous medium is preferably done in spatial Fourier-space. By using the convolution theorems and the properties of Fourier transforms introduced in Sec. 2.3.3, the PDEs and convolution integrals turn out to become simple algebraic equations with* $\mathbf{k}$ *being the unknown to be found. In contrast, the derivation of interface conditions is rather done in real space. The weak formulation of the wave equation shall serve as the tool for the purpose.*

4.1 Dispersion relation and additional modes

To study wave propagation in a medium with spatial dispersion, one has to solve the wave-type equation in $\mathbf{k}$-space. For crystals with spatial dispersion and without intrinsic magnetic response, the wave-like equation can be obtained by decoupling Maxwell's equations and it is given by [50]

$$\left[\mathbf{k}\times\mathbf{k}\times-k_0^2\hat{\hat{\mathbf{R}}}(\mathbf{k},k_0)\right]\tilde{\mathbf{E}}(\mathbf{k},k_0) = \boldsymbol{\mathcal{W}}(\mathbf{k},k_0)\tilde{\mathbf{E}}(\mathbf{k},k_0) = 0\,. \tag{4.3}$$

This equation is of paramount importance and represents an eigenvalue equation whose solutions are $\mathbf{k}(k_0)$, defining the dispersion relation of light in an infinitely extended homogeneous medium. The nontrivial solutions are obtained by posing the determinant of the wave-operator $\boldsymbol{\mathcal{W}}(\mathbf{k},k_0)$ to be zero. This ansatz is, however, only possible if $\mathbf{H}=\mathbf{B}$, i.e., $\boldsymbol{\mathcal{M}}=0$. Anyhow, if there exists an intrinsic magnetic response or because of a suitable gauge transformation (3.27), we would redefine the magnetic field such that $\tilde{\mathbf{H}}(\mathbf{k},k_0) = \hat{\hat{\mathbf{R}}}_{\text{magn}}(\mathbf{k},k_0)\tilde{\mathbf{B}}(\mathbf{k},k_0)$, and one has to solve the full Maxwell equations, which in their matrix form read

$$\hat{\mathcal{A}}(\mathbf{k},k_0)\cdot\begin{pmatrix}\tilde{\mathbf{E}}(\mathbf{k},k_0)\\ \tilde{\mathbf{H}}(\mathbf{k},k_0)\end{pmatrix} = \begin{pmatrix}0\\0\end{pmatrix}\,, \tag{4.4}$$

where $\hat{\mathcal{A}} \in \mathbb{C}^{8\times 6}$ refers to the dispersion matrix that is

$$\hat{\mathcal{A}}(\mathbf{k}, k_0) = \begin{pmatrix} k_0\hat{\tilde{\mathbf{R}}}(\mathbf{k}, k_0) & \mathbf{k}\times\cdot \\ \mathbf{k}\times\cdot & -k_0\hat{\tilde{\mathbf{R}}}_{\text{magn}}(\mathbf{k}, k_0) \\ \mathbf{k}\cdot\hat{\tilde{\mathbf{R}}}(\mathbf{k}, k_0) & 0 \\ 0 & \mathbf{k}\cdot\hat{\tilde{\mathbf{R}}}_{\text{magn}}(\mathbf{k}, k_0) \end{pmatrix}. \tag{4.5}$$

Nontrivial solutions require that the rank of $\hat{\mathcal{A}}(\mathbf{k}, k_0)$ is not maximal, i.e., that the determinant $\det\left(\hat{\mathcal{A}}^{\mathrm{T}}(\mathbf{k}, k_0)\hat{\mathcal{A}}(\mathbf{k}, k_0)\right) = 0$.

Without loss of generality, we consider the z direction as the principle propagation direction and focus only at the case where $k_x = 0$ or $k_y = 0$, i.e., we either have $\mathbf{k} = (k_x, 0, k_z)$ or $\mathbf{k} = (0, k_y, k_z)$. To encapsulate both cases in one notation, we denote the transverse component of $\mathbf{k}$ by k_t, where $t = x$ or $t = y$ and $t^* = x$ for $t = y$ and $t^* = y$ for $t = x$.[1] Under the assumption of central symmetry, optical activity vanishes and the polarization of the field is preserved. Therefore, it is sufficient to decompose the eigenmodes into decoupled transverse electric (TE) and transverse magnetic (TM) modes. In the TM-polarization case, the electric field $\tilde{\mathbf{E}}(\mathbf{k}, k_0)$ is in-plane with the propagation vector $\mathbf{k}$, while the magnetic field $\tilde{\mathbf{H}}(\mathbf{k}, k_0)$ is perpendicular to the plane extended by k_z-k_t. In fact, it holds for $\mathbf{k} = (k_t, k_z)$:

- TM-polarization: $\tilde{\mathbf{E}}(\mathbf{k}, k_0) = \tilde{E}_t(\mathbf{k}, k_0)\hat{\mathbf{e}}_t + \tilde{E}_t(\mathbf{k}, k_0)\hat{\mathbf{e}}_z$ and $\tilde{\mathbf{H}}(\mathbf{k}, k_0) = \tilde{H}_{t^*}(\mathbf{k}, k_0)\hat{\mathbf{e}}_{t^*}$
- TE-polarization: $\tilde{\mathbf{H}}(\mathbf{k}, k_0) = \tilde{H}_t(\mathbf{k}, k_0)\hat{\mathbf{e}}_t + \tilde{H}_t(\mathbf{k}, k_0)\hat{\mathbf{e}}_z$ and $\tilde{\mathbf{E}}(\mathbf{k}, k_0) = \tilde{E}_{t^*}(\mathbf{k}, k_0)\hat{\mathbf{e}}_{t^*}$

Remark 4.1.1. *We assume that the coordinate system of the laboratory is aligned with the coordinate system of the principle axis of the metamaterial. This allows the matrices $\hat{\epsilon}$, $\hat{\alpha}$, and $\hat{\gamma}$ being diagonal, which is convenient.*

In the following, we calculate the dispersion relations for three cases. First of all, we study the WSD approach, which will be also a starting point for the advanced models and will be developed into two directions. Second, we study the second order symmetry model (SYM), which strictly orients on symmetry considerations of a unit cell of a specific crystal. Here, we only include the $\hat{\beta}^j$ terms without considering fourth order terms, as it already gives significant improvements compared to WSD [117]. Third, and finally, we study the model that will be of most interest in this thesis, i.e. the fourth order model (SSD), where $\hat{\gamma} \neq 0$, but again $\hat{\beta}^j = 0$. Including, both $\hat{\gamma}$ and $\hat{\beta}^j$ into the analysis can, ideally, be done but the analysis becomes too complicated and is outside the framework of this thesis. Here, we wish to develop an effective medium model with the least number of effective material parameters.

4.1.1 Dispersion relation of WSD

For benchmarking, let us investigate the dispersion relation of the classical constitutive relation of anisotropic media with WSD

$$\tilde{\mathbf{D}}(\mathbf{k}, k_0) = \hat{\epsilon}(k_0)\tilde{\mathbf{E}}(\mathbf{k}, k_0) + \mathbf{k}\times\left(\hat{\alpha}(k_0)\mathbf{k}\times\tilde{\mathbf{E}}(\mathbf{k}, k_0)\right), \tag{4.6}$$

[1] For example, let $\mathbf{k} = (k_x, 0, k_z)$, then $k_t = k_x$ and $\mu_{t^*t^*} = \mu_{yy}$.

and, as usual, $\tilde{\mathbf{H}}(\mathbf{k}, k_0) = \tilde{\mathbf{B}}(\mathbf{k}, k_0)$. The dispersion relation can be derived by solving Eq. (4.3) that reads

$$\left(k_z^{\mathrm{WSD}}(k_t, k_0)\right)^2 = p_0(k_0) - q_0(k_0)k_t^2 \,. \tag{4.7}$$

Here, the complex coefficients $p_0(k_0)$ and $q_0(k_0)$ depend on both polarization and frequency and are, respectively, measures for the refractive index and for anisotropy. After the gauge transformation with $\tilde{\mathbf{Q}}(\mathbf{k}, k_0) = -\hat{\alpha}(k_0)\mathbf{k} \times \tilde{\mathbf{E}}(\mathbf{k}, k_0)$, we obtain for the TE-polarization

$$p_0^{\mathrm{TE}}(k_0) = k_0^2 \epsilon_{t^*t^*}(k_0)\mu_{tt}(k_0)\,, \quad \text{and} \quad q_0^{\mathrm{TE}}(k_0) = \frac{\mu_{tt}(k_0)}{\mu_{zz}(k_0)}\,, \tag{4.8}$$

and for TM-polarization

$$p_0^{\mathrm{TM}}(k_0) = k_0^2 \mu_{t^*t^*}(k_0)\epsilon_{tt}(k_0)\,, \qquad q_0^{\mathrm{TM}}(k_0) = \frac{\epsilon_{tt}(k_0)}{\epsilon_{zz}(k_0)}\,, \tag{4.9}$$

where

$$\mu_{tt}(k_0) := \frac{1}{1 - k_0^2 \alpha_{tt}(k_0)}\,, \tag{4.10}$$

according to the gauge transformation above. The dispersion relation contains only two independent parameters, namely p_0 and q_0. With these two degrees of freedom, the isofrequency contours described by Eq. (4.7) restrict to only two kinds, depending on the real part of the anisotropy parameter q_0 (cf. Fig. 4.1). Is $\Re q_0 > 0$, then the isofrequency surfaces are elliptic. While for $\Re q_0 < 0$, the isofrequency surfaces describe hyperbola. Such metamaterials are called hyperbolic metamaterials and are usually designed with anisotropic unit cells containing a mixture of a dielectric and a metal, and are employed at frequencies below the reduced plasma frequency of the diluted metal [119]. However, in the past [53], and as we will see in Ch. 5 in more detail, it was shown that most metamaterials of current interest show dispersion relations more complicated than the classical hyperbola and ellipses. These dispersion relations cannot be captured using the WSD approximation. There is a clear sign that the WSD approach is insufficient for a proper effective medium approach, that will be further developed in Ch. 5 on specific examples of optical metamaterials.

Furthermore, Eq. (4.7) has two complex solutions with the same absolute value, which, depending on the sign of $\Im k_z$, refer to the forward and backward propagating modes. The total field in the bulk is, therefore, the superposition of both modes that reads

$$\mathbf{E}(\mathbf{r}, k_0) = \mathbf{E}_0^+(k_0)\mathrm{e}^{\mathrm{i}\mathbf{k}\cdot\mathbf{r}} + \mathbf{E}_0^-(k_0)\mathrm{e}^{-\mathrm{i}\mathbf{k}\cdot\mathbf{r}}\,, \tag{4.11}$$

where $\mathbf{E}_0^{\pm}$ denote the field amplitudes of the two eigenmodes. The real part $\Re k_z$ indicates the oscillatory part, while the imaginary part $\Im k_z$ is connected to the energy loss in the principle propagation direction. As a consequence of the passivity condition (cf. Sec. 3.3), it must hold that $\Im k_z > 0$ in the principle propagation direction. We identify the forward propagating mode by the solution with the positive imaginary part $\Im k_z > 0$, and the backward one with $\Im k_z < 0$, as they are exponentially attenuated in their respective propagation direction.

To conclude this section, we would like to state once again that the WSD approach is equivalent to the local approach, where both electric permittivity and magnetic permeability are temporally dispersive, i.e., both depend on k_0.

Remark 4.1.2. *From now on, in all equations the parameter $\mu_{ii}(k_0)$ shall be identified via $\mu_{ii}(k_0) = \frac{1}{1-k_0^2\alpha_{ii}(k_0)}$ and is obtained from the gauge transformation $\tilde{\mathbf{Q}}(\mathbf{k}, k_0) = -\hat{\alpha}(k_0)\mathbf{k} \times \tilde{\mathbf{E}}(\mathbf{k}, k_0)$, as previously explained at multiple occasions.*

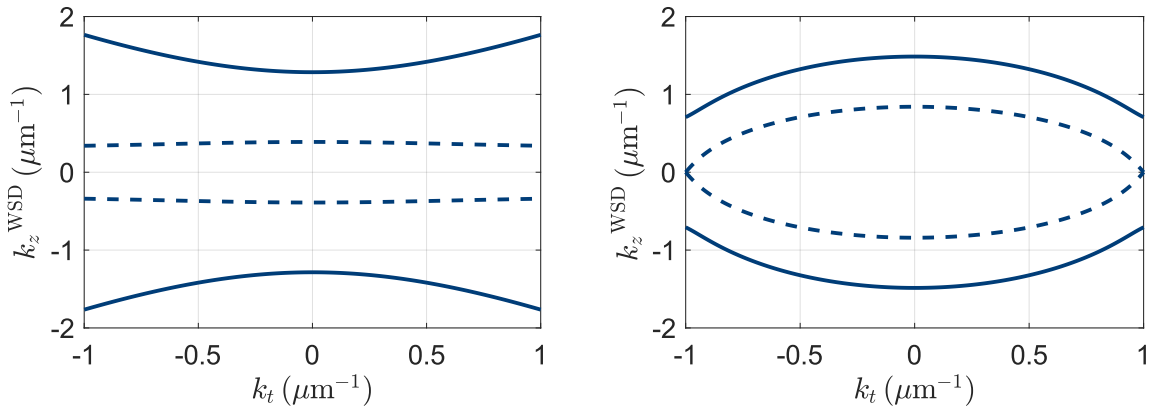

Figure 4.1: Examples of isofrequency contours for an anisotropic material with local constitutive relation, decomposed into real (solid) and imaginary (dashed) parts. On the left, a typical hyperbolic material where the different permittivity (permeability) components have different signs in TM (TE) polarizations. For the left figure we chose $p_0 = 1.5 + 1.1\mathrm{i}$, $q_0 = -1.5 - 0.2\mathrm{i}$ and for the right figure $p_0 = 1.5 + 2.5\mathrm{i}$, $q_0 = 1 + 2.5\mathrm{i}$.

4.1.2 Dispersion relation of the SYM model

The WSD approximation misses the second-order coefficients $\hat{\beta}^j(k_0)$ (c.f. Ref. [50]). Under a strict consideration of symmetry, there is *a priori* no reason why the $\hat{\beta}^j(k_0)$ could should be set to zero. Retaining these coefficients, the displacement field $\tilde{\mathbf{D}}(\mathbf{k}, k_0)$ reads

$$\tilde{\mathbf{D}}(\mathbf{k}, k_0) = \hat{\epsilon}(k_0)\tilde{\mathbf{E}}(\mathbf{k}, k_0) + \mathbf{k} \times \left(\hat{\alpha}(k_0)\mathbf{k} \times \tilde{\mathbf{E}}(\mathbf{k}, k_0)\right)) - \sum_{j\in\{x,y,z\}} k_j \left(\hat{\beta}^j(k_0) k_j \tilde{\mathbf{E}}(\mathbf{k}, k_0)\right) , \tag{4.12}$$

where $\hat{\beta}^j(k_0) = \beta_{jj}(k_0)\hat{\mathbf{e}}_j\hat{\mathbf{e}}_j$, with the dimension of m^2. According to the Taylor approximation (3.40), the terms proportional to $\hat{\beta}^j$ and $\hat{\alpha}$ emerge on equal footing. However, only $\hat{\alpha}(k_0)$ can be linked to a local magnetic permeability and leads to the WSD, while $\hat{\beta}^j(k_0)$ will always remain in the context of spatial dispersion, i.e., explicit $\mathbf{k}$ dependent material law. This term will be regarded as a higher-order susceptibility contribution that longitudinally couples $\tilde{E}_i$ with $\tilde{D}_i$, via k_i^2. Such purely longitudinal coupling will, however, only affect dispersion relation (and later also the interface conditions) of the TM-polarized mode. The dispersion relation of the TE-polarized wave for such constitutive relation continues to be

$$\left(k_z^{\mathrm{SYM}}(k_t, k_0)\right)^2 = p_0^{\mathrm{TE}}(k_0) - q_0^{\mathrm{TE}}(k_0)k_t^2 \tag{4.13}$$

and is identical to Eq. (4.7) with the same coefficients and, therefore, the same degree of freedom. Consequently, $\hat{\beta}^j$ has no effect in the TE-polarization, mainly because of the absence of cross coupling terms between the displacement field and the electric field. On the other hand, we obtain advanced dispersion relations for the TM-polarized wave that read

$$\begin{aligned} &k_z^2\left(1 + \beta_{zz}\frac{\epsilon_{tt}}{\epsilon_{zz}}\mu_{t^*t^*}k_0^2\right) + k_t^2\left(\frac{\epsilon_{tt}}{\epsilon_{zz}} + \beta_{tt}\mu_{t^*t^*}k_0^2\right) \\ &-k_z^2k_t^2\frac{\beta_{zz}}{\epsilon_{zz}}\beta_{tt}\mu_{t^*t^*}k_0^2 - k_z^4\frac{\beta_{zz}}{\epsilon_{zz}} - k_t^4\frac{\beta_{tt}}{\epsilon_{zz}} = \epsilon_{tt}\mu_{t^*t^*}k_0^2 . \end{aligned} \tag{4.14}$$

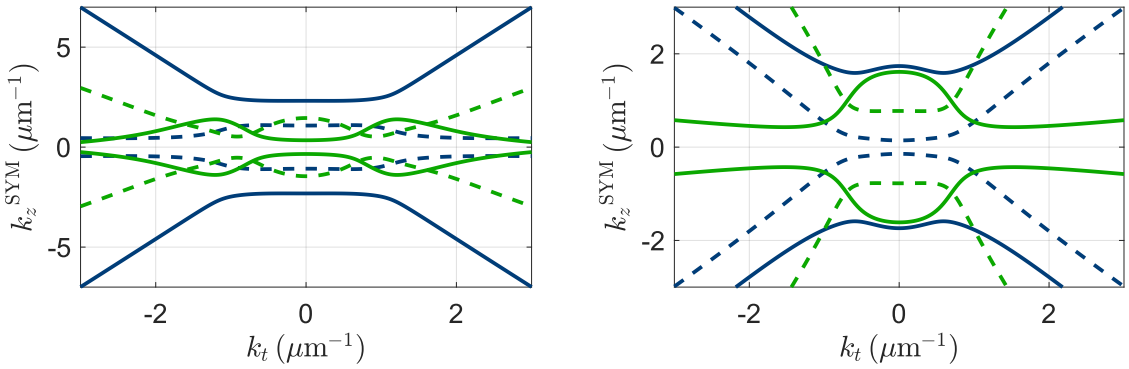

Figure 4.2: Examples of isofrequency contours obtained from the SYM model, decomposed into real (solid) and imaginary (dashed) parts. The $k_{z,+}^{\mathrm{SYM}}$ and $k_{z,-}^{\mathrm{SYM}}$ solutions are, respectively, plotted in blue and green. For the figure on the left we chose $p_0^{\mathrm{TM}} = -1+0.5\mathrm{i}$, $q_0^{\mathrm{TM}} = 2.1 + 2.5\mathrm{i}$, $p_1^{\mathrm{TM}} = 2.1 + 0.1\mathrm{i}$, $q_1^{\mathrm{TM}} = -2 + 0.5\mathrm{i}$ and for the figure on the right $p_0^{\mathrm{TM}} = 1 + 1.25\mathrm{i}$, $q_0^{\mathrm{TM}} = 1.5 - 0.25\mathrm{i}$, $p_1^{\mathrm{TM}} = -2.5 - \mathrm{i}$, $q_1^{\mathrm{TM}} = -2.5 + 4\mathrm{i}$.

Obviously, this is a biquadratic equation in k_t and k_z and particularly leads to advanced isofrequency contours beyond hyperbolas and ellipses, e.g., those functional dependencies given by WSD. Definitely, the local limit, i.e., $(\beta_{tt}, \beta_{zz}) \to (0, 0)$ restores the dispersion relation given by WSD. The solutions to Eq. (4.14) end up to be

$$\left(k_{z,\sigma}^{\mathrm{SYM}}(k_t, k_0)\right)^2 = p_1^{\mathrm{TM}} k_t^2 + q_0^{\mathrm{TM}} p_0^{\mathrm{TM}} + \sigma \sqrt{(p_1^{\mathrm{TM}} k_t^2 - q_0^{\mathrm{TM}} p_0^{\mathrm{TM}})^2 + 2 q_1^{\mathrm{TM}} \left(\frac{p_1^{\mathrm{TM}}}{p_0^{\mathrm{TM}}} k_t^4 + k_t^2 \right)}, \tag{4.15}$$

where $\sigma = \pm 1$ and the frequency-dependent coefficients

$$\begin{aligned} q_0^{\mathrm{TM}}(k_0) &= \frac{\epsilon_{zz}(k_0)}{2\beta_{zz}(k_0)}, \qquad & p_0(k_0)^{\mathrm{TM}} \quad &= \frac{k_0^2}{2} \epsilon_{tt(k_0)} \mu_{t^* t^*}(k_0), \\ q_1^{\mathrm{TM}}(k_0) &= \frac{\epsilon_{tt}(k_0)}{2\beta_{zz}(k_0)}, \qquad & p_1^{\mathrm{TM}}(k_0) \quad &= -\frac{k_0^2}{2} \beta_t(k_0) \mu_{t^* t^*}(k_0)\,. \end{aligned} \tag{4.16}$$

This finding is crucial. We have four solutions in which each two of them differ in their amplitude, as in general $|k_{z,+}^{\mathrm{SYM}}| \neq |k_{z,-}^{\mathrm{SYM}}|$ holds. The fact that multiple solutions to the wave question exist is equivalent to the existence of multiple plane waves for a given pair of frequency k_0 and transverse wave vector component k_t. This effect is clearly linked to spatial dispersion and is missing in the WSD approximation, where only one plane wave per propagation direction exists. Since the wave equation (4.3) is linear in $\mathbf{E}$ and has four distinct eigenvalues, the electric field is a superposition of four plane waves:

$$\mathbf{E}(\mathbf{r}, k_0) = \sum_{\sigma=\pm 1} \left(\mathbf{E}_{0,\sigma}^{+}(k_0) \mathrm{e}^{\mathrm{i}\mathbf{k}_\sigma \cdot \mathbf{r}} + \mathbf{E}_{0,\sigma}^{-}(k_0) \mathrm{e}^{-\mathrm{i}\mathbf{k}_\sigma \cdot \mathbf{r}} \right), \tag{4.17}$$

where $\mathbf{E}_{0,\sigma}^{+}(k_0)$ and $\mathbf{E}_{0,\sigma}^{-}(k_0)$ are the mode amplitudes. As a result, we obtain two forward and two backward propagating modes. Again, the forward modes are the ones with $\Im k_{z,\sigma}^{\mathrm{SYM}} > 0$ and are, in general, attenuated differently, as it can be seen in Fig. 4.2. The mode with the smallest $\Im k_{z,\sigma}^{\mathrm{SYM}}$, will be identified as the fundamental mode. In

principle, the imaginary parts $\Im k_{z,\sigma}^{\mathrm{SYM}}$ of the two modes can cross for a certain k_t and a mode transition must be considered. Such modal crossing was recently studied in the context of nonlocality in plasmonic wire media in Ref. [120]. In Fig. 4.2, we show some generic isofrequency contour plots for a set of parameters $(q_0^{\mathrm{TM}}, q_1^{\mathrm{TM}}, p_0^{\mathrm{TM}}, p_1^{\mathrm{TM}})$ for the TM-polarized modes. It is of imperative importance to mention that the dispersion relations with the four degrees of freedom above, give rise to more advanced isofrequency contours. They provide the possibility to an effective medium description of optical metamaterials with dispersive features, that are impossible to describe with the WSD (local) approach.

Eventually, one seeks to reproduce the local limit, i.e., the limit $\beta_{jj} \to 0$ for a sane convergence analysis. In fact, all results and findings for a non-vanishing nonlocality, i.e., $\beta_{jj} \neq 0$, must converge to the physics of local responses, i.e, $\beta_{jj} = 0$, considering we end up with the same material laws. Therefore, by taking the limit $\beta_{jj} \to 0$, we expect to reproduce the same results as in Sec. 4.1.1. However, here, the limit has to be done carefully. From Eq. (4.14) we note that the β_{jj} is the coefficient for the highest order polynomial (the unknown is k_z). Taking the local limit before solving the equation will yield the Eq. (4.7) for TM-polarization, where we only have one solution[2]. Not problematic at this stage. On the other hand, if one intends to take the local limit after solving the dispersion relation, i.e., at the level of Eq. (4.15). We find that one of the solutions $k_{z,\sigma}^{\mathrm{SYM}}$ converges to k_z^{WSD}, while the other one asymptotically behaves like $\frac{1}{\sqrt{\beta_{jj}}}$, as $\beta_{jj} \to 0$. Consequently, the corresponding eigenmode has an eigenvalue whose imaginary part goes to infinity, and is, therefore, exponentially decaying with negligible contribution, as to be expected.

At any rate, the material parameters β_{jj} cannot be *a priori* set to zero for all metamaterials per se. Only after a comparative analysis with the dispersion relation of a referential metamaterial, through full-wave simulations of Maxwell's equations, we can decide on the importance of $\hat{\beta}^j$. In other terms, if the inclusion of the parameter $\hat{\beta}^j$ leads to a closer matching between the dispersion relations from Eq. (4.14) and to the actual dispersion relations of a referential material, then $\hat{\beta}^j$ has to be taken into account.

4.1.3 Dispersion relation of the SSD model

In this model, instead of retaining the symmetry coefficients $\hat{\beta}^j$, we consider higher-order spatial dispersion terms proportional to $\hat{\gamma}$ in the expansion. This ansatz affects the dispersion relation of both TE and TM-polarization. In this approach, we intentionally do not include $\hat{\beta}^j$ terms as $\hat{\gamma}$ already gives significant improvement to WSD [117]. The goal is, again, to model metamaterials with the least number of free parameters. To proceed, we take the WSD approach as a starting point and extend it by a fourth order term, such that the constitutive relation becomes

$$\tilde{\mathbf{D}}(\mathbf{k}, k_0) = \hat{\epsilon}(k_0)\tilde{\mathbf{E}}(\mathbf{k}, k_0) + \mathbf{k} \times \big(\hat{\alpha}(k_0)\mathbf{k} \times \tilde{\mathbf{E}}(\mathbf{k}, k_0)\big)) + \mathbf{k} \times \mathbf{k} \times \big(\hat{\gamma}(k_0)\mathbf{k} \times \mathbf{k} \times \tilde{\mathbf{E}}(\mathbf{k}, k_0)\big) \,. \tag{4.18}$$

The fourth order term is a canonical extension to the second order contribution. This is particularly important as such term allows the derivation of the additional interface conditions using the weak formulation. It has to be noted that the position of $\hat{\gamma}$ between the cross products cannot be chosen arbitrarily. In Appendix A, we prove using Casimir-Onsager reciprocity relations that both $\hat{\alpha}$ and $\hat{\gamma}$ can only be located in a symmetric

[2]Strictly spoken, two solutions with the same absolute value, but different signs.

fashion, i.e., between an equal number of cross products from left and right[3]. In real space, this would translate into the condition that $\hat{\gamma}$ must be located between the same number of curl operators. Moreover, from a mathematical point of view, if $\hat{\gamma}$ is located before the first or second curl operator, we are not able to derive the required number of interface conditions. The details of this issue requires a subsection by itself and will be discussed in Sec. 4.2. Clearly, with a fourth order constitutive relation, the polynomial degree of the wave-equation increases as well. Meaning, that the number of solutions will be also higher than in the WSD approach. In fact, the dispersion relation for both TE- and TM-polarized modes are biquadratic equations in k_z and k_t. This is in contrast to the dispersion relation of the SYM model, where the consequences of spatial dispersion is only perceptible in the TM-polarization.

The dispersion relation for the TE-polarized case reads as

$$k_t^2 \frac{\mu_{tt}}{\mu_{zz}} + k_z^2 - \gamma_{t^*t^*}\mu_{tt}k_0^2 \left(k_t^2 + k_z^2\right)^2 = \epsilon_{t^*t^*}\mu_{tt}k_0^2\,, \tag{4.19}$$

where according to remark 4.1.2 $\mu_{ii} = \frac{1}{1-k_0^2\alpha_{ii}}$. Obviously, the biquadratic term is proportional to $\hat{\gamma}$. For $\hat{\gamma} \to 0$ the dispersion relation above reduces to the one obtained from WSD (c.f. Eq. (4.7)). Since the electric field in TE-polarization has only a single E_{t^*} component that is essentially nonzero, only the $\gamma_{t^*t^*}$ component comes into play. The solutions to the equation above are

$$\left(k_{z,\sigma}^{\mathrm{SSD}}(k_t,k_0)\right)^2 = -k_t^2 + p_0^{\mathrm{TE}} + \sigma\sqrt{\left(p_0^{\mathrm{TE}}\right)^2 - q_1^{\mathrm{TE}} + 2\left(p_1^{\mathrm{TE}} - p_0^{\mathrm{TE}}\right)k_t^2}\,, \tag{4.20}$$

where $\sigma = \pm 1$ and the frequency-dependent coefficients are

$$q_1^{\mathrm{TE}}(k_0) = \frac{\epsilon_{t^*t^*}}{\gamma_{t^*t^*}}, \qquad p_0^{\mathrm{TE}}(k_0) = \left[2k_0^2\gamma_{t^*t^*}\mu_{tt}\right]^{-1}, \qquad p_1^{\mathrm{TE}}(k_0) = \left[2k_0^2\gamma_{t^*t^*}\mu_{zz}\right]^{-1}. \tag{4.21}$$

In comparison to the WSD and to the SYM models with only two degrees of freedom, here, the dispersion relation has one additional degree of freedom that allows for even more complex isofrequency contours.

Concerning the TM-polarization, the electric field has two nonzero components that couple to $\hat{\gamma}$. Hence, we obtain

$$k_t^2\frac{\epsilon_{tt}}{\epsilon_{zz}} + k_z^2 - k_t^2k_z^2\left(\frac{\epsilon_{tt}}{\epsilon_{zz}}\gamma_{tt} + \gamma_{zz}\right)\mu_{t^*t^*}k_0^2 - \left(k_t^4\frac{\epsilon_{tt}}{\epsilon_{zz}}\gamma_{tt} + k_z^4\gamma_{zz}\right)\mu_{t^*t^*}k_0^2 = \epsilon_{tt}\mu_{t^*t^*}k_0^2\,, \tag{4.22}$$

where both nonlocal material parameters γ_{tt} and γ_{zz} are involved. Again, the local limit can be easily obtained from here by omitting these parameters. The solutions to the dispersion relation above are

$$\left(k_{z,\sigma}^{\mathrm{SSD}}(k_t,k_0)\right)^2 = -\frac{-1}{2}\left(q_0^{\mathrm{TM}} + q_1^{\mathrm{TM}}\right)k_t^2 + p_0^{\mathrm{TM}} + \sigma\sqrt{\left(p_0^{\mathrm{TM}} + \frac{q_0^{\mathrm{TM}} - q_1^{\mathrm{TM}}}{2}k_t^2\right)^2 - p_1^{\mathrm{TM}}}\,, \tag{4.23}$$

with the four degrees of freedom

$$q_0^{\mathrm{TM}} = \frac{\epsilon_{tt}}{\epsilon_{zz}}, \qquad q_1^{\mathrm{TM}} = \frac{\gamma_{zz}}{\gamma_{tt}}, \qquad p_0^{\mathrm{TM}} = \left[2k_0^2\gamma_{tt}\mu_{t^*t^*}\right]^{-1}, \qquad p_1^{\mathrm{TM}} = \frac{\epsilon_{tt}}{\gamma_{tt}}. \tag{4.24}$$

The fields are, once more, a superposition of four plane waves, in which two are forward and two are backwards propagating with pairwise different $|k_{z,\sigma}^{\mathrm{SSD}}(k_t,k_0)|$. Here, we can take the ansatz (4.17) as well. Obviously, retaining higher-order nonlocality gives access

[3]Under the assumption of isotropy, $\hat{\alpha}$ and $\hat{\gamma}$ become a multiples of the identity matrix. Only then, their position can be arbitrarily chosen.

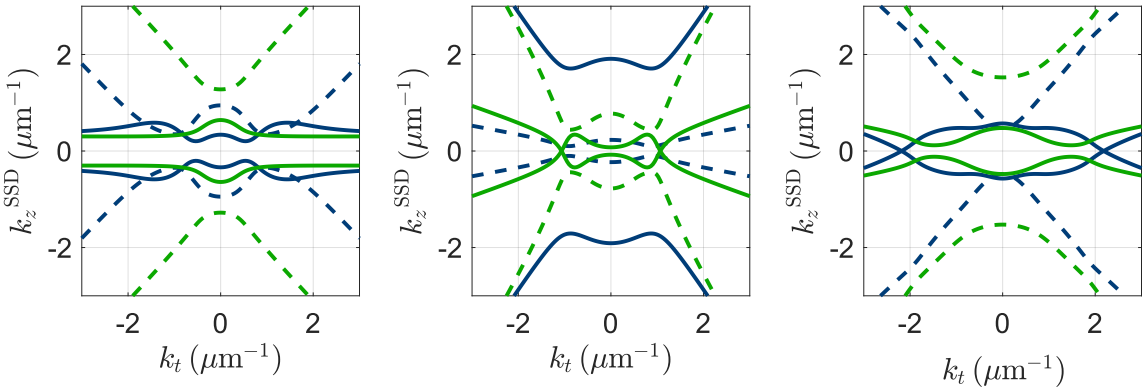

Figure 4.3: Examples of isofrequency contours obtained from the SSD model, decomposed into real (solid) and imaginary (dashed) parts. The $k_{z,+}^{\mathrm{SSD}}$ and $k_{z,-}^{\mathrm{SSD}}$ solutions are, respectively, plotted in blue and green. For the figure on the left corresponds to the TE-polarization with we set $p_0^{\mathrm{TE}} = -1+0.5\mathrm{i}$, $p_1^{\mathrm{TE}} = 1.5-\mathrm{i}$, $q_1^{\mathrm{TE}} = 2-0.5\mathrm{i}$. The center and the right figures belong to the isofrequencies in the TM-polarization with $p_0^{\mathrm{TM}} = 1.5-0.5\mathrm{i}$, $q_0^{\mathrm{TM}} = -2+0.5\mathrm{i}$, $p_1^{\mathrm{TM}} = -2.25-0.1\mathrm{i}$, $q_1^{\mathrm{TM}} = 2.5-\mathrm{i}$ and $p_0^{\mathrm{TM}} = -1+\mathrm{i}$, $q_0^{\mathrm{TM}} = 2-0.5\mathrm{i}$, $p_1^{\mathrm{TM}} = -1-\mathrm{i}$, $q_1^{\mathrm{TM}} = 1+0.5\mathrm{i}$, respectively.

to more advanced isofrequency contours for both TE- and TM-polarizations. In Fig. 4.3, we show the isofrequency contours decomposed into real and imaginary parts for both $k_{k,\pm}^{\mathrm{SSD}}$ solutions for each polarization for a given set of parameters. It is indubitable that Fig. 4.3 demonstrates the enhanced complexity of the isofrequency contours, in comparison to the previously proposed constitutive relations and for a metamaterial with local material laws (WSD). Moreover, even in the paraxial regime, the effect of nonlocality is visible. This becomes clear when we look at the expressions for the dispersion relations for zero transverse wave vector ($k_t = 0$), where we find that $k_{z,+}(0, k_0) \neq k_{z,-}(0, k_0)$, for all models and polarizations that sustain multiple modes. In general, the eigenvalues possess different imaginary parts and the corresponding eigenmodes are attenuated differently. Similarly to the identification procedure in the previous section, the mode with the smallest positive imaginary part will be identified as the fundamental mode. In a slab situation with thickness d_{slab}, this mode could carry the most energy as it is less amortized after propagating the distance d_{slab}.

Once more, the limit $\hat{\gamma} \to 0$ has to be taken carefully. One solution converges to the solution to WSD, and the other solution asymptotically behaves like $\frac{1}{\sqrt{\gamma_{ii}}}$ and diverges. Without loss of generality, let the divergent solution be always $k_{z,-}$.

To conclude this section, we pinpoint two important aspects we can learn from the study of dispersion relations. First of all, with the introduction of nonlocality, i.e., terms that cannot be reformulated to local material parameters using the gauge transformation (3.27), we obtain more advanced isofrequency contours, beyond those offered by the WSD approximation. Optical metamaterials with mesoscopic features show that the dispersion relation of the fundamental mode comprehend isofrequency contours that differ from hyperbola and/or ellipsoids [121], [122]. A clear sign that a nonlocal description of such metamaterials is required. In the second place, nonlocality introduces additional modes. This statement is known long time ago (c.f. Ch.1 of Ref. [50]), and was usually called "new (additional) wave". In spite of that, the additional modes were commonly disregarded, due to their requirement of additional constraints, which have to be set at

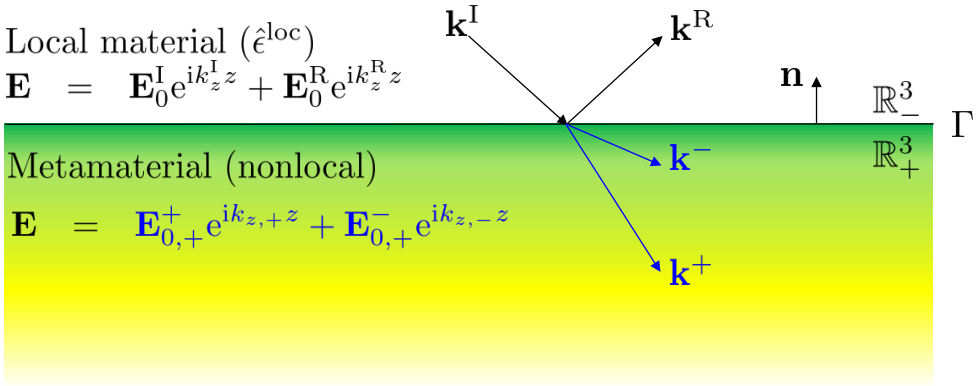

Figure 4.4: Schematics of a half-space problem with an interface $\Gamma = \overline{\mathbb{R}^3_-} \cap \overline{\mathbb{R}^3_+}$ between an ordinary material and a nonlocal metamaterial which, respectively, occupy the half-spaces $\mathbb{R}^3_-$ and $\mathbb{R}^3_+$ and from an interface at $z = 0$. The reflected field amplitude $\mathbf{E}_0^{\mathrm{R}}$ and both transmitted fields $\mathbf{E}_{0,+}^{\pm}$ are the unknown quantities to be found.

the interface between two distinct media.

By analytically solving dispersion relations, the propagation of the fields in bulk can be fully understood. However, this ability to describe the propagation of light in the bulk metamaterial is not yet the whole story. For each model, we further need to know how an external field coming from an external medium can excite these eigenmodes and how light is reflected and transmitted form a slab. To answer these questions, the respective interface conditions must be identified as well. This will be discussed in the following section.

4.2 Additional Interface Conditions

This section is based on a collaboration with the Institute for Analysis (IANA), Karlsruhe Institute for Technology (KIT), Karlsruhe. Credits to the mathematical rigour and, especially, to the clever choice of test functions go to my collaborator Dr. Andrii Khrabustovskyi [64], [117]. After he left KIT the cooperation continued with Dr. Fatima Z. Goffi.

Prior starting the derivation, we would like to stress that we cannot entirely remove the forthcoming mathematical details. Certainly, their involvement is substantial as these interface conditions do not just come out of nowhere but are indeed strictly derived on solid mathematical grounds. This clearly distinguishes our contribution from many others where these interface conditions were introduced on phenomenological grounds [123], [124]. The price to pay for the exact derivation is the additional mathematics, which here, requires the usage of some topics from functional analysis presented in Ch. 2.

When spatial dispersion occurs, the classical continuity equations for the electromagnetic fields, i.e., the continuity of the tangential component of $\mathbf{E}(\mathbf{r}, k_0)$ $\mathbf{H}(\mathbf{r}, k_0)$ and of normal components of $\mathbf{D}(\mathbf{r}, k_0)$ and $\mathbf{B}(\mathbf{r}, k_0)$, are neither sufficient (in terms of number), nor adequate (in terms of correctness) to unambiguously find all amplitudes of the involved modes at the interface. Moreover, due to the complicated expression of the displacement field as a function of the electric field and its spatial derivatives, we cannot simply imply the classical continuity condition for the magnetic field $\mathbf{H}(\mathbf{r}, k_0)$ from Maxwell's equations. To find the correct and the additional interface conditions for our

nonlocal response ansatz, we prefer to study the problem in the real space, where we define the interface $\Gamma = \overline{\mathbb{R}^3_+} \cap \overline{\mathbb{R}^3_-}$ between an ordinary material and a nonlocal metamaterial, which respectively, occupy the half-spaces $\mathbb{R}^3_-$ and $\mathbb{R}^3_+$ and meet at $z = 0$, as depicted in Fig. 4.4. The ordinary material is regarded as homogeneous and shall be fully characterized by a local permittivity $\hat{\epsilon}^{\text{loc}}(k_0)$. Meanwhile, the constitutive relation for the metamaterial including the nonlocal response in real space is given by Eq. (4.1). With $\mathbf{r} = (x, y, z)$, in the whole space we have

$$\mathbf{D}(\mathbf{E}) = \begin{cases} \hat{\epsilon}^{\text{loc}}\mathbf{E}(\mathbf{r}, k_0)\,, & \text{for } z < 0 \\ \hat{\epsilon}\mathbf{E}(\mathbf{r}, k_0) + \nabla \times (\hat{\alpha}\nabla \times \mathbf{E}(\mathbf{r}, k_0)) + \displaystyle\sum_{j\in(x,y,z)} \nabla_j(\hat{\beta}^j \nabla_j \mathbf{E}(\mathbf{r}, k_0)) & \\ \quad + \nabla \times \nabla \times (\hat{\gamma}\nabla \times \nabla \times \mathbf{E}(\mathbf{r}, k_0))\,, & \text{for } z > 0 \end{cases} \tag{4.25}$$

where $\hat{\epsilon}, \hat{\alpha}, \hat{\beta}^j, \hat{\gamma} : \mathbb{R}^3_+ \to \mathbb{C}^{3\times3}$ and $\hat{\epsilon}^{\text{loc}} : \mathbb{R}^3_- \to \mathbb{C}^{3\times3}$ are bounded with $\boldsymbol{\mathcal{E}}$-smoothness[4]. In the context of homogeneous metamaterials, all the material parameters are spatially independent. However, it must be always kept in mind, that they depend on the frequency.

We would like to emphasize once again that, here, mathematics is an essential component. The interface conditions are strictly derived on solid mathematical grounds. For achieving this, we start with the wave equation, which in its strong formulation reads

$$\begin{aligned} \nabla \times \nabla \times \mathbf{E} = k_0^2 \Big[& \bar{\epsilon}\mathbf{E}(\mathbf{r}, k_0) + \nabla \times (\bar{\alpha}\nabla \times \mathbf{E}(\mathbf{r}, k_0)) \\ & + \sum_{j\in(x,y,z)} \nabla_j(\bar{\beta}^j \nabla_j \mathbf{E}(\mathbf{r}, k_0)) + \nabla \times \nabla \times (\bar{\gamma}\nabla \times \nabla \times \mathbf{E}(\mathbf{r}, k_0)) \Big]\,, \end{aligned} \tag{4.26}$$

with the piecewise continuous material parameters

$$\bar{\epsilon} = \begin{cases} \hat{\epsilon}^{\text{loc}} & z < 0 \\ \hat{\epsilon} & z > 0 \end{cases} \qquad \bar{\alpha} = \begin{cases} 0 & z < 0 \\ \hat{\alpha} & z > 0 \end{cases} \qquad \bar{\beta}^j = \begin{cases} 0 & z < 0 \\ \hat{\beta}^j & z > 0 \end{cases} \qquad \bar{\gamma} = \begin{cases} 0 & z < 0 \\ \hat{\gamma} & z > 0 \end{cases}.$$

Prior starting with the derivation, we would like to recap some important facts from Ch. 2. First of all, we shall recall that $\boldsymbol{\mathcal{D}} = \boldsymbol{\mathcal{C}}_0^\infty$, is the space of infinitely continuous differentiable test functions with compact support, and its dual space $\boldsymbol{\mathcal{D}}'$. It is the space of distributions (generalized functions), i.e., the space of linear continuous functionals acting on $\boldsymbol{\mathcal{D}}$. Second, Lemma 2.1.1 stating that every locally integrable function, i.e., elements of $\boldsymbol{\mathcal{L}}^1_{\text{loc}}$ generates a regular distribution in $\boldsymbol{\mathcal{D}}'$. This also holds for locally square integrable functions $\boldsymbol{\mathcal{L}}^2_{\text{loc}}$. The dual mapping $\langle\cdot,\cdot\rangle_{\mathbb{R}^3}$ for integrable functions is given by Eq. (2.3), that reads for $\boldsymbol{\phi} \in \boldsymbol{\mathcal{D}}(\mathbb{R}^3)$ and $\mathbf{f} \in \boldsymbol{\mathcal{L}}^2_{\text{loc}}(\mathbb{R}^3)$

$$\mathbf{F}_{\mathbf{f}}[\boldsymbol{\phi}] := \langle \mathbf{f}, \boldsymbol{\phi}\rangle_{\mathbb{R}^3} = \int_{\mathbb{R}^3} \mathbf{f} \cdot \boldsymbol{\phi}\, \mathrm{d}r\,, \tag{4.27}$$

and $\mathbf{F} \in \boldsymbol{\mathcal{D}}'(\mathbb{R}^3)$. A concrete and useful example can be given is for $\mathbf{E} \in \boldsymbol{\mathcal{L}}^2_{\text{loc}}(\mathbb{R}^3)$. Then the distribution $\nabla \times \mathbf{E} \in \boldsymbol{\mathcal{D}}'(\mathbb{R}^3)$ is defined by the action

$$\nabla \times \mathbf{E}[\boldsymbol{\phi}] = \langle \nabla \times \mathbf{E}, \boldsymbol{\phi}\rangle_{\mathbb{R}^3} = \langle \mathbf{E}, \nabla \times \boldsymbol{\phi}\rangle_{\mathbb{R}^3}\,, \tag{4.28}$$

[4]Recall from Ch. 2 that $\boldsymbol{\mathcal{E}}$ is the space of infinitely differentiable functions.

which resembles integration by parts, where the boundary terms vanished due to $\boldsymbol{\phi}$ being compactly supported.

The third important matter that should be considered is the concept of weak formulation and traces. We described the tool in Sec. 2.2. We are going to use this tool for deriving the interface conditions in the next subsection. Strongly connected to this, is theorem 2.2.1, which gives strong statements to the continuity of normal and tangential field components at the interface, when specific regularity conditions are fulfilled. This theorem will be extensively used to prove some of the interface conditions.

4.2.1 Weak solutions

Due to the discontinuity of the material parameters (4.2) at the interface, i.e., the coefficients in the wave equation (4.26) above, it is impossible to consider the PDE in the classical sense [73]. To this end, a reasonable generalised ansatz is required. The unknown field $\mathbf{E}(\mathbf{r}, k_0)$ is supposed to solve Eq. (4.26) in $\mathbb{R}^3$, with some discontinues at the interface. One might, therefore, preliminary require that the restrictions $\mathbf{E}_-$ and $\mathbf{E}_+$ of $\mathbf{E}$ to the respective half-spaces $\mathbb{R}^3_-$ and $\mathbb{R}^3_+$ to satisfy the following regularity

$$\mathbf{E}_- \in \boldsymbol{\mathcal{C}}^4(\overline{\mathbb{R}^3_-}) \text{ and } \mathbf{E}_+ \in \boldsymbol{\mathcal{C}}^4(\overline{\mathbb{R}^3_+})\,, \tag{4.29}$$

where $\boldsymbol{\mathcal{C}}^4$ represents the space of four times continuously differentiable functions. Under the assumption of regularity (4.29), the interface conditions can be derived by means of partial integrations of continuous functions, i.e., by their restrictions on the interface separating the two half-spaces $\mathbb{R}^3_-$ and $\mathbb{R}^3_+$. However, we drop this assumption, and impose weaker regularity conditions (4.32), which allows us to calculate the interface conditions by evaluating the traces of weak functions.

Already at this stage, we can specify regularity conditions for the electric field $\mathbf{E}$ from a physical point of view. In particular, regarding the function spaces in which they are defined. Knowing these spaces is advantageous when it comes to the identification of the interface condition, which requires the analysis of the function space in which the solutions to Eq. (4.26) exist. From a physical perspective, it is legitimate to require that both the electric field $\mathbf{E} \in \boldsymbol{\mathcal{L}}^2_{\text{loc}}(\mathbb{R}^3)$ and the magnetic flux $\mathbf{B} \in \boldsymbol{\mathcal{L}}^2_{\text{loc}}(\mathbb{R}^3)$. This fact can be justified from the measurability of these functions everywhere in space, by means of the Aharonov-Bohm effect [125] or Lorentz force [81]. In addition, for time harmonic waves, Faraday's law reads $\nabla \times \mathbf{E}(\mathbf{r}, k_0) = \mathrm{i}k_0\mathbf{B}(\mathbf{r}, k_0)$. Hence, we obtain $\nabla \times \mathbf{E} \in \boldsymbol{\mathcal{L}}^2_{\text{loc}}(\mathbb{R}^3)$ as well. Ultimately, we have

$$\mathbf{E} \in \boldsymbol{\mathcal{H}}_{\text{loc}}(\text{curl}, \mathbb{R}^3)\,. \tag{4.30}$$

At this particular moment, we can already state the first interface condition by using Theorem 2.2.1. In other words, the continuity of the tangential components of $\mathbf{E}$ holds

$$(\mathbf{E}_+ - \mathbf{E}_-) \times \mathbf{n} = 0\,. \tag{4.31}$$

In analogy to the definition of the action (4.28), we can now define the action of $\nabla \times \mathbf{E}$. We would like to mention that regularity (4.30) is not given by the wave equation, but necessary to define the weak solutions to the wave equation. Actually, from the second term on the RHS of Eq. (4.26) we only have $\nabla \times \mathbf{E} \in \boldsymbol{\mathcal{L}}^2_{\text{loc}}(\mathbb{R}^3_+)$ and 0 in $\mathbb{R}^3_-$. From the third term on the RHS of the wave equation (4.26), we additionally require that for all $j \in \{x, y, z\}$: $\nabla_j \mathbf{E} \in \boldsymbol{\mathcal{L}}^2_{\text{loc}}(\mathbb{R}^3_+)$. Together with $\mathbf{E} \in \boldsymbol{\mathcal{L}}^2_{\text{loc}}(\mathbb{R}^3_+)$, we obtain $\mathbf{E} \in \boldsymbol{\mathcal{H}}^1_{\text{loc}}(\mathbb{R}^3_+)$.

The fourth term in the wave equation declares the requirement of $\nabla\times\nabla\times\mathbf{E} \in \boldsymbol{\mathcal{L}}^2_{\mathrm{loc}}(\mathbb{R}^3_+)$. In the final analysis, we require that the field $\mathbf{E}$ and its curl-derivatives satisfy the following regularities:

$$\mathbf{E} \in \boldsymbol{\mathcal{H}}_{\mathrm{loc}}(\mathrm{curl}, \mathbb{R}^3)\,, \mathbf{E} \in \boldsymbol{\mathcal{H}}^1_{\mathrm{loc}}(\mathbb{R}^3)\,, \nabla \times \nabla \times \mathbf{E} \in \boldsymbol{\mathcal{L}}^2_{\mathrm{loc}}(\mathbb{R}^3_+)\,. \tag{4.32}$$

Now that we have identified the function spaces of the solution and its partial derivatives, Eq. (4.26) can be understood as an equality in $\boldsymbol{\mathcal{D}}'(\mathbb{R}^3)$. Hence, according to the procedures described in Sec. 2.2, the weak formulation of the wave equation can be obtained by first multiplying with a test function $\boldsymbol{\phi} \in \boldsymbol{\mathcal{D}}(\mathbb{R}^3)$ and second integrating over $\mathbb{R}^3$. By using the definition of the generalized derivatives (see Def. (2.5)) we can shift the derivatives to the test function $\boldsymbol{\phi}$. Finally, the weak form of the wave equation reads for all $\boldsymbol{\phi} \in \boldsymbol{\mathcal{D}}(\mathbb{R}^3)$:

$$\begin{aligned}\langle \nabla \times \mathbf{E}, \nabla \times \boldsymbol{\phi}\rangle_{\mathbb{R}^3} =& k_0^2\Big[\langle \hat{\epsilon}^{\mathrm{loc}}\mathbf{E}, \boldsymbol{\phi}\rangle_{\mathbb{R}^3_-} + \langle \hat{\epsilon}\mathbf{E}, \boldsymbol{\phi}\rangle_{\mathbb{R}^3_+} + \langle \hat{\alpha}\nabla \times \mathbf{E}, \nabla \times \boldsymbol{\phi}\rangle_{\mathbb{R}^3_+} \\ &- \sum_{j\in\{x,y,z\}} \langle \hat{\beta}^j \nabla_j \mathbf{E}, \nabla_j \boldsymbol{\phi}\rangle_{\mathbb{R}^3_+} + \langle \hat{\gamma}\nabla \times \nabla \times \mathbf{E}, \nabla \times \nabla \times \boldsymbol{\phi}\rangle_{\mathbb{R}^3_+}\Big]\end{aligned} \tag{4.33}$$

If the vector field $\mathbf{E} : \mathbb{R}^3 \to \mathbb{C}^3$ meets the regularity conditions (4.32) and satisfies the weak form (4.33), then it is said to be a weak solution to the (strong) wave equation (4.26). *A priori*, it is not clear whether there is only one weak solution. Some existence and uniqueness tools that we mentioned in Sec. 2.2 may serve well. To not ending up with being too distracted from the core physics, we won't discuss the issue of existence and uniqueness in this chapter. Now, let $\mathbf{E}$ be a weak solution to Eq. (4.26)[5]. Then $\nabla\times\nabla\times\mathbf{E} \in \boldsymbol{\mathcal{L}}^2_{\mathrm{loc}}(\mathbb{R}^3_-)$.

Proof: Let $\boldsymbol{\phi} \in \boldsymbol{\mathcal{D}}(\mathbb{R}^3_-)$. Together with $\mathbf{E} \in \boldsymbol{\mathcal{H}}_{\mathrm{loc}}(\mathrm{curl}, \mathbb{R}^3)$ we have

$$\langle \mathbf{E}, \nabla \times \nabla \times \boldsymbol{\phi}\rangle_{\mathbb{R}^3_-} = \langle \nabla \times \mathbf{E}, \nabla \times \boldsymbol{\phi}\rangle_{\mathbb{R}^3_-} = \langle \underbrace{\nabla \times \nabla \times \mathbf{E}}_{\in \boldsymbol{\mathcal{L}}^2_{\mathrm{loc}}(\mathbb{R}^3_-)}, \boldsymbol{\phi}\rangle_{\mathbb{R}^3_-}\,.$$

The first two integrals exist due to the assumption of $\mathbf{E}$ and $\nabla \times \mathbf{E}$ being in $\boldsymbol{\mathcal{L}}^2_{\mathrm{loc}}(\mathbb{R}^3_-)$, respectively. The last equation holds by arguments of duality. By duality $\nabla \times \nabla \times \mathbf{E}$ must be in $\boldsymbol{\mathcal{D}}'(\mathbb{R}^3_-)$ in which $\boldsymbol{\mathcal{L}}^2_{\mathrm{loc}}(\mathbb{R}^3_-)$ is a dense subset. Moreover, we have

$$\nabla \times \nabla \times \mathbf{E} = k_0^2 \hat{\epsilon}^{\mathrm{loc}}\mathbf{E}\,, \text{ for almost all } \mathbf{r} \in \mathbb{R}^3_-\,. \tag{4.34}$$

Note that "almost all" means that (4.34) holds everywhere in $\mathbb{R}^3_+$ except on a set of Lebesque measure zero. Integrating over such set will not give a contribution. Analogously we can show that, by taking $\boldsymbol{\phi} \in \boldsymbol{\mathcal{D}}(\mathbb{R}^3_+)$ that

$$\nabla \times (\hat{\alpha}\nabla \times \mathbf{E}) + \sum_{j\in(x,y,z)} \nabla_j(\hat{\beta}^j \nabla_j \mathbf{E}) + \nabla \times \nabla \times (\hat{\gamma}\nabla \times \nabla \times \mathbf{E}) \in \boldsymbol{\mathcal{L}}^2_{\mathrm{loc}}(\mathbb{R}^3_+) \tag{4.35}$$

and

$$\begin{aligned}\nabla \times \nabla \times \mathbf{E} = k_0^2\Big(&\hat{\epsilon}\mathbf{E} + \nabla \times \hat{\alpha}(\nabla \times \mathbf{E}) \\ &+ \sum_{j\in\{x,y,z\}} \nabla_j(\hat{\beta}^j \nabla_j \mathbf{E}) + \nabla \times \nabla \times \hat{\gamma}(\nabla \times \nabla \times \mathbf{E})\Big)\,, \text{ for almost all } \mathbf{r} \in \mathbb{R}^3_+\,.\end{aligned} \tag{4.36}$$

[5]Please note that this also assumes that $\mathbf{E}$ satisfies the regularity condition (4.32)

Here, it is important to mention that the regularity property above corresponds to the whole sum of the functions and not to the individual terms. Therefore, we cannot simply imply that every term in Eq. (4.35) is in $\in \boldsymbol{\mathcal{L}}^2_{\mathrm{loc}}(\mathbb{R}^3_+)$.

With this, we have studied the weak solutions in the open half-spaces $\mathbb{R}^3_\pm$. In the following, we analyze them at the interface Γ, and in particular, derive the interface conditions.

4.2.2 Derivation of the interface conditions

Once more, we start by assuming $\mathbf{E}$ being a weak solution to the wave equation (4.26) . We recall that $\mathbf{E}_\pm$ are the restrictions of $\mathbf{E}$ to $\mathbb{R}^3_\pm$. Nonetheless, in the volume integrals over $\mathbb{R}^3_\pm$ we will remain using the notation $\mathbf{E}$, while in the surface integrals over the interface Γ, we explicitly write $\mathbf{E}_\pm$, to denote at which side of the interface the integral holds. Moreover, we will distinguish between fundamental and auxiliary interface conditions. The latter ones directly follow from Maxwell's equations and not from the weak formulation of the wave equation. However, they are needed for further simplification of the Fresnel Matrix, as we will see in Sec. 4.3.

Fundamental interface conditions: Let $\mathbf{n}$ be the vector normal to the interface Γ (c.f. Fig. 4.4). We now show that if $\mathbf{E}$ is a weak solution to Eq. (4.26) and it's restriction satisfy the regularity conditions (4.29), then $\mathbf{E}$ satisfies the following interface conditions on Γ:

$$(\mathbf{E}_- - \mathbf{E}_+) \times \mathbf{n} = 0\,, \tag{IC$_1$}$$

$$\begin{aligned}(\nabla \times \mathbf{E}_- - \nabla \times \mathbf{E}_+) \times \mathbf{n} + k_0^2(\hat{\alpha}\nabla \times \mathbf{E}_+) \times \mathbf{n} \\ +k_0^2(\nabla \times \hat{\gamma}\nabla \times \nabla \times \mathbf{E}_+) \times \mathbf{n} - k_0^2(\mathbb{1} - \mathbf{n}\mathbf{n}^{\mathrm{T}})\hat{\beta}^z\nabla_z\mathbf{E}_+ = 0\,,\end{aligned} \tag{IC$_2$}$$

$$(\hat{\gamma}\nabla \times \nabla \times \mathbf{E}_+) \times \mathbf{n} = 0\,, \tag{IC$_3$}$$

$$(\hat{\beta}^z\nabla_z\mathbf{E}_+) \cdot \mathbf{n} = 0\,. \tag{IC$_4$}$$

Conversely, if $\mathbf{E}$ satisfies regularity (4.29), independently solves the wave equation in $\mathbb{R}^3_+$ and $\mathbb{R}^3_-$, and additionally satisfies the interface conditions (IC$_1$)-(IC$_4$), then $\mathbf{E}$ is a weak solution to Eq. (4.26). The derived interface conditions above deserve some physical interpretation. The first interface condition simply states that the tangential component of the electric field is continuous across the interface. This we already know from common textbooks (e.g. Ref. [81] page 18). The second interface condition states that the discontinuity of the tangential component of curl $\mathbf{E}$ is caused by the nonlocal parameters $\hat{\alpha}$, $\hat{\beta}^z$, and $\hat{\gamma}$. In the limit of weak nonlocality or the WSD approximation, where $\hat{\beta}^j \to 0$ and $\hat{\gamma} \to 0$, we obtain the known interface condition for a local magnetic medium. In the WSD limit, only the first line in condition (IC$_2$) remains and reduces to

$$\begin{aligned}&(\nabla \times \mathbf{E}_- - \nabla \times \mathbf{E}_+) \times \mathbf{n} + k_0^2(\hat{\alpha}\nabla \times \mathbf{E}_+) \times \mathbf{n} = \\ &(\nabla \times \mathbf{E}_- - (\mathbb{1} - k_0^2\hat{\alpha})\nabla \times \mathbf{E}_+) \times \mathbf{n} = 0\,.\end{aligned}$$

With $\nabla \times \mathbf{E}(\mathbf{r}, k_0) = \mathrm{i}k_0\mathbf{B}(\mathbf{r}, k_0)$ and with the identification $\hat{\mu}^{-1}(k_0) = (\mathbb{1} - k_0^2\hat{\alpha}(k_0))$ we obtain the following classical continuity condition

$$(\mathrm{IC}_2) \Rightarrow (\mathbb{1}^{-1}\mathbf{B}_- - \hat{\mu}^{-1}\mathbf{B}_+) \times \mathbf{n} = (\mathbf{H}_- - \mathbf{H}_+) \times \mathbf{n} = 0\,. \tag{4.37}$$

This essentially means that in the absence of strong spatial dispersion the continuity of the tangential component of $\mathbf{H}$ across the interface is preserved. In fact, this is what we expect from this limit. Only by the introduction of the nonlocal parameters $\hat{\beta}^z$ and $\hat{\gamma}$, the continuity of $\mathbf{H}$ is broken.

Next, the interface conditions (IC_3) and (IC_4) are actually the additional ones and are directly proportional to the nonlocal parameters. At the first glance, they paradoxically seem to state that, respectively, the tangential and normal components of the field derivatives are zero at the interface. However, from the analysis of the dispersion relation of nonlocal media, we know that the eigenmodes are more than a single plane wave and additional modes exist. Meaning, that $\mathbf{E}_+$ is actually a superposition of multiple plane waves which renders (IC_3) and (IC_4) actually a sum of plane waves with different propagation constants $k_{z,\sigma}$. Precisely with both $\hat{\beta}^j$ and $\hat{\gamma}$ being simultaneously nonzero, $\mathbf{E}_+$ is a superposition of three forward propagating plane waves. This case requires the analysis of the dispersion relation with both $\hat{\beta}^j$ and $\hat{\gamma}$, which renders the wave Eq. (4.3) being a polynomial for k_z^2 of order 3. Furthermore, since we wish to model metamaterials with the least number of parameters, we intentionally omit this case in the analysis of the dispersion relation. The cases where one of the nonlocal parameters is zero were studied in Sec. 4.1. There, for each situation we find that we obtain two modes per propagation direction. This suggests that at an interface between two half-spaces, there are two forward propagating (transmitted) field amplitudes and one reflected field amplitude to find. To identify these three unknowns, three interface conditions are needed. Depending on the model, either condition (IC_3) or (IC_4) plays the role of the additional interface condition.

In Fig. 4.4 we show the situation of a half-space problem in which an incident field with incidence wave vector $\mathbf{k}^I$ coming from an ordinary material, gets reflected with $\mathbf{k}^R$ in the same half-space and transmitted into the nonlocal metamaterial to two plane waves with $\mathbf{k}_\pm$. Note that in general, there also exist two backward propagating solutions. They do not contribute here, as they won't give any feedback from the *fictitious* second interface at $+\infty$. Yet, in the slab problem (see e.g. Fig 4.5 with finite thickness d_{slab}, these backward (reflected) mode from the second interface at $z = d_{\mathrm{slab}}$ must be considered.

Auxiliary interface conditions: Additionally, we have $\mathbf{B}$ and $\nabla \cdot \mathbf{B}$ in $\boldsymbol{\mathcal{L}}^2_{\mathrm{loc}}(\mathbb{R}^3)$. Per definition this also means that $\mathbf{B} \in \boldsymbol{\mathcal{H}}_{\mathrm{loc}}(\mathrm{div}, \mathbb{R}^3)$ and according to Theorem 2.2.1 we have continuity of the normal component of $\mathbf{B}$. Using Faraday's law, we obtain

$$(\nabla \times \mathbf{E}_- - \nabla \times \mathbf{E}_+) \cdot \mathbf{n} = 0\,. \tag{IC$_5$}$$

Under the assumption of local constitutive relations, we have $\mathbf{D} = \bar{\epsilon}\mathbf{E} \in \boldsymbol{\mathcal{L}}^2_{\mathrm{loc}}(\mathbb{R}^3)$. Using Gauss law we have $\nabla \cdot (\bar{\epsilon}\mathbf{E}) = 0$, which is obviously also an element of $\boldsymbol{\mathcal{L}}^2_{\mathrm{loc}}(\mathbb{R}^3)$. Hence, $\bar{\epsilon}\mathbf{E} \in \boldsymbol{\mathcal{H}}_{\mathrm{loc}}(\mathrm{div}, \mathbb{R}^3)$ and, again by exploiting Theorem 2.2.1, we obtain $(\hat{\epsilon}^{\mathrm{loc}}\mathbf{E}_- - \hat{\epsilon}\mathbf{E}_+) \cdot \mathbf{n} = 0$, i.e., the classical continuity condition for the normal component of the displacement field. However, with retaining a nonlocal coupling term of longitudinal type, i.e. $\hat{\beta}^j \neq 0$, traces at the interface do not vanish and we cannot imply that $\mathbf{D} \in \boldsymbol{\mathcal{L}}^2_{\mathrm{loc}}(\mathbb{R}^3)$. In fact, we obtain for $\hat{\beta}^j \neq 0$ the following interface condition

$$\left(\hat{\epsilon}^{\mathrm{loc}}\mathbf{E} - -\hat{\epsilon}\mathbf{E}_+ - \sum_{j\in\{x,y,z\}} \nabla_i(\hat{\beta}^j \nabla_j \mathbf{E}_+)\right) \cdot \mathbf{n} - \nabla_\Gamma \cdot (\beta^z \nabla_z E_{z,+}) = 0\,, \tag{IC$_6$}$$

with the tangential differential operator $\nabla_\Gamma = (\nabla_x, \nabla_y, 0)$ on the surface Γ. The interface conditions (IC_1)-(IC_4) are the fundamental ones and necessary, to unambiguously link the field amplitudes at the interface. The remaining interface conditions, i.e., conditions (IC_5)-(IC_6) are the auxiliary ones and are only necessary to simplify the Fresnel matrix which will be constructed in Sec. 4.3. Depending on the polarization of the incident light, one of the auxiliary interface conditions trivially yields $0 = 0$ and is, therefore, redundant. For instance, For the TE-polarization there is no electric field component normal to the interface, i.e., no $\mathbf{E}_z$ component. Hence (IC_6) yields $0 = 0$ and no information can be gained from there. Following similar augments for the TM-polarization, we find that (IC_5) reduces to $0 = 0$, as there is no magnetic field component normal to the interface or, equivalently, $\nabla \times \mathbf{E}$ is purely tangential to the interface in TM mode.

Until now, some of the interface condition were just written down as they are. In the following, we shall prove (derive) them one by one. Please note that the proofs, that are not based on Theorem 2.2.1, are done by my collaborator Dr. Andrii Khrabustovskyi. Credits to the clever choice for the appropriate test functions go to him. This section was first published in the preprint [64] with more mathematical details and then adapted to the physics community in Ref. [126].

Derivation of the first and fifth interface condition

Since per supposition $\mathbf{E} \in \boldsymbol{\mathcal{H}}_{\mathrm{loc}}(\mathrm{curl}, \mathbb{R}^3)$, the interface conditions (IC_1) and (IC_5) directly follow from theorem 2.2.1.

Derivation of the second interface condition

The proof of the second interface condition requires some calculations and is based on the analysis in Refs. [64], [117]. To this end, let's consider the weak form (4.33) of the wave equation and decompose the integrals into a sum of integrals over the two half-spaces $\mathbb{R}^3_-$ and $\mathbb{R}^3_+$. Then, we reconstruct the strong form of the wave equation by partial integrations, such that we the derivatives on $\boldsymbol{\phi}$ are shifted back to $\mathbf{E}$. Finally, we separate the terms into volume integrals $\mathbb{R}^3$, $\mathbb{R}^3_-$, and $\mathbb{R}^3_+$ and into surface integrals over Γ. The latter integrals will directly yield the second interface condition (IC_2). By doing so, we obtain

$$
\begin{aligned}
&\langle \nabla \times \nabla \times \mathbf{E}, \boldsymbol{\phi} \rangle_{\mathbb{R}^3} - k_0^2 \langle \hat{\epsilon}^{\mathrm{loc}} \mathbf{E}, \boldsymbol{\phi} \rangle_{\mathbb{R}^3_-} \\
&- k_0^2 \langle \hat{\epsilon}\mathbf{E} + \nabla \times (\hat{\alpha} \nabla \times \mathbf{E}) + \sum_{j \in \{x,y,z\}} \nabla_j (\hat{\beta}^j \nabla_j \nabla_j \mathbf{E}) + \nabla \times \nabla \times \hat{\gamma} (\nabla \times \nabla \times \mathbf{E}_+), \boldsymbol{\phi} \rangle_{\mathbb{R}^3_+} \\
&= \langle \big(\nabla \times \mathbf{E}_- - \nabla \times \mathbf{E}_+ + k_0^2 \hat{\alpha} \nabla \times \mathbf{E}_+ + k_0^2 \nabla \times (\gamma \nabla \times \nabla \times \mathbf{E}_+) \big) \times \mathbf{n}, \boldsymbol{\phi} \rangle_\Gamma \\
&+ k_0^2 \langle (\hat{\gamma} \nabla \times \nabla \times \mathbf{E}_+) \times \mathbf{n}, \nabla \times \boldsymbol{\phi} \rangle_\Gamma - k_0^2 \langle \hat{\beta}^z \nabla_z \mathbf{E}_-, \boldsymbol{\phi} \rangle_\Gamma \,. \qquad (4.38)
\end{aligned}
$$

Note the different signs in front of $\mathbf{E}_+$ and $\mathbf{E}_-$ that arise from the fact that the normal vector $\mathbf{n}$ is pointing once outside and once inside the integration regions $\mathbb{R}^3_+$ and $\mathbb{R}^3_-$, respectively. The LHS of Eq. (4.38) represents the wave equation on both half-spaces $\mathbb{R}^3_-$ and $\mathbb{R}^3_+$. According to Eqs. (4.34) and (4.36), the LHS vanishes and only the integrals

over the interface Γ remain, which can be recast in the following way:

$$\begin{aligned}&\langle(\nabla\times\mathbf{E}_- - \nabla\times\mathbf{E}_+)\times\mathbf{n} + k_0^2(\hat{\alpha}\nabla\times\mathbf{E}_+)\times\mathbf{n}\\&+ k_0^2\left(\nabla\times(\hat{\gamma}\nabla\times\nabla\times\mathbf{E}_+)\right)\times\mathbf{n} - k_0^2(\mathbb{1}-\mathbf{n}\mathbf{n}^{\mathrm{T}})\hat{\beta}^z\nabla_z\mathbf{E}_+, \boldsymbol{\phi}\rangle_\Gamma\\&+ k_0^2\langle(\hat{\gamma}\nabla\times\nabla\times\mathbf{E}_+)\times\mathbf{n}, \nabla\times\boldsymbol{\phi}\rangle_\Gamma - k_0^2\langle\mathbf{n}\mathbf{n}^{\mathrm{T}}\hat{\beta}^z\nabla_z\mathbf{E}_-, \boldsymbol{\phi}\rangle_\Gamma = 0\,. \end{aligned}\tag{4.39}$$

Now, by suitably choosing the test functions, we can show that the integrals above are indeed zero. Let $\boldsymbol{\phi}\in\boldsymbol{\mathcal{D}}(\mathbb{R}^3)$ take the form

$$\boldsymbol{\phi}(\mathbf{r}) = (\phi_1(x,y)\eta(z), \phi_2(x,y)\eta(z), 0)^{\mathrm{T}}\,,$$

where ϕ_1, $\phi_1(x,y)\in\mathcal{D}(\mathbb{R}^2)$ and $\eta\in\mathcal{D}(\mathbb{R})$ being a mollifier. Additionally, let $\eta(z)=1$ for $|z|<\delta$, in a way the graph of η resembles the curve in Fig. 3.1. Hence, we obtain $\nabla\times\boldsymbol{\phi} = (-\phi_2\eta', \phi_1\eta', (\nabla_x\phi_2 - \nabla_y\phi_1)\eta)^{\mathrm{T}}$. Evaluated at the interface Γ, we obtain with $\eta'=0$

$$\nabla\times\boldsymbol{\phi}|_\Gamma = (0,0,\nabla_x\phi_2 - \nabla_y\phi_1)^{\mathrm{T}}\,.$$

Since the z-component of $\boldsymbol{\phi}$ is zero, the third integral in Eq. (4.39) disappears. Furthermore, the second term Eq. (4.39) vanishes as well. In fact, the integrand is the following scalar product, restricted at the interface Γ:

$$k_0^2\left(\hat{\gamma}\nabla\times\nabla\times\mathbf{E}_+\right)\times\mathbf{n})\cdot(\nabla\times\boldsymbol{\phi}|_\Gamma) = (\hat{\gamma}\nabla\times\nabla\times\mathbf{E}_+)\cdot(\mathbf{n}\times(\nabla\times\boldsymbol{\phi}|_\Gamma)) = 0\,.$$

The first equation holds due to the equality of the scalar triple product under symmetric permutation and the commutativity of the dot product. The second equation holds since $\mathbf{n}$ and $\nabla\times\boldsymbol{\phi}|_\Gamma$ are colinear. After all, Eq. (4.39) reduces to

$$\begin{aligned}&\langle(\nabla\times\mathbf{E}_- - \nabla\times\mathbf{E}_+)\times\mathbf{n} + k_0^2(\hat{\alpha}\nabla\times\mathbf{E}_+)\times\mathbf{n}\\&+ k_0^2\left(\nabla\times(\hat{\gamma}\nabla\times\nabla\times\mathbf{E}_+)\right)\times\mathbf{n} - k_0^2(\mathbb{1}-\mathbf{n}\mathbf{n}^{\mathrm{T}})\hat{\beta}^z\nabla_z\mathbf{E}_+, (\phi_1,\phi_2,0)^{\mathrm{T}}\rangle_\Gamma = 0\,. \end{aligned}\tag{4.40}$$

At last, since ϕ_1 and ϕ_2 are arbitrary test functions, we deduce from Eq. (4.40) the second interface condition (IC_2).

Derivation of the third interface condition

Concerning the third interface condition, we start from Eq. (4.39) and by choosing the test function $\boldsymbol{\phi}\in\boldsymbol{\mathcal{D}}(\mathbb{R}^3)$, such that

$$\boldsymbol{\phi}(\mathbf{r}) = (\phi_2(x,y)z\eta(z), -\phi_1(x,y)z\eta(z), 0)^{\mathrm{T}}\,.$$

As in the previous proof, ϕ_1, $\phi_1(x,y)\in\mathcal{D}(\mathbb{R}^2)$ and $\eta\in\mathcal{D}(\mathbb{R})$, with $\eta|_{\{|z|<\delta\}}=1$ for some $\delta>0$. With this clever choice[64], we obtain $\boldsymbol{\phi}$ and $\nabla\times\boldsymbol{\phi}$ at the interface Γ that, respectively, read

$$\boldsymbol{\phi}|_\Gamma = 0\,,\qquad \nabla\times\boldsymbol{\phi}|_\Gamma = (\phi_1,\phi_2,0)^{\mathrm{T}}\,.$$

Obviously, with $\boldsymbol{\phi}|_\Gamma=0$, the first and last term in Eq. (4.39) are zero. Thus, we get

$$\langle(\hat{\gamma}\nabla\times\nabla\times\mathbf{E}_+)\times\mathbf{n}, (\phi_1,\phi_2,0)^{\mathrm{T}}\rangle_\Gamma = 0\,.\tag{4.41}$$

Considering ϕ_1 and ϕ_2 being arbitrary test functions, we conclude from Eq. (4.41) the third interface condition (IC_3).

Derivation of the fourth interface condition

Ultimately, due to the interface conditions (IC_2) and (IC_3), the first two integrals in Eq. (4.39) disappear for any arbitrary test function $\boldsymbol{\phi} \in \boldsymbol{\mathcal{D}}(\mathbb{R}^3)$, and finally, it remains

$$\langle \mathbf{n}\mathbf{n}^{\mathrm{T}} \hat{\beta}^z \nabla_z \mathbf{E}_+, \boldsymbol{\phi} \rangle_\Gamma = 0\,, \tag{4.42}$$

which yields the fourth interface condition (IC_4).

Derivation of the sixth interface condition

Now, let us prove the sixth and last interface condition. As previously mentioned, by the introduction of the nonlocal parameter $\hat{\beta}^j$, we cannot conclude that $\mathbf{D} \in \boldsymbol{\mathcal{H}}_{\mathrm{loc}}(\mathrm{div}, \mathbb{R}^3)$ and, thus, the continuity of its normal component. To derive the corresponding interface condition, let us choose a curl-free test function, i.e.,

$$\boldsymbol{\phi} = \nabla \psi\,,$$

with the scalar test function with compact support. Inserting this test function in the weak form of the wave equation (4.33), all terms proportional to $\nabla \times \boldsymbol{\phi}$ vanish and we obtain

$$\langle \hat{\epsilon}^{\mathrm{loc}} \mathbf{E}, \nabla \psi \rangle_{\mathbb{R}^3_-} + \langle \hat{\epsilon} \mathbf{E}, \nabla \psi \rangle_{\mathbb{R}^3_+} - \sum_{j \in \{x,y,z\}} \langle \hat{\beta}^j \nabla_j \mathbf{E}, \nabla_j \nabla \psi \rangle_{\mathbb{R}^3_+} = 0\,. \tag{4.43}$$

Moreover, let us assume that $\mathrm{supp}(\psi) \subset \mathbb{R}^3_+$. Integrating by parts in Eq. (4.43) yields

$$\forall \psi \in \mathcal{D}(\mathbb{R}^3_+) : \Big\langle \nabla \cdot \big(\hat{\epsilon} \mathbf{E} + \sum_{j \in \{x,y,z\}} \nabla_j (\hat{\beta}^j \nabla_j \mathbf{E}) \big), \psi \Big\rangle_{\mathbb{R}^3_+}\,. \tag{4.44}$$

Additionally, since $\mathcal{D}(\mathbb{R}^3_+)$ is a dense subset of $\mathcal{L}^2(\mathbb{R}^3_+)$, it holds

$$\nabla \cdot \big(\hat{\epsilon} \mathbf{E} + \sum_{j \in \{x,y,z\}} \nabla_j (\hat{\beta}^j \nabla_j \mathbf{E}) \big) = 0 \ \text{ for almost all } \mathbf{r} \in \mathbb{R}^3_+\,. \tag{4.45}$$

Along the same lines, by using $\psi \in \mathcal{D}(\mathbb{R}^3_-) \big(\subset \mathcal{L}^2(\mathbb{R}^3_-)$, dense$\big)$, we obtain

$$\nabla \cdot \big(\hat{\epsilon}^{\mathrm{loc}} \mathbf{E} \big) = 0 \ \text{ for almost all } \mathbf{r} \in \mathbb{R}^3_-\,. \tag{4.46}$$

Next, by plugging an arbitrary $\psi \in \mathcal{D}(\mathbb{R}^3)$ into Eq. (4.43), and subsequently integrating by parts in each half-spaces $\mathbb{R}^3_\pm$, we obtain

$$\begin{aligned} &\langle \nabla \cdot \big(\hat{\epsilon}^{\mathrm{loc}} \mathbf{E} \big), \psi \rangle_{\mathbb{R}^3_-} + \langle \nabla \cdot \big(\hat{\epsilon} \mathbf{E} + \sum_{j \in \{x,y,z\}} \nabla_j (\hat{\beta}^j \nabla_j \mathbf{E}) \big), \psi \rangle_{\mathbb{R}^3_+} \\ &\Big\langle \big(\hat{\epsilon}^{\mathrm{loc}} \mathbf{E}_- - \hat{\epsilon} \mathbf{E}_+ - \sum_{j \in \{x,y,z\}} \nabla_j (\hat{\beta}^j \nabla_j \mathbf{E}_+) \big) \cdot \mathbf{n}, \psi \Big\rangle_\Gamma + \langle \hat{\beta}^z \nabla_z \mathbf{E}_+, \nabla \psi \rangle_\Gamma = 0\,. \end{aligned} \tag{4.47}$$

Following Eqs. (4.45) and (4.46), the first two volume integrals over $\mathbb{R}^3_\pm$ are zero. Furthermore, taking into account interface condition (IC_4), the last term can be rewritten in the following form

$$\langle \hat{\beta}^z \nabla_z \mathbf{E}_+, \nabla \psi \rangle_\Gamma = \langle (\mathbb{1} - \mathbf{n}\mathbf{n}^{\mathrm{T}}) \hat{\beta}^z \nabla_z \mathbf{E}_+, \nabla_\Gamma \psi \rangle_\Gamma = -\langle \nabla \cdot (\hat{\beta}^z \nabla_z \mathbf{E}_+), \psi \rangle_\Gamma\,, \tag{4.48}$$

where $\nabla_\Gamma = (\nabla_x, \nabla_y, 0)$ is the differential operator, tangential to Γ. The last equality above was obtained by integrating by parts and shifting the derivative from ψ to $\mathbf{E}_+$. Finally, since $\psi \in \mathcal{D}(\mathbb{R}^3)$ is arbitrary, we conclude from Eqs. (4.47) and (4.48) the sixth and last interface condition (IC_6) on Γ.

Proof of equivalence

In the analysis above, the interface conditions have been calculated from the weak formulation of the wave equation. We have shown that if $\mathbf{E}$ is a weak solution to the wave Eq. (4.26) in $\mathbb{R}^3$, implying it meets the regularity properties given in conditions (4.32) and satisfies the Eq. (4.33), and if $\mathbf{E}$ fulfills assumption (4.29), then $\mathbf{E}$ satisfies the interface conditions (IC_1)-(IC_4). This is the forward direction "⇒". Now, we would like to prove that the backward direction "⇐" holds as well. I.e., we want to prove that if $\mathbf{E}$ satisfies (4.29), solves Eq. (4.34) in $\mathbb{R}^3_-$, solves Eq. (4.36) in $\mathbb{R}^3_+$, and let the interface conditions (IC_1)-(IC_4) hold, then $\mathbf{E}$ is a weak solution to the wave Eq. (4.26).

Proof: First, we have to show that $\mathbf{E}$ fulfils the regularity conditions (4.32) and second, solves the weak form (4.33) of the wave equation.

By density arguments (c.f. Ref. [73] for mathematical details), assumption (4.29) implies that $\mathbf{E} \in \boldsymbol{\mathcal{L}}^2_{\mathrm{loc}}(\mathbb{R}^3)$, $\mathbf{E} \in \boldsymbol{\mathcal{H}}^1_{\mathrm{loc}}(\mathbb{R}^3_+)$, and $\nabla \times \nabla \times \mathbf{E} \in \boldsymbol{\mathcal{L}}^2_{\mathrm{loc}}(\mathbb{R}^3)$. Additionally, according to Theorem 2.2.1, from interface condition (IC_1) we further obtain that $\nabla \times \mathbf{E} \in \boldsymbol{\mathcal{L}}^2_{\mathrm{loc}}(\mathbb{R}^3)$. Hence, regularity conditions (4.32) are fulfilled.

Next, let $\boldsymbol{\phi} \in \boldsymbol{\mathcal{D}}(\mathbb{R}^3)$. After integrating by parts in Eq. (4.38), we obtain

$$\begin{aligned}&\langle \nabla \times \mathbf{E}, \nabla \times \boldsymbol{\phi} \rangle_{\mathbb{R}^3} - k_0^2 \langle \hat{\epsilon}^{\mathrm{loc}} \mathbf{E}, \boldsymbol{\phi} \rangle_{\mathbb{R}^3_-} - k_0^2 \langle \hat{\epsilon} \mathbf{E}, \boldsymbol{\phi} \rangle_{\mathbb{R}^3_+} + \langle \hat{\alpha} \nabla \times \mathbf{E}, \nabla \times \boldsymbol{\phi} \rangle \\ &- \sum_{j\{x,y,z\}} \langle \hat{\beta}^j \nabla_j \mathbf{E}, \nabla_j \boldsymbol{\phi} \rangle_{\mathbb{R}^3_+} + \langle \hat{\gamma} \nabla \times \nabla \times \mathbf{E}, \nabla \times \nabla \times \boldsymbol{\phi} \rangle_{\mathbb{R}^3_+} = \mathrm{LHS}_{(4.33)} - \mathrm{RHS}_{(4.33)} \,,\end{aligned} \tag{4.49}$$

where $\mathrm{LHS}_{(4.33)}$ and $\mathrm{RHS}_{(4.33)}$ are the expressions on the LHS and RHS of Eq. (4.33). Since, we assume that Eqs. (4.34) and (4.36) hold, the integral terms $\mathrm{LHS}_{(4.33)} = 0$. Furthermore, with the interface conditions (IC_2)-(IC_4), the $\mathrm{RHS}_{(4.33)} = 0$ as well. Therefore, $\mathrm{LHS}_{(4.49)} = 0$, and finally $\mathbf{E}$ satisfies Eq. (4.33). In conclusion, $\mathbf{E}$ is a weak solution to the wave Eq. (4.26). □

Further remarks concerning traces

Another fact is, the interface Γ has a Lebesgue measure zero. Therefore, neither the electric field $\mathbf{E}$ nor the displacement field $\mathbf{D}$ can be defined as classical functions, but rather as generalized ones, i.e., as distributions, unless the additional regularity (smoothness) assumptions (4.29) in the closure $\overline{\mathbb{R}^3_+}$ and $\overline{\mathbb{R}^3_-}$ are given. In other terms, it is possible to derive the interface conditions without the request of the additional regularities (4.29). This difficulty can be lifted by defining suitable traces of $\mathbf{E}$ and of its partial derivatives on Γ as elements of $\boldsymbol{\mathcal{D}}'(\Gamma)$. However, the study of traces won't affect the interface conditions (IC_1)-(IC_4) at all, they only need to be reformulated in a generalized sense. Hence, we gain no further physical insights thereof. Even though the formal introduction of traces is important for mathematical research, for the sake of a thesis in theoretical physics, we drop their discussion here[6] and would like to refer the analysis of the traces on Γ can be found in Sec. VI of our paper [64].

Besides, for the study of the slab problem, both bulk and interface aspects need to be merged. For the joint analysis of dispersion relations and interface conditions, we require

[6] As mentioned in Ch. 2, the strict introduction of traces requires a deeper course in Sobolev spaces with fractional order [69]. We spare the reader these details.

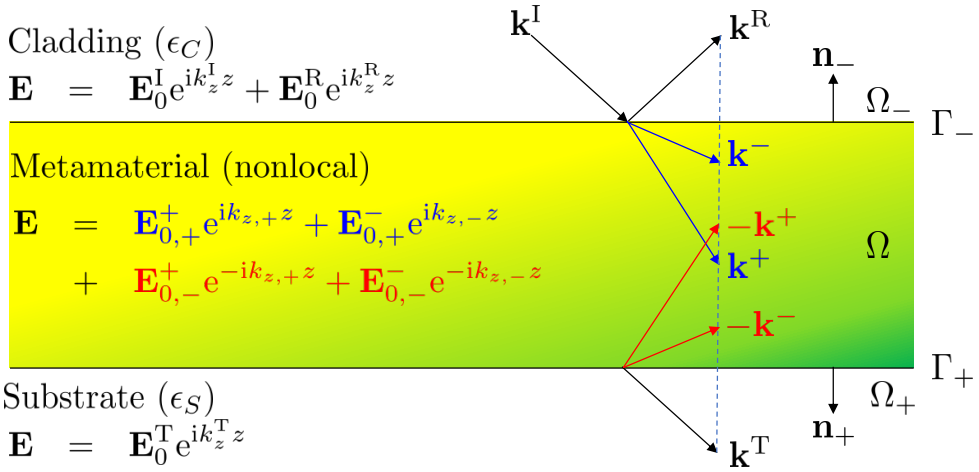

Figure 4.5: Schematics of a generic problem where a slab Ω separates substrate and cladding into two half-spaces Ω_- and Ω_+, respectively, and defining the interfaces $\Gamma_- := \overline{\Omega_-} \cap \overline{\Omega}$ and $\Gamma_+ := \overline{\Omega_+} \cap \overline{\Omega}$. Here, the backward propagating modes reflect from the second interface and contribute to the total reflection in the cladding.

that the electric field is at least four times continuously differentiable, i.e., an element of $\mathcal{C}^4$. Otherwise, the wave equation with four spatial derivatives on $\mathbf{E}$ cannot be solved. Therefore, we always assume that the eclectic field $\mathbf{E}$ satisfies the regularity condition (4.29) anyways.

4.3 Establishing the Fresnel Equations

In this section, we incorporate the subjects of both dispersion relations (Sec. 4.1) and interface conditions (Sec. 4.2) to study the problem of light propagation through a slab of a nonlocal metamaterial, as well as its electromagnetic response, i.e., reflection and transmission. As we mentioned in the previous section, the relevant interface conditions are (IC_1)-(IC_4).

Now, suppose we have an infinitely extended metamaterial in the xy-plane with a finite thickness d_{slab} in the z-direction. The space occupied by the metamaterial shall be denoted as $\Omega =: \mathbb{R}^2 \times (0, d_{\mathrm{slab}})$, which separates the two half-spaces Ω_- and Ω_+, as depicted in Fig. 4.5. Let $\Omega_- := \mathbb{R}^2 \times (-\infty, 0)$ be the half-space in which the incident light $(\mathbf{k}^I, \mathbf{E}^I, \mathbf{H}^I)$ and the reflected light $(\mathbf{k}^R, \mathbf{E}^R, \mathbf{H}^R)$ exist, and let $\Omega_+ := \mathbb{R}^2 \times (d_{\mathrm{slab}}, \infty)$ be the half-space in which the light is transmitted out of the slab with $(\mathbf{k}^T, \mathbf{E}^T, \mathbf{H}^T)$. The half-spaces $\Omega_\pm$ shall later represent the cladding and substrate, respectively. We assume that they consist of ordinary, isotropic, local, and homogeneous materials without magnetic response. Further, they shall be fully described with a local permittivity $\hat{\epsilon}^{\mathrm{loc}} = \epsilon_C \mathbb{1}$ and $\epsilon_S \mathbb{1}$, respectively, where ϵ_C and ϵ_S are both scalar functions of the frequency k_0. As depicted in Fig. 4.5, the insertion of a metamaterial between a cladding and a substrate defines two interfaces. These interfaces are denoted as

$$\Gamma_- := \overline{\Omega_-} \cap \overline{\Omega} = \{\mathbf{r} \in \mathbb{R}^3 \big|\, z = 0\}\,, \text{ and } \Gamma_+ := \overline{\Omega_+} \cap \overline{\Omega} = \{\mathbf{r} \in \mathbb{R}^3 \big|\, z = d_{\mathrm{slab}}\}\,.$$

The aim of this analysis here, is to find the field amplitudes of the reflected $\mathbf{E}^R$ and transmitted wave $\mathbf{E}^T$, when the metamaterial slab is illuminated with an incident plane wave $\mathbf{E}^I$ from Γ_-. Despite the fact that we only discuss plane waves here, an arbitrary

illumination can always be written as a superposition of plane waves [80]. Hence, the plane wave assumption is not a limitation.

Without loss of generality, we additionally assume that the incidence plane is either the xz- or yz-planes and the principle propagation direction is the z-direction. The incident wave vector is, therefore, either $\mathbf{k}^I = (k_x, 0, k_z)$ or $\mathbf{k}^I = (0, k_y, k_z)$. To cover both cases in one notation, we shall recall our previously introduced abbreviation, where the single transverse component of $\mathbf{k}$ is denoted by k_t, where t is either x or y and $t^* = x$ if $t = y$ and vice versa (see Sec. 4.1).

Remark 4.3.1. *Due to the translational symmetry of the homogeneous interface, all electromagnetic field waves share the same transverse wave vector k_t. Consequently, for all wave vectors $\mathbf{k}$, their transverse component is denoted by k_t, without any further superscript.*

Furthermore, we assume that the coordinate system of the laboratory is aligned with the coordinate system of the principle axis of the centrosymmetric metamaterial. Then, the metamaterial preserves the polarization of light, i.e., polarizations do not mix. In other words, each solution $\mathbf{E}$ of Eq. (4.26) can be decomposed into

$$\mathbf{E} = \mathbf{E}^{\mathrm{TE}} + \mathbf{E}^{\mathrm{TM}}$$

and each of $\mathbf{E}^{\mathrm{TE}}$ and $\mathbf{E}^{\mathrm{TM}}$ individually solve Eq. (4.26) as well. Accordingly, TE- and TM-polarized incident waves can be studied separately. Treating both polarizations simultaneously may in principle be done, but due to the different dispersion relations (check formulas (4.13), (4.15) for the SYM model and (4.20), (4.22) for the SSD model) and the different numbers of modes, the analysis and the different case studies will be too cumbersome to read. Therefore, we start with TE-polarization in the following subsection and discuss afterwards the case of TM-polarization.

4.3.1 Illumination with TE-polarized light

Let the incident field be

$$\mathbf{E}^I(\mathbf{r}, k_0) = \mathbf{E}_0^I(k_0)\mathrm{e}^{\mathrm{i}\mathbf{k}^I\cdot\mathbf{r}}\,,\ \text{for } \mathbf{r} \in \Omega_-\,,$$

with $\mathbf{k}^I = (k_t, k_z)$ and $\mathbf{E}_0^I = E_{t^*}^I\hat{\mathbf{e}}_{t^*}$, where $\hat{\mathbf{e}}_{t^*}$ is the unit vector in t^* direction. The dispersion relation in this half-space is given by Eq. (4.7) with $\hat{\mu} = \mathbb{1}$ and $\epsilon_{t^*t^*} = \epsilon_{zz} = \epsilon_C$, i.e., we have $\left(k_z^I(k_t, k_0)\right)^2 = \epsilon_C k_0^2 - k_t^2$. Since the reflected field resides in the same half-space Ω_-, it obeys the same dispersion relation as for the incident field, with a reversed propagation to the $(-z)$ direction, simply $k_z^R = -k_z^I$. Due to the preservation of polarization of light, the reflected field is t^*-polarized as well, such that

$$\mathbf{E}^R(\mathbf{r}, k_0) = E_{t^*}^R(k_0)\mathrm{e}^{\mathrm{i}\mathbf{k}^R\cdot\mathbf{r}}\hat{\mathbf{e}}_{t^*}\,,\ \text{for } \mathbf{r} \in \Omega_-\,.$$

The total field in Ω_- is the superposition of both incident and reflected fields $\mathbf{E}^I + \mathbf{E}^R$. In the transmission half-space Ω_+, we only have the transmitted field

$$\mathbf{E}^T(\mathbf{r}, k_0) = E_{t^*}^T(k_0)\mathrm{e}^{\mathrm{i}\mathbf{k}^T\cdot(\mathbf{r}-d_{\mathrm{slab}}\hat{\mathbf{e}}_z)}\hat{\mathbf{e}}_{t^*}\,,\ \text{for } \mathbf{r} \in \Omega_+\,,$$

with the dispersion $\left(k_z^T(k_t, k_0)\right)^2 = \epsilon_S k_0^2 - k_t^2$. Note the phase shift in the transmitted field, which has been introduced as that field can only start propagating from a distance

$z = d_{\text{slab}}$ from the origin of the coordinate system. To make sure that no artificial phases occur, we subtract a $(d_{\text{slab}}\hat{\mathbf{e}}_z)$-term in the exponential function above.

Ultimately, in the slab Ω the metamaterial is described by the constitutive relation (4.1). In Sec. 4.1.2, we have shown that the nonlocal parameter $\hat{\beta}^j$ does not couple to the TE-polarized field and, therefore, does neither affect the dispersion relation nor increase the number of modes. On the contrary, $\hat{\gamma}$ indeed advances the dispersion relations and raises the number of modes to four, which are pairwise forward and backwards propagating. In that sense, the total field in the slab is

$$\mathbf{E}^{\text{slab}}(k_0, \mathbf{r}) = \sum_{\sigma=\pm 1} \left(E^{+}_{t^*,\sigma}(k_0) \mathrm{e}^{\mathrm{i}\mathbf{k}_\sigma \cdot \mathbf{r}} + E^{-}_{*,\sigma}(k_0) \mathrm{e}^{-\mathrm{i}\mathbf{k}_\sigma \cdot \mathbf{r}} \right) \hat{\mathbf{e}}_{t^*} \,, \text{ for } \mathbf{r} \in \Omega \,,$$

with the wave vectors $\mathbf{k}_\sigma = (k_t, k_{z,\sigma})$ and the eigenvalue $k_{z,\sigma}$ given by Eq. (4.20).

In our scenario, the incident field $E^I_{t^*}$ is the only known field amplitude, while all other six amplitudes $(E^R_{t^*}, E^+_{t^*,+}, E^+_{t^*,-}, E^-_{t^*,+}, E^-_{t^*,-}, E^T_{t^*})$ have to be found. These field amplitudes are linked together through the interface conditions. For instance, interface condition (IC_1) on both interfaces Γ_+ and Γ_- links the tangential component of the electric field for all $(x, y) \in \mathbb{R}^2$

$$\begin{cases} E^I_{t^*} + E^R_{t^*} - \sum_{\sigma=\pm 1} \left(E^+_{t^*,\sigma} + E^-_{t^*,\sigma} \right) = 0 & \text{on } \Gamma_- \text{ where } z = 0 \,, \\ \sum_{\sigma=\pm 1} \left(E^+_{t^*,\sigma} \mathrm{e}^{\mathrm{i}k_{z,\sigma} d_{\text{slab}}} + E^-_{t^*,\sigma} \mathrm{e}^{-\mathrm{i}k_{z,\sigma} d_{\text{slab}}} \right) - E^T_{t^*} = 0 & \text{on } \Gamma_+ \text{ where } z = d_{\text{slab}} \,. \end{cases} \tag{4.50}$$

In fact, form the interface conditions we also notice that the term proportional to $\hat{\beta}^z$ in (IC_2) vanishes as $\hat{\beta}^z \mathbf{E}^{\text{slab}} = 0$ in TE-polarization. Furthermore, interface condition (IC_4) reduces to the trivial equation $0 = 0$. Hence, even at the level of interface conditions, $\hat{\beta}^j$ has no effect in TE-polarization. Besides, we find that (IC_5) yields the same continuity conditions for the fields as in Eq. (4.50), multiplied by k_t. Since k_t is always the same in all three media, (IC_5) and (IC_1) are linearly dependent and, therefore (IC_5) does not give any further information. Finally, for TE-polarization, (IC_6) reads $0 = 0$ by default, as there is no electric field component that is normal to the interface. For that reason, we have three non-trivial equations at each interface. With two interfaces being present, it makes in total six linearly independent equations with six unknowns. The system is, therefore, said to be determined and can be uniquely solved.

Finally, by inserting our plane wave ansatzes into (IC_1)-(IC_2) and after further sorting the field amplitudes, we reach to the following linear algebraic system

$$\underline{\underline{\mathbf{F}}}^{\text{SSD,TE}} \cdot \underline{\mathbf{E}} = \underline{\mathbf{I}}$$

for $\underline{\mathbf{E}} = (E^R_{t^*}, E^+_{t^*,+}, E^+_{t^*,-}, E^-_{t^*,+}, E^-_{t^*,-}, E^T_{t^*})^{\mathrm{T}}$, with the Fresnel matrix

$$\underline{\underline{\mathbf{F}}}^{\text{SSD,TE}} = \begin{pmatrix} 1 & -1 & -1 & -1 & -1 & 0 \\ k_z^R & B_+ & B_- & -B_+ & -B_- & 0 \\ 0 & C_+ & C_- & C_+ & C_- & 0 \\ 0 & -\mathrm{e}^{\mathrm{i}k^{\text{SSD}}_{z,+} d_{\text{slab}}} & -\mathrm{e}^{\mathrm{i}k^{\text{SSD}}_{z,-} d_{\text{slab}}} & -\mathrm{e}^{-\mathrm{i}k^{\text{SSD}}_{z,+} d_{\text{slab}}} & -\mathrm{e}^{-\mathrm{i}k^{\text{SSD}}_{z,-} d_{\text{slab}}} & 1 \\ 0 & B_+ \mathrm{e}^{\mathrm{i}k^{\text{SSD}}_{z,+} d_{\text{slab}}} & B_- \mathrm{e}^{\mathrm{i}k^{\text{SSD}}_{z,-} d_{\text{slab}}} & -B_+ \mathrm{e}^{-\mathrm{i}k^{\text{SSD}}_{z,+} d_{\text{slab}}} & -B_- \mathrm{e}^{-\mathrm{i}k^{\text{SSD}}_{z,-} d_{\text{slab}}} & k_z^T \\ 0 & C_+ \mathrm{e}^{\mathrm{i}k^{\text{SSD}}_{z,+} d_{\text{slab}}} & C_- \mathrm{e}^{\mathrm{i}k^{\text{SSD}}_{z,-} d_{\text{slab}}} & C_+ \mathrm{e}^{-\mathrm{i}k^{\text{SSD}}_{z,+} d_{\text{slab}}} & C_- \mathrm{e}^{-\mathrm{i}k^{\text{SSD}}_{z,-} d_{\text{slab}}} & 0 \end{pmatrix} \tag{4.51}$$

and input vector $\underline{\mathbf{I}} = -E^I_{t^*}(1, k^I_z, 0, 0, 0, 0)^{\mathrm{T}}$, containing only the information of the incident field and the angle of incidence. These quantities are usually known in the experiment

or in simulations and can be used for predicting reflection and transmission coefficients for different angles of incidence and frequency. Here, $B_\sigma = -k_{z,\sigma}^{\mathrm{SSD}}\left(\frac{1}{\mu_{tt}} - k_0^2\gamma_{t^*t^*}\left(\mathbf{k}_+^{\mathrm{SSD}}\right)^2\right)$, $C_\sigma = \gamma_{t^*t^*}\left(\mathbf{k}_\sigma^{\mathrm{SSD}}\right)^2$, and $\left(\mathbf{k}_\sigma^{\mathrm{SSD}}\right)^2 = k_t^2 + \left(k_{z,\sigma}^{\mathrm{SSD}}\right)^2$.

The Fresnel matrix above encapsulates everything we studied so far. It contains both dispersion relations and interface conditions and must be interpreted as follows. The first three rows contain the three interface conditions (IC_1)-(IC_3) at the first interface Γ_- where $z = 0$, while the last three rows contain these interface conditions evaluated at the second interface Γ_+ where $z = d_{\mathrm{slab}}$. This is reflected in the accumulated phase $\mathrm{e}^{\mathrm{i}k_{z,\sigma}^{\mathrm{SSD}}d_{\mathrm{slab}}}$. The first and the last columns, respectively, incorporate the coefficients for the reflected and transmitted field. Clearly, there is no reflected field at the second interface and no transmitted field at the first interface, hence, the zeroes on bottom left and top right, respectively. The four centered columns accommodate the field amplitudes within the slab, in which the first two consist of the forward propagating modes with $\Im k_{z,\sigma} > 0$, while the last two consist of the backward propagating modes, where $\Im k_{z,\sigma} < 0$. Here, the backward modes are important as back reflections from the second interface need to be considered for the correct calculation of the reflection coefficient.

Eventually, one seeks to reproduce the local limit by taking $\hat{\gamma} \to 0$. Again $\hat{\beta}^j$ has no effect here. First, when $\hat{\gamma} \to 0$, the third and sixth row, i.e., the third interface condition, vanish. Second, one pair of the eigenmodes, which we identified to be $\pm k_{z,-}$ diverge with $\frac{1}{\sqrt{\gamma_{ii}}}$, as $\hat{\gamma} \to 0$. This would lead to a huge imaginary part which causes exponentially decaying the field amplitudes and, therefore, do not contribute neither to reflection nor to transmission. Hence, in this WSD limit, two columns vanish as well and the dimension of the Fresnel matrix cuts down to a 4×4 matrix, which reads

$$\underline{\underline{\mathbf{F}}}^{\mathrm{WSD,TE}} = \begin{pmatrix} 1 & -1 & -1 & 0 \\ k_z^R & \frac{-k_z^{\mathrm{WSD}}}{\mu_{tt}} & \frac{k_z^{\mathrm{WSD}}}{\mu_{tt}} & 0 \\ 0 & -\mathrm{e}^{\mathrm{i}k_z^{\mathrm{WSD}}d_{\mathrm{slab}}} & -\mathrm{e}^{-\mathrm{i}k_z^{\mathrm{WSD}}d_{\mathrm{slab}}} & 1 \\ 0 & \frac{-k_z^{\mathrm{WSD}}}{\mu_{tt}}\mathrm{e}^{\mathrm{i}k_z^{\mathrm{WSD}}d_{\mathrm{slab}}} & \frac{k_z^{\mathrm{WSD}}}{\mu_{tt}}\mathrm{e}^{-\mathrm{i}k_z^{\mathrm{WSD}}d_{\mathrm{slab}}} & k_z^T \end{pmatrix}. \tag{4.52}$$

Since the material parameter $\hat{\beta}^j$ does neither affect the dispersion relation, nor the interface conditions in the TE-polarized case, the Fresnel matrix (4.52) is identical for the SYM model as well. Therefore, also in terms of reflection and transmission coefficients, there is no gain from taking further symmetry terms $\hat{\beta}^j$ in the second-order expansion, at least for the TE-polarized case.

To finalize this section, the complex valued reflection and transmission coefficients are obtained by inverting the Fresnel matrix $\underline{\underline{\mathbf{F}}}$, multiplying it by the input vector $\underline{\mathbf{I}}$ and, respectively, taking the first and last component. Thus, for the SSD model

$$\begin{aligned} \rho^{\mathrm{SSD,TE}}(k_t, k_0, \hat{\epsilon}, \hat{\mu}, \hat{\gamma}, d_{\mathrm{slab}}) &= \left[\left(\underline{\underline{\mathbf{F}}}^{\mathrm{SSD,TE}}\right)^{-1} \cdot \underline{\mathbf{I}}\right]_1, \\ \tau^{\mathrm{SSD,TE}}(k_t, k_0, \hat{\epsilon}, \hat{\mu}, \hat{\gamma}, d_{\mathrm{slab}}) &= \left[\left(\underline{\underline{\mathbf{F}}}^{\mathrm{SSD,TE}}\right)^{-1} \cdot \underline{\mathbf{I}}\right]_6, \end{aligned} \tag{4.53}$$

and for both WSD and SYM models

$$\begin{aligned} \rho^{\mathrm{WSD,TE}}(k_t, k_0, \hat{\epsilon}, \hat{\mu}, d_{\mathrm{slab}}) &= \left[\left(\underline{\underline{\mathbf{F}}}^{\mathrm{WSD,TE}}\right)^{-1} \cdot \underline{\mathbf{I}}\right]_1, \\ \tau^{\mathrm{WSD,TE}}(k_t, k_0, \hat{\epsilon}, \hat{\mu}, d_{\mathrm{slab}}) &= \left[\left(\underline{\underline{\mathbf{F}}}^{\mathrm{WSD,TE}}\right)^{-1} \cdot \underline{\mathbf{I}}\right]_4, \end{aligned} \tag{4.54}$$

where ρ and τ, respectively, denote the reflection and transmission coefficients. For the sake of readability, we do not write the (very) lengthy expressions for $\rho^{\mathrm{SSD,TE}}$ and $\tau^{\mathrm{SSD,TE}}$ explicitly. Concerning, the WSD model, the formulas we obtain from (4.60) coincide with the results from the literature [82] for a local anisotropic medium with magnetic response.

The formulas above are one of the central results in this work and will be employed in the Chapter 5 for the parameter retrieval of concrete optical metamaterials.

4.3.2 Illumination with TM-polarized light

In the case of TM-polarized light, the field of the incident plane wave lies in the incidence plane, such that for $\mathbf{k}^I = (k_t, k_z)$ we have $\mathbf{E}^I = (E_t^I, E_z^I)\mathrm{e}^{\mathrm{i}\mathbf{k}^I\cdot\mathbf{r}}$, for $\mathbf{r} \in \Omega_-$. Here again, the reflected and transmitted fields $\mathbf{E}^R$ and $\mathbf{E}^T$ share the same polarization as the incident field and all the wave vectors have the same k_t component.

Traditionally, for the TM-polarized case, the reflection and transmission coefficients are calculated from the ratio of the reflected and transmitted to the incident magnetic fields. The reason is simple. In TM-polarization, there exists only one magnetic field component that is essentially nonzero. However, our interface conditions are formulated for the electric fields, where here we have two nonzero components. The question is then, how should the reflection and transmission coefficients be defined. Is it rather the ratios of the normal components, i.e. the E_z fields or the tangential components, i.e., the E_t fields. The answer is, up to a sign or a constant prefactor, it does not matter. In the half-spaces $\Omega_\pm$ filled with an isotropic local medium characterized with $\epsilon_{C,S}$, one has $\nabla\cdot(\epsilon_{C,S}\mathbf{E}) = 0$. Consequently,

$$k_t E_t + k_z E_z = 0 \;\Rightarrow\; E_t = -\frac{k_z}{k_t} E_z\,,$$

which holds true for all incident, reflected, and transmitted fields. Subsequently, the pairs of reflection and transmission coefficients (ρ_t, τ_t), and (ρ_z , τ_z) which are defined as

$$\begin{aligned} \rho_t^{\mathrm{TM}} &:= \frac{E_t^R}{E_t^I}\,,\; \tau_t^{\mathrm{TM}} := \frac{E_t^T}{E_t^I}\,, \\ \rho_z^{\mathrm{TM}} &:= \frac{E_z^R}{E_z^I}\,,\; \tau_z^{\mathrm{TM}} := \frac{E_z^T}{E_z^I}\,. \end{aligned} \tag{4.55}$$

Using the divergence equation above, we obtain

$$\rho_z^{\mathrm{TM}} = -\rho_t^{\mathrm{TM}}\,,\; \tau_t^{\mathrm{TM}} = \frac{k_z^T}{k_z^I}\tau_z^{\mathrm{TM}}\,. \tag{4.56}$$

The minus sign in front of the reflection coefficient arises from $k_z^R = -k_z^I$. Concerning the transmission coefficient, the fields reside in different media. Therefore, from the dispersion relations, it holds for $\epsilon_C \neq \epsilon_S \Rightarrow k_z^I \neq k_z^T$. However, if we consider a symmetric configuration, i.e., if the metamaterial slab is located between two identical media, i.e, $\epsilon_C = \epsilon_S$, then $k_z^I = k_z^T$ and the transmission coefficients coincide. In the end, the reflection coefficients do only change by a minus sign. When measuring energies, i.e., $R = |\rho|^2$, this sign has no impact. In this thesis, we decide to chose the ratios of the z-components of the field, which is by no means a limitation, as discussed above. Nonetheless, there exists one pathological case, where there should be no worries in general. At normal incidence, i.e. $k_t = 0$, all $E_z = 0$, and the expressions for ρ_z^{TM} and τ_z^{TM} above have "$\frac{0}{0}$" ratios. It

turns out that this is a removable singularity and, hence, makes the expressions even at normal incidence being well-defined.

Note, that in the TM-polarized case both parameters $\hat{\beta}^j$ and $\hat{\gamma}$ couple to the electric field and in a way they both contribute to the dispersion relation in the bulk and to the existence of additional interface conditions. Similar to the study of the bulk properties, here, we wish to derive the Fresnel matrices for both SYM and SSD models separately, with only one of the nonlocal parameters above being nonzero.

Fresnel matrix of the SYM model

In the slab Ω, the total field consists of the superposition of two forward and two backward modes

$$\mathbf{E}^{\text{slab}}(k_0, \mathbf{r}) = \sum_{\sigma=\pm 1} \left(\mathbf{E}^{+}_{0,\sigma}(k_0) \mathrm{e}^{\mathrm{i}\mathbf{k}_\sigma \cdot \mathbf{r}} + \mathbf{E}^{-}_{0,\sigma}(k_0) \mathrm{e}^{-\mathrm{i}\mathbf{k}_\sigma \cdot \mathbf{r}} \right) ,$$

where $\mathbf{E}^{\pm}_{0,\sigma} = E^{\pm}_{t,\sigma}\hat{\mathbf{e}}_t + E^{\pm}_{z,\sigma}\hat{\mathbf{e}}_z$. To get rid of the E_t components, we use the divergence equation in Ω, which reads for each mode $\nabla \cdot \left(\hat{\epsilon}\mathbf{E}^{\pm}_{\sigma} + \sum_{j\in\{x,y,z\}} \nabla_j (\hat{\beta}^j \nabla \cdot \mathbf{E}^{\pm}_{\sigma}) \right) = 0$ and thereby

$$k_t(\epsilon_{tt} - \beta_{tt}k_t^2)E^{\pm}_{t,\sigma} \pm k_{z,\sigma}(\epsilon_{zz} - \beta_{zz}k^2_{z,\sigma})E^{\pm}_{z,\sigma} = 0 \Rightarrow E^{\pm}_{t,\sigma} = -\frac{(\epsilon_{zz} - \beta_{zz}k^2_{z,\sigma})}{(\epsilon_{tt} - \beta_{tt}k_t^2)} \frac{\pm k_{z,\sigma}}{k_t} E^{\pm}_{z,\sigma} .$$

In the special case where $\epsilon_{tt} - \beta_{tt}k_t^2 = 0$, the inversion above is not possible and will therefore not be treated here.

Following the same procedures as for the TE-polarized case, we evaluate the three interface conditions (IC_1), (IC_2) with $\hat{\gamma} = 0$, and (IC_4) at both interfaces Γ_- and Γ_+. With these equations, we can unambiguously determine the six unknowns $\underline{\mathbf{E}} = (E^R_z, E^+_{z,+}, E^+_{z,-}, E^-_{z,+}, E^-_{z,-}, E^T_z)^{\mathrm{T}}$ Here, the Fresnel matrix for the SYM model reads

$$\underline{\underline{\mathbf{F}}}^{\text{SYM,TM}} = \begin{pmatrix} k^R_z & A_+ & A_- & -A_+ & -A_- & 0 \\ \left(\mathbf{k}^R\right)^2 & B_+ & B_- & B_+ & B_- & 0 \\ 0 & C_+ & C_- & -C_+ & -C_- & 0 \\ 0 & A_+\mathrm{e}^{\mathrm{i}k^{\text{SYM}}_{z,+}d_{\text{slab}}} & A_-\mathrm{e}^{\mathrm{i}k^{\text{SYM}}_{z,-}d_{\text{slab}}} & -A_+\mathrm{e}^{-\mathrm{i}k^{\text{SYM}}_{z,+}d_{\text{slab}}} & -A_-\mathrm{e}^{-\mathrm{i}k^{\text{SYM}}_{z,-}d_{\text{slab}}} & k^T_z \\ 0 & B_+\mathrm{e}^{\mathrm{i}k^{\text{SYM}}_{z,+}d_{\text{slab}}} & B_-\mathrm{e}^{\mathrm{i}k^{\text{SYM}}_{z,-}d_{\text{slab}}} & B_+\mathrm{e}^{-\mathrm{i}k^{\text{SYM}}_{z,+}d_{\text{slab}}} & B_-\mathrm{e}^{-\mathrm{i}k^{\text{SYM}}_{z,-}d_{\text{slab}}} & \left(\mathbf{k}^T\right)^2 \\ 0 & C_+\mathrm{e}^{\mathrm{i}k^{\text{SYM}}_{z,+}d_{\text{slab}}} & C_-\mathrm{e}^{\mathrm{i}k^{\text{SYM}}_{z,-}d_{\text{slab}}} & -C_+\mathrm{e}^{-\mathrm{i}k^{\text{SYM}}_{z,+}d_{\text{slab}}} & -C_-\mathrm{e}^{-\mathrm{i}k^{\text{SYM}}_{z,-}d_{\text{slab}}} & 0 \end{pmatrix} . \tag{4.57}$$

which links the unknown fields $\underline{\mathbf{E}}$ to the input vector $\underline{\mathbf{I}}$ as follows

$$\underline{\underline{\mathbf{F}}}^{\text{SYM,TM}} \cdot \underline{\mathbf{E}} = \underline{\mathbf{I}} ,$$

with $\underline{\mathbf{I}} = -E^I_z \left(k^I_z, \left(\mathbf{k}^I\right)^2, 0, 0, 0, 0 \right)^{\mathrm{T}}$, containing only the known parameters from the incident light. Further, the coefficients in the Fresnel matrix read $A_\sigma = -\frac{\epsilon_{zz} - \beta_{zz}\left(k^{\text{SYM}}_{z,\sigma}\right)^2}{\epsilon_{tt} - \beta_{tt}(k_t)^2} k^{\text{SYM}}_{z,\sigma}$, $B_\sigma = \mu^{-1}_{t^*t^*}\left(A_\sigma k^{\text{SYM}}_{z,\sigma} - k_t^2\right)$, and $C_\sigma = \beta_{zz}k^{\text{SYM}}_{z,\sigma}$.

Again, the reflection and transmission coefficients are calculated by inverting the Fresnel matrix:

$$\begin{aligned} \rho^{\text{SYM,TM}}(k_t, k_0, \hat{\epsilon}, \hat{\mu}, \hat{\beta}^j, d_{\text{slab}}) &= \left[\left(\underline{\underline{\mathbf{F}}}^{\text{SYM,TM}}\right)^{-1} \cdot \underline{\mathbf{I}} \right]_1 , \\ \tau^{\text{SYM,TM}}(k_t, k_0, \hat{\epsilon}, \hat{\mu}, \hat{\beta}^j, d_{\text{slab}}) &= \left[\left(\underline{\underline{\mathbf{F}}}^{\text{SYM,TM}}\right)^{-1} \cdot \underline{\mathbf{I}} \right]_6 , \end{aligned} \tag{4.58}$$

Shortly, we want to note that in the local limit, i.e. for $\hat{\beta}^j \to 0$, the Fresnel Matrix above reduced to the for the WSD case in the TM-polarization which reads

$$\underline{\underline{\mathbf{F}}}^{\mathrm{WSD,TM}} = \begin{pmatrix} k_z^R & -\frac{\epsilon_{zz}}{\epsilon_{tt}} k_z^{\mathrm{WSD}} & \frac{\epsilon_{zz}}{\epsilon_{tt}} k_z^{\mathrm{WSD}} & 0 \\ \left(\mathbf{k}^R\right)^2 & -\epsilon_{zz} k_0^2 & -\epsilon_{zz} k_0^2 & 0 \\ 0 & -\frac{\epsilon_{zz}}{\epsilon_{tt}} k_z^{\mathrm{WSD}} \mathrm{e}^{\mathrm{i}k_z^{\mathrm{WSD}} d_{\mathrm{slab}}} & \frac{\epsilon_{zz}}{\epsilon_{tt}} k_z^{\mathrm{WSD}} \mathrm{e}^{-\mathrm{i}k_z^{\mathrm{WSD}} d_{\mathrm{slab}}} & k_z^T \\ 0 & -\epsilon_{zz} k_0^2 \mathrm{e}^{\mathrm{i}k_z^{\mathrm{WSD}} d_{\mathrm{slab}}} & -\epsilon_{zz} k_0^2 \mathrm{e}^{-\mathrm{i}k_z^{\mathrm{WSD}} d_{\mathrm{slab}}} & \left(\mathbf{k}^T\right)^2 \end{pmatrix}. \tag{4.59}$$

Consequently, the reflection and transmission coefficients converge to the expected expressions, which may be found in Ref. [82] or obtained by

$$\begin{aligned} \rho^{\mathrm{WSD,TM}}(k_t, k_0, \hat{\epsilon}, \hat{\mu}, d_{\mathrm{slab}}) &= \left[\left(\underline{\underline{\mathbf{F}}}^{\mathrm{WSD,TM}}\right)^{-1} \cdot \underline{\mathbf{I}}\right]_1, \\ \tau^{\mathrm{WSD,TM}}(k_t, k_0, \hat{\epsilon}, \hat{\mu}, d_{\mathrm{slab}}) &= \left[\left(\underline{\underline{\mathbf{F}}}^{\mathrm{WSD,TM}}\right)^{-1} \cdot \underline{\mathbf{I}}\right]_4. \end{aligned} \tag{4.60}$$

Fresnel matrix of the SSD model

The analysis of the SSD model is analogous to the previous cases. Except that, here the divergence equation is simpler and reads $\nabla \cdot (\hat{\epsilon} \mathbf{E}_\sigma^\pm) = 0$ and, therefore, we have

$$\epsilon_{tt} k_t E_{t,\sigma}^\pm \pm \epsilon_{zz} k_{z,\sigma} E_{z,\sigma}^\pm = 0 \Rightarrow E_{t,\sigma}^\pm = -\frac{\epsilon_{zz}}{\epsilon_{tt}} \frac{\pm k_{z,\sigma}}{k_t} E_{z,\sigma}^\pm .$$

To construct the Fresnel matrix, we benefit from the interface conditions (IC_1), (IC_2) with $\hat{\beta}^j = 0$, and (IC_3). The Fresnel matrix reads

$$\underline{\underline{\mathbf{F}}}^{\mathrm{SSD,TM}} = \begin{pmatrix} k_z^R & A_+ & A_- & -A_+ & -A_- & 0 \\ \left(\mathbf{k}^R\right)^2 & B_+ & B_- & B_+ & B_- & 0 \\ 0 & C_+ & C_- & -C_+ & -C_- & 0 \\ 0 & A_+ \mathrm{e}^{\mathrm{i}k_{z,+}^{\mathrm{SYM}} d_{\mathrm{slab}}} & A_- \mathrm{e}^{\mathrm{i}k_{z,-}^{\mathrm{SYM}} d_{\mathrm{slab}}} & -A_+ \mathrm{e}^{-\mathrm{i}k_{z,+}^{\mathrm{SYM}} d_{\mathrm{slab}}} & -A_- \mathrm{e}^{-\mathrm{i}k_{z,-}^{\mathrm{SYM}} d_{\mathrm{slab}}} & k_z^T \\ 0 & B_+ \mathrm{e}^{\mathrm{i}k_{z,+}^{\mathrm{SYM}} d_{\mathrm{slab}}} & B_- \mathrm{e}^{\mathrm{i}k_{z,-}^{\mathrm{SYM}} d_{\mathrm{slab}}} & B_+ \mathrm{e}^{-\mathrm{i}k_{z,+}^{\mathrm{SYM}} d_{\mathrm{slab}}} & B_- \mathrm{e}^{-\mathrm{i}k_{z,-}^{\mathrm{SYM}} d_{\mathrm{slab}}} & \left(\mathbf{k}^T\right)^2 \\ 0 & C_+ \mathrm{e}^{\mathrm{i}k_{z,+}^{\mathrm{SYM}} d_{\mathrm{slab}}} & C_- \mathrm{e}^{\mathrm{i}k_{z,-}^{\mathrm{SYM}} d_{\mathrm{slab}}} & -C_+ \mathrm{e}^{-\mathrm{i}k_{z,+}^{\mathrm{SYM}} d_{\mathrm{slab}}} & -C_- \mathrm{e}^{-\mathrm{i}k_{z,-}^{\mathrm{SYM}} d_{\mathrm{slab}}} & 0 \end{pmatrix}, \tag{4.61}$$

which relates the unknown fields $\underline{\mathbf{E}}$ and the input vector $\underline{\mathbf{I}}$ via the equation

$$\underline{\underline{\mathbf{F}}}^{\mathrm{SSD,TM}} \cdot \underline{\mathbf{E}} = \underline{\mathbf{I}},$$

with $\underline{\mathbf{I}} = -E_z^I \left(k_z^I, \left(\mathbf{k}^I\right)^2, 0, 0, 0, 0\right)^{\mathrm{T}}$, as previously. Here, the coefficients that appear in the matrix read $A_\sigma = -\frac{\epsilon_{zz}}{\epsilon_{tt}} k_{z,\sigma}^{\mathrm{SSD}}$, $B_\sigma = \left[k_0^2 \left(\gamma_{zz} k_t^2 + \gamma_{tt} \left(k_{z,\sigma}^{\mathrm{SSD}}\right)^2\right) - \mu_{t^*t^*}^{-1}\right] \left(A_\sigma k_{z,\sigma}^{\mathrm{SYM}} - k_t^2\right)$, and $C_\sigma = \gamma_{tt} \left(A_\sigma k_{z,\sigma}^{\mathrm{SYM}} - k_t^2\right) k_{z,\sigma}^{\mathrm{SSD}}$.

Finally, the reflection and transmission coefficients for the SSD model are

$$\begin{aligned} \rho^{\mathrm{SSD,TM}}(k_t, k_0, \hat{\epsilon}, \hat{\mu}, \hat{\gamma}, d_{\mathrm{slab}}) &= \left[\left(\underline{\underline{\mathbf{F}}}^{\mathrm{SSD,TM}}\right)^{-1} \cdot \underline{\mathbf{I}}\right]_1, \\ \tau^{\mathrm{SSD,TM}}(k_t, k_0, \hat{\epsilon}, \hat{\mu}, \hat{\gamma}, d_{\mathrm{slab}}) &= \left[\left(\underline{\underline{\mathbf{F}}}^{\mathrm{SSD,TM}}\right)^{-1} \cdot \underline{\mathbf{I}}\right]_6, \end{aligned} \tag{4.62}$$

Once more, the limit $\hat{\gamma} \to 0$ reproduces the results we know from the literature Ref. [82], where the third and last rows, as well as the third and fifth columns in Eq. (4.61) vanish.

4.3.3 Half-space problem and further remarks

In some applications, it is important to study the half-space problem, where the metamaterial is infinitely thick, i.e. $d_{\text{slab}} \to \infty$ such that $\Omega \to \mathbb{R}^3_+$, or alternatively, at least thick enough such that all light is absorbed and no transmission occurs. A concrete example of such applications is the study of surface plasmon polaritons sustained at an interface of a nonlocal metamaterial as discussed in detail in Ref. [127]. The majority of the work has been done by Joshua Feis in the context of a B. Sc. thesis that I supervised. In this work, we investigated the impact of nonlocality at the dispersion of surface plasmon polaritons and discussed the ATR spectrum in an Otto setup [128]. For the reflection from a half-space, the second interface would be located at $z = +\infty$. Meaning that there is no feedback from the second interface and the backward propagating modes would not contribute to the reflection coefficient. Technically, the dimensions of the Fresnel matrices reduce to 2×2 for the WSD model and to 3×3 for both SYM and SSD models. In all cases, it holds for the reflection from a half-space

$$\rho_{\text{HS}}(k_t, k_0, \text{EMP}) = \left[\underline{\underline{\mathbf{F}}}_{\text{HS}}^{-1} \cdot \underline{\mathbf{I}}\right]_1 , \tag{4.63}$$

where $\underline{\underline{\mathbf{F}}}_{\text{HS}}$ denotes the half-space Fresnel matrix of the corresponding model with the appropriate effective material parameters (EMP).

One remark concerning the derivation of the reflection and transmission coefficients is in order. Here, we require that the Fresnel matrices are regular and can be inverted, or precisely $\underline{\underline{\mathbf{F}}}$ is generically invertible. By *generically* invertible, it is meant that the set of effective material parameters $\hat{\epsilon}$, $\hat{\alpha}$, $\hat{\gamma}$, and $\hat{\beta}^j$ for which $\det(\underline{\underline{\mathbf{F}}}) = 0$ has a Lebesque measure zero in the space of all possible parameters. Throughout this work, the invertibility of the Fresnel matrices will be always assumed.

4.4 Basic homogenization models

Eventually, a comparison with the present homogenization approaches from the literature needs to be made. Therefore, in this section, we summarize two frequently used, but fundamentally different, models for the homogenization of optical metamaterials. First, we have the Maxwell-Garnett formula that is mostly applicable only in the quasi-static regime. There, to a random permittivity distribution with a certain concentration in a finite volume, a spatially averaged effective permittivity is assigned. Second, we present the nonlocal wire medium model, which as its name reveals, is specially conceived to effectively describe plasmonic wire media with a nonlocal response. This model was developed by several authors [57]–[59], [120], and is regarded as the prototype model for nonlocality.

These two presented models from the literature will be compared in Ch. 5 to the ones we have proposed in Eq. (4.1) in the very beginning of this chapter.

4.4.1 Maxwell-Garnett mixing rule

In this subsection, we present the basic steps for the derivation of the Maxwell-Garnett mixing rule. Details can be found in Ch. 16 of Ref. [129] and in the Review paper [130]. In general, mixing rules play an important role in the homogenization of deep-subwavelength

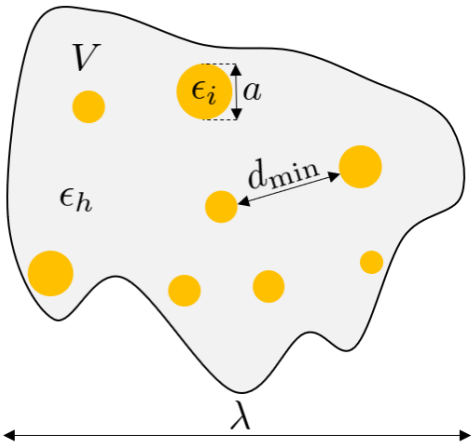

Figure 4.6: A simple mixture of spherical inclusions in a homogeneous background medium with volume V (Island of Djerba). The permittivity of the inclusions is ϵ_i and that of the host is ϵ_h. The validity of Maxwell-Garnett theory requires that the wavelength λ of light is much longer than any characteristic length-scale. The inclusions must be far away, such that their interaction is merely weak. De facto $\lambda \gg d_{\min} \gg a$.

structures, as they offer a simplified analysis when dealing with a certain density ν of particles in a finite volume V, as shown in Fig 4.6. However, such homogenization procedure has a lot of assumptions. First of all, which is common to all homogenization approaches, the size of the particles, or inclusions, is much smaller than the operational wavelength of light. In this limit, the electromagnetic field cannot probe the microscopic details of the structure, but perceives the small particles as ellipsoids. However, the effective permittivity still depends on the aspect ratio of the inclusions, whose shapes are approximated by ellipsoids. Second, the particles are not allowed to strongly interact with each other, meaning that they are required to be sufficiently far from each other, such that one particle does only weakly distort the local field field exerted at a neighbouring particle. This latter condition can be lifted by instead of studying inclusions embedded into an environment, but rather studying a mixing between two phases, where (at least) two materials are treated symmetrically. This is dealt with in the Bruggeman mixing rule [130]. Consequently, the Maxwell-Garnett mixing rule can only be valid for low volume concentrations, or alternatively, for a low filling factor $f := \nu V$. For the sake of simplicity, we assume that the particles to be spheres. More complicated inclusions are studied in Ref. [130] as well. If the assumptions above hold, the local response approximation is valid and the displacement field upon an illumination with a spatially uniform external field $\tilde{\mathbf{E}}_{\text{ext}}$ is given by

$$\tilde{\mathbf{D}}(\mathbf{k}, k_0) = \epsilon_{\text{eff}}(k_0)\tilde{\mathbf{E}}_{\text{ext}}(\mathbf{k}, k_0) = \epsilon_h \tilde{\mathbf{E}}_{\text{ext}}(\mathbf{k}, k_0) + 4\pi\tilde{\boldsymbol{\mathcal{P}}}(\mathbf{k}, k_0)\,, \tag{4.64}$$

where ϵ_{eff} is the effective, averaged permittivity and ϵ_h the permittivity of the environment (host) medium. Traditionally, the host medium is assumed to be non-dispersive. Now, the task reduces to finding an expression for the polarization density $\tilde{\boldsymbol{\mathcal{P}}}$ as a function of the external field $\tilde{\mathbf{E}}_{\text{ext}}$.

As discussed in Sec. 3.1 in the deep-subwavelength regime a particle can be described by an electric dipole polarizability α_{el}, where the induced polarization density due to the external field of light is given by the linear relationship

$$\tilde{\boldsymbol{\mathcal{P}}}(\mathbf{k}, k_0) = \nu\tilde{\mathbf{p}}(\mathbf{k}, k_0) = \nu\alpha_e(k_0)\tilde{\mathbf{E}}_{\text{loc}}(\mathbf{k}, k_0)\,. \tag{4.65}$$

In a sufficiently dense structure, the local field $\tilde{\mathbf{E}}_{\text{loc}}$ must forcibly differ from the external field $\tilde{\mathbf{E}}_{\text{ext}}$, as the surrounding polarization from other inclusions locally increases the field effect by means of the superposition principle. For very diluted mixtures, they are equal, but for a non-negligible concentration n of spherical inclusions, it holds

$$\tilde{\mathbf{E}}_{\text{loc}}(\mathbf{k}, k_0) = \tilde{\mathbf{E}}_{\text{ext}}(\mathbf{k}, k_0) + \frac{4\pi}{3\epsilon_h}\tilde{\boldsymbol{\mathcal{P}}}(\mathbf{k}, k_0)\,, \tag{4.66}$$

where $\frac{1}{3\epsilon_h}\tilde{\boldsymbol{\mathcal{P}}}(\mathbf{k}, k_0)$ is the polarization field. Due to the isotropy of the sphere, we have the prefactor 1/3 which refers to its depolarization factor. Combining Eqs.(4.65-4.66) and solving for the averaged polarization density, we arrive at the formula

$$\tilde{\boldsymbol{\mathcal{P}}}(\mathbf{k}, k_0) = \frac{\nu\alpha_{el}(k_0)}{1 - \frac{4\pi\nu\alpha_{el}(k_0)}{3\epsilon_h}}\tilde{\mathbf{E}}_{\text{ext}}(\mathbf{k}, k_0) = \chi(k_0)\tilde{\mathbf{E}}_{\text{ext}}(\mathbf{k}, k_0)\,. \tag{4.67}$$

Finally, the effective permittivity $\epsilon_{\text{eff}}(k_0) = \epsilon_h + 4\pi\chi(k_0)$ reads

$$\epsilon_{\text{eff}}(k_0) = \epsilon_h + 4\pi\frac{\nu\alpha_{el}(k_0)}{1 - \frac{4\pi\nu\alpha_{el}(k_0)}{3\epsilon_h}}\,. \tag{4.68}$$

For our purposes, we rather want to express the effective permittivity as a function of the permittivity $\epsilon_i(k_0)$ of the inclusions, rather than by their polarizabilities. For a sphere, the polarizability is easy to calculate. It is proportional to the internal field within the inclusions and to the permittivity contrast $(\epsilon_i - \epsilon_h)$ between the inclusion and the environment. Moreover, a uniform external field across a sphere induces a uniform field $\tilde{\mathbf{E}}_{\text{int}}$ within the sphere, which reads (c.f. Ref. [81] Ch. 4.4)

$$\tilde{\mathbf{E}}_{\text{int}}(\mathbf{k}, k_0) = \frac{3\epsilon_h}{\epsilon_i(k_0) + 2\epsilon_h}\tilde{\mathbf{E}}_{\text{ext}}(\mathbf{k}, k_0)\,. \tag{4.69}$$

With $\tilde{\mathbf{p}}(\mathbf{k}, k_0) = \alpha_{el}(k_0)\tilde{\mathbf{E}}_{\text{ext}}(\mathbf{k}, k_0)$, we obtain

$$\alpha_{el}(k_0) = \frac{V}{4\pi}(\epsilon_i(k_0) - \epsilon_h)\frac{3\epsilon_h}{\epsilon_i(k_0) + 2\epsilon_h}\,. \tag{4.70}$$

Inserting this equation into the Clausius-Mossotti formula (4.68) and together with $f = \nu V$, we end up with the Maxwell-Garnett equation

$$\epsilon_{\text{eff}}(k_0) = \epsilon_h + 3f\epsilon_h\frac{\epsilon_i(k_0) - \epsilon_h}{\epsilon_i(k_0) + 2\epsilon_h - f(\epsilon_i(k_0) - \epsilon_h)}\,. \tag{4.71}$$

In the limiting cases $f \to 0$ and $f \to 1$, which correspond to filling factors of 0% and 100%, respectively, we obtain as expected the permittivities $\epsilon_{\text{eff}} = \epsilon_h$ and $\epsilon_{\text{eff}}(k_0) = \epsilon_i(k_0)$.

Note that other more advanced mixing rules that incorporate multiphase mixtures with anisotropic inclusions exist [130]. They are not of relevance here and, therefore, will not be discussed. Soon, for the wire-medium, we require the usage of the Maxwell-Garnett formula for cylindrical inclusions. There, the effective permittivity cannot be simply regarded as a scalar but is rather a matrix of a uniaxial medium. The effective permittivity (tensor) for cylindrical inclusions are found in Ref. [131].

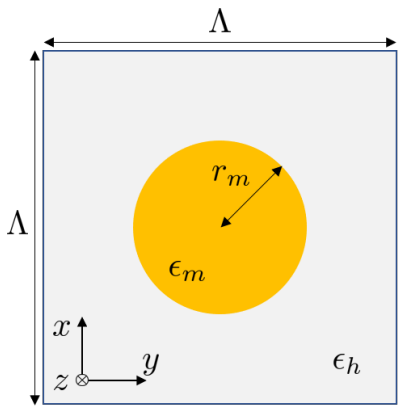

Figure 4.7: Top view a square unit cell consisting of a cylindrical metallic wire with radius r_m and permittivity ϵ_m embedded in a dielectric host medium with permittivity ϵ_h. Being periodically arranged in the xy-plane and arbitrarily extruded in the z-direction, they form an a square lattice where the metallic wires are along the z-axis.

4.4.2 Nonlocal wire medium model

In the framework of nonlocal homogenization, one of the most studied materials is the plasmonic wire medium. Here, we would like to recap some important facts about the effective medium approach for the nonlocal wire medium. The main results concerning the dispersion relations are found in Ref. [61] and the associated (additional) interface conditions in Ref. [59].

Let's consider an array of metallic nanowires with a dispersive permittivity $\epsilon_m(k_0)$, that is embedded in a dielectric host medium ϵ_h. The host medium is again assumed to be non-dispersive. The plasmonic nanowires are assumed to be intrinsically nonmagnetic and are fully described by a Drude-type permittivity (3.65). The nanowires have a radius r_m and are periodically aligned in the x- and y-directions with lateral periods Λ forming a square unit cell and infinitely extended in the z-direction. The basic geometry for the structure is depicted in Fig. 4.7. The structure has three perpendicular mirror planes and is, therefore, centrosymmetric, with an additional invariance along the z-direction. Such structures have a C_4-symmetry and can, accordingly, be regarded as a uniaxial medium.

In the limit of small surface concentrations of plasmonic nanowires, i.e., for $f = \frac{\pi r_m^2}{\Lambda^2} \ll 1$, the tangential components of the effective response tensor can be approximated by the Maxwell-Garnett permittivities for small cylinders, that read

$$\epsilon_{xx}^{\mathrm{loc}}(k_0) = \epsilon_{yy}^{\mathrm{loc}}(k_0) = \epsilon_h \frac{(1+f)\epsilon_m(k_0) + (1-f)\epsilon_h}{(1+f)\epsilon_h + (1-f)\epsilon_m(k_0)}\,. \tag{4.72}$$

By virtue of the C_4-symmetry of the unit cell, the transverse permittivities $\epsilon_{xx}^{\mathrm{loc}}(k_0)$ and $\epsilon_{yy}^{\mathrm{loc}}(k_0)$ are equal.

Dispersion relations

In the last decades, it was shown that such structures experience a strong nonlocal response, when excited with a TM-polarized electromagnetic wave [57], [60]. In physical terms, the z-component of the electric field longitudinally couples to the free charge carriers in the metallic wires and induces a nonlocal current therein. Hence, all nonlocal

effects are encoded in the z-component of the spatially dispersive permittivity, in form of a k_z-dependent function. Therefore, we shall only discuss the TM-polarized case here. Under the usage of the coherent potential approximation [132], it was shown from solid physical grounds that

$$\epsilon_z(k_z, k_0) = \frac{\epsilon_z^{\mathrm{loc}}(k_0) + \epsilon_m(k_0)\eta(k_0)\left(\frac{k_z}{k_0}\right)^2}{1 + \eta(k_0)\left(\frac{k_z}{k_0}\right)^2}\,, \tag{4.73}$$

with the Maxwell-Garnett averaged permittivity

$$\epsilon_z^{\mathrm{loc}}(k_0) = (1-f)\epsilon_h + f\epsilon_m(k_0)\,. \tag{4.74}$$

The parameter η in (4.73) is dimensionless and is a measure for the nonlocality, which reads $\eta(k_0) = \frac{\Gamma_{\mathrm{E}}}{4}(k_0 r_m)^2$, where $\Gamma_{\mathrm{E}} \approx 0.5772...$ is the Euler-Mascheroni constant. For vanishing small nanorods, i.e. $r_m \to 0$, we have $\eta(k_0) \to 0$ and, therefore, converge to the local limit $\epsilon_z(k_z, k_0) \to \epsilon_z^{\mathrm{loc}}(k_0)$. The nonlocal response in Eq. (4.73) can be regarded as a Padé-type response with

$$\hat{\tilde{\mathbf{q}}}(k_z, k_0)\tilde{\mathbf{D}}(\mathbf{k}, k_0) = \hat{\tilde{\mathbf{p}}}(k_z, k_0)\tilde{\mathbf{E}}(\mathbf{k}, k_0)\,. \tag{4.75}$$

Here we have

$$\hat{\tilde{\mathbf{p}}}(k_z, k_0) = \mathrm{diag}\left(\epsilon_x^{\mathrm{loc}}, \epsilon_y^{\mathrm{loc}}, \epsilon_z^{\mathrm{loc}}\right) + \epsilon_m\eta\left(\frac{k_z}{k_0}\right)^2 \mathbf{e}_z \otimes \mathbf{e}_z$$

and

$$\hat{\tilde{\mathbf{q}}}(k_z, k_0) = \mathbb{1} + \eta\left(\frac{k_z}{k_0}\right)^2 \hat{\mathbf{e}}_z \otimes \hat{\mathbf{e}}_z\,.$$

By $\otimes$, we denote the tensor product between two vectors. A Padé-type response is an approximation by a rational function (here a function of k_z), i.e., by a Padé-approximant. The Taylor approximation is just a special case of the Padé-approximation, where the denominator is one and, therefore, a polynomial function. The nonlocal response function for the wire medium model, i.e., (4.73) is specifically a rational function of k_z^2 and, therefore, of Padé-type.

To calculate the dispersion relations in the bulk, the wave equation has to be solved. By inserting ansatz (4.75) into the wave-equation. (4.3), we obtain for Padé-type responses the following equation

$$\hat{\tilde{\mathbf{q}}}(k_z, k_0)\mathbf{k} \times \mathbf{k} \times \tilde{\mathbf{E}}(\mathbf{k}, k_0) = k_0^2 \hat{\tilde{\mathbf{q}}}(k_z, k_0)\tilde{\mathbf{E}}(\mathbf{k}, k_0)\,. \tag{4.76}$$

Similar to the nonlocal models we discussed in Sec. 4.1, the wave equation is here a k_z-polynomial of fourth degree, where the solution in the TM-polarization are

$$\begin{aligned}\left(k_{z,\sigma}^{\mathrm{WM}}(k_t, k_0)\right)^2 = {} & \frac{\eta\epsilon_{tt}^{\mathrm{loc}}\left(\epsilon_m k_0^2 - k_t^2\right) - k_0^2\epsilon_z^{\mathrm{loc}}}{2\eta\epsilon_m} \\ & + \sigma\sqrt{\frac{4\eta\epsilon_m\epsilon_{tt}^{\mathrm{loc}}\left(\epsilon_z^{\mathrm{loc}}k_0^4 - k_0^2k_t^2\right) + \left[k_0^2\epsilon_z^{\mathrm{loc}} - \eta\epsilon_{tt}^{\mathrm{loc}}\left(\epsilon_m k_0^2 - k_t^2\right)\right]^2}{4\eta^2\epsilon_m^2}}\,,\end{aligned} \tag{4.77}$$

where $\sigma = \pm 1$, denotes the mode mode index, which propagate in one direction in the medium. For the sake of readability, we omitted the explicit frequency dependence of the material parameters on the RHS of Eq. (4.77).

The dispersion relation above deserves some comments. First of all, the functional dependence of the wave vector component in the main propagation direction is expressed by all parameters describing the actual geometry of the wire medium, i.e., radius r_m, permittivities ϵ_m and ϵ_h of both the dielectric host and metallic wires, in an entirely analytical way. Second, in the homogeneous picture the eigenmodes are, again, plane waves and the wave-equation has four different eigenvalues (4.77), where each pair differs by a sign. This suggests that for every given set of material parameters, the total field is a superposition of pairwise two forward and two backward propagating plane waves with a different propagation constants $k_{z,\sigma}^{\mathrm{WM}}$. In order to uniquely determine these plane wave amplitudes, additional interface conditions must be taken into account.

Additional interface conditions

Specially conceived for the wire medium, an additional interface condition was phenomenologically proposed in Ref. [59]. To this end, let's again consider an interface $\Gamma = \overline{\mathbb{R}^3_-} \cap \overline{\mathbb{R}^3_+}$ separating these two half-spaces, where $\overline{\mathbb{R}^3_-}$ is filled with a local scalar permittivity ϵ_C and $\overline{\mathbb{R}^3_+}$ is occupied by the wire medium. The interface conditions for the wire medium model read

$$(\mathbf{E}_- - \mathbf{E}_+) \times \mathbf{n} = 0\,, \tag{4.78}$$

$$(\nabla \times \mathbf{E}_- - \nabla \times \mathbf{E}_+) \times \mathbf{n} = 0\,, \tag{4.79}$$

$$(\epsilon_C \mathbf{E}_- - \epsilon_h \mathbf{E}_+) \cdot \mathbf{n} = 0\,, \tag{4.80}$$

where $\mathbf{E}_-$ and $\mathbf{E}_+$ are, respectively, the restrictions of $\mathbf{E}$ to $\mathbb{R}^3_-$ and $\mathbb{R}^3_+$ and $\mathbf{n}$ being the unit vector, normal to the interface. The first two interface conditions are the classical ones, which state the continuity of the tangential components of, first, $\mathbf{E}(\mathbf{r}, k_0)$ and, second, of $\nabla \times \mathbf{E}(\mathbf{r}, k_0)$. The second interface condition is equivalent to the continuity of the tangential component of $\mathbf{H}(\mathbf{r}, k_0)$, which suggests that the nonlocal wire medium model does not maintain an artificial magnetic response. This is in a good approximation, if, and only if, the metallic wires are very thin compared to the wavelength. Only then, the skin penetration depth of the conducting wires is negligible. Finally, the third interface condition (4.80) is the actual new one, which was phenomenologically proposed by enforcing that the normal component of the macroscopic current density vanishes at the interface, and does not leak out from the half-space, independent from the operating wavelength. Here, one has to be careful and Eq. (4.80) should not be confused with the continuity of the normal component of the displacement field $\mathbf{D}(\mathbf{r}, k_0)$. These are completely different interface conditions, since the latter one would further comprise the permittivity $\epsilon_m(k_0)$ of the metallic wires. Besides, in real space $\mathbf{D}(\mathbf{r}, k_0)$ and $\mathbf{E}(\mathbf{r}', k_0)$, and are not simply connected by an algebraic product, but are rather correlated by a spatial convolution (c.f. Eq. (3.31)), through a nonlocal response kernel which depends on the relative vector $\mathbf{r} - \mathbf{r}'$. Therefore, interface condition (4.80) is truly an additional interface condition and not a reformulation of the classical continuity condition for $\mathbf{D}$.

Reflection and transmission from a slab

Putting both dispersion relations (4.77) and interface conditions (4.78)-(4.80) together, we can fully derive and evaluate the Fresnel matrix for a slab of a nonlocal wire medium,

with thickness d_{slab}, which we find to be

$$\underline{\underline{\mathbf{F}}}^{\text{WM,TM}} = \begin{pmatrix} k_z^R & A_+ & A_- & -A_+ & -A_- & 0 \\ \left(\mathbf{k}^R\right)^2 & B_+ & B_- & B_+ & B_- & 0 \\ \epsilon_C & -\epsilon_h & -\epsilon_h & -\epsilon_h & -\epsilon_h & 0 \\ 0 & A_+ \mathrm{e}^{\mathrm{i}k_{z,+}^{\text{WM}} d_{\text{slab}}} & A_- \mathrm{e}^{\mathrm{i}k_{z,-}^{\text{WM}} d_{\text{slab}}} & -A_+ \mathrm{e}^{-\mathrm{i}k_{z,+}^{\text{WM}} d_{\text{slab}}} & -A_- \mathrm{e}^{-\mathrm{i}k_{z,-}^{\text{WM}} d_{\text{slab}}} & k_z^T \\ 0 & B_+ \mathrm{e}^{\mathrm{i}k_{z,+}^{\text{WM}} d_{\text{slab}}} & B_- \mathrm{e}^{\mathrm{i}k_{z,-}^{\text{WM}} d_{\text{slab}}} & B_+ \mathrm{e}^{-\mathrm{i}k_{z,+}^{\text{WM}} d_{\text{slab}}} & B_- \mathrm{e}^{-\mathrm{i}k_{z,-}^{\text{WM}} d_{\text{slab}}} & \left(\mathbf{k}^T\right)^2 \\ 0 & -\epsilon_h \mathrm{e}^{\mathrm{i}k_{z,+}^{\text{WM}} d_{\text{slab}}} & -\epsilon_h \mathrm{e}^{\mathrm{i}k_{z,-}^{\text{WM}} d_{\text{slab}}} & -\epsilon_h \mathrm{e}^{-\mathrm{i}k_{z,+}^{\text{WM}} d_{\text{slab}}} & -\epsilon_h \mathrm{e}^{-\mathrm{i}k_{z,-}^{\text{WM}} d_{\text{slab}}} & \epsilon_S \end{pmatrix}, \tag{4.81}$$

with matrix elements $A_\sigma = -\frac{\epsilon_{zz}}{\epsilon_{tt}} k_{z,\sigma}^{\text{WM}}$ and $B_\sigma = \left(A_\sigma k_{z,\sigma}^{\text{WM}} - k_t^2\right)$, and ϵ_S and ϵ_C refer to the permittivities of the substrate and cladding, respectively. Here as well, each line in the matrix represents the interface conditions (4.78)-(4.80), in the same order.

Ultimately, the complex valued reflection and transmission coefficients from the wire medium slab are

$$\begin{aligned} \rho^{\text{WM,TM}}(k_t, k_0, \epsilon_m, \epsilon_h, r_m, d_{\text{slab}}) &= \left[\left(\underline{\underline{\mathbf{F}}}^{\text{WM,TM}}\right)^{-1} \cdot \underline{\mathbf{I}}\right]_1 , \\ \tau^{\text{WM,TM}}(k_t, k_0, \epsilon_m, \epsilon_h, r_m, d_{\text{slab}}) &= \left[\left(\underline{\underline{\mathbf{F}}}^{\text{WM,TM}}\right)^{-1} \cdot \underline{\mathbf{I}}\right]_6 , \end{aligned} \tag{4.82}$$

with the input vector $\underline{\mathbf{I}} = \left(k_z^I, \left(\mathbf{k}^I\right)^2, \epsilon_C, 0, 0, 0\right)$.

Concerning the TE-polarized case, the reflection and transmission coefficients for the nonlocal wire medium model is equivalent to those of the WSD case (4.60) with the further restriction of $\hat{\mu} = 1$.

We will discuss the difference between the wire medium model and the SSD model by comparing reflection and transmission coefficients obtained from both homogenization models in comparison to the exact response from a concrete slab in Sec. 5.3.3 of the next chapter.

4.5 Chapter summary and concluding remarks

In this chapter, we first studied light propagation in optical metamaterials with strong spatial dispersion. As a starting-pont, we departed from the commonly used WSD model, where the material's response is assumed to be local and characterized by a dispersive permittivity and magnetic permeability. We extended the WSD approximation by introducing nonlocal parameters in two ways. Once we introduced second-order symmetry terms (SYM model), which are usually unjustifiably neglected, and second, we included a more advanced fourth-order contribution (SSD model), which retains higher-order spatial derivatives of the electric field, giving a more accurate description the metamaterial in the slightly-subwavelength regime. Our nonlocal models can be generically used for any centrosymmetric metamaterial and, in contrast to other nonlocal approaches, e.g. the wire medium model, they are not linked to a specific metamaterial geometry.

In the analysis of the dispersion relations, i.e. in Sec. 4.1, one major finding is the enhancement of the functional dependency of the isofrequency contours, which were limited to hyperbolas and ellipses in the local description. This was illustrated in Figs. 4.1-4.3 for generically chosen effective material parameters. The complexity of the curves is a clear indication of the ability to capture the effects of spatial dispersion. Moreover, we have shown that the proposed models with a nonlocal response increase the number of

plane waves being excited in the bulk metamaterial. In each nonlocal model, we find two forward and two backward propagating modes. While concentrating on the modes with $\Im k_{z,\sigma} > 0$, which in our sign convention correspond to modes that would exponentially decay while they propagate in the positive z-direction, we find that these two modes clearly distinguish themselves from the magnitude of both real and imaginary parts of $k_{z,\sigma}$. The solution with the larger imaginary part is being more absorbed in the medium and corresponds, therefore, to the additional wave. The fundamental wave is defined by the wave with the smallest positive imaginary part in the dispersion relation.

This would also mean that an illumination of a metamaterial half-space with a plane wave, will cause the propagation of a superposition of two linearly independent transmitted modes in the half-space occupied by such nonlocal metamaterials. Previously, i.e., in the WSD approach, only one plane wave is transmitted. To uniquely find these field amplitudes at the interface, we derived in Sec. 4.2 the necessary (additional) interface conditions.

We would like to emphasize again, that the interface conditions (IC_1)-(IC_6) do not just come out of the blue. They were rather derived on solid mathematical grounds, using the weak formulation of the wave equation, ergo, a specific variational method. In theory, taking into account an arbitrary high order of spatial derivatives would also mean that the number of additional modes will be arbitrary high as well, with different propagation constants $k_{z,j}$, where j denotes the mode number. Consequently, a higher number of interface conditions is necessary. Using the general formalism proposed here, further types of nonlocal constitutive relations can be analyzed.

Ultimately, in Sec. 4.3, we combined both bulk and interface aspects above to reconstruct the Fresnel equations for all discussed models in both TE- and TM-polarizations. These are the final equations in our theory, which can be used to predict both reflection and transmission from a slab upon illuminating with a plane wave. Also, the limit of a reflection form a half-space metamaterial was discussed which can be used in the study of surface plasmons polaritons excited at the interface of a nonlocal metamaterial.

In conclusion, to decide on the applicability of the different models, a comparison of their prediction to the actual response of a referential material is mandatory. Hence, each metamaterial that is subject to homogenization, has to be studied individually. Only after a comparison with the bulk properties and, more importantly, the reflection and transmission from a slab for a specific frequency range, a judgment on the model can be made. This will be the topic of the next Chapter 5, where all the theory developed thus far, finally comes into action. To this end, a parameter retrieval method will be introduced and employed for different optical metamaterials.

Besides, we introduced in Sec. 4.4.1 the commonly used Maxwell-Garnett formula, which will be used in the next Chapter as a benchmark for the parameter retrieval of a material consisting of dielectric spheres on a cubic lattice. It has to be mentioned that this is the most basic homogenization approach, but also the easiest one to apply in practice. Additionally, we presented the prototype model for the effective description of wire media with nonlocal effects in Sec. 4.4.2. In the Sec. 5.3.3 of the next chapter, we will compare the wire medium model and the SSD model at the stage of homogenizing a concrete wire medium structure. We will show that the effective description is not unique and that different constitutive relations can be used to homogenize metamaterials.

5 | Effective parameter retrieval

We must trust to nothing but facts: These are presented to us by Nature, and cannot deceive.

Antoine Lavoisier - Elements of Chemistry

In the preceding chapter, we proposed models for a homogenization of metamaterials with spatial dispersion. We derived the dispersion relations, the necessary interface conditions, and lastly the corresponding reflection and transmission coefficients. Each model has a set of parameters, namely the effective material parameters that are to be assigned to a given metamaterial. In this chapter, we will impose these models to effectively describe certain metamaterials. We will check the validity of each model and answer the question whether a metamaterial can be actually replaced by a homogeneous one. This can be done at first by comparing the bulk properties in terms of eigenmodes. In particular, this requires to study the isofrequency contours given by the analytical expressions of the models, compared to those of the referential metamaterial. If a model is valid for the effective description of that give metamaterial, then we can retrieve meaningful effective material parameters. To this end, there are many tools for the retrieval, with mixed advantages and disadvantages. The Maxwell-Garnett homogenization is easiest to apply and directly gives the effective permittivity of a heterogeneous mixture (c.f. Eq. (4.71)). However, this only works in the quasi-static regime, which is not of interest in the research of optical metamaterials. Other techniques such as the homogenization by field averaging [35] can be applied to metamaterials as well, but they are computationally very intensive and essentially require simulations. They are unfortunately not accessible for experiments. Very commonly used is also the Lorentz-Drude Model Optimization Approach [133], where the metamaterial is, again, described by an effective permeability and permittivity (local approach). These material parameters have a frequency dependency either of Lorentz (3.64) or Drude type (3.65), and the method relies on optimizing the free parameters appearing in these equations, i.e., plasma frequency, resonance frequency, and the damping coefficient, such that the error between the response of the calculated model and that reference material is minimized.

Despite the versatile number of methods, none of them incorporates spatial dispersion effects. Only few methods [134] consider such effects, but again are by no means general-purpose tools and require the metamaterial to possess a specific geometry, such as a wire medium structure [135] or spheres on a cubic lattice [136]. Fact is, there is no absolutely best tool for the retrieval, but the one which is accessible for both numerical and experimental setups is the scattering parameter retrieval, also known as S-parameter retrieval. This retrieval method was already introduced by Nicolson and Ross [137] followed by Weir [138] in the early 1970s. Three decades later Smith *et al.* applied the S-parameter retrieval to metamaterials [38]. In this approach, having the analytical expressions for the reflection and transmission coefficients from a slab with finite thickness is mandatory. From these expressions, the effective material parameters can be deduced. The latter quantities are then functions of reflection and transmission coefficients, which are easily calculated numerically. Experimentally, amplitude and phase measurements lead to complex valued reflection and transmission coefficients as well. This data can be used as input for the retrieval procedure.

In its early stage however, the S-parameter retrieval was limited to the normal incidence only, and to the assumption of isotropic material laws. Later on, Menzel *et al.* proposed an extension to bi-isotropic [139] and then to anisotropic [53] material laws, including the retrieval at oblique incidence. In their latter work they have shown the validity of their retrieval only in the paraxial regime. The invalidity at higher angles of incidence goes back to the assumption of local material laws. In our contribution [126], we were to extended this method while retaining nonlocal constitutive relations and have shown that the effective material parameters can be meaningfully retrieved beyond the paraxial regime. One huge drawback of the S-parameter retrieval is the complex branch cuts. The expressions for reflection and transmission coefficients contain exponential functions of type $\mathrm{e}^{\mathrm{i}k_z d_{\mathrm{slab}}}$ with complex arguments, whose inversion have multiple solutions. Hence, it is possible that the inverted quantities may land on different Riemann sheets, when evaluating the complex logarithm at different frequencies or angles of incidence. To lift this issue, at least two measurements/simulations with different slab thicknesses d_{slab} are required to find the right branch [140]. Alternatively, the slab can be chosen to be very thin compared to the propagation constant k_z, such that $k_z d_{\mathrm{slab}} \ll 1$. However, the material is in this case so thin, that bulk properties cannot be reliably retrieved.

This chapter is structured as follows. In the following two sections, we explain the S-parameter retrieval and the way the referential reflection and transmission coefficients from a periodic metamaterial slab are numerically obtained. In Sec. 5.3, apply the S-parameter retrieval to three different structures, namely a layer of dielectric spheres on a cubic lattice, the fishnet metamaterial, and the plasmonic wire medium. We particularly show that going from a second order to a fourth order constitutive relation allows for a better prediction of the actual optical coefficients of heterogeneous metamaterials when compared to full wave reference simulations. In Sec. 5.4, going back to the examples of fishnet and wire medium, we show the limits of the homogenization approaches considered here and the drawbacks of the S-parameter retrieval method. We also discuss potential solutions that may lift some issues discussed in the corresponding subsections.

5.1 S-parameter optimization approach

The retrieval is done for each frequency individually. The number of required pairs of reflection and transmission coefficients depends on the number of effective material parameters. For instance, under the assumption of WSD and isotropy, the only material parameters are the two complex numbers ϵ and μ. They may be retrieved by direct inversion of the complex valued ρ^{WSD} and τ^{WSD} from Eqs. (4.60) at normal incidence [140]. If the material is additionally anisotropic, the material parameters ϵ_{zz} and μ_{zz}, which, respectively, couple to the field components E_z and H_z, can only be probed at oblique incidence [141]. However, it turned out that the latter authors find that the retrieved effective material parameters depend on the angle of incidence, which cannot be correct for homogeneous metamaterials. Simply, because the material parameters are supposed to be independent from $\mathbf{k}$[1]. Certainly, this is linked to the assumption of local constitutive relations for the attempt of homogenizing mesoscopic metamaterials. In their example, the authors took the fishnet metamaterial with a lateral periodicity of about only a third

[1]Note that this is not in contradiction with spatial dispersion. The response tensor $\hat{\tilde{\mathbf{R}}}(\mathbf{k}, k_0)$ remains $\mathbf{k}$-dependent, even when isotropy is assumed. However, the coefficients $\tilde{\mathbf{C}}_\alpha(k_0)$ from Eq. (3.41), e.g., $\hat{\epsilon}(k_0)$, $\hat{\mu}(k_0)$, $\hat{\beta}^j(k_0)$, and $\gamma(k_0)$ do not depend on $\mathbf{k}$.

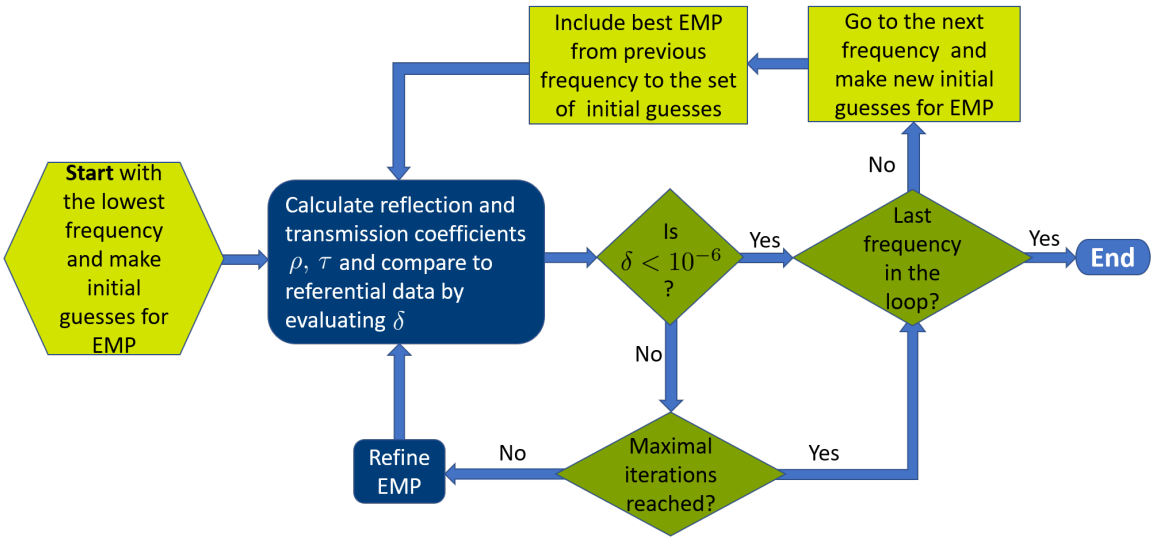

Figure 5.1: The used optimization algorithm to determine effective material parameters (EMP). Several initial guesses for the EMP will be probed and refined in order to minimize the objective function δ, that is given in Eq. (5.1). To improve the performance of the retrieval method and to lift the issue with different branch cuts, the best fit from the previous frequency will be used as an initial guess for the current frequency.

of the wavelength in the effective medium. Clearly, the dynamics of the fields of light, i.e., nonlocality are relevant and should have been considered. However, with nonlocality, the reflection and transmission coefficients are highly nonlinear functions of the effective material parameters and cannot be simply inverted as in the WSD case.

For these reasons, we have to reformulate the S-parameter retrieval from an inversion problem to a fitting problem. We call this the S-parameter optimization problem. The algorithm is represented in the flowchart in Fig. 5.1. At each individual frequency k_0, the analytically calculated reflection and transmission coefficients ρ and τ have to be fitted to a pair of referential reflection and transmission ρ^{REF} and τ^{REF} coefficients obtained either from measurements or simulations of the actual metamaterial, by means of minimizing an objective function δ with respect to the material parameters and for all possible angles of incidence $k_t \in [0, k_0)$. The objective function reads

$$\delta(k_0) = \min_{\substack{\hat{\epsilon},\hat{\mu},\\ \hat{\beta}^j,\hat{\gamma}}} \sum_{k_t=0}^{k_0} \frac{w(k_t)}{2} \left(\left| 1 - \frac{\rho(k_t, k_0, \hat{\epsilon}, \hat{\mu}, \hat{\beta}^j, \hat{\gamma}, d_{\mathrm{slab}})}{\rho^{\mathrm{ref}}(k_t, k_0, d_{\mathrm{slab}})} \right| + \left| 1 - \frac{\tau(k_t, k_0, \hat{\epsilon}, \hat{\mu}, \hat{\beta}^j, \hat{\gamma}, d_{\mathrm{slab}})}{\tau^{\mathrm{ref}}(k_t, k_0, d_{\mathrm{slab}})} \right| \right) , \tag{5.1}$$

which is a measure how well a model applies to homogenize a structure. Here, ρ and τ correspond to the analytically derived reflection and transmission coefficients for either the WSD ($\hat{\beta}^j = \hat{\gamma} = 0$), the SYM ($\hat{\gamma} = 0$), or the SSD ($\hat{\beta}^j = 0$) models, which were calculated for both TE- and TM-polarizations in Sec. 4.3. For the lowest frequency, a set of initial guesses for the material parameters are assumed. The function $w(k_t)$ is a weight function, which depends on the angle of incidence, and chosen in a way, such that the fitting procedure is more focused for small k_t. Here, we chose an exponentially decaying weight, such that

$$w(k_t) = \mathrm{e}^{-\alpha k_t} ,$$

where $\alpha = 2.5\Lambda_t$, with Λ_t being the lateral period of the metamaterial in t-direction. The choice of such weight function is justified by our requirement to be able to reproduce at

least reflection and transmission in the paraxial regime, and look subsequently how far we can extend this region of applicability also to higher oblique incidence angles. For the optimization purposes, the set of $(\hat{\epsilon}, \hat{\mu}, \hat{\beta}^j, \hat{\gamma})$ that minimize δ at frequency $k_{0,i}$, will be used as initial guess for the next frequency $k_{0,i+1}$. Since the material parameters are assumed to be smooth functions of k_0, this step will first lift the problem with complex branch-cuts, and second, speeds up the retrieval process tremendously. Of course, this approach remains slower than a direct inversion of the equations. However, it is more adaptable and can be used when no closed form for the effective material parameters exist.

TE-polarized light		TM-polarized light	
$(k_x, 0, k_z)$	$(0, k_y, k_z)$	$(k_x, 0, k_z)$	$(0, k_y, k_z)$
ϵ_{yy}	ϵ_{xx}	ϵ_{xx}	ϵ_{yy}
μ_{xx}	μ_{yy}	ϵ_{zz}	ϵ_{zz}
μ_{zz}	μ_{zz}	μ_{yy}	μ_{xx}
γ_{yy}	γ_{xx}	β_{xx} or γ_{xx}	β_{yy} or γ_{yy}
-	-	β_{zz} or γ_{zz}	β_{zz} or γ_{zz}

Table 5.1: Relevant material parameters that couple to light depending on the polarization and the incidence plane.

As a consequence of anisotropy, all effective material parameters can only be retrieved by considering the four independent illumination directions and polarizations. Here, we consider the four $(\mathrm{TM}, \mathrm{TE}) \times (k_x, k_y)$ illuminations. The retrievable material parameters for each case are summarized in Tab. 5.1. We notice that the nonlocal parameter $\hat{\gamma}$ acts similarly to the permittivity $\hat{\epsilon}$, i.e., it couples only to the electric field components that appear in the considered polarization. For example, in the TM-k_y polarized case, the electric field is $\mathbf{E} = (0, E_y, E_z)$ and couples to $(\epsilon_{yy}, \epsilon_{zz})$ and to $(\gamma_{yy}, \gamma_{zz})$, while the magnetic field $\mathbf{H} = H_x \hat{\mathbf{e}}_x$ couples to μ_{xx}. Concerning the parameters β_{jj}, for $j \in \{x, y, z\}$, they are only relevant in the TM-polarization, but then, they couple similarly to ϵ_{jj}.

Now that the retrieval is introduced, we need to know how to numerically obtain the referential reflection and transmission coefficients ρ^{REF} and τ^{REF} from a periodic metamaterial slab. In this work, we have not access to experimental data.

5.2 Reflection and transmission from a periodic metamaterial

The description of the Fourier Modal Method (FMM) in this section is predominantly adopted from Ref. [142]. Since we aim to homogenize periodic metamaterials with sub-wavelength unit cells, a rigorous full-wave description of the periodic metamaterial is indispensable to determine both dispersion relations in the bulk as well as the reflection and transmission coefficients form a slab. These quantities will serve then in the parameter retrieval as the referential quantities describing the actual metamaterial. For the periodic metamaterial considered here, the Bloch theorem may simplify the treatment as it is not necessary to consider in these full-wave simulations the entire space but only a single unit cell. [27]. In this section, we suppress the frequency dependence of the fields and material parameters, as we intend demonstrate the FMM at a fixed frequency k_0. According to

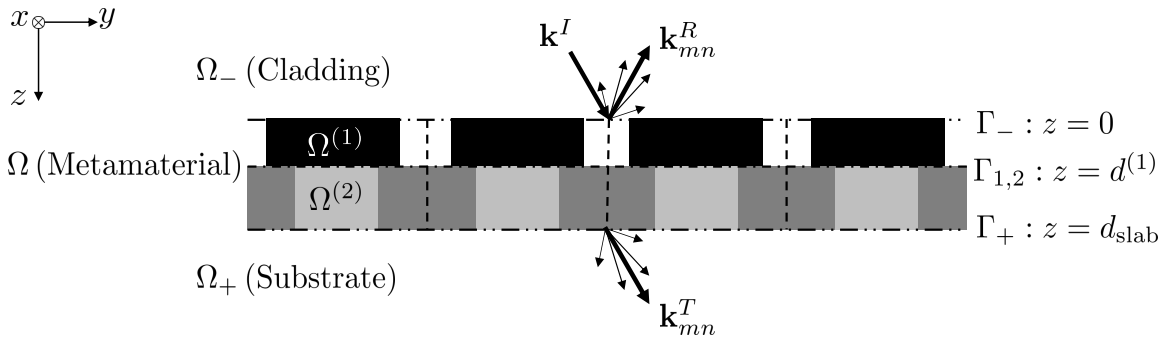

Figure 5.2: Reflection and transmission from a periodic metamaterial with thickness d_{slab} upon illumination with a single plane wave $\mathbf{k}^I$. At the first interface Γ_-, part of the fields will be reflected back as a superposition of diffracted plane waves with $\mathbf{k}^R_{mn}$, and a portion propagates through metamaterial slab. At the interface Γ_+ we obtain the transmitted fields with wave vectors $\mathbf{k}^T_{mn}$. The periodic metamaterial occupying the space Ω is decomposed here into two subspaces $\Omega^{(1)}$ and $\Omega^{(2)}$ with permittivities $\epsilon^{(1)}(x, y)$, $\epsilon^{(2)}(x, y)$ that are invariant in the z-direction. Here, we illustrate the decomposition on the example of a two-layered system, but is in general applicable of any arbitrary multilayer system.

Sec. 3.1, the mesoscopic features of the metamaterial made from nonmagnetic and nonchiral made from can be described in a very good approximation by a spatially dependent local permittivity. Therefore, we assume that the unit cell V possesses a permittivity distribution $\epsilon(\mathbf{r})$, where $\mathbf{r} \in V$.

Theorem 5.2.1. *(Bloch theorem) Let $\mathbb{G}$ be the set of lattice vectors. Then, $\forall \mathbf{r}_0 \in \mathbb{G}$ it holds $\epsilon(\mathbf{r} + \mathbf{r}_0) = \epsilon(\mathbf{r})$ with $\mathbf{r} \in V$. Further there exists a periodic function $\mathbf{F}_\mathbf{q}(\mathbf{r} + \mathbf{r}_0) = \mathbf{F}_\mathbf{q}(\mathbf{r})$, with*

$$\mathbf{F}(\mathbf{r}) = \mathbf{F}_\mathbf{q}(\mathbf{r}) \mathrm{e}^{\mathrm{i}\mathbf{q}\cdot\mathbf{r}}\,, \tag{5.2}$$

where $\mathbf{F}(\mathbf{r})$ refers to the electric field $\mathbf{E}(\mathbf{r})$ or magnetic field $\mathbf{H}(\mathbf{r})$. The quantities $\mathbf{q}$ and $\mathbf{F}_\mathbf{q}(\mathbf{r})$ denote the Bloch wave vector and the Bloch amplitude, respectively.

According to this theorem, it is sufficient to calculate $\mathbf{q}$ and $\mathbf{F}_\mathbf{q}(\mathbf{r})$ in a single unit cell to obtain the electromagnetic field $\mathbf{F}(\mathbf{r})$ in the entire periodic metamaterial.

In Ref. [27] it was shown that in a three-dimensional periodic metamaterial, the fields are rather a superposition of many Bloch modes, which might couple to the incoming plane wave at the interface. Now, let us assume to have a periodic structure being replicated infinitely often in the xy-plane with lateral periods Λ_x and Λ_y. Further, consider a finite number of unit cells in the z-direction, forming a slab that is doubly periodic in the xy-plane with finite thickness d_{slab} in the z-direction. The basic geometry is depicted in Fig. 5.2, where the periodic metamaterial slab occupies the region Ω and separates the two half-spaces $\Omega_\pm$ of the cladding and substrate. In the homogeneous half-spaces $\Omega_\pm$, the reflected and transmitted fields can then be expanded into a Fourier series that read

$$\mathbf{E}^{R/T}(\mathbf{r}) = \sum_{m=-M}^{M} \sum_{n=-N}^{N} \mathbf{E}^{R/T}_{mn} \mathrm{e}^{\mathrm{i}\mathbf{k}^{R/T}_{mn}\cdot\mathbf{r}}\,. \tag{5.3}$$

Here, m and n denote the diffraction orders of the wave, where M and N refer to the expansion orders in x- and in y-directions. The corresponding dispersion relations in the

homogeneous cladding with permittivity ϵ_C and substrate with permittivity ϵ_S read

$$\left(k_{z,mn}^{R/T}\right)^2 = \epsilon_{C/S}k_0^2 - k_{x,m}^2 - k_{y,n}^2 = \epsilon_{C/S}k_0^2 - \left(k_x + \frac{2\pi m}{\Lambda_x}\right)^2 - \left(k_y + \frac{2\pi n}{\Lambda_y}\right)^2 , \tag{5.4}$$

where $k_{x,0} = k_x$ and $k_{x,0} = k_y$ are determined by the angle of incidence given by $\mathbf{k}^I$ and, by virtue of the interface conditions, they are invariant in all domains $\Omega_\pm$ and $\Omega^{(l)}$.

In general, the dispersion relations inside the periodic metamaterial are very complicated and a closed form is missing. Nonetheless, they can be calculated numerically. In the Fourier Modal Method (FMM), the periodic metamaterial is considered as composition of L stacked layers, that are invariant in the z-direction [142]–[144]. Hence, the region Ω occupied by the periodic metamaterial is decomposed into L subdomains $\Omega^{(l)}$ with thicknesses $d^{(l)}$ having a permittivity distribution that is periodic in the xy-plane and invariant in the z-direction, such that

$$\Omega = \bigcup_{l=1}^{L} \Omega^{(l)} , \quad d_{\text{slab}} = \textstyle\sum_{l=1}^{L} d^{(l)} \text{ , and } \quad \epsilon^{(l)}(x,y,z) = \epsilon^{(l)}(x,y) .$$

Adjacent domains with different permittivities define the interface $\Gamma_{l,l+1} = \overline{\Omega^{(l)}} \cap \overline{\Omega^{(l+1)}}$, at which light propagation changes according to the dispersion relations in the respective layer. Please note, that the dispersion relations in each layer l are not those from the entire metamaterial. The xy-periodic permittivity distribution and its inverse in the l^{th} layer may be expanded in a Fourier series

$$\begin{aligned} \epsilon^{(l)}(x,y) &= \sum_{mn} \epsilon_{mn}^{(l)} \mathrm{e}^{\mathrm{i}\left[\left(\frac{2\pi m}{\Lambda_x}\right)+\left(\frac{2\pi n}{\Lambda_y}\right)\right]} , \\ \left[\epsilon^{(l)}(x,y)\right]^{-1} &= \sum_{mn} \zeta_{mn}^{(l)} \mathrm{e}^{\mathrm{i}\left[\left(\frac{2\pi m}{\Lambda_x}\right)+\left(\frac{2\pi n}{\Lambda_y}\right)\right]} , \end{aligned} \tag{5.5}$$

where $\sum_{mn} = \sum_{m=-M}^{M} \sum_{n=-N}^{N}$ is a sum with $(2M+1)(2N+1)$ elements. Consequently, due to the z-invariance of $\epsilon^{(l)}$, a Bloch mode $\mathbf{E}_{\mathbf{q}^{(l)}}^{(l)}(\mathbf{r})$ in the l^{th} layer is a biperodic function with the wave vector $\mathbf{q}_{mn}^{(l)} = (k_{x,m}, k_{y,n}, q_z^{(l)})$ and is given as

$$\mathbf{E}_{\mathbf{q}^{(l)}}^{(l)}(\mathbf{r}) = \sum_{mn} \mathbf{E}_{mn}^{(l)} \mathrm{e}^{\mathrm{i}(k_{x,m}x + k_{y,n}y)} \mathrm{e}^{\mathrm{i}q_z^{(l)}z} , \text{with } \mathbf{r} \in \Omega^{(l)} , \tag{5.6}$$

that is an expansion into plane waves with amplitudes $\mathbf{E}_{mn}^{(l)}$ in the xy-plane that share the propagation constant $q_z^{(l)}$ in the z-direction. Note that Eq. (5.6) analogously holds for the magnetic field $\mathbf{H}^{(l)}(\mathbf{r})$. The fields within a thin layer l couple by virtue of the Maxwell equations

$$\nabla \times \mathbf{E}^{(l)}(\mathbf{r}) = \mathrm{i}k_0 \mathbf{H}^{(l)}(\mathbf{r}) , \qquad \nabla \times \mathbf{H}^{(l)}(\mathbf{r}) = -\mathrm{i}k_0 \epsilon^{(l)}(x,y) \mathbf{E}^{(l)}(\mathbf{r}) , \tag{5.7}$$

for $\mathbf{r} \in \Omega^{(l)}$. With these coupled-wave equations, the eigenmodes in layer l may be calculated.

The full-wave computation of the exact problem associated with the diffracted fields in the cladding and substrate requires to satisfy Maxwell's equations in each layer l, cladding Ω_- and substrate Ω_+, but also to fulfill the continuity conditions of the tangential components of both electric and magnetic fields applied between two consecutive layers.

In other terms, interface conditions (IC_1) and (IC_2) (with $\hat{\alpha} = \hat{\beta}^j = \hat{\gamma} = 0$) must be applied to the fields between cladding, first metamaterial layer, i.e. at the first interface Γ_- at $z = 0$, then at the interface $\Gamma_{1,2}$ at $z = d^{(1)}$ between first and second metamaterial layer, and so on, until the interface Γ_+ between the last metamaterial layer and the substrate at $z = d_{\mathrm{slab}}$. Finally, the resulting system of interface conditions is solved for the reflection and transmission coefficients of the diffracted fields. A generalized analysis with an arbitrary number of L layers at oblique incidence [143] and with conical diffraction (non-planar) is handled in Ref. [144]. Here, for demonstration, we show the analysis for a single layer with thickness d_{slab} that is invariant in the z-direction, and the incident field being TM-k_y polarized[2]. The following derivation is adopted from Ref. [142] and adapted to our own needs.

Using Maxwell's Eq. (5.7) we eliminate the z-component of the electric field by substituting it with

$$E_z(\mathbf{r}) = -[\mathrm{i}k_0\epsilon(\mathbf{r})]^{-1}[\nabla \times \mathbf{H}(\mathbf{r})]_z = [\mathrm{i}k_0\epsilon(\mathbf{r})]^{-1}\nabla_y H_x(\mathbf{r})\,.$$

Under these considerations, Maxwell's Eqs. (5.7) together with the Fourier decompositions from Eq. (5.5) and Eq. (5.6) of the permittivity and its inverse yield the following coupled-wave Eqs.

$$\begin{aligned} k_0 q_z E_{y,mn} &= -k_0^2 H_{x,mn} + k_{y,n} \sum_{pq} \zeta_{m-p,n-q} k_{y,q} H_{x,pq}\,, \\ k_0 q_z H_{x,mn} &= k_{x,m}^2 E_{y,mn} - k_0^2 \sum_{pq} \epsilon_{m-p,n-q} E_{y,pq}\,. \end{aligned} \tag{5.8}$$

This represents an eigenvalue problem with $2(2M+1)(2N+1)$ eigenvalues $q_{z,j}$ and eigenfunctions $E_{y,mnj}$ and $H_{x,mnj}$, where $j \in (1, 2(2M+1)(2N+1))$. They are ordered by their imaginary parts such that $\Im q_{z,0} \leq \Im q_{z,1} \leq \cdots$. Here, $q_{z,0}$ refers to the propagation constant of the fundamental mode, i.e., the mode that transfers the most energy to the second interface Γ_+ after a propagation through a distance d_{slab}. We note that the FMM rigorously takes all modes, up to the given truncation order M and N, into account and does not make the fundamental mode approximation. Both eigenvalues $\Im q_{z,j}$ and eigenfunctions $E_{y,mnj}$ and $H_{x,mnj}$ are numerically obtained using an eigenvalue solver. Hence, the total field is a superposition these eigenmodes and of both forward and backward propagating ones:

$$E_y(\mathbf{r}) = \sum_j \left[\left(a_j \mathrm{e}^{\mathrm{i}q_{z,j}z} + b_j \mathrm{e}^{-\mathrm{i}q_{z,j}(z-d_{\mathrm{slab}})} \right) \sum_{mn} E_{y,mnj} \mathrm{e}^{\mathrm{i}(k_{x,m}x + k_{y,m}y)} \right], \tag{5.9}$$

$$H_x(\mathbf{r}) = \sum_j \left[\left(a_j \mathrm{e}^{\mathrm{i}q_{z,j}z} - b_j \mathrm{e}^{-\mathrm{i}q_{z,j}(z-d_{\mathrm{slab}})} \right) \sum_{mn} H_{x,mnj} \mathrm{e}^{\mathrm{i}(k_{x,m}x + k_{y,m}y)} \right], \tag{5.10}$$

where a_j and b_j are unknown coefficients of the forward and backward propagating modes, respectively, and to be determined from the interface conditions. Note the phase $\exp(\mathrm{i}q_{z,j}d_{\mathrm{slab}})$ that has been added for the backward propagating modes. This guarantees that they start to propagate from the second interface, which in the reference frame is situated at a distance $z = d_{\mathrm{slab}}$ from the origin.

[2]Later in the numerical analysis we will only consider this polarization, so it makes sense to restrict to this case here.

For a single layer problem, such as periodic wire medium array with length d_{slab}, the reflection and transmission problem is, up to the finite truncation M and N, numerically exact. Since the material is locally described by a scalar permittivity only, interface conditions (IC_1) and (IC_2) (with $\hat{\alpha} = \hat{\beta}^j = \hat{\gamma} = 0$), are sufficient to determine both reflected and transmitted field amplitudes at both interfaces Γ_- and Γ_+. In this case, the tangential components of both electric and magnetic fields are continuous across the interfaces. Consequently, at the first interface with $z = 0$ we have

$$\frac{k_z^I}{\sqrt{\epsilon_C}k_0}\delta_{m0}\delta_{n0} + E^R_{ymn} = \sum_j \left(a_j + b_j \mathrm{e}^{\mathrm{i}q_{z,j}d_{\text{slab}}}\right) E_{y,mnj}\,, \qquad (\text{IC}_1) \text{ at } \Gamma_- \tag{5.11}$$

$$-\frac{\left|\mathbf{k}^I\right|}{k_0}\delta_{m0}\delta_{n0} + \frac{k_{y,m}}{k_0}E^R_{z,mn} + \frac{k_z^I}{k_0}E^R_{y,mn} = \sum_j \left(a_j - b_j \mathrm{e}^{\mathrm{i}q_{z,j}d_{\text{slab}}}\right) H_{x,mnj}\,, \qquad (\text{IC}_2) \text{ at } \Gamma_- \tag{5.12}$$

where k_z^I is the propagation constant of the incident field and δ_{nm} the Kronecker-Delta symbol. The first term on the LHS of both Eqs. (5.11) and (5.12) refer to the incident field, that is only one single plane wave, while the remaining terms on the LHS correspond to the reflected amplitudes of the $(2M+1)(2N+1)$ diffracted plane waves. The z-component $E^R_{z,mn}$ of the electric field for the reflected waves are involved in the continuity of the tangential field components due to the substitution of $H_x(\mathbf{r})$ that is given by $\nabla \times \mathbf{E}(\mathbf{r})$ (Maxwell's equation). On the RHS of Eqs. (5.11) and (5.12), we have the fields at the other side of the interface, namely the transmitted ones including the backward propagating modes. The backward propagating modes that arise at the second interface Γ_+ accumulate a phase after propagating an optical path of length $q_{z,j}d_{\text{slab}}$ towards the first interface Γ_-.

Next, by applying the interface conditions the second interface with $z = d_{\text{slab}}$ we obtain

$$\sum_j \left(a_j \mathrm{e}^{\mathrm{i}q_{z,j}d_{\text{slab}}} + b_j\right) E_{y,mnj} = E^T_{y,mn}\,, \qquad (\text{IC}_1) \text{ at } \Gamma_+ \tag{5.13}$$

$$\sum_j \left(a_j \mathrm{e}^{\mathrm{i}q_{z,j}d_{\text{slab}}} - b_j\right) H_{x,mnj} = \frac{k_{y,n}}{k_0}E^T_{z,mn} - \frac{k_z^T}{k_0}E^T_{y,mn}\,. \qquad (\text{IC}_2) \text{ at } \Gamma_+ \tag{5.14}$$

The transmitted fields are the fields on the RHS, while on the LHS we have the fields in the periodic metamaterial slab evaluated at the distance $z = d_{\text{slab}}$. Here again, the z-component $E^T_{z,mn}$ of the transmitted electric field arise from to the substitution of the transmitted magnetic field $\mathbf{H}$ by means of Maxwell's Eq. (5.7). By virtue of $\nabla \cdot \mathbf{E}^R(\mathbf{r}) = 0$ and $\nabla \cdot \mathbf{E}^T(\mathbf{r}) = 0$, the z-components of the reflected and transmitted fields may be eliminated, and the system of Eqs. (5.11)-(5.14) above may be unambiguously solved for reflection and transmission coefficients $E^R_{y,mn}$ and $E^T_{y,mn}$.

Further, we are interested in the far-field response only. For a subwavelength structure, only the zeroth diffraction-order with $(m,n) = (0,0)$ significantly contributes, while all other diffracted fields $(m,n) \neq (0,0)$ are attenuated after propagating distances over several wavelengths by means of Eq. (5.4). Nonetheless, to correctly compute reflection and transmission coefficients of the zeroth diffraction-order that are comparable to those obtained from experimental measurements, sufficiently high truncation orders M and N have to be considered in the full-wave analysis. To illustrate the numerical convergence

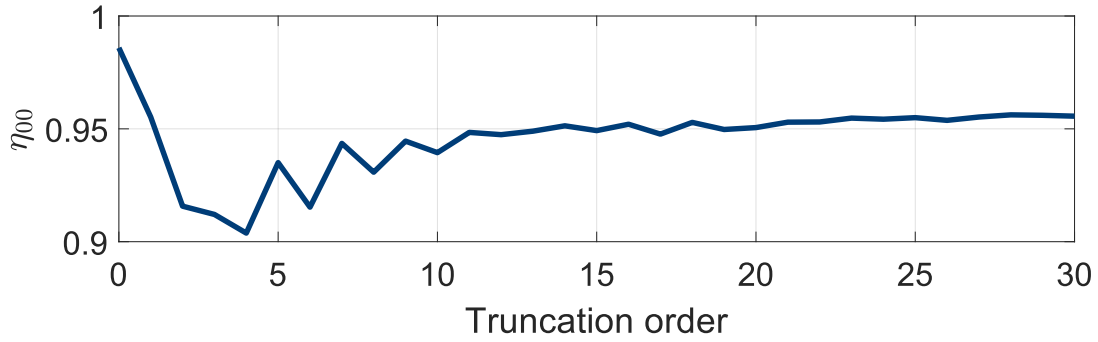

Figure 5.3: Convergence plot of the diffraction efficiency of the zeroth diffraction order $\eta_{00} = \eta_{00}^R + \eta_{00}^T$ as function of the truncation orders M and N. Here, we choose $M = N$ varying from 0 to 30 and evaluate η_{00} at a selected frequency of $k_0 = 7\,\mu\text{m}^{-1}$ and at normal incidence, for the example of the wire medium slab, that is subject to homogenization in Sec. 5.3.3. The wire medium slab has a thickness of $d_{\text{slab}} = 300\,\text{nm}$, lateral periodicities $\Lambda_x = \Lambda_y = 60\,\text{nm}$, with metallic wires with radius $r_m = 12.5\,\text{nm}$ and permittivity $\epsilon_m(7\,\mu\text{m}^{-1}) = -32.58 + \text{i}4.03$ embedded in a host medium with permittivity $\epsilon_h = 2.74$.

of the FMM, the diffraction efficiencies, that are defined as

$$\begin{aligned} \eta_{mn}^R &= \Re\left(\frac{k_{z,mn}^R}{k_{z,00}^R}\right)\left|\mathbf{E}_{mn}^R\right|^2 , \\ \eta_{mn}^T &= \Re\left(\frac{k_{z,mn}^T}{k_{z,00}^T}\right)\left|\mathbf{E}_{mn}^T\right|^2 \end{aligned} \tag{5.15}$$

are calculated. The convergence of the diffraction efficiency for the zeroth diffraction order, are plotted in Fig. 5.3 as function of the retained Fourier orders M and N. We exemplary choose the wire medium which will be studied in Sec. 5.3.3 and evaluated the diffraction efficiencies at a selected frequency $k_0 = 7\,\mu\text{m}^{-1}$ and normal incidence. With $M = N = 7-10$ we obtain an accuracy up to two decimals, whereas $M = N \geq 11$ provide an accuracy of at least three decimals, but also the computational time polynomially increases with $\mathcal{O}(M^3)$-complexity [145]. For the numerical references in this thesis, we chose $M = N = 12$ to calculate with good accuracy within a reasonable amount of time.

This method will be used in the following sections for obtaining the referential reflection and transmission coefficients for the fishnet metamaterial and for the wire medium. The FMM as presented here, can be directly applied to the periodic wire medium slab, as its unit cell consists of a single layer with thickness d_{slab}. In the case of the fishnet, however, the scattering scenario is quite more involved as the unit cell consists of a stacking of five different material layers: air, metal, dielectric, metal, air. Henceforth, for a single functional fishnet layer the unit cell must be discretized into five different layers that are invariant in the z-direction, and into ten layers for two functional fishnet layers. Concerning the material consisting of spheres arranged in a cubic lattice, the FMM would require to mesh the sphere in many layers in the propagation direction, i.e. defining many layers in the z-direction, where interface conditions between each of them needs to be calculated to successively match the tangential field components. This method is computationally inefficient and we, therefore, prefer to use the Korringa-Kohn-Rostoker (KKR) method [146] for the spheres. There, the unit cell containing the sphere is modeled as it is as a single object, which is computationally favorable.

5.3 Implementation on concrete structures

In this section, we apply the S-parameter optimization approach to concrete periodic metamaterial structures, where the electromagnetic response is calculated using the numerical tools mentioned above. Our main target here is the fishnet metamaterial. In the studied spectral range, the fishnet shows a negative index behaviour. We intend to capture with dispersion relations this feature and reproduce the reflection and transmission coefficients at high angles of incidence using the three WSD, SYM, and SSD models in Sec. 5.3.2. This structure is, however, highly anisotropic and incorporates intrinsic losses and the retrieval is quite challenging to discuss at first hand. Therefore, prior discussing the complicated fishnet structure, we study an easier example of a metamaterial made by isotropic unit cells, namely a layer of dielectric spheres arranged on a cubic lattice. This structure can be homogenized with scalar material parameters, which renders the retrieval procedure less challenging and the example suitable for a better understanding of our approach. Such all-dielectric structure has a clear spectral signature in terms of the Brewster effect in the TM-polarized case. In Sec. 5.3.1, we demonstrate the ability of the Brewster angle being captured more accurately using the nonlocal approach, especially at frequencies slightly below the first band gap. The third example we aim to study is a wire medium, for which a closed-form nonlocal characterization is available. The general structure as well as the wire medium model were introduced in Sec. 4.4.2. In Sec. 5.3.3, we compare our nonlocal approach by reconstructing the reflection and transmission coefficients from a concrete wire medium slab.

In Ref. [117], we have shown that both SYM and SSD models are better approaches for homogenizing metamaterials beyond the paraxial regime compared to the WSD model. Further, in the same reference we find that the improvement of reconstructing the dispersion relation of the fundamental mode is better when considering the fourth order spatial dispersion, namely the SSD model, than when considering the second-order symmetry terms, namely the SYM model. This finding can be seen in Fig. 5.8 and will be elaborated in depth in the appropriate section. We, therefore, opt to retain in our following examples rather the fourth order term $\hat{\gamma}$ instead of the second-order symmetry term $\hat{\beta}$. This choice is done with the purpose to describe the metamaterial with the least number of effective material parameters. Therefore, we have chosen the seemingly more suitable model for capturing the reflection and transmission coefficients.

In all the numerical experiments below, we simulate the bulk dispersion relations and the reflection and transmission from a slab with 240 frequencies k_0 ranging from $k_{0,\min}$ to $k_{0,\max}$. At each frequency, we change the angles of incidence θ with 100 samples from 0° to 89.99°. We intentionally omit the angle 90.00° due to numerical reasons. The transverse momentum is then $k_t = \epsilon_C k_0 \sin(\theta)$. Without loss of generality, in the following examples, we constantly assume both substrate and cladding being air, i.e., $\epsilon_C = \epsilon_S = 1$.

In the following subsections, we will study three fundamentally different structures, where emphasis is put on the importance of taking a local response into account for a proper homogenization of the structures. The limitation the considered homogenization approach and the S-parameter retrieval used here, is the focus of the next section 5.4. There, we will study the fishnet and the wire medium in different situations where both homogenization and the S-parameter retrieval are challenged.

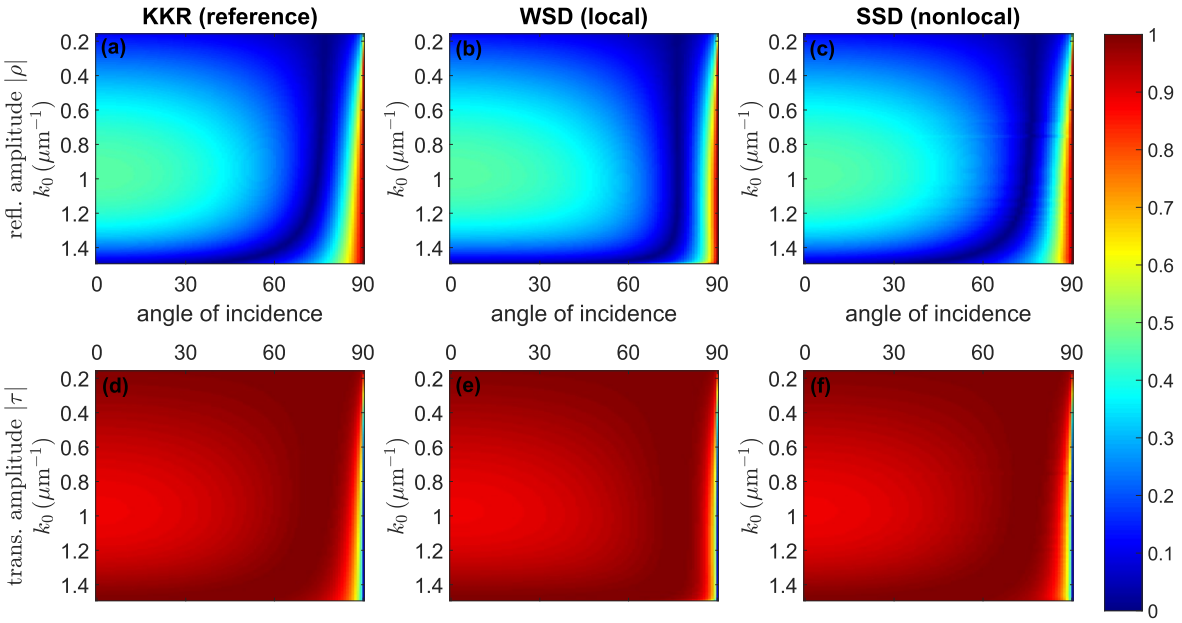

Figure 5.4: **(a)**-**(c)** Amplitudes of the reflected light $|\rho|$ and **(d)**-**(f)** of the transmitted light $|\tau|$ from a layer of dielectric spheres with thickness $d_{\mathrm{slab}} = 1\mu$m using different approaches. The left figures (**(a)** and **(d)**) correspond to the full-wave simulation of the actual slab as done with the KKR. This can be considered as the reference data. I thank my colleague Andreas Vetter from TFP at KIT for these reference data using KKR. The centered figures (**(b)** and **(e)**) are the fitted reflection and transmission amplitudes from a homogeneous slab with the same thickness as the heterogeneous slab using the WSD approach. The figures on the right (**(c)** and **(f)**) are obtained from considering a homogeneous slab with SSD. The figure indicates the improvement in capturing the reflection and transmission of the reference material using SSD (nonlocal) compared to WSD (local).

5.3.1 Dielectric spheres on a cubic lattice: A basic material

Please note that the findings of this were previously published in Ref. [126].
In our first numerical experiment, we consider an array of Germanium spheres arranged on a simple cubic lattice. The permittivity of Germanium in the infrared region is $\epsilon_{\mathrm{Ge}} = 16$ (c.f. Ref. [147]). The host medium is air with $\epsilon_h = 1$. The assumption of a frequency independent permittivity results in the scalability of Maxwell's equations. Therefore, the only critical parameter here is the period-to-wavelength ratio a/λ. Hence, and without loss of generality, we assume a period $a = \Lambda_x = \Lambda_y = d_{\mathrm{slab}} = 1\,\mu$m. The radius of the spheres is $r_{\mathrm{Ge}} = 0.45a$, that represents a filling factor $f = \frac{4\pi}{3}\left(\frac{r_{\mathrm{Ge}}}{a}\right)^3 \approx 0.38$. The free-space wavelength of the incident light is chosen such that $\lambda \in (4a, 40a)$, i.e., the critical parameter a/λ ranges from $\frac{1}{40}$ to $\frac{1}{4}$. The factor 4 guarantees that the wavelength in the medium with the highest refractive index remains longer than the period of the structure. Therefore, the unit cell safely remains subwavelength and homogenization is in principle possible.

In order to numerically predict the reflection and transmission coefficients for such spherical structures, we use the KKR method [146]. The scattered fields from such materials are expressed as a superposition of plane waves. Here, we consider a single layer of the metamaterial with a total thickness of $d_{\mathrm{slab}} = 1\,\mu$m being illuminated with a TM-

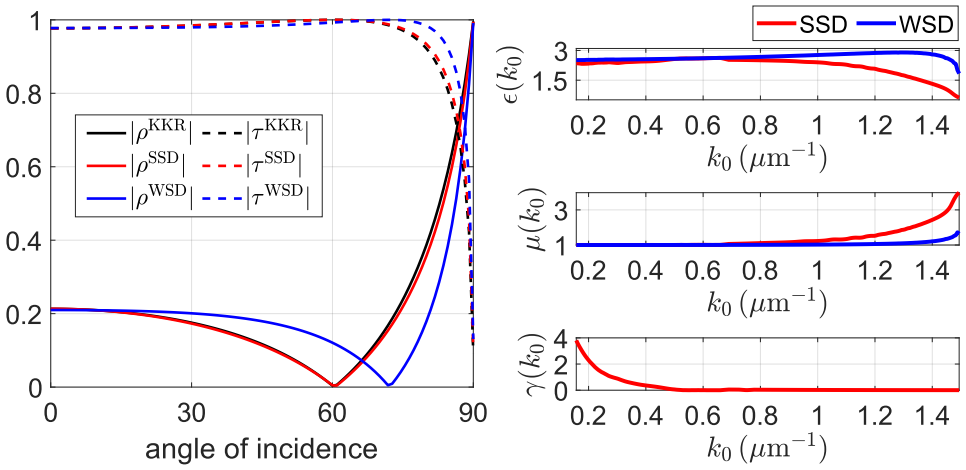

Figure 5.5: (left) Reflection and transmission amplitude close to the first band gap at a selected frequency $k_0 = 0.9\frac{\pi}{2a}$. In the paraxial regime, both WSD (blue) and SSD (red) models are adequate for homogenization. However, at higher angles of incidence only the SSD model agrees with the reference curves (black) and may even capture the Brewster angle with very high precision. (right) Retrieved effective material parameters from a layer of spheres using the local WSD (blue) and the nonlocal SSD (red) approaches.

polarized plane wave. For all angles of incidence and wave numbers k_0, the referential reflection and transmission coefficients are shown in Figs. 5.4**(a)** and **(d)**, respectively. They correspond to the TM-polarized mode for frequencies below the first band gap. In the graph of the reflection coefficient we observe a dark line which indicates the angles with a vanishing reflection. These are the expected Brewster angles that are encountered in the TM polarization. The numerical data were obtained from a simulation done by my colleague Andreas Vetter using the KKR method, I thank him for that.

Next, the retrieval is based on minimizing the objective function δ which is defined in Eq. (5.1), by means of the fitting procedure described in Sec. 5.1. As a consequence of the isotropy of the unit cell and the absence of loss in its constituents, the S-parameter optimization approach reduces to a two-dimensional or three-dimensional fitting problem. For the WSD (local) model, the free parameters to fit are two real numbers ϵ and μ. Concerning the SSD (nonlocal) model, we additionally include the nonlocal parameter γ into the fitting procedure.

The obtained reflection and transmission coefficients from fitting each model to the reference data are revealed in Fig. 5.4. In view of the simplicity of the material, it is not extraordinary that both WSD and SSD models properly achieve to capture the electromagnetic response in the paraxial regime. Yet, by getting closer to the band gap and with increasing angles of incidence, we notice that the WSD model misses to recover the Brewster angle, while the SSD model still manages to coincide with the reference with a very high accuracy. For the sake of clarity, we refer to Fig. 5.5(left) where the absolute values of reflection and transmission coefficients are depicted at a selected frequency of $k_0 = 0.9\frac{\pi}{2a}$. In the paraxial regime, both WSD and SSD models are conform with the reference. For higher angles of incidence higher than 20°, the WSD model deviates strongly and we observe that only the SSD model matches with the reference, and especially, captures the Brewster angle with very good precision, whereas the WSD approach fails to do so.

The retrieved effective material parameters are depicted in Fig. 5.5(right). In the

quasi-static limit, i.e. for $k_0 \approx 0$, the retrieved permittivity roughly corresponds to the predicted value from the Maxwell-Garnett mixing formula given by Eq. (4.71). For our geometrical configuration, the Maxwell-Garnett permittivity is frequency independent with $\epsilon_{\mathrm{MG}} \approx 2.40$.

Further, as expected from a mixture of nonmagnetic inclusions, we retrieve in the quasi-static limit a rather trivial magnetic permeability $\mu(k_0) \approx 1$. This is just expected, as the materials themselves do not offer an intrinsic magnetic response and no resonances is supported that could induce a magnetic response. At higher frequencies, however, both homogenization models experience a dispersive permeability $\mu(k_0)$. Close to the band gap, μ shows a resonance, which is linked the first magnetic Mie resonance at $\lambda \approx 2a\sqrt{\epsilon_{\mathrm{Ge}}}$. Concerning the nonlocal parameter $\gamma(k_0)$, it shows a k_0^{-4} dependency, which causes the huge values in the small-frequency region. This behaviour is expected given the appearance of γ on the fourth order of the Taylor approximation $\propto |\mathbf{k}|^4$, which cancels the divergence at zero frequency in the effective response tensor $\hat{\hat{\mathbf{R}}}(\mathbf{k}, k_0)$. Nonetheless, apart from this relatively unimportant scaling, $\gamma(k_0)$ at higher frequencies is rather small compared to the local parameters, but is not negligible. It has to be taken into account to accurately describe the optical response of the studied metamaterial, even at small frequencies.

We further want to remark that such proportionality is not present in the permeability $\mu(k_0)$, as the term appearing in the second-order Taylor approximation, i.e. $\alpha(k_0)$ in Eq. (4.18) has been already appropriately scaled by k_0^2 with $\mu^{-1}(k_0) = 1 - k_0^2\alpha(k_0)$.

Note that this structure allowed for a very simplified version of the retrieval procedure with only three parameters. Anyhow, a direct inversion of Eqs. (4.62) for the reflection and transmission coefficients remains impossible, as the nonlocal parameter γ does not allow for it, even at normal incidence. Next, for the fishnet metamaterial, the retrieval tends to be more complicated. Due to the anisotropy and the intrinsic losses, we have to consider three complex numbers for the local WSD approach and five complex numbers for the nonlocal SSD approach. In total, there are six and ten real numbers to be fitted for the WSD and SSD approaches, respectively.

5.3.2 Fishnet metamaterial: A negative index material

Please note that the findings concerning the bulk dispersion relations of this subsection were previously published in Ref. [117] and for the effective parameter retrieval from a slab in Ref. [126]. In a broader perspective, the fishnet metamaterial is formed of a stacking of a thin dielectric layer, sandwiched between two symmetric metallic layers, as depicted in Fig. 5.6. The three layers are periodically perforated and have rectangular holes. It is regarded as the prototype structure for achieving a negative index behaviour with a high figure of merit at optical frequencies. A high figure of merit can be especially reached when choosing silver instead of gold or copper for the metallic layers [148]. The structure itself is biaxial anisotropic. Further, it has three independent mirror symmetries, i.e., the permittivity distribution $\epsilon(\mathbf{r})$ within the heterogeneous unit cell is symmetric under the transformation $\epsilon(\pm x, \pm y, \pm z)$, where the inversions w.r.t a coordinate are meant to be performed independently. The corresponding symmetry class is called orthorhombic-dipyramidal symmetry [50], and is denoted as $\mathrm{D_{2h}}$. Unlike the structure made out of spheres on a cubic lattice, the electromagnetic response of the fishnet depends on the polarization of light. For instance, a TM-k_x polarized light would couple differently to the material than a TM-k_y polarized one, as different material parameters will be probed.

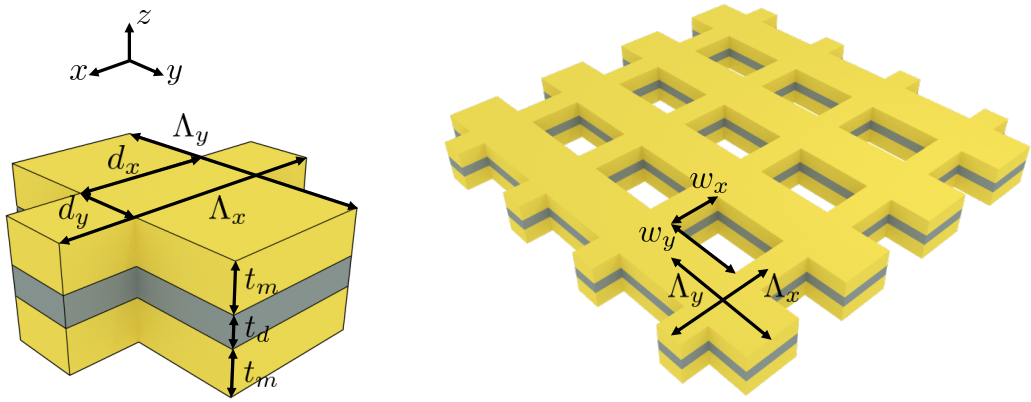

Figure 5.6: (Left) Unit cell of the fishnet metamaterial and (right) its periodic replica on the xy-plane. One functional layer of the fishnet metamaterial made of a stacking of three metal-dielectric-metal layers. It is a biperiodic structure with periods Λ_x and Λ_y and consists of rectangular holes with the widths w_x and w_y. The structure is assumed to be infinitely extend in the xy-plane.

The full list of probed material parameters is summarized in Tab. 5.1. If the wholes were additionally square, i.e. $w_x = w_y$, then the structure has a four-fold symmetry, i.e. D_{4h}-symmetry and would respond independently from the polarization, but of curse only at normal incidence. Here, we study a fishnet metamaterial with a D_{2h} symmetry.

Design idea of the fishnet and the origin of the negative index

The fishnet metamaterial can be regarded as a combination of a pair of rectangular plates connected to plasmonic wires, which are separated by a dielectric spacer. The thin plasmonic wires are oriented in the direction of the electric field of the incident light. These wires act as a diluted metal with a reduced plasma frequency yielding a negative effective permittivity when operated below that frequency. The dilution corresponds in good approximation to the filling factor of the metallic wires within the unit cell. The rectangular plates are made of the same metal as the nanowires and are separated by the same dielectric medium. When the metallic plates are excited with an electric field that is polarized parallel to the plates, a polarization current will be induced. When the dielectric spacer is very thin, these currents might resonantly couple either in a symmetric way, when the induced currents are parallel, or in an antisymmetric fashion, when they are antiparallel. In a symmetric coupling scenario, the polarization current is curl-free and the effective response will resemble a strong electric dipole and the whole fishnet material will simply act as a diluted metal. The antisymmetric coupling, however, is particularly interesting as the antisymmetric current distribution is not curl-free and generates a resonant magnetic response. This phenomenon may be linked to an magnetic permeability in the effective picture. This coupling phenomena is understood very well in the hybridization model for the plasmonic response of nano-structures [149], [150]. The antisymmetric coupling represents a bound state, such that the magnetic permeability can be effectively described as a Lorentzian (see e.g. Eq. (3.64)). The fishnet structure is constructed by joining these two constituents together, where a negative index behaviour can be reached at a desired wavelength. This peculiar effect occurs when both permittivity and permeability have simultaneously negative real parts, which takes place when the resonance frequency of the Lorentzian permeability is lower than the plasma frequency of the diluted metal.

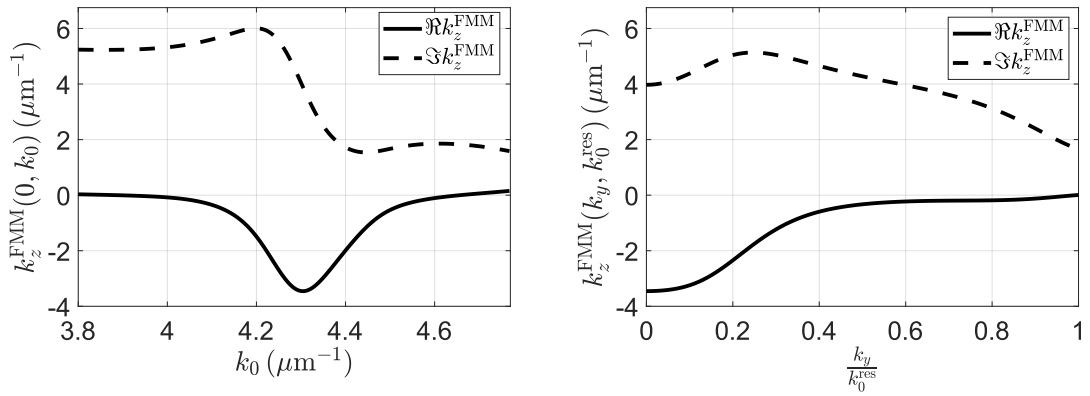

Figure 5.7: Fundamental dispersion relation at $k_y = 0$ (left) and isofrequency contours at the resonance frequency $k_0^{\mathrm{res}} = 4.3\,\mu\mathrm{m}^{-1}$ (right) of the fishnet metamaterial as function of k_y. The real part of k_z is negative, meaning that the fishnet has a negative index. In the effective medium approach, this translates to a simultaneously negative permittivity and permeability.

The effective permittivity can be independently designed from the magnetic permeability by varying the thickness of the wires. Both resonance strength and and position of the magnetic permeability can be tuned by varying the thickness of the dielectric spacer in the fabrication process [151].

The fabrication process of the fishnet metamaterial is usually divided into two major steps, commonly starting with a tri-layer system consisting of a sacrificial photoresist, a hard mask, and a thick imaging photoresist layer being put on top of a substrate [152]. In the first step, by means of an interference lithography, an array of pillars are formed, which will keep the place for the holes of the fishnet [153]. In the second step, alternating layers of metal and dielectric layers are deposited by electron beam evaporation, which will form the functional layers of the fishnet structure. The remaining photoresist pillars are dissolved in the last step leaving only the fishnet metamaterial with its rectangular holes.

Retrieval results

In our numerical experiment, we consider a fishnet metamaterial with lateral periods of $\Lambda_x = \Lambda_y = 600\,\mathrm{nm}$, and with rectangular holes of widths $w_x = 100\,\mathrm{nm}$ and $w_y = 316\,\mathrm{nm}$. For the metal layers, we use silver with thickness $t_m = 45\,\mathrm{nm}$ due to its high figure of merit at the frequencies of interest. The silver can be modeled by a Drude-type permittivity with the plasma frequency $\omega_p = 13\,700$ THz and relaxation rate (loss) $\Gamma_L = 85$ THz. The silver layers are separated by thin dielectric spacer made of magnesium fluoride MgF_2 of thickness $t_d = 30\,\mathrm{nm}$. In the frequency band of interest, the permittivity is assumed to be nondispersive with $\epsilon_{\mathrm{MgF_2}} = 1.9044$. Both geometrical and material parameters are adopted from Ref. [154]. Furthermore, the stacking in the z-direction can be chosen arbitrarily. The closer the adjacent metallic layers are, the stronger they couple. A very dense packing might, therefore, lead to a resonant response, where higher-order Bloch modes become important and can have considerable influence on the results for a periodically stacked structure [155]. On the other hand, if the structure is very diluted, the layers will only weakly couple, and the induced resonances have weak (or no) influence

on the total dispersion of the material. Therefore, one aims to preferably balance these regimes with a moderate density that results in high resonances and the weak coupling of next unit cell and, thereby, maintaining the response of a single unit cell [156], [157]. In Ref. [156], this sweet-spot was found to be when the period in the z-direction is $\Lambda_z = 200\,\mathrm{nm}$.

The dispersion relation of the fundamental TM-k_y polarized Bloch mode of the infinitely extended fishnet structure is shown in Fig. 5.7 (left) for frequencies k_0 ranging from $3.8\,\mu\mathrm{m}^{-1}$ and $4.8\,\mu\mathrm{m}^{-1}$. The numerical data were obtained by a plane wave ansatz using the FMM. Notably, the fundamental mode has a resonance around the frequency $4.3\,\mu\mathrm{m}^{-1}$ and most importantly a negative real part in the dispersion relation, which translates to a negative index $\Re n_z(k_y, k_0) = \Re k_z^{\mathrm{FMM}}(k_y, k_0)/k_0 < 0$ in the propagation direction. At the resonance frequency $\Re n_z$ goes down to -0.8. In Fig. 5.7 (right), we show the isofrequency contour of the fundamental mode at the resonance frequency for the TM-k_y polarized field, while $k_x = 0$. Both curves reveal a negative index behaviour in the TM-k_y polarized mode. This makes illuminating the fishnet with TM-k_y polarized light of utmost interest in the effective parameter retrieval from reflection and transmission coefficients.

Reconstructing the dispersion relations In this paragraph, we aim to reproduce the dispersion relations at oblique incidence using the local homogenization model WSD, and the two nonlocal models SYM, and SSD. This work has been presented first in Ref. [117]. The comparison relies on fitting the parameters (p_0, q_0, p_1, q_1) that appear in the dispersion relations for the TM-polarized modes in Eqs. (4.7), (4.15), and (4.22) for the WSD, SYM, and SSD models, respectively. The fitting is based on minimizing the least absolute deviations functional

$$\delta^{\mathrm{DISP}}(k_0) = \min_{\substack{\hat{\epsilon},\hat{\mu},\\ \hat{\beta}^j,\hat{\gamma}}} \sum_{k_y=0}^{k_0} w(k_y) \left| 1 - \frac{\left(k_z^i(k_y, k_0, \mathrm{EMP})\right)^2}{\left(k_z^{\mathrm{FMM}}\right)^2 (k_y, k_0)} \right| , \tag{5.16}$$

where the index $i \in \{\mathrm{WSD}, \mathrm{SYM}, \mathrm{SSD}\}$ refers to the model and EMP is the set of effective material parameters of the respective model. Here again, $w(k_y) = \exp(-2.5\Lambda_y k_y)$ as in Eq. (5.1). The fitting algorithm is identical with the one described in Sec. 5.1 and in Fig. 5.1.

The results of fitting the dispersion relations of the fundamental TM-k_y mode are summarized in Fig. 5.8 which reveals strong improvements when considering nonlocal constitutive relations for a homogenization beyond the paraxial regime. In Fig. 5.8**(a)**, we show the obtained dispersion relations, i.e. $k_z(k_y, k_0)$ as function of the frequency k_0 for fixed k_y values. In the paraxial regime, all homogenization models are in accordance with the reference curves (black) of the heterogeneous fishnet. By increasing the transverse momentum k_y, the propagation constant k_z of the WSD model starts to show strange Lorentzians that are not present in the dispersion relation of the original structure. The nonlocal models match with the references up to $k_y = 0.4k_{0,\mathrm{res}}$ for the SYM model and $k_y = 0.5k_{0,\mathrm{res}}$ for the SSD model, whereas the WSD is valid only up to $k_y = 0.2k_{0,\mathrm{res}}$. Impressively, the nonlocal models manage to capture the position of the resonance frequency, that is shifting with increasing k_y. The shift of the resonance frequency was explained in the literature [82], [158] in relation to the phase advance between two subsequent metallic layers that is accumulated under the oblique propagation through the dielectric spacer. This leads to a shift of the resonance position of the antisymmetric mode that is causing

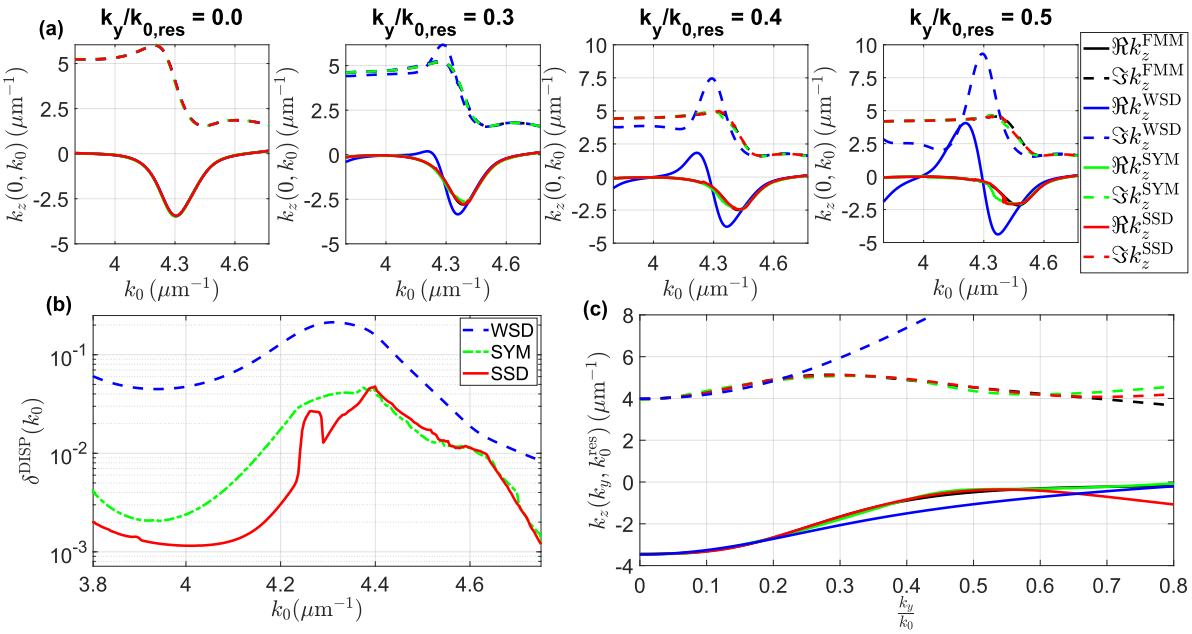

Figure 5.8: Reconstructed dispersion relations and isofrequency contours of the fundamental TM-k_y mode of fishnet (black) at different transverse wave vectors and frequencies using WSD (blue), SYM (green), and SSD (red) models. **(a)** $k_z(k_y, k_0)$ as a function of frequency k_0 for discrete k_y values. For small k_y all three models coincide with the reference dispersion relations. For $k_y \geq 0.3k_{0,\mathrm{res}}$ the local model starts to deviate, while the nonlocal models are in accordance with the reference. The SYM model starts to show inconsistencies from $k_y = 0.4k_{0,\mathrm{res}}$. The SSD model shows an agreement even for k_y values up to $0.5k_{0,\mathrm{res}}$. **(b)** The objective function δ^{DISP} from Eq. (5.16) as a function of k_0 in logarithmic scale. Overall, the nonlocal models allow for a realistic homogenization. **(c)** The isofrequency contour at the resonance frequency $k_{0,\mathrm{res}} = 4.3\,\mu\mathrm{m}^{-1}$ as a function of k_y. The local WSD approach is only valid in the paraxial regime. The nonlocal ones are valid up to $k_y = 0.5k_{0,\mathrm{res}}$ and may be applied for a parameter retrieval at oblique incidence.

the artificial magnetization. Conversely, keeping k_y fixed and varying the thickness t_d of the dielectric spacer will cause a change of both resonance position and amplitude as well [151]. In Fig. 5.8**(c)**, we exemplary show the isofrequency contour at the resonance frequency, i.e., the worst case scenario. Obviously, the local WSD approach (blue) is only valid in the paraxial regime, while both nonlocal models (green for SYM and red for SSD) may go up to $k_y = 0.5k_{0,\mathrm{res}}$ and adequately describe the complicated isofrequency contour of the reference (black). This is a direct consequence from the complexity of their dispersion relations (4.15) and (4.22), which unlock contours beyond the usual ellipses and hyperbolas, that represent the limits of the WSD model. In order to lift this limitation it is, therefore, essential to consider nonlocal effects when homogenizing complex metamaterials such as the fishnet.

To further quantify the improvements of nonlocality, in Fig. 5.8**(b)** we plot the merit function given in Eq. (5.16) as a function of frequency that is a measure of how good a specific constitutive relation can explain the dispersion relation of a certain metamaterial. We clearly see that the figure shows improvements in the effective description of the metamaterial when considering nonlocal material laws. For all studied frequencies, both SYM and SSD approaches are more accurate than the local WSD approach. For

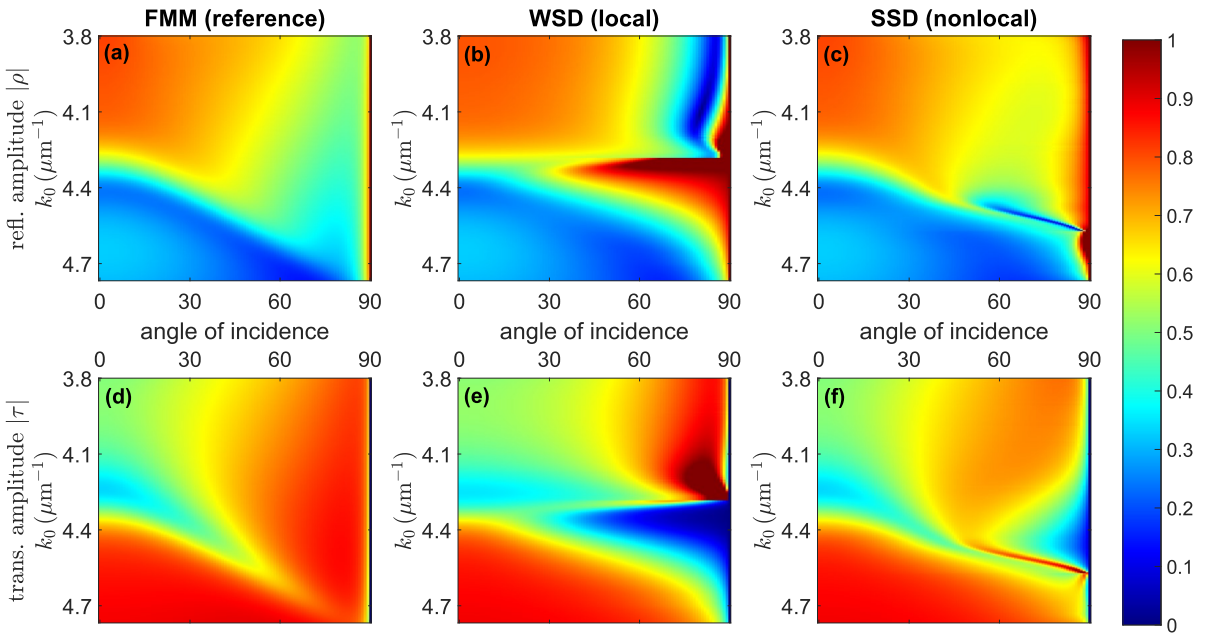

Figure 5.9: **(a)**-**(c)** amplitude of the reflected light $|\rho|$ and **(d)**-**(f)** of the transmitted light $|\tau|$ from one fishnet layer with thickness $d_{\mathrm{slab}} = 200$ nm using different approaches. The left figures (**(a)** and **(d)**) correspond to the full-wave simulation of the actual fishnet slab as done with the FMM. This can be considered as the reference data. The centered figures (**(b)** and **(e)**) are the fitted reflection and transmission amplitudes from a homogeneous slab with the same thickness as the fishnet using the WSD, i.e., the local approach. The figures on the right (**(c)** and **(f)**) are obtained from considering a homogeneous slab with SSD, i.e., retaining nonlocal effects in the effective description. The figure indicates the improvement in capturing the reflection and transmission of the reference material using SSD (nonlocal) compared to WSD (local).

frequencies below the resonance frequency $4.3\,\mu\mathrm{m}^{-1}$, the SSD model even surpasses the SYM model. We further notice that all considered models show the strongest deviations from the reference around that resonance frequency. Yet, this is not surprising as the effective description generally tends to become improper in the resonance regime. With that being said, the findings immediately imply that retaining nonlocal material laws are necessary for a more realistic effective description of metamaterials and that these should be considered for the full homogenization by retrieving the effective material parameters from reflection and transmission from a slab. Since the SSD model outperforms the SYM model, we will only focus on the former approach in the full homogenization process.

The partial homogenization, based on reconstructing the dispersion relations of the fundamental mode, serves as an *a priori* quick quality check of a certain homogenization model, without the requirement of the hard-to-find additional interface conditions. However, it does not fully retrieve the effective material parameters, but rather wave parameters such as $\mathbf{k}$, or refractive index, or anisotropy parameters of the structure. An example concerning the latter quantity, we may only retrieve the ratio $\frac{\epsilon_{yy}}{\epsilon_{zz}}$ for the local WSD model in the TM-k_y polarization. To, further, unambiguously determine each individual effective material parameter, a retrieval based on reflection and transmission from a slab is a necessary step.

Effective parameter retrieval from a slab The real utility of the effective medium description of a metamaterial is not only to reproduce the bulk dispersion that may be obtained with other techniques, but also to relate the response of a metamaterial to its reflection and transmission from a slab. To this end, the wave impedance, which is the second characteristic quantity besides the refractive index that influences light-matter interaction, is required. Retrieving the impedance from the reflection from a half-space is technically feasible. However, it does not accommodate bulk propagation in the medium. It is, therefore, not possible to conclude on the validity of the fundamental mode approximation from the reflection from a half-space only and, hence, it must be generally assumed that the reflection coefficient is actually the superposition of many Bloch modes. Further, we loose important information concerning the transmission. If that happens none of the properties could be accessed that require to probe for the propagation of light inside the metamaterial. This is, of course, a huge loss of information. Therefore, it is important and more efficient to simultaneously consider both reflection and transmission of light through a metamaterial slab sandwiched between some surrounding media. Here, both propagation and scattering aspects that amount the excitation of multiple modes in experimentally observable quantities are simultaneously taken into account. Some constraints need to be formulated on the slab to render it useful. For example, the slab should not be very thick when made from lossy materials, e.g. metallic inclusions. The light propagating inside the slab is strongly absorbed while propagating towards the second interface, such that the transmission becomes too small to be useful in the retrieval. As soon as the transmission gets comparable to the numerical noise level, the retrieval can only rely on the reflection values. Here the slab can, again, be considered as a half-space, that gives no feedback from the second interface with a considerable amount of missing information. Therefore, a suitable thickness for the slab needs to be chosen to balance between significant propagation and enough transmission. In this study, we will consider slabs obtained from stacking one and two functional fishnet layers, only. We have shown in Ref. [126] that the effective material parameters remain rather consistent when considering two functional layers, but of course small changes do occur as well. So, a further increase of the number of functional layers would rather only cause a further reduction of the transmission amplitude and, therefore, negatively influence on the reliability of the retrieval.

The numerically calculated reflection and transmission coefficients are obtained using the FMM as well, by matching the classical interface conditions between the cladding, the individual layers of the fishnet, and the substrate. To guarantee convergence to realistic values obtained from an actual experimental laboratory, a large number of Bloch modes are taken into account. As a consequence from the subwavelength size of the unit cell, only the zeroth-diffraction order in both reflection and transmission significantly contributes to the far field response, while the higher-order diffraction fields are suppressed. We denote former fields as ρ^{FMM} and τ^{FMM}, respectively. In Fig. 5.9**(a)** and **(d)**, we show the amplitude of the zeroth-order reflection and transmission coefficients. As expected from the analysis of the dispersion relation, the structure has a resonance frequency at $k_0 = 4.3\,\mu\mathrm{m}^{-1}$ that shifts towards higher frequencies with increasing angles of incidence. There, most part of light gets absorbed by the fishnet. We always show the amplitude of the reflection and transmission coefficients, but of course, in the retrieval process the complex coefficients are involved.

The reconstruction of the response of the referential fishnet metamaterial using different homogenization approaches is based on the retrieval method explained Sec. 5.1.

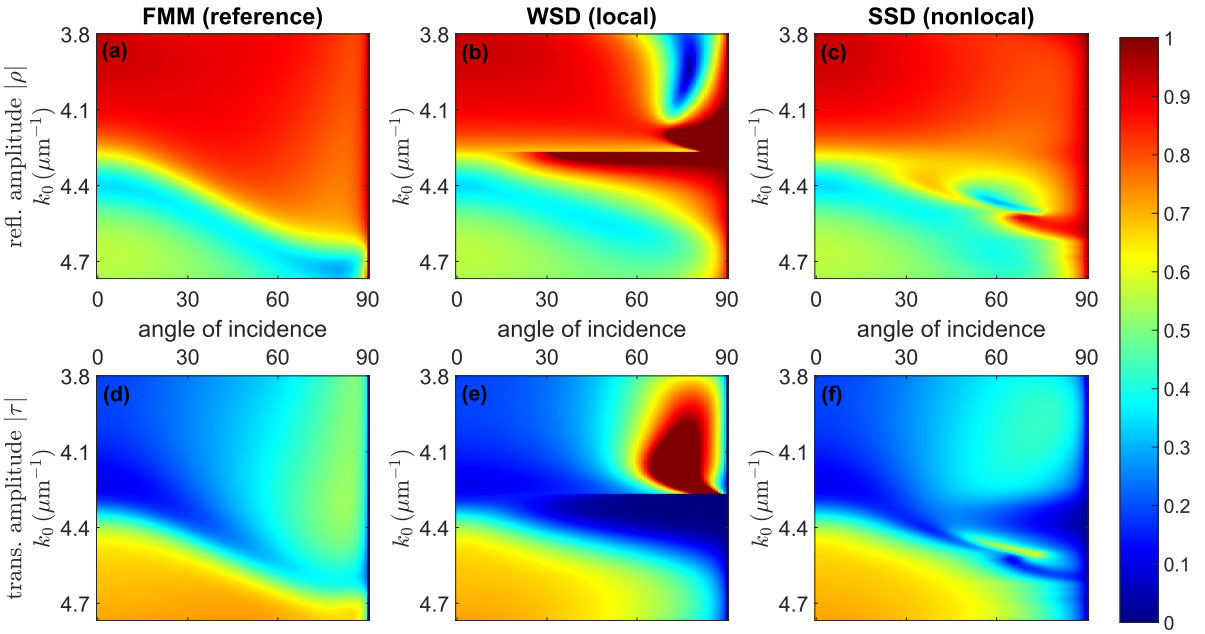

Figure 5.10: Amplitude of the reflected light $|\rho|$ and of the transmitted light $|\tau|$ from two fishnet layers with thickness $d_{\text{slab}} = 400$ nm using different approaches. The rest of the caption is identical to that of Fig. 5.9.

The resulting reflection and transmission coefficients are depicted in Fig. 5.9**(b)** and **(e)** for WSD, and **(c)** and **(f)** for the SSD approach. As expected from the analysis of the dispersion relations, both WSD and SSD models seem to be valid in the paraxial regime, even at the resonance frequency. Further, the figure reveals significant improvements at higher angles of incidence when considering SSD compared to WSD. For the sake of clarity, we refer to Fig. 5.11(right), where we particularly show the improvement at a selected frequency $k_0 = 4.3629\,\mu\text{m}^{-1}$, which roughly corresponds to the average of the resonance frequencies that shift with increasing angles of incidence. By considering SSD, we do not only push the agreement with the reference from 25° to 50°, but are also able to capture the functional dependency, i.e., the curvature of both reflection and transmission coefficients as function of angle of incidence. This is a sound evidence in favor for the importance of retaining nonlocal constitutive relations in the effective description of mesoscopic metamaterials. Of course, this is not perfect yet and other models for homogenization with an even higher expansion order in Eq. (3.40) in real space or, alternatively, in Eq. (3.41) in spatial Fourier-space might further lead to additional improvements at significantly higher angles of incidence. Similarly, for a stacking of two functional fishnet layers with a total thickness of $d_{\text{slab}} = 400\,\text{nm}$, we reconstruct with the same method the reflection and transmission coefficients using WSD and SSD. Please note, in that case we retrieve a different set of effective properties that will be compared to those retrieved from a single functional layer further below. The corresponding reflection and transmission coefficients are shown in Fig. 5.10. Due to the propagation through two absorbing fishnet layers, we notice in Fig. 5.10**(d)** that at frequencies below $4.3\,\mu\text{m}^{-1}$ the transmission is strongly reduced down to values below 0.2 in the paraxial regime, with almost no significant spectral features. However, the retrieval relies on significant transmission. Therefore, it is not recommended to stack a further functional fishnet layer which would further increase the thickness and leads to a much smaller transmission. Eventually, the

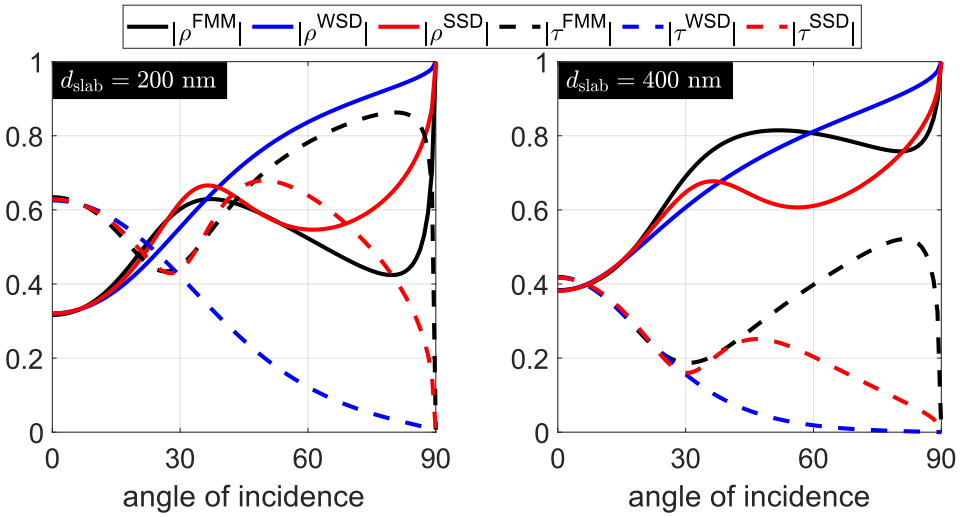

Figure 5.11: Reflection (solid) and transmission (dashed) amplitudes for one (left) and two (right) functional fishnet layer(s) at a selected frequency $k_0 = 4.3629\,\mu\text{m}^{-1}$ with thicknesses $d_{\text{slab}} = 200\,\text{nm}$ and $d_{\text{slab}} = 400\,\text{nm}$, respectively. Here, the WSD (blue) matches with the reference (black) up to an angle of incidence of 20° an, while the SSD (red) is valid up to 30° for the reflection and 50° for the transmission coefficient.

transmission gets too small to be useful in the retrieval.

Concerning the results, here again, both homogenization models serve fine in the paraxial regime. However, both models start to strongly deviate with increasing angle of incidence. For instance, at the resonance frequency the WSD model already fails to reproduce the reference data for angles beyond 20° and the SSD extends its validity up to 30° for the reflection and 50° for the transmission coefficient. Despite of that, the smaller angle defines the region of applicability of a certain model. The results for the selected frequency of $k_0 = 4.3629\,\mu\text{m}^{-1}$ for two fishnet layers are depicted in Fig. 5.11(right). Again, the SSD manages to roughly mimic the functional dependency at higher angles of incidence, which is a clear signal that the homogenization with a nonlocal approach is more appropriate.

To further elucidate the quality of the nonlocal homogenization approach, we show in Fig. 5.12 the absolute deviations in percent between the complex valued reflection and transmission coefficients computed with the FMM to those fitted using either WSD or SSD to one (left) and two (right) fishnet layers. To better quantify the deviations, we truncated the color axis to 10%. In principle, we distinguish between two areas. The dark areas denote the pairs of frequencies and angles of incidence where the reflection and transmission coefficients can be properly reproduced with the retrieved material parameters, leading to a meaningful homogenization. On the contrary, the bright regions indicate deviations from the reference above 10%, namely the regions where the homogenization with a specific model breaks down. For both thicknesses, the nonlocal approach extends the validity to higher angles of incidence compared to the local approach. Naturally, as we also anticipated, both models struggle to properly homogenize the fishnet around the resonance frequency $k_0 = 4.3\,\mu\text{m}^{-1}$. In view of this analysis, the dark regions of Fig. 5.12 represent the domains, where the fishnet metamaterial can be reasonably homogenized with meaningful retrieved effective material parameters.

The extracted effective material parameters from one and two fishnet layers are de-

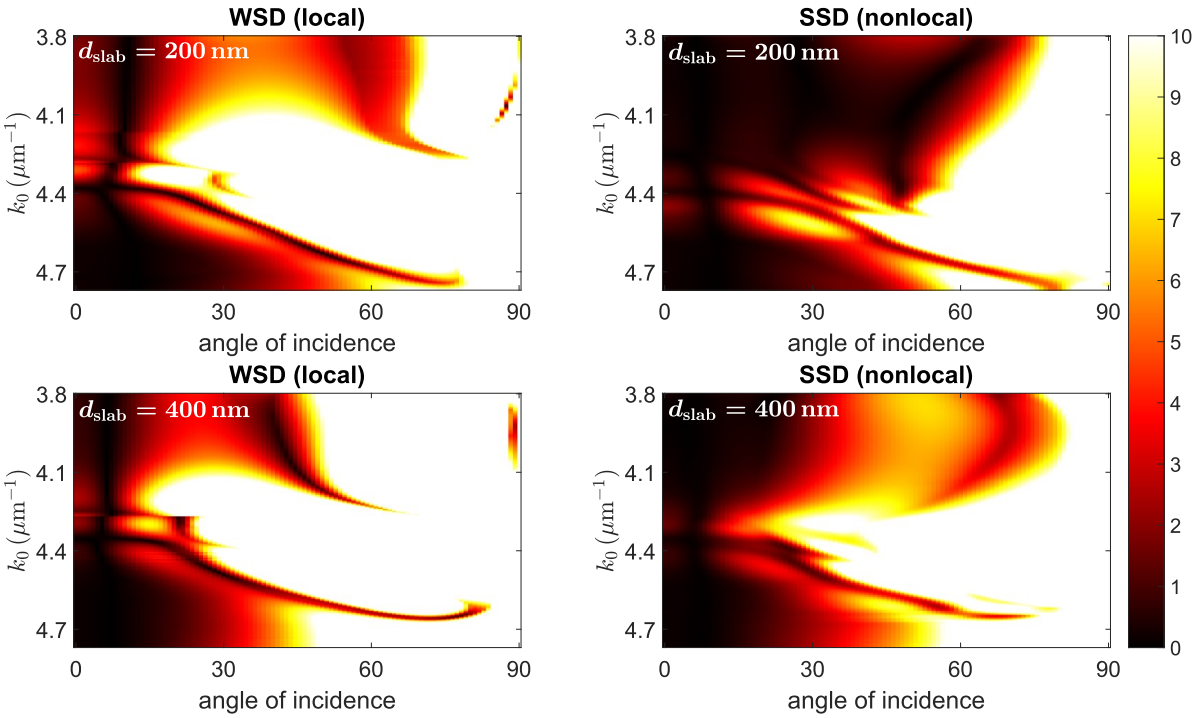

Figure 5.12: Deviations of the homogenization approaches from the fishnet response using the local WSD (left) and nonlocal SSD (right) approaches for one (top) and two (bottom) fishnet layers with thicknesses $d_{\text{slab}} = 200\,\text{nm}$ and $d_{\text{slab}} = 400\,\text{nm}$, respectively. The deviations to the reference data are given in percent, limited to 10% and plotted as a function of the frequency and the angle of incidence. Both WSD and SSD serve well in the paraxial regime, while the SSD notably stretches the agreement to higher angles of incidence for all frequencies. As expected, the deviation around the resonance is high for both models, as the effective wavelength in the effective medium is shorter at these frequencies, which renders the critical parameter (Λ_y/λ) closer to unity.

picted in Fig. 5.13. The blue curves correspond to the retrieved material parameters using the local WSD approach and the red curves to those using the nonlocal SSD approach. The solid curves are obtained from a retrieval from one fishnet layer and the dashed curves from two functional layers of the fishnet metamaterial, i.e., two times the sequence of five different material layers. The effective material parameters seem to not significantly change by doubling the thickness, except for the y-component of the permittivity that shows a Drude-Lorentzian behaviour at the resonance frequency. As expected, the y-component of the permittivity is negative in the studied frequency range. There is one important remark concerning the permittivity ϵ_{yy} obtained from the local homogenization method. The permittivity ϵ_{yy} shows an anti-Lorentzian behaviour in the vicinity of the resonance frequency. First of all, this antiresonance has an anomalous negative slope-dispersion curve that breaks causality [159] and is, therefore, unphysical. Second, the same antiresonance causes that $\Im\epsilon_{yy} < 0$ for a small frequency band. Such negative imaginary part suggests that the medium, that is actually made out of absorbing constituents, is rather gainy, if considered as an isolated material property. This is, again, unphysical. In the early 2000s, such anti-Lorentzian was associated to the finite unit cell size [160], while there, the authors assume the WSD approximation for homogenization. It is somewhat suspicious that a metamaterial made out of passive and causal materi-

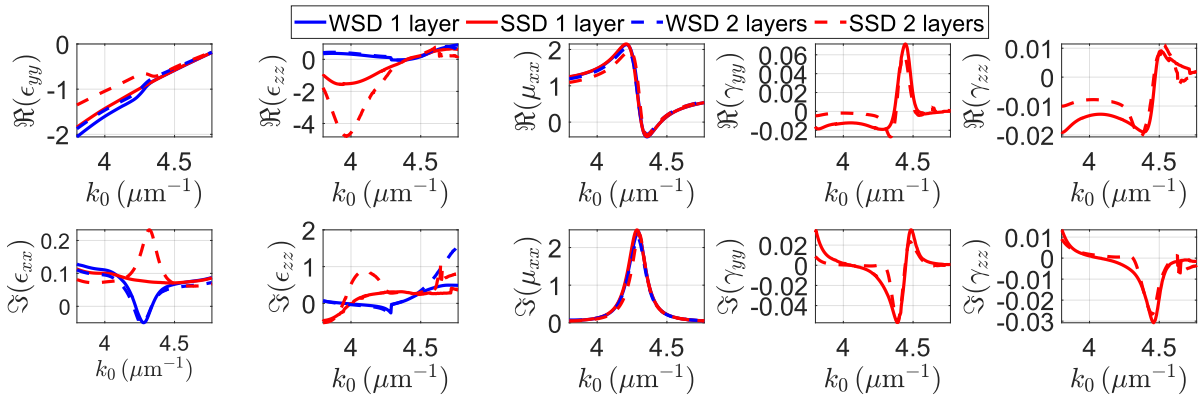

Figure 5.13: Real and imaginary parts of the retrieved effective material parameters for the fishnet metamaterial for one (solid) and two (dashed) layers. In blue, we have the retrieved material parameters used the local WSD approach and in red using the nonlocal SSD approach. The results were obtained from minimizing the merit function Eq. (5.1) using the respective model.

als, ends up breaking these two fundamental aspects in its effective picture. The truth, however, is rather linked to the fact of enforcing local constitutive relations to the homogenization of mesoscopic metamaterials. By the introduction of the nonlocal parameter $\hat{\gamma}$, i.e., considering SSD, this anti-resonance could be lifted and is no longer existing in the permittivity ϵ_{yy} that is retrieved using that nonlocal approach. Despite of that matter, the permittivity is rather dominated by a Drude-type dispersion. This is the usual response expected for a diluted metal.

Concerning the permeability μ_{xx}, both local and nonlocal show practically indistinguishable Lorenztians, and are in good approximation independent from the number of fishnet layers. The real part attains negative values in a central frequency region of interest. This dispersion is the desired effect here and is one major reason for the study of fishnet metamaterials. This peculiar response emerges due to the antisymmetric coupling between the two silver layers, that are separated by the dielectric layer. Finally, circular currents are induced by the y-component of the electric field in different metallic layers and an effective magnetization arises. In our geometrical configuration, the resonance frequency of the effective magnetic permeability μ_{xx} happens to be at $k_0 = 4.3\,\mu\mathrm{m}^{-1}$. It corresponds to the spectral region where the $\Im k_z$ has its maximum value. As noted in Sec. 3.2, and specifically proved in inequality (3.25), the magnetic characteristics of metamaterials at optical frequencies become trivial in the zero-cell-size limit. Thus, such strong resonant magnetic response can only be achieved if the size of the unit cell has an appreciable fraction of the wavelength. Here at resonance, we roughly have a period-to-wavelength ratio $\Lambda_x/\lambda \approx 0.4$, where λ is the free-space wavelength[3]. Ultimately, with both ϵ_{yy} and μ_{xx} being simultaneously negative, the desired negative index behaviour is reached.

Further, under the consideration of oblique incidence, the z-component of the electric field of the incoming TM-polarized wave couples to the z-component of the permittivity and we may, therefore, retrieve the ϵ_{zz} parameter. Unfortunately, this parameter is quite tricky to make sense of for two reasons. First, in contrast to the previously discussed

[3]The effective in-medium wavelength at resonance is 25% longer than in vacuum with $\lambda \leftarrow \frac{\lambda}{|\Re n(k_0)|} = \frac{\lambda}{0.8} = 1.25\lambda$, where $\Re n_z(4.3\,\mu\mathrm{m}^{-1}) = \frac{\Re k_z(0,4.3\,\mu\mathrm{m}^{-1})}{4.3\,\mu\mathrm{m}^{-1}} = -0.8$ is the refractive index at normal incidence.

material parameters, here, both homogenization models predict different values. Given the fact that the SSD model is more accurate than the WSD at oblique incidence, we tend to consider the ϵ_{zz} retrieved using SSD is actually the rather true effective parameter to be assigned for the fishnet. Second, the retrieval of this parameter in the present geometry is tough. It turns out that the reflection and transmission from a slab is rather insensitive on that specific material parameter, even though it can be only probed at oblique incidence. This causes the retrieval from reflection and transmission being only weakly dependent on this specific parameter and indeed a deviating choice of the specific material parameter provides nearly the same optical coefficients. We will discuss and explain this issue later in Sec. 5.4.1.

Finally, the nonlocal parameters γ_{xx} and γ_{zz} are shown in Fig. 5.13 and, of course, there are no blue curves as they do not exist in the local model. First, we notice that both nonlocal parameters show a resonance at a slightly higher frequency compared to that of the local ones at around $4.5\,\mu\mathrm{m}^{-1}$. This higher resonance frequency might suggest that these parameters are related to higher-order multipoles. Second, they are at least one order of magnitude smaller than the local parameters $\hat{\epsilon}$ and $\hat{\mu}$. This completely makes sense as they are higher-order contributions in the Taylor approximation (4.18) with nonlocal corrections. Despite of that fact, these nonlocal parameters are quite important as they allow for a significant improvement in the effective description of the considered fishnet metamaterial. This especially holds true when describing the optical response at oblique incidence, as largely demonstrated in Figs. 5.9-5.12.

To conclude this subsection, we investigated the fishnet metamaterial. The aim here was to apply two homogenization models to the fishnet. First, we studied the infinitely extended bulk in terms of dispersion relations and, and second the biperiodic slab with finite thickness, in terms of reflection and transmission. In both cases, we have shown that nonlocal material laws are urgently needed to effectively homogenize the fishnet metamaterial and to predict its electromagnetic response beyond the paraxial regime. However, the issue that was encountered in the retrieval approach concerning the liability of the retrieved ϵ_{zz} parameter, is still open. Further, a homogeneous medium is independent on its termination, whereas mesoscopic metamaterials such as the fishnet do not fulfill this requirement. To address these two aforementioned issues, in Sec. 5.4.1 we provide a sensitivity analysis to first give details why some specific material parameters can be more reliably retrieved while others are not. In the same section, we also study the behaviour of the effective material parameters when changing the sequence of the individual fishnet layers, i.e., by redefining the unit cell such that infinitely extended bulk remains the same.

5.3.3 Plasmonic wire medium: A prototypical material with strong spatial dispersion

Please note that the findings of this subsection were previously published in Ref. [161].

A particularly interesting metamaterial that exhibits strong spatial dispersion is the array of metallic wires in the vicinity of the epsilon near-zero regime. This structure further allows for a negative refraction, but in contrast to the fishnet metamaterial, it is polarization independent, which is a necessary condition for the design of isotropic negative index metamaterials. Let us recall its basic geometry that is depicted in Fig. 5.14. It consists of an array of cylindrical metallic nanowires with permittivity ϵ_m and radius r_m, embedded in a dielectric host medium with a nondispersive permittivity ϵ_h. Arising

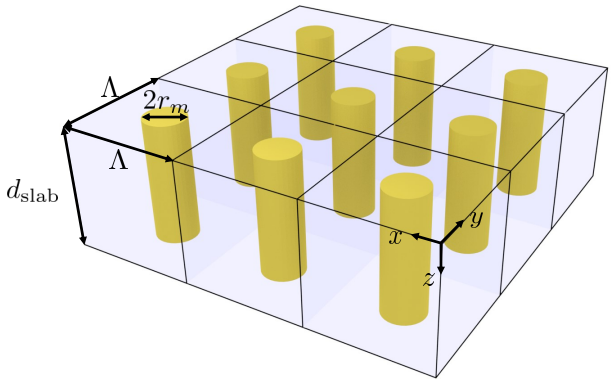

Figure 5.14: A slab of a wire medium consisting of metallic wires with length d_{slab} and radius r_m being embedded in a dielectric host medium. The wires are parallel to the z-direction and periodically arranged in a square lattice with lateral periodicity Λ.

from the microwave regime towards infrared and optical wavelengths, it gained significant attention due to its versatile applications ranging from antenna applications [162], by exploiting its near-zero refractive index, to subwavelength imaging [163] in the negative permittivity regime. Almost two decades ago, it was proven [57] that wire media show strong spatial dispersion in the TM-polarized case, even in the very long wavelength regime. In the effective description, the effective permittivity was modeled using the hydrodynamic model described in Sec. 4.4.2. Here, we will apply that wire medium model (WM) from the literature, i.e. Eq. (4.73) in this thesis, and compare its retrieval performance against the SSD model, i.e. Eq. (4.18) we have been proposing, while predicting the reflection and transmission coefficients from an actual wire medium slab. Here, we will not discuss the local WSD approach in this part of the study. The WM model only holds for very thin wires and does not account for any artificial magnetization. Hence, and for the sake of a reasonable comparison between both WM and SSD models, we will assume a disappearing effective magnetic response in the SSD model, i.e., $\hat{\mu} = \mathbb{1}$ by choosing $\hat{\alpha} = 0$. In brief, we solely study the impact of the nonlocal parameter $\hat{\gamma}$.

Before we proceed with the retrieval results, let us discuss the fundamental similarities and differences of both nonlocal models. First of all, the WM model is predictive and directly yields the reflection and transmission coefficients. It only requires to know the geometrical and material data for a given wire medium structure. On the contrary, the SSD model rather relies on a fitting procedure, which might take a couple of hours, that needs to be done for each structure individually. However, we have found in Ref. [161] that the SSD model is rather more robust when period to wavelength ratio is getting closer to unity and manages to capture the reflection and transmission coefficients more adequately at normal incidence (see Sec. 5.4.1). Second, in the absence of an interface, we have shown as well [161] that both models are in principle equivalent, i.e., the light propagation within an infinitely extended medium is identical for all frequencies k_0 and transverse momentum k_y. This is only possible for a further restriction of the SSD model, by enforcing the dispersion relations $k_{z,\sigma}(k_y, k_0)^{\mathrm{SSD}} \stackrel{!}{=} k_{z,\sigma}^{\mathrm{WM}}(k_y, k_0)$ to be equal. Imposing

WM model	SSD model
$[\mathbf{E}(\mathbf{r},k_0)\times\mathbf{n}]=0$	$[\mathbf{E}(\mathbf{r},k_0)\times\mathbf{n}]=0$
$[(\nabla\times\mathbf{E}(\mathbf{r},k_0))\times\mathbf{n}]=0$	$[(\nabla\times\mathbf{E}(\mathbf{r},k_0))\times\mathbf{n}]=$ $-k_0^2(\nabla\times\gamma(k_0)\nabla\times\nabla\times\mathbf{E}(\mathbf{r},k_0))\times\mathbf{n}$
$[(\epsilon_h\mathbf{E}(\mathbf{r},k_0))\cdot\mathbf{n}]=0$	$(\gamma(k_0)\nabla\times\nabla\times\mathbf{E}(\mathbf{r},k_0))\times\mathbf{n}=0$

Table 5.2: Interface conditions for the two nonlocal WM and SSD models with $\hat{\alpha}=0$. The brackets $[\cdot]$ refer to the discontinuity of the quantity across the interface. The last row represents the additional interface condition of the corresponding model.

this, implies the parameters in the SSD model to be

$$\begin{aligned}\frac{1}{\epsilon_{yy}}&=\frac{1}{\epsilon_{yy}^{\mathrm{loc}}}-\eta\frac{\epsilon_m}{\epsilon_{zz}^{\mathrm{loc}}},\quad \frac{1}{\gamma_{yy}}=k_0^{-4}\left(\epsilon_{yy}^{\mathrm{loc}}-\frac{\epsilon_{zz}^{\mathrm{loc}}}{\eta\epsilon_m}\right),\\ \frac{1}{\epsilon_{zz}}&=\frac{1}{\epsilon_{zz}^{\mathrm{loc}}},\qquad\qquad \frac{1}{\gamma_{zz}}=k_0^{-4}\frac{\left(\eta\epsilon_m\epsilon_{yy}^{\mathrm{loc}}-\epsilon_{zz}^{\mathrm{loc}}\right)^2}{\eta\epsilon_{yy}^{\mathrm{loc}}\left(\epsilon_m+\eta\epsilon_m\epsilon_{yy}^{\mathrm{loc}}-\epsilon_{zz}^{\mathrm{loc}}\right)}.\end{aligned}\tag{5.17}$$

where on the LHS we have the free parameters of the SSD model and on the RHS we have the effective parameters of the WM model. The permittivities $\epsilon_{yy}^{\mathrm{loc}}$ and $\epsilon_{zz}^{\mathrm{loc}}$ are the Maxwell-Garnett averaged permittivities for cylindrical inclusions and given by Eqs. (4.72) and (4.74), respectively. Let us recall that η is the actual nonlocal parameter of the WM model and is directly proportional to the ratio $(r_m/\lambda)^2\ll 1$. By considering the limit of vanishing wires, i.e. $r_m\to 0$, the nonlocal parameter η tends to zero and the effective material parameters of the SSD model converge to the expected values

$$\epsilon_{yy}\to\epsilon_{yy}^{\mathrm{loc}}\,,\epsilon_{zz}\ \ \to\epsilon_{zz}^{\mathrm{loc}}\,,\gamma_{yy}\to 0\,,\gamma_{zz}\ \ \to 0\,.$$

With this, the local limit is verified as well.

However, regardless of assumption (5.17) and the implied similarity in the dispersion relations, the SSD and WM models are still fundamentally different. The dissimilarity emerges at the presence of an interface, as the interface conditions differ and cannot be mapped to each other like in the study of the bulk dispersion relations. We summarize the three interface conditions for each model in Tab. 5.2. The first row states the continuity of the tangential component of $\mathbf{E}(\mathbf{r},k_0)$ in both models. This is always the case as $\mathbf{E}(\mathbf{r},k_0)\in\boldsymbol{\mathcal{H}}_{\mathrm{loc}}(\mathrm{curl},\mathbb{R}^3)$, independent from the model in question. The second interface condition refers to the (dis)continuity of the tangential component of $\nabla\times\mathbf{E}(\mathbf{r},k_0)$, i.e., the tangential component of $\mathbf{H}(\mathbf{r},k_0)$. The WM model assumes the continuity of the latter quantity, while the SSD model breaks this continuity with a jump proportional to the nonlocal parameter $\hat{\gamma}$. Ultimately, the third row in Tab. 5.2 contains the actual additional interface conditions. Concerning the WM model, this interface condition is purely normal, i.e., it makes statements only on the normal component of the electric field. On contrary, the additional interface condition obtained from the SSD model is purely tangential. Hence, there is no way to map one interface condition into another, as they both describe different field components. Therefore, it is reasonable to expect that both models lead to a different set of reflection and transmission coefficients from an array of wire media with finite length, ergo a slab. In the following section, we will study the electromagnetic response of both models and compare them to that of an actual wire medium slab.

Retrieval results Let us consider a wire medium made of metallic nanowires with radius $r_m = 12.5\,\text{nm}$ embedded in a nondispersive medium made of aluminum oxide (Al_2O_3) with a permittivity $\epsilon_h = 2.74$. The nanowires are periodically arranged in the xy-plane forming a square lattice with period $\Lambda = 60$ nm with a small surface concentration of wires $f = \frac{\pi r_m^2}{\Lambda^2} = 13\%$. The wires are made of gold with the permittivity ϵ_m given by

$$\epsilon_m(\omega) = \epsilon_{\text{bulk}}(\omega) + \frac{\mathrm{i}\omega_p^2\tau(R_b - R)}{\omega(\omega\tau + \mathrm{i})(\omega\tau R + \mathrm{i}R_b)}\,, \tag{5.18}$$

where $R_b = 35.7$ nm and $R = 10$ nm denote the mean-free path and the effective mean-free path of the electrons, respectively [26]. The plasma frequency is $\omega_p = 13\,700\,\text{THz}$ and the relaxation time of the conducting electrons in gold $\tau = 2.53 \times 10^{-14}\text{s}$. The permittivity consists of two terms. The first term ϵ_{bulk} denotes the permittivity of bulk gold and is obtained from Johnson and Christy [164]. The second term describes additional effects to the finite size of the nanowires that constraints the motion of the free electrons in the nanowires. The finite length of the nanowires is $d_{\text{slab}} = 300\,\text{nm}$ that also represents the slab thickness. Both material and geometrical data above were adopted from Refs. [26], [120]. Here again, the reference data for the reflection and transmission coefficients were obtained using the FMM, where the field is expanded into Bloch modes in the xy-direction and into plane waves in the z-direction. As the wire medium is invariant in the z-direction, only one layer is enough in the numerical calculation. This requires less computation of interface conditions and is much faster compared to the case of the fishnet with five material layers[4]. In our simulations, we calculate the reflection and transmission coefficients of the wire medium in a frequency range of $k_0 \in (7\ \ \mu\text{m}^{-1}, 11\ \ \mu\text{m}^{-1})$ with the angles of incidence $\theta = \arcsin\left(\frac{k_y}{k_0}\right)$, where $k_y \in [0, k_0)$. We intentionally omitted the grazing incidence at $k_y = k_0$, due to numerical reasons. An angle of incidence of 90° does first, make no sense and second, leads to divergences of type "$\frac{1}{0}$" in the simulations.

The numerically calculated reflection and transmission coefficients of the mesoscopic structure upon an illumination by a TM-k_y polarized plane wave are, respectively, depicted in Figs. 5.15**(a)** and **(d)** as function of frequency and angle of incidence. The reconstruction of this reference data using the wire medium (WM) model is straightforward. It suffices to insert the material and geometrical details of the mesoscopic structure given above into the corresponding equations for the reflection and transmission coefficients, i.e., into Eq. (4.82). By doing so, we obtain the predicted response depicted in Figs. 5.15**(b)** and **(e)**. On the other hand, the SSD model still requires the fitting procedure, that is described in Sec. 5.1, to obtain the effective material parameters that lead to the reflection and transmission coefficients shown in Figs. 5.15**(c)** and **(f)**.

Despite the difference in the approaches, both homogenization models are satisfying, especially in the paraxial regime. The WM model yields reflection coefficients that are more conforming with the reference for higher angles of incidence, whereas the SSD model shows an inexplicable huge reflection, that is not present in neither the reference, nor in the WM model. This inconsistency might be linked to the Taylor approximation in the SSD model, i.e., Eq. (4.18), which is an expansion in the vicinity of $k_y \approx 0$ and further, to the weight function $w(k_y)$ that is implemented to optimize the fitting procedure around the paraxial regime, to the detriment of the retrieval quality at higher angles of incidence.

[4]In the fishnet one functional layer consists of a stacking of Air-metal-spacer-metal-spacer layers, where between two consecutive material layers interface conditions have to be calculated. Of course, in addition to the two interface conditions between slab, cladding, and substrate.

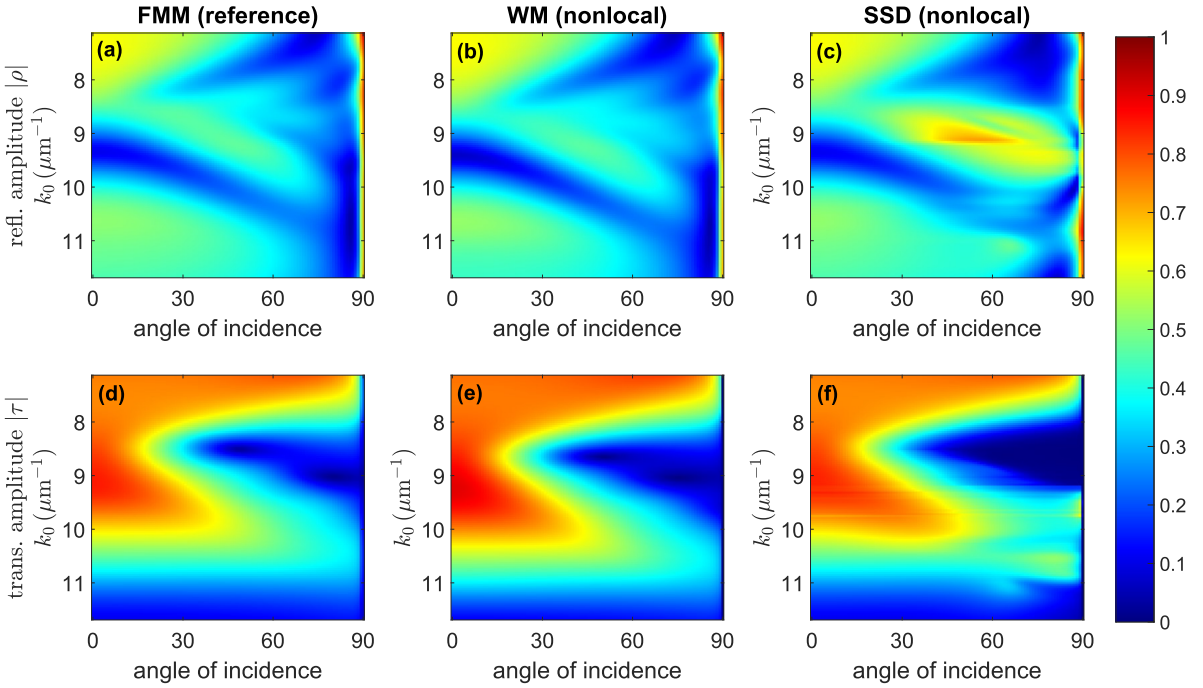

Figure 5.15: Amplitude of the reflected light $|\rho|$ and of the transmitted light $|\tau|$ from a metallic wire medium with thickness $d_{\mathrm{slab}} = 300\,\mathrm{nm}$ and lateral periodicity $\Lambda = 60\,\mathrm{nm}$ using different approaches.

Notwithstanding the foregoing statements, it is quite welcoming to note that the SSD approach, that is not specially conceived for wire media, offers reasonable prediction of the electromagnetic response. In addition, we reveal in Fig. 5.16**(a)** the reflection and transmission coefficients at a selected frequency of $k_0 = 10.25\,\mu\mathrm{m}^{-1}$ as a function of the angle of incidence. The black curves represent the reference data obtained from the FMM. We notice that both nonlocal models are in compliance with the reference data. Though, the WM model shows deviations especially for the transmission coefficients and even at normal incidence, where the SSD model is almost exact. Given the fact that the SSD model is not only specially derived for the homogenization of wire media, but also serves as a general-purpose model that can be implemented to other metamaterials whose unit cell have a central symmetry, this outcome is quite promising. Hence, the SSD model may be regarded as a reasonable alternative model for wire media and homogenization is not unique. Finally, the retrieved effective material parameters of the SSD model are summarized in Fig. 5.16**(b)**. We remark that all material parameters have a Lorentzian or anti-Lorentzian resonance around $k_0 \approx 9.5\,\mu\mathrm{m}^{-1}$, there, where both reflection and transmission coefficient abruptly drop, which suggests that most light is absorbed by the medium. Only parameter γ_{zz} seems to sustain an additional resonance at a lower frequency, which might explain the drop of the reflection coefficient at $k_0 \approx 8\,\mu\mathrm{m}^{-1}$.

Let us briefly summarize the findings of this subsection. First, we studied on an analytical level the difference and similarities of both nonlocal approaches. In the bulk, with further restrictions to the SSD model, both models may be identical. However, at the presence of an interface, the models fundamentally differ, as in the WM the additional interface condition only involves the normal component of the electric fields, while the SSD model only contains their tangential components. Second, a numerical study was done on a test subject from the literature [26], [120]. We find that both nonlocal models

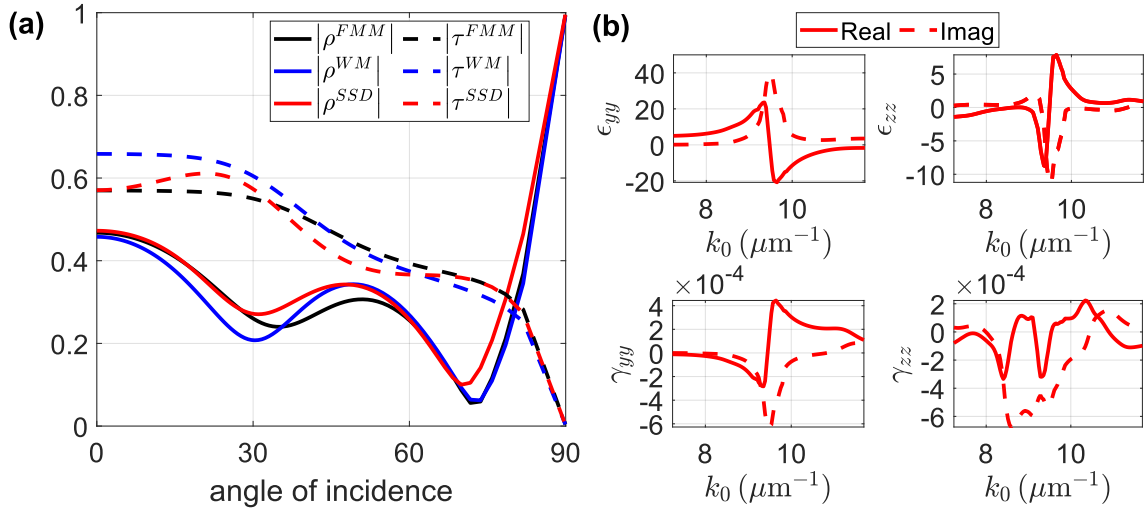

Figure 5.16: **(a)** Reflection and transmission amplitudes from the original wire medium with period $\Lambda = 60\,\mathrm{nm}$ at a selected frequency $k_0 = 10.25\,\mu\mathrm{m}^{-1}$. The solid (dashed) curves represent the reflection (transmission) coefficients, while the black curves represent the reference simulations. Generally, both models WM and SSD models show a good agreement with the reference, but the SSD model is, especially up to 45°, much closer to the reference than the wire medium model. **(b)** Real (solid) and imaginary (dashed) parts of the retrieved effective material parameters of the SSD model as a function of the frequency k_0.

are able to predict the reflection and transmission coefficients of a concrete wire medium slab. Especially the WM model shows good results at high angles of incidence. Since there is an explicit expression at hand, no further optimization method is required, which renders the approach being fast. However, the details shown in Fig. 5.16**(a)** suggest that the WM model does not perfectly correspond to the reference, especially in the paraxial region. This issue does not occur with the SSD model when characterizing wire medium, which is actually very accurate near the normal incidence. However, it takes a certain amount of time to reproduce the reflection and transmission of the reference and shows inconsistencies in the range of grazing angles. This is a consequence of the normal incidence-focused sensitivity during the retrieval and Taylor approximation for small k_y values. The mismatch of the WM at normal incidence might be linked to the additional interface condition that states $0 = 0$, while the dispersion relation still dictates an additional mode as $k_z \neq 0$ in the k_z-dependent permittivity (see e.g. Eq. (4.73)).

The next question that we want to answer is, how do these two effective medium models perform under a scaling of the unit cell, with the same filling factor? We will address this question in Sec. 5.4.2 by studying a three-times scaled unit cell of the same wire medium and will elaborate on the reasons of the failure of the homogenization models, especially at higher angles of incidence.

5.4 On the limits of homogenization and parameter retrieval

Until now, we were mostly showing the positive aspects of the homogenization models and of the retrieval technique. Here, we will give details why different material parameters are retrieved with different accuracy and also show the limits of the homogenization. For the former matter, we provide here a sensitivity analysis and elaborate on the challenge in retrieving the z-component of the permittivity. Basically, we show that the complex reflection coefficient is weakly sensitive with respect to ϵ_{zz}.

Recently [165], it was experimentally confirmed that the reflection and transmission from a multilayered structure depends on the sequence of layers, even if the layers are deeply subwavelength. In this thesis, we will substantiate this claim at the example of the fishnet metamaterial by redefining the unit cell. We have shown in Ref. [126] that the effective parameters do change, but only in their resonance strength and not on their type of dispersion, e.g., Drude, Lorentz, and anti-Lorentz.

Further, we show the importance of the fundamental mode approximation and the critical parameter (Λ/λ), where Λ is the lateral period of periodic structure, and λ the wavelength of light. On the example of the wire medium, we will show that the nonlocal homogenization methods discussed in Sec. 5.3.3 are pushed towards their limits of validity, by laterally scaling up the unit cell while keeping the filling factor constant. This was done in Ref. [161] and will be elaborated in Sec. 5.4.2 with details.

5.4.1 Sensitivity analysis and robustness of the retrieval method

The test subject of this analysis is the fishnet metamaterial from the previous section. First, we do a sensitivity analysis to explain the difficulty of retrieving z-components of the material parameters. Second, we discuss the retrieval from a rearranged fishnet made from the same multilayer structure but with a slightly different definition of the unit cell. To be specific, the considered unit cell has been shifted by half a unit cell in z-direction (normal to the interface). In the infinitely extended bulk, both original and redefined fishnet structures are identical, as the shifting only represents a translation of the coordinate system along the z-direction, such that $z \leftarrow z - \Lambda_z/2$.

Sensitivity analysis To further estimate in detail the reliability of the retrieved effective material parameters, let us study the Jacobian matrix of the reflection coefficient w.r.t. the material parameters, i.e., the partial derivatives

$$J_\rho = \left(\frac{\partial \rho}{\partial p}\right) , \tag{5.19}$$

where $p = (\epsilon_{yy}, \epsilon_{zz}, \mu_{xx}, \gamma_{yy}, \gamma_{zz})$ denotes the vector containing the effective material parameters. The matrix elements of the Jacobian contain the partial derivatives that serve as a measure of sensitivity. They indicate how strong the analytical reflection coefficient ρ varies by changing the respective material parameter. We present our analysis for the reflection coefficient. This is no limitation in general as we may draw identical conclusions when doing the analysis with the transmission coefficient.

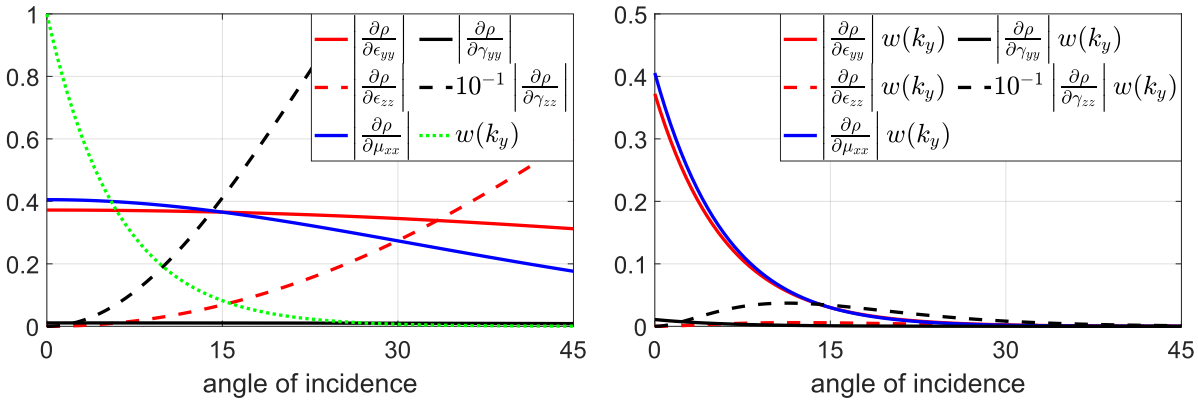

Figure 5.17: Matrix elements of the Jacobian as a measure for the sensitivity of the reflection coefficient in terms of the effective material parameters retrieved from one functional fishnet layer with thickness $d_{\text{slab}} = 200\,\text{nm}$. The partial derivatives are evaluated at $k_0 = 4.3\,\mu\text{m}^{-1}$, the resonance frequency of the fishnet metamaterial. On the left figure we display the absolute values of the partial derivatives J_ρ and the weight function $w(k_y)$. The figure on the right shows the effective sensitivity in the retrieval procedure, where the weight $w(k_y)$ has been considered into the partial derivatives. The parameters ϵ_{yy}, μ_{xx} and γ_{zz} seem to be very sensitive ones, while ϵ_{zz} and γ_{yy} are rather less important in the retrieval procedure.

In Fig. 5.17(left) we show the Jacobian for the reflection coefficient of the SSD model evaluated at $k_0 = 4.3\,\mu\text{m}^{-1}$, the resonance frequency of the fishnet. Here, we concentrate only on the real parts of the effective material parameters retrieved from one functional fishnet layer with thickness $d_{\text{slab}} = 200\,\text{nm}$, as they contain the propagation aspect. Meanwhile, derivatives w.r.t. the imaginary parts only translate to how much the reflection coefficient is affected w.r.t. loss. They are not of main importance here and will, therefore, not be considered in the analysis. We further included the weighting function $w(k_y$ in Fig. 5.17(left) that is plotted in green dotted line. Recall that we introduced the weight into the fitting procedure with the purpose to capture at least the reflection and transmission coefficients in the paraxial regime. The adjusted sensitivity that also incorporates that weight is depicted in Fig. 5.17(right). There, we show the product $J_\rho w(k_y)$. At normal incidence, the retrieval is obviously very sensitive against the change of the local parameters ϵ_{yy} and μ_{xx}, while it is less sensitive with regards to ϵ_{zz}. Also, at higher angles of incidence the impact of the latter parameter remains rather small. Therefore, ϵ_{zz} can be retrieved but due to the rather small influence on the overall merit function $\delta(k_0)$ the retrieval is not reliable. A quite noticable different dispersion of ϵ_{zz} might only cause a small change to the overall merit function.

Concerning the nonlocal parameters, their sensitivity is significantly different. The nonlocal parameter γ_{zz} seems to be a very sensitive one (note the downscale by 10^{-1} in the legend), which might also explain the importance of retaining nonlocality in the homogenization of the fishnet. On the other hand, γ_{yy} is apparently not important even in the paraxial regime. Such low sensitivity suggests that a huge change in the parameter would only weakly affect the reflection and transmission values. Therefore, we obtain a specific dispersion for the material parameter, but it makes the interpretation of the functional dependency complicated.

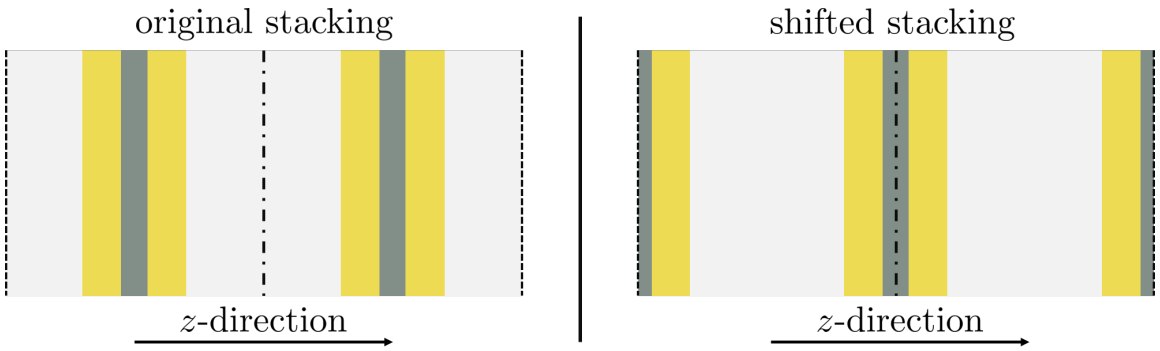

Figure 5.18: Lateral view of two functional fishnet layers. The orange layers refer to the metal, dark gray to the dielectric spacer, and light gray to the air layers. On the left, we have a stacking of the two original fishnet layers, where in each unit cell we have a pair of metallic layers that are separated by a thin dielectric spacer. On the right, we have the fishnet with a shifted unit cell, where the metallic layers only couple at the interface of two unit cells.

Robustness of the retrieval method The electromagnetic response from a homogeneous medium is independent on its termination, as in the homogeneous picture the incoming light interacts with the slab as one entity rather than with its individual layers. In contrast, the response from mesoscopic systems such as the fishnet does depend on the order of the material layers. For instance, the transmission coefficient depends on the impedance of the layer adjacent to the substrate, whereas the effective propagation constant does not change. In Ref. [93], it was shown that a purely dielectric structure made of alternating, deep-subwavelength layers change the reflection and transmission spectra, especially when operated at the critical angle of total internal reflection, that is predicted from an effective medium approach (there it is the local model without magnetization). Here, we will show on the example of the fishnet that, with the S-parameter retrieval, we retrieve different material parameters for different terminations.

To this end, let us consider a unit cell being shifted by half of its period in the z-direction. In the original fishnet, the unit cell compromises a stack of air-metal-dielectric-metal-air layers. The redefined unit cell now consists of a stack of dielectric-metal-air-metal-dielectric layers, where the air thickness is doubled, and the dielectric layer is halved compared to the original structure. Note that now, the dielectric layer is adjacent to the cladding and substrate. The stacking of two of such unit cells is depicted on Fig. 5.18. It is important to bear in mind that an infinite number of such unit cells in the z-direction would lead to the same bulk material as previously. This symmetry is only broken by the introduction of an interface.

Analogously to the situation of the original structure, we numerically calculate the reflection and transmission coefficients for the fishnet with the redefined unit cell. Afterwards, we performed the S-parameter optimization approach by fitting the analytically calculated reflection and transmission coefficients to those of the reference material. Here, we studied one and two functional layers of such shifted unit cells. The retrieved effective material parameters from one functional fishnet layer for the slabs with different terminations are depicted in Fig. 5.19**(a)**. Concerning the slab made from two functional fishnet layers, the retrieved effective material parameters are depicted in Fig. 5.19**(b)**.

As expected, for a single functional layer of this modified geometry, the induced dipole moments in the metallic layers are now spatially separated by rather thick air layer. Their

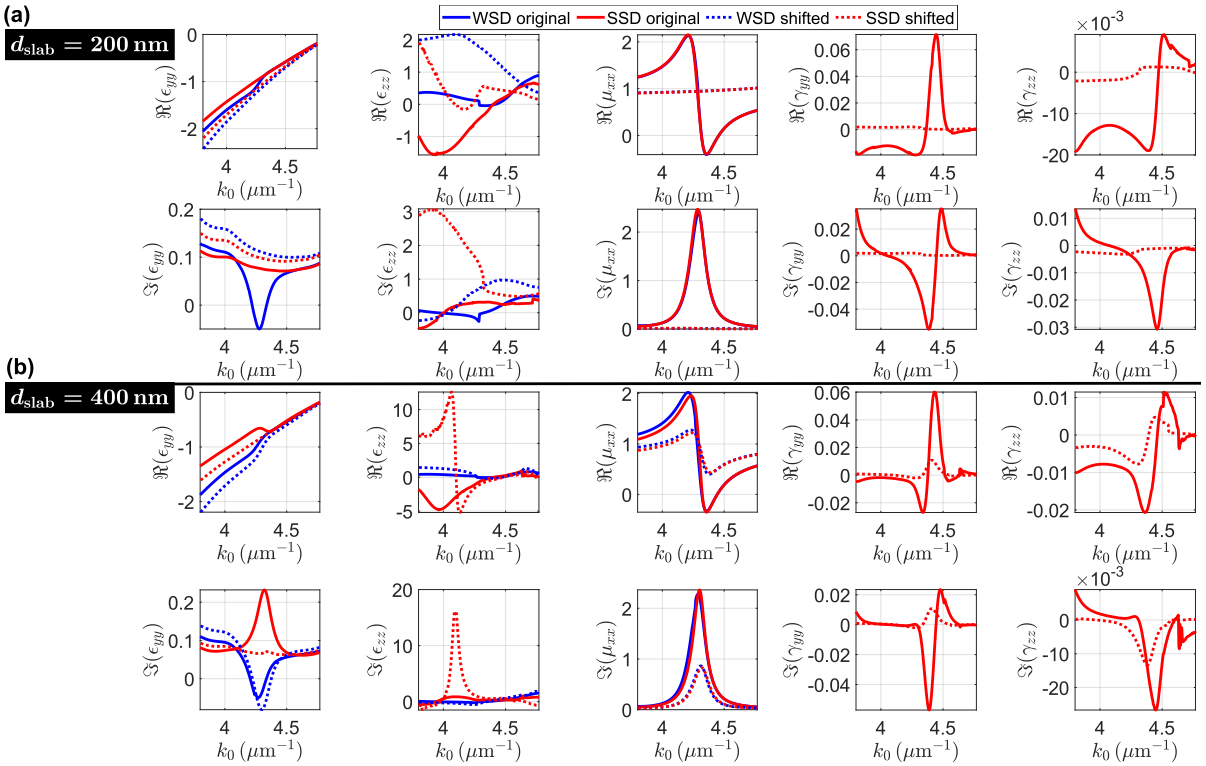

Figure 5.19: Real and imaginary parts of the retrieved effective material parameters for the fishnet metamaterial from the original unit cell (solid) and from shifted unit cell (dotted). We consider **(a)** a single stacking in the z-direction with slab thickness $d_{\text{slab}} = 200\,\text{nm}$ and **(b)** a double stacking with slab thickness $d_{\text{slab}} = 400\,\text{nm}$. In blue, we have the retrieved material parameters used the local WSD approach and in red using the nonlocal SSD approach. The permittivity strongly depends on the stacking. Notably, the permeability μ_{xx} vanishes for one layer of the shifted unit cell. As expected, with a stacking of two unit cells, the Lorentzian in the permeability μ_{xx} reappears with a smaller amplitude, due to the dilution of the metamaterial. The nonlocal parameters for the shifted unit cell are one order of magnitude smaller than for the original fishnet.

antisymmetric coupling has been previously responsible to induce the magnetic response. This larger separation leads to the disappearance of the effective magnetic response in the frequency range of interest. Therefore, the absence of a magnetic resonance and $\mu_{xx} \approx 1$. This is a clear indication that the definition of the unit cell affects the response. The magnetic resonance, however, appears again in a stack of two functional layers in the z-direction, such that the second metal layer of the first unit cell is only separated by $2 \times 1/2$-dielectric layers from the first metal layer of the second unit cell, as depicted in Fig. 5.18(right). This restores the original configuration and leads to an antisymmetric and strong coupling between the induced dipole moments in the consecutive metal layers. Therefore, at a qualitative level we restore the same material dispersion, but of course, we also observe a weakening of the overall dispersion. This is a mere consequence of the actual dilution of the metamaterial.

The electric permittivity ϵ_{yy} for one layer in contrast seems to depend only weakly on such a shift. This makes sense because the electric response, in the lowest order approximation, only depends on the individual metallic layers and not on their coupling. Nonetheless, we suppose that by including further functional fishnet layers the retrieved

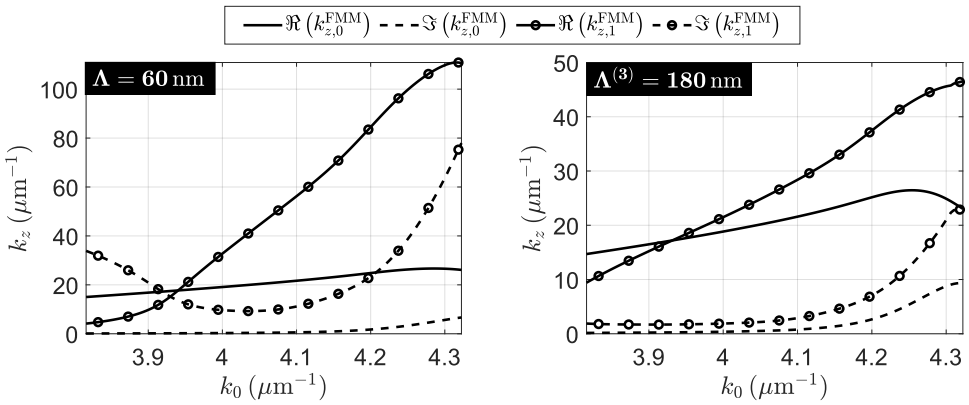

Figure 5.20: Dispersion relation of the fundamental and the first higher-order mode of (left) the original structure with periodicity $\Lambda = 60\,\mathrm{nm}$, and (right) for the stretched structure with periodicity $\Lambda^{(3)} = 180\,\mathrm{nm}$ with $k_x = k_y = 0$. For the original structure, the fundamental mode with propagation number $k_{z,0}^{\mathrm{FMM}}$ is very well isolated from the higher order mode, as $\Im\left(k_{z,0}^{\mathrm{FMM}}\right) \ll \Im\left(k_{z,1}^{\mathrm{FMM}}\right)$. For the stretched structure it is, however, not the case as only $\Im\left(k_{z,0}^{\mathrm{FMM}}\right) < \Im\left(k_{z,1}^{\mathrm{FMM}}\right)$ holds. Here, the first-order mode is not sufficiently attenuated to be neglected.

effective material parameters obtained from the two different unit cells converge to the same values. However, due to to absorption, by adding a further fishnet layer the transmission drops to very low values that are eventually too small for the retrieval.

Concerning the nonlocal parameters γ_{yy} and γ_{zz}, they show a much smaller resonance amplitude for both one and two shifted layers compared to those retrieved from the original structure. At last, only the ϵ_{zz} parameter seem to vary a lot below the resonance frequency, where it shows a Lorentz resonance. Anyway, the interpretation of this parameter is quite delicate, as it is a very insensitive one and hard to retrieve, as discussed above. Altogether, our findings are in agreement with the findings documented in the references [93], [165].

5.4.2 Homogenization of wire media at extreme conditions

In this subsection, we study on the example of the wire medium the importance of the fundamental mode approximation, even in the nonlocal regime and push the nonlocal models towards their limits and study their performance at extreme conditions. To this end, let us consider the wire medium from Sec. 5.3.3 and laterally enlarge the unit cell by a factor three. The period of the enlarged structure $\Lambda^{(3)} = 3\Lambda$ and its corresponding wire radius is $r_m^{(3)} = 3r_m$. By doing so, we keep the surface concentration $f^{(3)} = \frac{4\pi}{3}\left(\frac{3r_m}{3\Lambda}\right)^3 = f$ equal to that of the original structure. Particularly important is that such scaling changes the period-to-wavelength ratio, that is $(\Lambda/\lambda) \ll 1$ for the original structure, while $\left(\Lambda^{(3)}/\lambda\right) \approx 0.3$ for the enlarged one. Notable differences may be already observed in a modal analysis in terms of the dispersion relations of the fundamental mode $k_{z,0}^{\mathrm{FMM}}$ and of the next higher-order mode $k_{z,1}^{\mathrm{FMM}}$. Both are numerically calculated using the plane wave expansion ansatz that is part of the FMM and are depicted in Fig. 5.20 for both original and enlarged structure for $k_x = k_y = 0$. Concerning the original structure, the fundamental mode is well separated from the next higher-order mode, as the imaginary part $\Im(k_{z,0}^{\mathrm{FMM}}) \ll \Im(k_{z,1}^{\mathrm{FMM}})$ by at least one order of magnitude. Thus, the validity of the

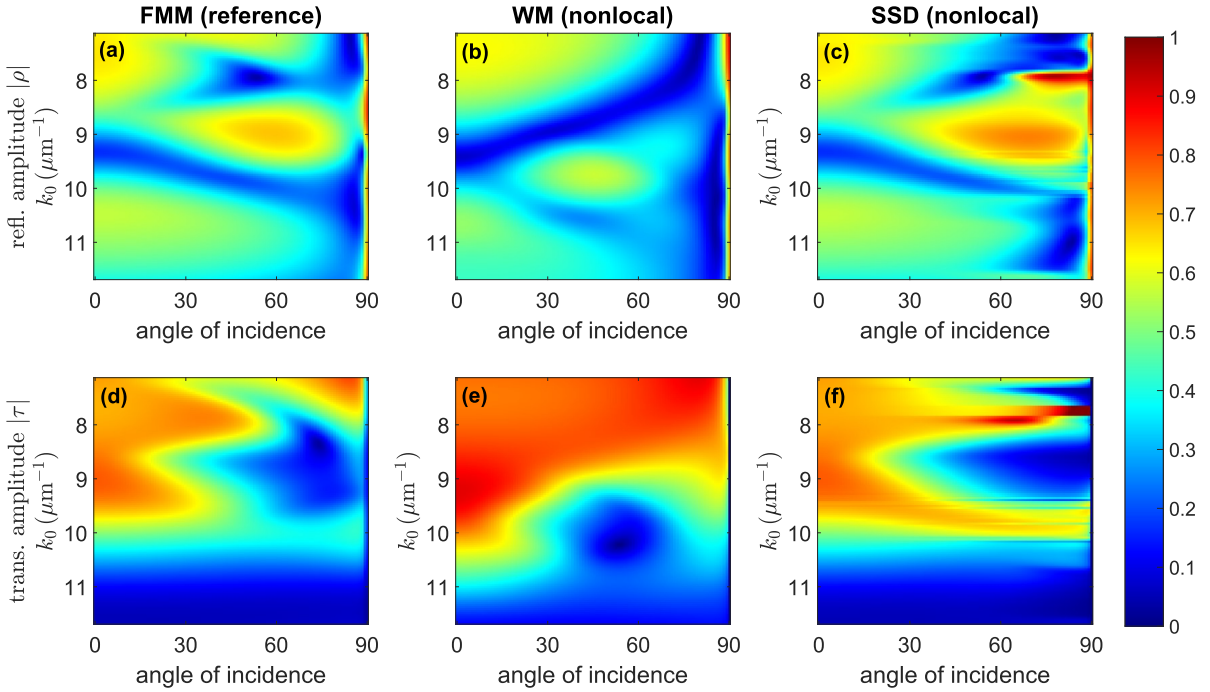

Figure 5.21: Amplitude of the reflected light $|\rho|$ and of the transmitted light $|\tau|$ from from the enlarged wire medium with thickness $d_{\mathrm{slab}} = 300\,\mathrm{nm}$ and lateral periodicity $\Lambda = 180\,\mathrm{nm}$ using different approaches.

fundamental mode approximation is assured. However, for the enlarged wire medium, where $\left(\Lambda^{(3)}/\lambda\right)$ is getting larger, $\Im(k_{z,0}^{\mathrm{FMM}})$ is only 5 times smaller than $\Im(k_{z,1}^{\mathrm{FMM}})$, hence, the breakdown of the fundamental mode approximation is expected. With this, we drive the system into a regime where we can legitimately anticipate that both theories should encounter difficulties in homogenizing the enlarged structure.

In order to compare the analytical and numerical results, we show the reflection and transmission coefficients spectra from the laterally enlarged wire medium slab, with the same thickness $d_{\mathrm{slab}} = 300\,\mathrm{nm}$ as in the original structure in Fig. 5.21. Again, the reference data **(a)** and **(d)** are obtained using the FMM data, the WM results **(b)** and **(e)** from the predictive Eqs. (4.82), and the SSD results **(c)** and **(f)** from the fitting procedure described in Sec. 5.1 using the reflection and transmission Eqs. (4.62). Obviously, the wire medium model starts to experience issues in predicting the optical coefficients, particularly when it comes to the transmission coefficients, for high frequencies and almost all angles of incidence, even in the paraxial regime. On the other hand, the SSD model is capable of adequately reproducing both reflection and transmission coefficients up to an angle of incidence of 30°. However, strong deviations from the reference are visible beyond that angle, which renders this model inapplicable as well in that regime. A more precise picture of this finding, and in particular the agreement of the SSD model with the reference at small angles of incidence, is illustrated in Fig. 5.22**(a)**, where we show the reflection and transmission coefficients at a selected frequency $k_0 = 10.25\,\mu\mathrm{m}^{-1}$. Here as well, and even more pronounced than previously seen in Fig. 5.16**(a)**, the mismatch between the analytically predicted and numerically calculated optical coefficients in the paraxial regime might be linked to the phenomenologically imposed additional interface condition for the WM model, which at normal incidence is equivalent to the tautology $0 = 0$. We recall that even at normal incidence spatial dispersion is still present, as the

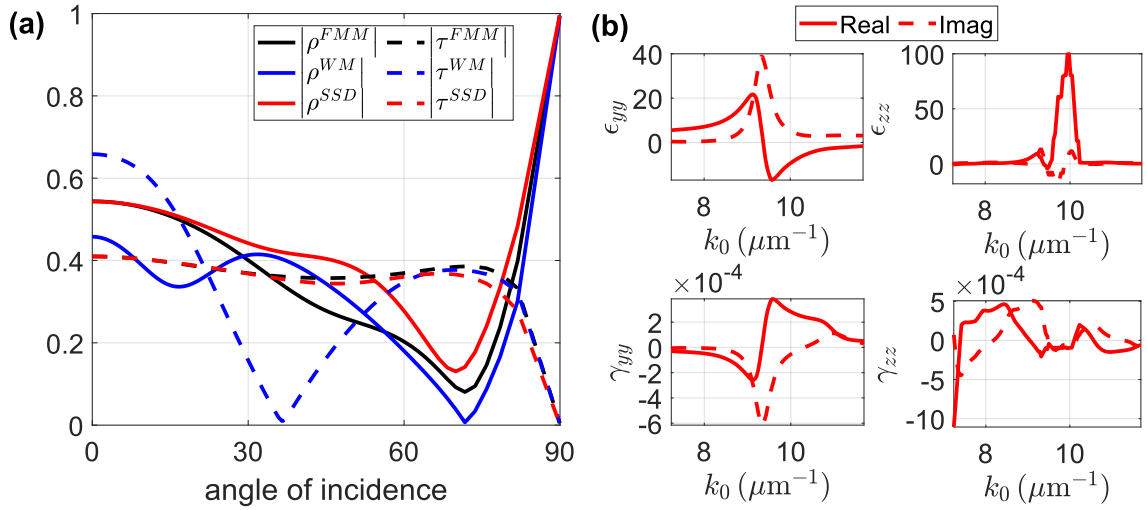

Figure 5.22: **(a)** Reflection and transmission amplitudes from the enlarged wire medium with period $\Lambda = 180\,\mathrm{nm}$ at a selected frequency $k_0 = 10.25\,\mu\mathrm{m}^{-1}$. The solid (dashed) curves represent the reflection (transmission) coefficients, while the black curves represent the reference simulations. The WM model (blue curves) completely misses the reference data, even at normal incidence, whereas the SSD model (red curves) manages to capture both optical frequencies at least to an angle of incidence of 30°. **(b)** Real (solid) and imaginary (dashed) parts of the retrieved effective material parameters of the SSD model as a function of the frequency k_0.

effective permittivity remains k_z-dependent (see Eq. (4.73)) and field is still a superposition of two plane waves with different wave vectors $\mathbf{k}_{\pm}^{\mathrm{WM}}$ (cf Eq. (4.77)). Ultimately, the effective material parameters of the SSD model for the enlarged wire medium are shown in Fig. 5.22**(b)**. The retrieved x-components show Lorentzians with a resonance frequency $k_0 = 9.5\,\mu\mathrm{m}^{-1}$, whereas the z-components become noisy and less coherent. We cannot extract a clean functional dependency, such as a Lorentzian or Drude curve. This might be linked to the fact that these parameters are less sensitive in the retrieval method, as discussed in Sec. 5.4.1.

One last remark concerning the resulting reflection and transmission coefficients from both models is in order. We would like to emphasize once more that the WM model predicts the optical coefficients within minutes, by only knowing the geometrical data, i.e., thickness, radius, and filling factor, and the material parameters, i.e., the permittivities of metal and host medium. On the contrary, the SSD model requires the passage through the S-parameter optimization approach, i.e., a fitting procedure that lasts hours to present the results shown in this section. In a nutshell, the WM model is straightforward, and fast, while the SSD model is slow and more precise. That being said, concerning homogenization in general, no effective medium model can be *a priori* trusted and a rigorous numerical simulation is frequently required to check the validity of the approaches. This was entirely considered in the thesis.

5.5 Chapter summary and discussion

To conclude, in this chapter we applied the homogenization models developed in Ch. 4 on centrosymmetric metamaterials of different kinds to retrieve their effective material

parameters. Due to the complicated expressions of the derived reflection and transmission coefficients in the nonlocal approach, the classical S-parameter retrieval method, based on direct inversion of these optical coefficients, is not applicable here. Therefore, we presented in Sec. 5.1 the parameter retrieval method, that we called the S-parameter optimization approach. It is based on a fitting procedure that takes oblique incidence into account. In order to get first hands on this method, we first studied an easy material, made from dielectric spheres arranged on a cubic lattice. Despite the isotropy of this material, a fitting at oblique incidence has been considered as well. At frequencies close to the first band gap, we have found that the nonlocal SSD model is able to capture the Brewster angle, whereas the local WSD model fails to do so.

The spotlight in this chapter was put on the fishnet metamaterial, a peculiarly interesting material with a negative index in the studied frequency range. From the analysis of the dispersion relations, we confirm the importance of a nonlocal description of that material. We studied two nonlocal approaches, namely the SYM model, that incorporates the second-order symmetry terms, the SSD model, the four-order approach, and of course the local WSD model for benchmarking. We find that the SSD model surpasses both WSD and SYM models in the studied frequency range. From the analysis of the bulk dispersion relations, we got first insights on the wave parameters such as the refractive index, but not on the individual material parameters. The actual full homogenization process requires the assignment of effective material parameters to a structure. This can only be done when reflection and transmission from a slab is considered. There, we studied the WSD and the SSD models side by side and have found that the WSD model predicts a causality- and passivity-breaking permittivity ϵ_{yy}. This unphyiscal behaviour was lifted with the introduction of nonlocality and is not present in the permittivity of the SSD model. Further, the SSD model adequately predicts the optical coefficients at higher angles of incidence, whereas the applicability of the WSD approach is limited to the paraxial regime. This is another indication that nonlocality should be considered for a meaningful homogenization.

While the retrieved parameters were roughly independent from the number of layers, and hence, from the thickness of the material, they, however, strongly depend on the sequence of the individual layers of the fishnet. We repeat in Sec. 5.4.1 the same simulations for the same structure, but with a dielectric spacer as a first layer, instead of air. For a single functional fishnet layer, the induced electric dipoles in the metallic layers (that are now far apart) do not couple and we find that the magnetic resonance vanishes. Hence, the material effectively behaves as a diluted metal. The magnetic resonance reappears again when at least two functional fishnet layers are stacked in the z-direction. There, the last metal layer of a unit cell strongly couples to the first metal layer of the next unit cell, as the distance between metals is again the thickness of the dielectric spacer of the original structure. Further, we find that some of the parameters are rather hard to interpret. As already discussed in Sec. 5.3.2, the z-component of the permittivity is hard to retrieve as at normal incidence the incident field does not couple at all to this component. Also, at higher angles of incidence the impact remains rather small. Therefore, the parameter can be retrieved but due to the rather small influence on the overall merit function the retrieval is not reliable. A weakly different dispersion of the material parameter might only cause a small change to the overall merit function $\delta(k_0)$. To emphasize on this aspect, which also applies to some of the nonlocal material parameters, we made a sensitivity analysis in Sec. 5.4.1 and discussed it. It clearly stresses that some parameters are hard to retrieve as the optical response from the slab geometry is rather insensitive against

these parameters. Therefore, we obtain a specific dispersion for the material parameters, but it makes the interpretation of the functional dependency complicated.

At last, we studied in Sec. 5.3.3 the wire medium model for which an analytical model already exists, namely the nonlocal wire medium (WM) model. In this study we provided numerical benchmarks for both theories and have shown that there is no unique effective medium description for metamaterials. We compare two substantially different nonlocal effective medium models and find that, if the fundamental mode approximation is verified, both WM and SSD models give fairly good outcomes in the effective picture compared to the full wave simulation of the reference. We obtained further findings from a second wire medium, where the unit cell is larger. There, the period-to-wavelength ratio gets closer to unity and the fundamental mode approximation breaks down. As a consequence, the WM model breaks down for all studied frequencies and angles of incidence, even at normal incidence, and fails to predict the optical coefficients from a slab. The SSD model, however, manages to capture this response up an angle of incidence of 30°. This finding is in favor for the SSD model, and was unexpected. We first anticipated that the WM model, that is specially conceived for wire media is rather the robust one while the SSD model would have shown inconsistencies. For that reason, we conclude that there is no assurance that an effective medium theory can predict the electromagnetic response of a metamaterial, unless and a rigorous numerical simulation is done to check the validity of the theory.

6 | Thesis summary and perspectives

In this thesis, we introduced a viable route to effectively describe homogenized metamaterials with the assumption of a nonlocal response. The effective properties shall allow us to reproduce in a best possible sense the full wave response from the actual metamaterial with all its fine details while considering the metamaterial at an effective level, i.e., as homogeneous. We showed the importance to go beyond the usually employed local constitutive equations and took nonlocality into account to adequately describe homogenized metamaterials on equal footing as natural materials. Of course, we are not the first to work in this direction, but the approach we have chosen is generally applicable and does not hinge on the assumption of a specific geometry for the centrosymmeric metamaterial. Our approach is based on a Taylor approximation of the nonlocal kernel in $\mathbf{k}$-space, that linearly links the displacement field to the electric field of light, while retaining terms up to the fourth order.

We showed that, contrary to local materials, for any given set of a specific frequency $k_0(\mathbf{k})$ and two chosen components of the wave vector $\mathbf{k}$, multiple plane waves exist as solutions with different propagation constants k_z. This is a consequence of the polynomial order of the wave equation in $\mathbf{k}$, i.e., dispersion relation that increases with an increasing truncation order of the Taylor approximation of the nonlocal kernel $\hat{\hat{\mathbf{R}}}(\mathbf{k}, k_0)$. Accordingly, the study of how light couples at the interface from one medium to another requires the derivation of additional interface conditions. The ordinary interface conditions are not enough to unambiguously fix all the amplitudes of the plane waves involved when considering reflection and transmission at an interface between an ordinary medium and the considered nonlocal metamaterial. With the collaboration of Dr. Andrii Khrabustovskyi, the interface conditions have been derived using the weak formulation of the wave equation. This required some concepts of functional analysis and distribution theory. These fields of mathematics are rather unfamiliar to the physics community, and the analysis here, required going deeper therein. Therefore, in Ch. 2 we gave the necessary mathematical background and elaborate on the basics of distribution theory and on the concept of the weak formulation, the tool with which the interface conditions were derived. The chapter is written in a mathematical style, but nevertheless, each topic is accompanied with a physical example for motivation.

In Ch. 3, we gave the theoretical background behind spatial dispersion in periodic metamaterials at optical frequencies. We discussed two possibilities causing nonlocal effects to appear. Either the material has strong multipolar resonances and is excited close to a resonance line and/or the mesoscopic feature of the structure are visible to the incoming electromagnetic wave. The latter case was discussed in terms of the critical parameter (a/λ), where a denotes a characteristic length of the metamaterial, e.g., a dimension of the unit cell. For a local homogenization approach, we discussed the weak spatial dispersion approximation (WSD) that is only valid if $(a/\lambda) \ll 1$. This became particularly clear in the study of an array of dielectric spheres on a cubic lattice for zero frequencies up to the first photonic band gap. Further, we discussed the origin of the artificial magnetic response of metamaterials at optical frequencies. Via a suitable gauge transformation, we identify such response as a second-order nonlocal response in the electric field. This is still captured by the WSD. However, in our numerical examples, it has been later shown in the thesis that the WSD turns to be insufficient when considering

light propagation inside the metamaterial in an arbitrary direction, or it only works in a parameter regime where the operational wavelength is much longer than the size of the unit cells. Unfortunately, the relevant dispersive effects are not observable in such long-wavelength regime. Therefore, to effectively capture the physics, material laws must be considered that go beyond the local response, i.e. they have to be nonlocal.

Nonlocality beyond the WSD approach was the main topic of Ch. 4. For the case of centrosymmetric metamaterials, we started from the WSD approach and extended it into two directions that incorporate nonlocal material laws, that only rely on the assumption of a specific symmetry class of the unit cell, namely centrosymmetry, but not on the detailed geometry. First, the symmetry model that retains all nonzero second-order symmetry terms for materials whose unit cell have a D_{2h} symmetry, e.g. the fishnet metamaterial, and second, the strong spatial dispersion model (SSD) that takes derivatives up to the fourth order into account. In the analysis of bulk dispersion relations, we showed that the obtained isofrequency contours give rise to more advanced curves that allow to homogenize metamaterials with dispersive features not captured by a local material law. Later, on the example of the fishnet, we find that both proposed nonlocal models indeed offered a more accurate description of the bulk properties of this metamaterial. Further, we find that both nonlocal models sustain an additional mode that requires an additional interface condition to be formulated in order to unambiguously determine the amplitude of that mode. The interface conditions are derived from first principles and were not phenomenologically introduced, as it was the case in the wire medium (WM) model [59]. The derivation of the interface conditions relies on the evaluation of a weak formulation of the wave equation in a small volume enclosing the interface. With the interface conditions at hand, we derived the corresponding Fresnel matrices for both slab and half-space problem. They are required to obtain the analytical expressions for the reflection and transmission coefficients, and to be able to compare them to those of a heterogeneous metamaterial.

The application of these homogenization models was essentially done in Ch. 5, where the effective parameters are determined from the S-parameters of the original structure. Due to the complexity of the analytical expressions of the optical coefficients, we extended the classical S-parameter retrieval method to an S-parameter optimization problem. We introduce this approach in Sec. 5.1. It is essentially a fitting procedure where we define a merit function and minimize it w.r.t. the effective material parameters and also include illuminations at oblique incidence. In the first two case studies, namely the array of dielectric spheres and the fishnet metamaterial, we demonstrated the importance of considering nonlocality by showing the improved matching between the reflection and transmission coefficients to those of a mesoscopic metamaterial by considering SSD instead of WSD. In addition, the permittivity ϵ_{yy} retrieved using WSD approach showed an anti-Lorentzian resonance, that drives its imaginary part to negative values. This is unphysical and breaks both causality and passivity, if considered as an isolated material parameter. Such features disappear when SSD is considered, which is a further indication that nonlocality should be considered in the effective description of metamaterials. We further compared two nonlocal models, the WM model and the SSD model for the homogenization of the wire medium. First, with an analytical analysis of the dispersion relations and interface conditions for both WM and SSD models, we confirm that the models are fundamentally different. It shall be emphasized that this discrepancy was not present in the bulk properties, i.e. dispersion relations, but it only emerges at the level of interface conditions. Further, we studied and showed the importance of the period-to-wavelength ratio in the

validity of the approaches, and more importantly, we concluded that homogenization is not unique. In a strict sense, the study implies that multiple models of homogenization can be applied to describe the optical response from a certain metamaterial.

With that being said, we have further shown in Sec. 5.4, on both fishnet structure and wire medium, that homogenization is not perfect yet and that the retrieval method still has its weaknesses. The retrieval method, for instance, could profit from further optimizations, to reliably capture the z-component of the permittivity. The sensitivity analysis in Sec. 5.4.1, clearly shows that this parameter is not properly considered into the fitting procedure, mainly due to the introduced weighting function that focuses in the paraxial regime. However, in the cause of the time we came to the conclusion that such weighting is essential to at least capture the reflection and transmission at normal incidence, with a reasonable amount of time. We did not show it here, but omitting the weight gave inconsistent results after an even longer minimization of the merit function. For instance, with the current numerical method, a uniform weighting leads to a long-lasting fitting that renders the parameter retrieval very slow. The trend nowadays is to improve such optimization problems with machine learning algorithms to speed up the parameter retrieval. A trained neural network would tremendously reduce the amount of time required for the fitting procedure. The network training itself, depending on the problem, may demand a lot of efforts. But in the retrieval case, the problem is quite simple so the network training doesn't end up very computationally expensive anyway. This is different from cases for inverse design for example, where networks have to produce a two-dimensional output of surface geometry from input spectra. Besides, if the trained network for the parameter retrieval is universal, then the trained the network is quite useful for large variety of cases. But this claim must be proven or verified in the first place.

Further, by virtue of the general formalism we've been developing here, other kinds of nonlocal constitutive relations can be explored. In Sec. 5.3, we particularly showed that going from a second order to a fourth order constitutive relation allows for a better prediction of the actual optical coefficients of heterogeneous metamaterials when compared to full wave reference simulations. This is encouraging and motivates further research with constitutive relations with an even higher truncation order. Taking even higher order terms into account, would definitely make the homogenization more accurate. Of course, more degrees of freedom would, again, require more time for the fitting procedure, but with the right optimization methods, this can be speed up as well. Nonetheless, rigorous numerical simulations are necessary to check the validity of the approach. Quite honestly, the absolute validity of a homogenization model can never be proven, as there will always be a point of insufficiency, i.e., an illumination scenario of some metamaterial from which the effective description predicts a different optical response than the full wave consideration of the actual structure does. An example of such subtle failure was demonstrated in Sec. 5.4.1, where the retrieved effective material parameters depend on the definition of the unit cell, even though, the bulk material remains unchanged.

Without demanding such absoluteness, the present work can be rationally extended to a more general class of metamaterials where a nonlocal description is an important and timely issue, namely the study of nonlocality in metamaterials without central symmetry. Lifting such restriction enables chirality and, perhaps, effects beyond. The state-of-the art model is the set of bi-anisotropic constitutive relations, see Eqs. (3.54-3.55), that form a general case of the WSD model for gyrotropic media. On the other hand, there is no reason to exclusively approximate the nonlocal kernel by a polynomial of $\mathbf{k}$, i.e., by a Taylor

approximation. Even though such approach can capture the dispersion relations quite well for an increasing interval of the transversal wave vector component, an approximation with a higher polynomial degree causes stronger divergences beyond the interval considered to determine the material parameters. An alternative route to relax or even circumvent such divergences which has at least better predictive strength with a smaller or at least the same number of degrees of freedom is the approximation of the nonlocal response kernel by a Padé-approximant. A Padé-approximant is a rational function of $\mathbf{k}$, where the Taylor-approximant is just a special case of. A relevant physical example of a Padé-approximant is the hydrodynamic model for describing nonlocality in wire media. We discussed this special case in Sec. 4.4.2, and in particular Eq. (4.73). We have shown in Sec. 5.4.2 that such model with polynomials of second degree in both numerator and denominator, remains insufficient and prompts further research. A consideration of a Padé-approximant with higher orders will definitely bring us closer to the reconstruction of the nonlocal response function for a certain metamaterial.

Besides the seek for different nonlocal response functions, further research in the context of metamaterials is immediately possible where the physics of such nonlocal metamaterials can be investigated. It starts by analyzing basic optical phenomena in the presence of metamaterials with strong nonlocal response. Just to give one example, after studying guided surface modes sustained at interfaces of nonlocal materials in our previously published work [127], it would be intellectually interesting to investigate the properties of guided modes propagating in structured wave guides of slab form. One may also study further potential applications that depend on such nonlocal metamaterials, that will eventually enter in future textbooks and lectures on optics. Finally, the development of suitable numerical tools to study light propagation in nonlocal metamaterials is of contemporary interest.

Acknowledgements

After all the presented work in this thesis, I want to express my gratitude to all people that supported me during my time as a PhD student. I learned a lot during these years, both in physics and mathematics.

First and foremost, I want to thank my wonderful wife Ouiem, for making this thesis only the second most important thing I made. Thank you for our amazing son Adam and the great support and motivation, especially during the time of writing this thesis! Thank you, Adam, for waiting for me whenever I came late home and for your cheerful smiles that shed light into my life. Having you midway during my Ph.D. was certainly not easy for me but you had made my life wonderful.

Of course, I want to thank my supervisor Prof. Dr. Carsten Rockstuhl for providing a great deal of encouragement and support throughout my time as a PhD student. You gave me the opportunity to work on the fascinating topic of metamaterials, even though I came from a very different field and had much to learn in the beginning. I know, the supervision was sometimes a hard job for you, but I thank you for your endurance with me during the last years. You taught me a lot in physics and beyond.

I would also like to thank my co-supervisor Prof. Dr. Michael Plum for his guidance throughout the mathematical topics and for the fruitful collaboration. Thank you for staying in the late evening giving me a private lesson in the spectral theory of self-adjoint operators and explaining the concept of tempered distributions. I really appreciate that I had the opportunity to work with you.

I am greatly indebted to both of you for making the years of my PhD studies inspiring and pleasurable, both on a physical and a mathematical level. When I was a young teenager, I faced a hard decision during choose between physics or mathematics. Now doing a PhD in theoretical physics with a decent mathematical content collaboration with the department of mathematics, is the best end of my academic studies I can imagine.

Further, I would like to thank my collaborators from the department of mathematics. First, I would like to thank Dr. Andrii Khrabustovskyi for his successful collaboration from the very beginning of my PhD. Without your mathematical rigor and without your expertise in functional analysis, this work would not exist the way it is now. I would like to thank Dr. Christian Stohrer for his support in numerical mathematics and for the optimization of my parameter retrieval method, which tremendously shortened my waiting times. I would further like to thank Dr. Fatima Z. Goffi for your collaboration which just started during my final stage. Also, many thanks for your kind support in answering my mathematical questions again and again. Thank you for proof-reading my mathematical Chapter 2. I also thank my colleagues at the CRC 1173 for the great discussions during the annual meetings and during the iRTG seminars.

I really liked the atmosphere in my working group. I would like to start thanking my prior office mate Dr. Aimi Abass for his help in answering many questions related to optics where I was a stranger in the beginning. I thank you for trying to push my Tekken skills to the limit. Also, for the honey you constantly ordered from your contact person whenever I ran out of stock. Such good stuff! Special thanks go to Dr. Radius Suryadharma for your support, both academically and personally. Thank you for your uncountable invitations and for the great menus we cooked together. It was a great time! Thank you, Andreas Vetter, for your support whenever I had a question concerning

fabrication methods and for your support during the revision of my second manuscript and especially for your simulation data using the KKR method. Further, I would like to thank Dr. Ivan Fernandez-Corbaton for your warnings concerning homogenization in general and for putting many things in question, that I took as granted. Thank you for making me aware of many things I was blind against. I would also like to thank Aristeidis Lamprianidis and Taavi Repän for carefully proof-reading a draft Chapter 3 and 4, respectively, and for making some helpful comments.

For the harmonious and friendly atmosphere, I want to thank all my other colleagues in the Photonics group. I also thank my KSOP mentor Dr. Guillaume Gomard for your advices and efficient mentoring and for never letting me down whenever I needed your support. Furthermore, I thank the Deutsche Forschungsgemeinschaft (DFG) for supporting me via CRC 1173 "Wave Phenomena" and the Karlsruhe School of Optics and Photonics (KSOP) for providing a comprehensive PhD Training program and covering all the tuition fees for the MBA fundamentals program.

Last but not least, I would like to thank my family for all their love and encouragement. For my parents, thank you so much for your confidence and invaluable support over all these years, and for giving me the opportunities and experiences that have made me who I am. Also, I thank my brother for his presence who raised me with a love of science. Grandma, thank you for your support during the last ten years of my life. You have been always taking care of me and making sure that nothing is missing. Finally, I thank the family of my wife who have also been generous with their love and encouragement despite the long distance between us. Thank you all!

Karim Mnasri
October 2019

A | General symmetry properties for centrosymmetric metamaterials

The general expression of the nonlocal response tensor $\hat{\mathbf{R}}$ up to second order is

$$D_i(\mathbf{r}, k_0) = \hat{R}_{ij}(\nabla, k_0) E_j(\mathbf{r}, k_0) := \epsilon_{ij} E_j(\mathbf{r}, k_0) + c_{ijlm} \nabla_l \nabla_m E_j \,. \tag{A.1}$$

According to Casimir-Onsager symmetry relations for reciprocal media (3.30), it must hold that $\hat{R}_{ij} = \hat{R}_{ji}$, which also implies

$$c_{ijkl} = c_{jikl} \,. \tag{A.2}$$

We further require that the electric field $\mathbf{E}$ is at least a $\mathcal{C}^2(\mathbb{R}^3)$-function. Consequently, according to the equality of mixed partials (Schwartz's theorem), the second-order derivatives can be interchanged which renders

$$c_{ijlm} \nabla_l \nabla_m E_j = c_{ijlm} \nabla_m \nabla_l E_j = c_{ijml} \nabla_l \nabla_m E_j \,.$$

In the first equality we put the fact that $\mathbf{E} \in \boldsymbol{\mathcal{C}}^2(\mathbb{R}^3)$ and in the second equation, we simply relabeled the indices. In fact, we have

$$c_{ijlm} = c_{jilm} = c_{ijml} = c_{jiml} \,. \tag{A.3}$$

These are the fundamental symmetry conditions for the fourth-rank tensor c_{ijlm}. This reduces the number of different components from 81 to only 36 [50].
If we consider a concrete crystal with specific symmetries, the number of independent components can be further reduced. In the monoclinic system, the unit-cell is described by vectors of unequal lengths. They form a rectangular unit-cell with a parallelogram as its base. Hence two vectors are perpendicular (meet at right angles), while the third vector meets the other two at an angle other than 90°. Here, 16 components of the tensor c_{ijlm} vanish, particularly, all components in which an index appears only once or exactly three times vanish, e.g., $c_{xyyy} = 0$ and $c_{xyzz} = 0$, etc.. Hence, only 20 independent components are non-vanishing [50].
The Fishnet metamaterial that we consider, and all other structures we previously study as well, are at least of D_{2h} symmetry (Orhtorhombic system) with three twofold (rotation by π) symmetry axes. Orthorhombic crystals result from stretching a cubic lattice along two of its orthogonal pairs by two different factors, resulting in a rectangular unit-cell with a rectangular base. All three bases intersect at 90° angles, so the three lattice vectors remain mutually orthogonal . It follows that only 12 components survive [50]. These are

$$c_{iiii} \qquad \text{for } i \in \{x, y, z\} \tag{A.4}$$

$$c_{iijj} \qquad \text{for } (i, j) \in \{x, y, z\} \times \{x, y, z\} \text{ and } i \neq j \,, \tag{A.5}$$

$$c_{ijij} \qquad \text{for } (i, j) \in \{x, y, z\} \times \{x, y, z\} \text{ and } i \neq j \,. \tag{A.6}$$

Remark A.0.1. *The components c_{iiii} were only considered in our first manuscript and correspond to the (usually neglected) symmetry-terms that we called β.*

In a crystal with cubic symmetry, the number of independent components decreases dramatically. Only 4 independent components remain which are

$$c_1 = c_{xxxx} = c_{yyyy} = c_{zzzz}\,, \qquad c_2 = c_{xxzz} = c_{yyxx} = c_{zzyy}\,, \tag{A.7}$$

$$c_3 = c_{xyxy} = c_{yzyz} = c_{zxzx}\,, \qquad c_4 = c_{zzxx} = c_{xxyy} = c_{yyzz}\,. \tag{A.8}$$

In an isotropic medium, the non-vanishing components are the same as for the cubic system with the further constraint that $c_2 = c_4$ and $c_3 = c_1 - c_2$. Altogether, we have two independent components only [50].

In the following, we shall study case by case the validity of Casimir-Onsager for three different positions of $\hat{\alpha}(k_0)$ in the second order expansion for $\mathbf{D}(\mathbf{r}, k_0)$. In other terms we analyze the three constitutive relations

$$\begin{aligned}
\mathbf{D}(\mathbf{r}, k_0) &= \hat{\epsilon}\mathbf{E}(\mathbf{r}, k_0) + \nabla \times \hat{\alpha}\nabla \times \mathbf{E}(\mathbf{r}, k_0)\,,\\
\mathbf{D}(\mathbf{r}, k_0) &= \hat{\epsilon}\mathbf{E}(\mathbf{r}, k_0) + \nabla \times \nabla \times \hat{\alpha}\mathbf{E}(\mathbf{r}, k_0)\,,\\
\mathbf{D}(\mathbf{r}, k_0) &= \hat{\epsilon}\mathbf{E}(\mathbf{r}, k_0) + \hat{\alpha}\nabla \times \nabla \times \mathbf{E}(\mathbf{r}, k_0)\,,
\end{aligned}$$

and show that only the first one satisfies Casimir-Onsager reciprocity. The other two are, therefore, unphysical.

A.1 Let $\mathbf{D}(\mathbf{r}, k_0) = \hat{\epsilon}\mathbf{E}(\mathbf{r}, k_0) + \nabla \times \hat{\alpha}\nabla \times \mathbf{E}(\mathbf{r}, k_0)$

This is the usual case that we always considered in the Taylor approach. This constitutive relation requires that

$$c_{ijlm}\nabla_l\nabla_m E_j \stackrel{!}{=} \left[\nabla \times (\hat{\alpha}\nabla \times \mathbf{E})\right]_i\,. \tag{A.9}$$

Then, it holds

$$\begin{pmatrix}
\alpha_{yy}\nabla_x\nabla_z E_z - \alpha_{yy}\nabla_z\nabla_z E_x + \alpha_{zz}\nabla_x\nabla_y E_y - \alpha_{zz}\nabla_y\nabla_y E_x\\
\alpha_{xx}\nabla_y\nabla_z E_z - \alpha_{xx}\nabla_z\nabla_z E_y + \alpha_{zz}\nabla_x\nabla_y E_x - \alpha_{zz}\nabla_x\nabla_x E_y\\
\alpha_{xx}\nabla_y\nabla_z E_x - \alpha_{xx}\nabla_y\nabla_y E_z + \alpha_{yy}\nabla_x\nabla_z E_x - \alpha_{yy}\nabla_x\nabla_x E_z
\end{pmatrix}\,, \tag{A.10}$$

where it has been assumed that $\hat{\alpha}$ is a diagonal matrix. Comparing the coefficients yields

$$\begin{pmatrix}
c_{xzxz} = \alpha_{yy}\,, & c_{xxzz} = -\alpha_{yy}\,, & c_{xyxy} = \alpha_{zz}\,, & c_{xxyy} = -\alpha_{zz}\\
c_{yzyz} = \alpha_{xx}\,, & c_{yyzz} = -\alpha_{xx}\,, & c_{yxyx} = \alpha_{zz}\,, & c_{xxyy} = -\alpha_{zz}\\
c_{zyzy} = \alpha_{xx}\,, & c_{zzyy} = -\alpha_{xx}\,, & c_{zxzx} = \alpha_{yy}\,, & c_{zzxx} = -\alpha_{yy}
\end{pmatrix}$$

The coefficients in the same color are related to the same material parameter α_{ii}. From the comparison, we note that the assumption in Eq. (A.9) is compatible with the fundamental symmetry constraints in Eq. (A.3). For example we systematically obtain terms such as $c_{xyxy} = c_{yxyx} = \alpha_{zz}$ or $c_{yzyz} = c_{zyzy} = \alpha_{xx}$. We also note that there are constraints that impose $c_{iijj} = c_{jjii}$ for all $(i, j) \in \{x, y, z\} \times \{x, y, z\}$ and $i \neq j$, which are not part of the fundamental symmetry constraints. For instance, we have $c_{xxzz} = c_{zzxx} = -\alpha_{yy}$. Furthermore the fact that such terms differ by a minus sign as well, i.e., $c_{ijij} = -c_{iijj}$ for all $(i, j) \in \{x, y, z\} \times \{x, y, z\}$ and $i \neq j$ suggests that the assumption in Eq. (A.9) is of higher symmetry than simply spatial inversion symmetry. The first constraints, i.e., $c_{iijj} = c_{jjii}$ for all $(i, j) \in \{x, y, z\} \times \{x, y, z\}$ and $i \neq j$ renders the crystal of a tetragonal system, i.e., of fourfold symmetry. They define the symmetry classes C_4 and D_{4h}.

Remark A.1.1. *The fishnet metamaterial is of* D_{2h} *symmetry (only), while we assume Eq.* (A.9) *to hold. We technically try to describe a system with lower symmetry* (D_{2h}) *with coefficients of higher symmetry* (D_{4h}).

Remark A.1.2. *The second constraint* $c_{ijij} = -c_{iijj}$ *for all* $(i, j) \in \{x, y, z\} \times \{x, y, z\}$ *and* $i \neq j$*, is not linked to a symmetry.*

A.2 Let $\mathbf{D}(\mathbf{r}, k_0) = \hat{\epsilon}\mathbf{E}(\mathbf{r}, k_0) + \nabla \times \nabla \times \hat{\alpha}\mathbf{E}(\mathbf{r}, k_0)$

In this case we enforce the coefficients to obey

$$c_{ijlm}\nabla_l\nabla_m E_j \stackrel{!}{=} [\nabla \times \nabla \times (\hat{\alpha}\mathbf{E})]_i \ . \tag{A.11}$$

Then, it holds

$$\begin{pmatrix} -\alpha_{xx}\nabla_y\nabla_y E_x - \alpha_{xx}\nabla_z\nabla_z E_x + \alpha_{yy}\nabla_x\nabla_y E_y + \alpha_{zz}\nabla_x\nabla_z E_z \\ -\alpha_{yy}\nabla_x\nabla_x E_y - \alpha_{yy}\nabla_z\nabla_z E_y + \alpha_{xx}\nabla_x\nabla_y E_x + \alpha_{zz}\nabla_y\nabla_z E_z \\ -\alpha_{zz}\nabla_y\nabla_y E_z - \alpha_{zz}\nabla_x\nabla_x E_z + \alpha_{xx}\nabla_x\nabla_z E_x + \alpha_{yy}\nabla_y\nabla_z E_y \end{pmatrix} , \tag{A.12}$$

Comparing the coefficients yields

$$\begin{pmatrix} c_{xxyy} = -\alpha_{xx} \ , & c_{xxzz} = -\alpha_{xx} \ , & c_{xyxy} = \alpha_{yy} \ , & c_{xzxz} = \alpha_{zz} \\ c_{yyxx} = -\alpha_{yy} \ , & c_{yyzz} = -\alpha_{yy} \ , & c_{yxyx} = \alpha_{xx} \ , & c_{yzyz} = -\alpha_{zz} \\ c_{zzyy} = -\alpha_{zz} \ , & c_{zzxx} = -\alpha_{zz} \ , & c_{zxzx} = \alpha_{xx} \ , & c_{zyzy} = \alpha_{yy} \end{pmatrix}$$

From this comparison, we read out that the assumption in Eq. (A.11) yields that simultaneously $c_{xyxy} = \alpha_{yy}$ and $c_{yxyx} = \alpha_{xx}$ hold. Following the fundamental symmetry constraints (A.3), it must hold that

$$c_{xyxy} = c_{yxyx} \Rightarrow \alpha_{yy} = \alpha_{xx}$$

Furthermore, we have $c_{yzyz} = \alpha_{zz}$ and $c_{zyzy} = \alpha_{yy}$ that results in $\alpha_{zz} = \alpha_{yy}$. Finally, it must hold that

$$\alpha_{xx} = \alpha_{yy} = \alpha_{zz} \ .$$

Consequently, the system has to be isotropic, otherwise physical symmetries are violated. In this case, the position of $\hat{\alpha}$ among the curl operators is irrelevant and can be placed in another position. Hence, this case is essentially trivial.

A.3 Let $\mathbf{D}(\mathbf{r}, k_0) = \hat{\epsilon}\mathbf{E}(\mathbf{r}, k_0) + \hat{\alpha}\nabla \times \nabla \times \mathbf{E}(\mathbf{r}, k_0)$

Here, $\hat{\alpha}$ is positioned on the left. This supposition imposes that

$$c_{ijlm}\nabla_l\nabla_m E_j \stackrel{!}{=} (\hat{\alpha}\nabla \times \nabla \times \mathbf{E})_i \ . \tag{A.13}$$

Then, it holds

$$\begin{pmatrix} \alpha_{xx}\nabla_x\nabla_y E_y - \alpha_{xx}\nabla_y\nabla_y E_x + \alpha_{xx}\nabla_x\nabla_z E_z - \alpha_{xx}\nabla_z\nabla_z E_x \\ \alpha_{yy}\nabla_x\nabla_y E_x - \alpha_{yy}\nabla_x\nabla_x E_y + \alpha_{yy}\nabla_y\nabla_z E_z - \alpha_{yy}\nabla_z\nabla_z E_y \\ \alpha_{zz}\nabla_x\nabla_z E_x - \alpha_{zz}\nabla_x\nabla_x E_z + \alpha_{zz}\nabla_y\nabla_z E_y - \alpha_{zz}\nabla_y\nabla_y E_z \end{pmatrix} , \tag{A.14}$$

Comparing the coefficients yields

$$\begin{pmatrix} c_{xyxy} = \alpha_{xx}\,, & c_{xxyy} = -\alpha_{xx}\,, & c_{xzxz} = \alpha_{xx}\,, & c_{xxzz} = -\alpha_{xx} \\ c_{yxyx} = \alpha_{yy}\,, & c_{yyxx} = -\alpha_{yy}\,, & c_{yzyz} = \alpha_{yy}\,, & c_{yyzz} = -\alpha_{yy} \\ c_{zxzx} = \alpha_{zz}\,, & c_{zzyy} = -\alpha_{zz}\,, & c_{zyzy} = \alpha_{zz}\,, & c_{zzyy} = -\alpha_{zz} \end{pmatrix}$$

From this comparison, we read out that the assumption in Eq. (A.13) yields that $c_{xyxy} = \alpha_{xx}$, $c_{yxyx} = \alpha_{yy}$ and $c_{xzxz} = \alpha_{xx}$, $c_{zyzy} = \alpha_{zz}$ hold simultaneously. Following the fundamental symmetry constraints (A.3), it must hold that

$$\alpha_{xx} = \alpha_{yy} = \alpha_{zz}\,.$$

Finally, the system has to be isotropic as well. In this case, the position of $\hat{\alpha}$ among the curl operators is irrelevant and can be placed in another position. Hence, this case is essentially trivial as well.

Bibliography

[1] E. Shamonina and L. Solymar, "Metamaterials: How the subject started," *Metamaterials*, vol. 1, no. 1, pp. 12–18, 2007. DOI: 10.1016/j.metmat.2007.02.001.

[2] N. Engheta, "Ideas for potential applications of metamaterials with negative permittivity and permeability," in *Advances in Electromagnetics of Complex Media and Metamaterials*, Springer, Dordrecht, 2002, pp. 19–37. DOI: 10.1007/978-94-007-1067-2_2.

[3] T. J. Cui, D. Smith, and R. Liu, *Metamaterials - Theory, Design, and Applications*, 2010th ed. Berlin Heidelberg: Springer Science & Business Media, 2009. DOI: 10.1007/978-1-4419-0573-4.

[4] J. B. Pendry, "Negative refraction makes a perfect lens," *Physical Review Letters*, 2000. DOI: 10.1103/PhysRevLett.85.3966.

[5] S. Guenneau and S. A. Ramakrishna, "Negative refractive index, perfect lenses and checkerboards: Trapping and imaging effects in folded optical spaces," *Comptes Rendus Physique*, vol. 10, no. 5, pp. 352–378, 2009. DOI: 10.1016/j.crhy.2009.04.002.

[6] G. Rosenblatt and M. Orenstein, "Perfect lensing by a single interface: Defying loss and bandwidth limitations of metamaterials," *Physical Review Letters*, vol. 115, no. 19, p. 195 504, 2015. DOI: 10.1103/PhysRevLett.115.195504.

[7] M. G. Silveirinha, A. Alù, and N. Engheta, "Infrared and optical invisibility cloak with plasmonic implants based on scattering cancellation," *Physical Review B*, vol. 78, no. 7, p. 075 107, 2008. DOI: 10.1103/PhysRevB.78.075107.

[8] N. Landy and D. R. Smith, "A full-parameter unidirectional metamaterial cloak for microwaves," *Nature materials*, vol. 12, no. 1, p. 25, 2013. DOI: 10.1038/nmat3476.

[9] R. Fleury, F. Monticone, and A. Alù, "Invisibility and cloaking: Origins, present, and future perspectives," *Physical Review Applied*, vol. 4, no. 3, p. 037 001, 2015. DOI: 10.1103/PhysRevApplied.4.037001.

[10] J. Zhang, P. A. R. Ade, P. Mauskopf, *et al.*, "New artificial dielectric metamaterial and its application as a terahertz antireflection coating," *Applied Optics*, vol. 48, no. 35, pp. 6635–6642, 2009. DOI: 10.1364/AO.48.006635.

[11] P. Spinelli, M. Verschuuren, and A. Polman, "Broadband omnidirectional antireflection coating based on subwavelength surface mie resonators," *Nature communications*, vol. 3, p. 692, 2012. DOI: 10.1038/ncomms1691.

[12] S. Fahr, C. Rockstuhl, and F. Lederer, "Negative refractive index materials for improved solar cells," *Physical Review B*, vol. 88, no. 11, p. 115 403, 2013. DOI: 10.1103/PhysRevB.88.115403.

[13] E. E. Narimanov and A. V. Kildishev, "Optical black hole: Broadband omnidirectional light absorber," *Applied Physics Letters*, vol. 95, no. 4, p. 041 106, 2009. DOI: 10.1063/1.3184594.

[14] N. Mohammadi Estakhri, B. Edwards, and N. Engheta, "Inverse-designed metastructures that solve equations," *Science*, vol. 363, no. 6433, pp. 1333–1338, 2019. DOI: 10.1126/science.aaw2498.

[15] C. Rockstuhl and T. Scharf, *Amorphous Nanophotonics*. Wiesbaden: Springer Berlin Heidelberg, 2013. DOI: /10.1007/978-3-642-32475-8.

[16] S. Hrabar, I. Krois, I. Bonic, *et al.*, "Ultra-broadband simultaneous superluminal phase and group velocities in non-foster epsilon-near-zero metamaterial," *Applied Physics Letters*, vol. 102, no. 5, p. 054 108, 2013. DOI: 10.1063/1.4790297.

[17] V. G. Veselago, "The electrodynamics of substances with simultaneously negative values of epsilon and mu," *Soviet Physics Uspekhi*, vol. 10, no. 4, pp. 509–514, 1968. DOI: 10.1070/pu1968v010n04abeh003699.

[18] D. R. Smith, W. J. Padilla, D. C. Vier, *et al.*, "Composite medium with simultaneously negative permeability and permittivity," *Physical Review Letters*, vol. 84, no. 18, pp. 4184–4187, 2000. DOI: 10.1103/PhysRevLett.84.4184.

[19] J. B. Pendry, A. J. Holden, D. J. Robbins, *et al.*, "Magnetism from conductors and enhanced nonlinear phenomena," *IEEE Transactions on Microwave Theory and Techniques*, vol. 47, no. 11, pp. 2075–2084, 1999. DOI: 10.1109/22.798002.

[20] A. Boltasseva and V. M. Shalaev, "Fabrication of optical negative-index metamaterials: Recent advances and outlook," *Metamaterials*, vol. 2, no. 1, pp. 1–17, 2008. DOI: https://doi.org/10.1016/j.metmat.2008.03.004.

[21] C. M. Soukoulis and M. Wegener, "Past achievements and future challenges in the development of three-dimensional photonic metamaterials," *Nature Photonics*, vol. 5, no. 9, p. 523, 2011. DOI: 10.1038/nphoton.2011.154.

[22] S. Mühlig, A. Cunningham, S. Scheeler, *et al.*, "Self-assembled plasmonic core–shell clusters with an isotropic magnetic dipole response in the visible range," *American Chemical Society Nano*, vol. 5, no. 8, pp. 6586–6592, 2011. DOI: 10.1021/nn201969h.

[23] M. Fruhnert, S. Mühlig, F. Lederer, *et al.*, "Towards negative index self-assembled metamaterials," *Physical Review B*, vol. 89, no. 7, p. 075 408, 2014. DOI: 10.1103/PhysRevB.89.075408.

[24] M. Kafesaki, I. Tsiapa, N. Katsarakis, *et al.*, "Left-handed metamaterials: The fishnet structure and its variations," *Physical Review B*, vol. 75, no. 23, p. 235 114, 2007. DOI: 10.1103/PhysRevB.75.235114.

[25] C. R. Simovski, P. A. Belov, A. V. Atrashchenko, *et al.*, "Wire metamaterials: Physics and applications," *Advanced Materials*, vol. 24, no. 31, pp. 4229–4248, 2012. DOI: 10.1002/adma.201200931.

[26] R. J. Pollard, A. Murphy, W. R. Hendren, *et al.*, "Optical nonlocalities and additional waves in epsilon-near-zero metamaterials," *Physical Review Letters*, vol. 102, no. 12, p. 127 405, 2009. DOI: 10.1103/PhysRevLett.102.127405.

[27] K. Sakoda, *Optical properties of photonic crystals*. Berlin: Springer Science & Business Media, 2004, vol. 80. DOI: 10.1007/b138376.

[28] M. Kadic, G. W. Milton, M. van Hecke, *et al.*, "3D metamaterials," *Nature Reviews Physics*, vol. 1, pp. 198–210, 2019. DOI: 10.1038/s42254-018-0018-y.

[29] L. Lifeng, "New formulation of the fourier modal method for crossed surface-relief gratings," *Journal of the Optical Society of America A*, vol. 14, no. 10, pp. 2758–2767, 1997. DOI: 10.1364/JOSAA.14.002758.

[30] J.-M. Jin, *The finite element method in electromagnetics*. New york: John Wiley & Sons, 2015.

[31] A. Taflove and S. C. Hagness, *Computational electrodynamics: the finite-difference time-domain method*. Artech house, 2005. DOI: 10.1016/B978-012170960-0/50046-3.

[32] A. Andryieuski, A. V. Lavrinenko, and S. V. Zhukovsky, "Anomalous effective medium approximation breakdown in deeply subwavelength all-dielectric photonic multilayers," *Nanotechnology*, vol. 26, no. 18, p. 184 001, 2015. DOI: 10.1088/0957-4484/26/18/184001.

[33] V. A. Markel, "Introduction to the maxwell garnett approximation: Tutorial," *Journal of the Optical Society of America A*, vol. 33, no. 7, pp. 1244–1256, 2016. DOI: 10.1364/JOSAA.33.001244.

[34] A. Sihvola, "Homogenization principles and effect of mixing on dielectric behavior," *Photonics and Nanostructures - Fundamentals and Applications*, vol. 11, no. 4, pp. 364–373, 2013. DOI: https://doi.org/10.1016/j.photonics.2013.01.004.

[35] D. R. Smith and J. B. Pendry, "Homogenization of metamaterials by field averaging (invited paper)," *Journal of the Optical Society of America B*, vol. 23, no. 3, pp. 391–403, 2006. DOI: 10.1364/JOSAB.23.000391.

[36] A. Andryieuski, S. Ha, A. A. Sukhorukov, *et al.*, "Bloch-mode analysis for retrieving effective parameters of metamaterials," *Physical Review B*, vol. 86, no. 3, p. 035 127, 2012. DOI: 10.1103/PhysRevB.86.035127.

[37] M. G. Silveirinha, "Metamaterial homogenization approach with application to the characterization of microstructured composites with negative parameters," *Physical Review B*, vol. 75, no. 11, p. 115 104, 2007. DOI: 10.1103/PhysRevB.75.115104.

[38] D. R. Smith, D. C. Vier, T. Koschny, *et al.*, "Electromagnetic parameter retrieval from inhomogeneous metamaterials," *Physical Review E*, vol. 71, no. 3, p. 036 617, 2005. DOI: 10.1103/PhysRevE.71.036617.

[39] V. A. Markel and J. C. Schotland, "Homogenization of maxwell's equations in periodic composites: Boundary effects and dispersion relations," *Physical Review E*, vol. 85, no. 6, p. 066 603, 2012. DOI: 10.1103/PhysRevE.85.066603.

[40] G. Papanicolau, A. Bensoussan, and J.-L. Lions, *Asymptotic analysis for periodic structures*. Amsterdam: Elsevier, 1978, vol. 5. DOI: 10.1090/chel/374.

[41] G. Milton and A. Sawicki, "Theory of composites. cambridge monographs on applied and computational mathematics," *Applied Mechanics Reviews*, vol. 56, no. 2, B27–B28, 2003. DOI: 10.1115/1.1553445.

[42] O. Ouchetto, C. Qiu, S. Zouhdi, *et al.*, "Homogenization of 3-d periodic bianisotropic metamaterials," *IEEE Transactions on Microwave Theory and Techniques*, vol. 54, no. 11, pp. 3893–3898, 2006. DOI: 10.1109/TMTT.2006.885082.

[43] D. Cioranescu and J. S. J. Paulin, *Homogenization of Reticulated Structures*. Berlin Heidelberg: Springer Science & Business Media, 2012. DOI: 10.1007/978-1-4612-2158-6.

[44] G. Bouchitte and B. Schweizer, "Homogenization of maxwell's equations in a split ring geometry," *Multiscale Modeling and Simulation*, vol. 8, no. 3, pp. 717–750, 2010. DOI: 10.1137/09074557X.

[45] J. Zhou, T. Koschny, M. Kafesaki, *et al.*, "Saturation of the magnetic response of split-ring resonators at optical frequencies," *Physical Review Letters*, vol. 95, no. 22, p. 223 902, 2005. DOI: 10.1103/PhysRevLett.95.223902.

[46] D. A. Kirzhnitz, L. V. Keldysh, and A. A. Maradudin, *The Dielectric Function of Condensed Systems*. Amsterdam: Elsevier, 2012.

[47] A. A. Rukhadze and V. P. Silin, "Electrodynamics of media with spatial dispersion," *Soviet Physics Uspekhi*, vol. 4, no. 3, pp. 459–484, 1961. DOI: 10.1070/pu1961v004n03abeh003357.

[48] A. B. Pippard and W. L. Bragg, "The surface impedance of superconductors and normal metals at high frequencies ii. the anomalous skin effect in normal metals," *Proceedings of the Royal Society of London Series A Mathematical and Physical Sciences*, vol. 191, no. 1026, pp. 385–399, 1947. DOI: 10.1098/rspa.1947.0122.

[49] R. G. Chambers and O. R. Frisch, "The anomalous skin effect," *Proceedings of the Royal Society of London. Series A. Mathematical and Physical Sciences*, vol. 215, no. 1123, pp. 481–497, 1952. DOI: 10.1098/rspa.1952.0226.

[50] V. M. Agranovich and V. Ginzburg, *Crystal optics with spatial dispersion, and excitons*. Berlin: Springer Science & Business Media, 2013, vol. 42. DOI: 10.1007/978-3-662-02406-5.

[51] C. Simovski, *Composite Media with Weak Spatial Dispersion*. New York: Jenny Stanford Publishing, 2018. DOI: 10.1201/9781351166249.

[52] J. Kaschke and M. Wegener, "Gold triple-helix mid-infrared metamaterial by sted-inspired laser lithography," *Optics Letters*, vol. 40, no. 17, pp. 3986–3989, 2015. DOI: 10.1364/OL.40.003986.

[53] C. Menzel, T. Paul, C. Rockstuhl, *et al.*, "Validity of effective material parameters for optical fishnet metamaterials," *Physical Review B*, vol. 81, no. 3, p. 035 320, 2010. DOI: 10.1103/PhysRevB.81.035320.

[54] I. Tsukerman and V. A. Markel, "A non-asymptotic homogenization theory for periodic electromagnetic structures," *Proceedings of the Royal Society A: Mathematical, Physical and Engineering Sciences*, vol. 470, no. 2168, p. 20 140 245, 2014. DOI: 10.1098/rspa.2014.0245.

[55] R. V. Craster, J. Kaplunov, and A. V. Pichugin, "High-frequency homogenization for periodic media," *Proceedings of the Royal Society A: Mathematical, Physical and Engineering Sciences*, vol. 466, no. 2120, pp. 2341–2362, 2010. DOI: 10.1098/rspa.2009.0612.

[56] D. Harutyunyan, G. W. Milton, and R. V. Craster, "High-frequency homogenization for travelling waves in periodic media," *Proceedings of the Royal Society A: Mathematical, Physical and Engineering Sciences*, vol. 472, no. 2191, p. 20 160 066, 2016. DOI: 10.1098/rspa.2016.0066.

[57] P. A. Belov, R. Marqués, S. I. Maslovski, *et al.*, "Strong spatial dispersion in wire media in the very large wavelength limit," *Physical Review B*, vol. 67, no. 11, p. 113 103, 2003. DOI: 10.1103/PhysRevB.67.113103.

[58] M. G. Silveirinha, "Nonlocal homogenization model for a periodic array of -negative rods," *Physical Review E*, vol. 73, no. 4, p. 046 612, 2006. DOI: 10.1103/PhysRevE.73.046612.

[59] M. G. Silveirinha, "Additional boundary condition for the wire medium," *IEEE Transactions on Antennas and Propagation*, vol. 54, no. 6, pp. 1766–1780, 2006. DOI: 10.1109/TAP.2006.875920.

[60] B. M. Wells, A. V. Zayats, and V. A. Podolskiy, "Nonlocal optics of plasmonic nanowire metamaterials," *Physical Review B*, vol. 89, no. 3, p. 035 111, 2014. DOI: 10.1103/PhysRevB.89.035111.

[61] T. Geng, S. Zhuang, J. Gao, *et al.*, "Nonlocal effective medium approximation for metallic nanorod metamaterials," *Physical Review B*, vol. 91, no. 24, p. 245 128, 2015. DOI: 10.1103/PhysRevB.91.245128.

[62] P. Y. Yu and M. Cardona, "Spatial dispersion in the dielectric constant of gaas," *Solid State Comm.*, vol. 9, no. 16, pp. 1421–1424, 1971. DOI: 10.1016/0038-1098(71)90409-1.

[63] G. H. Cocoletzi and W. L. Mochán, "Spatial dispersion effects on the optical properties of an insulator–excitonic-semiconductor superlattice," *Physical Review B*, vol. 39, no. 12, pp. 8403–8408, 1989. DOI: 10.1103/PhysRevB.39.8403.

[64] A. Khrabustovskyi, K. Mnasri, M. Plum, *et al.*, "Interface conditions for a metamaterial with strong spatial dispersion," *arXiv:1710.03676*, 2017.

[65] H. Bremermann, *Distributions, Complex Variables, and Fourier Transforms*. Berkeley/California: Addison-Wesley Publishing Company, inc., 1965.

[66] E. J. Beltrami and M. R. Wohlers, *Distributions and the Boundary Values of Analytic Functions*. New York and London: Academic Press, 1966. DOI: 10.1016/C2013-0-12415-4.

[67] M. Struwe, *Variational Methods Applications to Nonlinear Partial Differential Equations and Hamiltonian Systems*. Berlin: Springer Science & Business Media, 2008. DOI: 10.1007/978-3-540-74013-1.

[68] L. Hörmander, *Linear Partial Differential Operators*. Wiesbaden: Springer Berlin Heidelberg, 2012. DOI: 10.1007/978-3-642-46175-0.

[69] S. Soboleff, "Sur un théorème d'analyse fonctionnelle," *Matematicheskii Sbornik*, vol. 46, no. 3, pp. 471–497, 1938.

[70] F. G. Friedlander and M. S. Joshi, *Introduction to the theory of distributions*, 2. ed. Cambridge: Cambridge Univ. Press, 1998.

[71] H. Brezis, *Functional Analysis, Sobolev Spaces and Partial Differential Equations*, 2011th ed. Berlin Heidelberg: Springer Science & Business Media, 2010. DOI: 10.1007/978-0-387-70914-7.

[72] F. Z. Goffi, "Approximation de l'impédance d'une multicouche mince contrastée pour le système de maxwell harmonique," PhD thesis, Université des Sciences et de la Technologie Houari Boumédiène, 2017.

[73] P. Monk *et al.*, *Finite element methods for Maxwell's equations*. Oxford: Oxford University Press, 2003. DOI: 10.1093/acprof:oso/9780198508885.001.0001.

[74] A. V. A. Alonso, "Unique solvability for high-frequency heterogeneous time-harmonic maxwell equations via the fredholm alternative theory," *Mathematical Methods in the Applied Sciences*, vol. 21, no. 6, pp. 463–477, 1998. DOI: 10.1002/(SICI)1099-1476(199804)21:6<463::AID-MMA947>3.0.CO;2-U.

[75] M. L. C. Hazard, "On the solution of time-harmonic scattering problems for maxwell's equations," *SIAM Journal on Mathematical Analysis*, vol. 27, no. 6, pp. 1597–1630, 1996. DOI: 10.1137/S0036141094271259.

[76] E. M. Stein and G. Weiss, *Introduction to Fourier Analysis on Euclidean Spaces*. Kassel: Princeton University Press, 1971.

[77] L. Hörmander, *The Analysis of Linear Partial Differential Operators I - Distribution Theory and Fourier Analysis*. Berlin: Springer Berlin Heidelberg, 2015. DOI: 10.1007/978-3-642-61497-2.

[78] V. I. Bogachev, *Measure Theory*. Berlin Heidelberg: Springer Science & Business Media, 2007. DOI: 10.1007/978-3-540-34514-5.

[79] R. E. Raab, O. L. De Lange, and O. L. de Lange, *Multipole theory in electromagnetism: classical, quantum, and symmetry aspects, with applications*. Oxford University Press on Demand, 2005, vol. 128. DOI: 10.1093/acprof:oso/9780198567271.001.0001.

[80] H. Römer, *Theoretical optics*. Weinheim: Wiley Online Library, 2005. DOI: 10.1002/3527604294.

[81] J. D. Jackson, "Classical electrodynamics, 3rd ed.," *American Journal of Physics*, vol. 67, no. 9, pp. 841–842, 1999. DOI: 10.1119/1.19136.

[82] C. Menzel, "Characterisation of optical metamaterials: Effective parameters and beyond," PhD thesis, 2012. [Online]. Available: www.db-thueringen.de/receive/dbt_mods_00019598.

[83] O. Kidwai, S. V. Zhukovsky, and J. E. Sipe, "Dipole radiation near hyperbolic metamaterials: Applicability of effective-medium approximation," *Optics Letters*, vol. 36, no. 13, pp. 2530–2532, 2011. DOI: 10.1364/OL.36.002530.

[84] B. E. B. Graham and R. E. Raab, "Non-reciprocal optical rotation in cubic antiferrornagnets," *Philosophical Magazine B*, vol. 64, no. 3, pp. 267–274, 1991. DOI: 10.1080/13642819108207619.

[85] L. Landau and E. Lifshitz, "Chapter V - Fferromagnetism and antiferromagnetism," in *Electrodynamics of Continuous Media (Second Edition)*, vol. 8, Amsterdam: Pergamon, 1984, pp. 130–179. DOI: 10.1016/B978-0-08-030275-1.50011-4.

[86] L. Landau and E. Lifshitz, "Chapter IX - The electromagnetic Wave Equations," in *Electrodynamics of Continuous Media (Second Edition)*, vol. 8, Amsterdam: Pergamon, 1984, pp. 257–289. DOI: 10.1016/B978-0-08-030275-1.50015-1.

[87] B. Bokut and A. Serdyukov, "On the phenomenological theory of natural optical activity," *Sov. Phys. JETP*, vol. 34, no. 5, pp. 962–964, 1972. [Online]. Available: www.jetp.ac.ru/cgi-bin/e/index/e/34/5/p962?a=list.

[88] A. P. Vinogradov, "On the form of constitutive equations in electrodynamics," *Physics Uspekhi*, vol. 45, no. 3, pp. 331–338, 2002. DOI: 10.1070/pu2002v045n03abeh001079.

[89] L. Landau and E. Lifshitz, "Chapter XII - Spatial Dispersion," in *Electrodynamics of Continuous Media (Second Edition)*, vol. 8, Amsterdam: Pergamon, 1984, pp. 358–371. DOI: 10.1016/B978-0-08-030275-1.50018-7.

[90] A. Serdyukov, I. Semchenko, S. Tertyakov, *et al.*, *Electromagnetics of bi-anisotropic materials - Theory and Application*, ser. Electrocomponent Science Monographs. Amsterdam: Gordon and Breach Science Publishers, 2001, vol. 11.

[91] L. Landau and E. Lifshitz, "Chapter XII - Fluctuations," in *Statistical Physics Part 1 (Third Edition)*, vol. 5, Pergamon, 1980, pp. 333–400. DOI: 10.1016/B978-0-08-023039-9.50018-4.

[92] P. Lalanne and D. Lemercier-lalanne, "On the effective medium theory of subwavelength periodic structures," *Journal of Modern Optics*, vol. 43, no. 10, pp. 2063–2085, 1996. DOI: 10.1080/09500349608232871.

[93] H. Herzig Sheinfux, I. Kaminer, Y. Plotnik, *et al.*, "Subwavelength multilayer dielectrics: Ultrasensitive transmission and breakdown of effective-medium theory," *Physical Review Letters*, vol. 113, no. 24, p. 243 901, 2014. DOI: 10.1103/PhysRevLett.113.243901.

[94] C. R. Simovski and S. A. Tretyakov, "Local constitutive parameters of metamaterials from an effective-medium perspective," *Physical Review B*, vol. 75, no. 19, p. 195 111, 2007. DOI: 10.1103/PhysRevB.75.195111.

[95] C. R. Simovski, S. A. Tretyakov, A. H. Sihvola, *et al.*, "On the surface effect in thin molecular or composite layers," *The European Physical Journal - Applied Physics*, vol. 9, no. 3, pp. 195–204, 2000. DOI: 10.1051/epjap:2000105.

[96] C. R. Simovski, M. Popov, and S. He, "Dielectric properties of a thin film consisting of a few layers of molecules or particles," *Physical Review B*, vol. 62, no. 20, pp. 13 718–13 730, 2000. DOI: 10.1103/PhysRevB.62.13718.

[97] C. R. Simovski, "Material parameters of metamaterials (a review)," *Optics and Spectroscopy*, vol. 107, no. 5, p. 726, 2009. DOI: 10.1134/S0030400X09110101.

[98] A. Wünsche, "Grenzbedingungen der elektrodynamik für medien mit r"aumlicher dispersion und übergangsschichten," *Annalen der Physik*, vol. 492, no. 2, pp. 121–142, 1980. DOI: 10.1002/andp.19804920205.

[99] J. W. Gibbs, "Notes on the electromagnetic theory of light; part ii," *American Journal of Science*, vol. Series 3 Vol. 23, no. 138, pp. 460–476, 1882. DOI: 10.2475/ajs.s3-23.138.460.

[100] J. K. Gansel, M. Thiel, M. S. Rill, *et al.*, "Gold helix photonic metamaterial as broadband circular polarizer," *Science*, vol. 325, no. 5947, pp. 1513–1515, 2009. DOI: 10.1126/science.1177031.

[101] J. Kaschke and M. Wegener, "Gold triple-helix mid-infrared metamaterial by sted-inspired laser lithography," *Optics Letters*, vol. 40, no. 17, pp. 3986–3989, 2015. DOI: 10.1364/OL.40.003986.

[102] D. B. Burckel, J. R. Wendt, G. A. Ten Eyck, *et al.*, "Micrometer-scale cubic unit cell 3d metamaterial layers," *Advanced Materials*, vol. 22, no. 44, pp. 5053–5057, 2010. DOI: 10.1002/adma.201002429.

[103] B. Wang, J. Zhou, T. Koschny, *et al.*, "Nonplanar chiral metamaterials with negative index," *Applied Physics Letters*, vol. 94, no. 15, p. 151 112, 2009. DOI: 10.1063/1.3120565.

[104] H. A. Lorentz, "Über die beziehung zwischen der fortpflanzungsgeschwindigkeit des lichtes und der körperdichte," *Annalen der Physik*, vol. 245, no. 4, pp. 641–665, 1880. DOI: 10.1002/andp.18802450406.

[105] J. Pastrnak and K. Vedam, "Optical anisotropy of silicon single crystals," *Physical Review B*, vol. 3, no. 8, pp. 2567–2571, 1971. DOI: 10.1103/PhysRevB.3.2567.

[106] A. V. Chebykin, M. A. Gorlach, and P. A. Belov, "Spatial-dispersion-induced birefringence in metamaterials with cubic symmetry," *Physical Review B*, vol. 92, no. 4, p. 045 127, 2015. DOI: 10.1103/PhysRevB.92.045127.

[107] M. A. Gorlach, S. B. Glybovski, A. A. Hurshkainen, *et al.*, "Giant spatial-dispersion-induced birefringence in metamaterials," *Physical Review B*, vol. 93, no. 20, p. 201 115, 2016. DOI: 10.1103/PhysRevB.93.201115.

[108] B. Lahiri, S. G. McMeekin, A. Z. Khokhar, *et al.*, "Magnetic response of split ring resonators (srrs) at visible frequencies," *Optics Express*, vol. 18, no. 3, pp. 3210–3218, 2010. DOI: 10.1364/OE.18.003210.

[109] R. S. Penciu, M. Kafesaki, T. Koschny, *et al.*, "Magnetic response of nanoscale left-handed metamaterials," *Physical Review B*, vol. 81, no. 23, p. 235 111, 2010. DOI: 10.1103/PhysRevB.81.235111.

[110] C. Menzel, E. Hebestreit, R. Alaee, *et al.*, "Extreme coupling: A route towards local magnetic metamaterials," *Physical Review B*, vol. 89, no. 15, p. 155 125, 2014. DOI: 10.1103/PhysRevB.89.155125.

[111] H. O. Hågenvik and J. Skaar, "Magnetic permeability in fresnel equation," *Journal of the Optical Society of America B*, vol. 36, no. 5, pp. 1386–1395, 2019. DOI: 10.1364/JOSAB.36.001386.

[112] J. Skaar, H. O. Hågenvik, and C. A. Dirdal, "Four definitions of magnetic permeability for periodic metamaterials," *Physical Review B*, vol. 99, no. 6, p. 064 407, 2019. DOI: 10.1103/PhysRevB.99.064407.

[113] M. A. Gorlach and P. A. Belov, "Nonlocality in uniaxially polarizable media," *Physical Review B*, vol. 92, no. 8, p. 085 107, 2015. DOI: 10.1103/PhysRevB.92.085107.

[114] S. S. Kruk, D. A. Powell, A. Minovich, *et al.*, "Spatial dispersion of multilayer fishnet metamaterials," *Optics Express*, vol. 20, no. 14, pp. 15 100–15 105, 2012. DOI: 10.1364/OE.20.015100.

[115] M. G. Silveirinha and P. A. Belov, "Spatial dispersion in lattices of split ring resonators with permeability near zero," *Physical Review B*, vol. 77, no. 23, p. 233 104, 2008. DOI: 10.1103/PhysRevB.77.233104.

[116] M. A. Gorlach and P. A. Belov, "Effect of spatial dispersion on the topological transition in metamaterials," *Physical Review B*, vol. 90, no. 11, p. 115 136, 2014. DOI: 10.1103/PhysRevB.90.115136.

[117] K. Mnasri, A. Khrabustovskyi, C. Stohrer, *et al.*, "Beyond local effective material properties for metamaterials," *Physical Review B*, vol. 97, no. 7, p. 075 439, 2018. DOI: 10.1103/PhysRevB.97.075439.

[118] I. Tsukerman and V. A. Markel, "Nonasymptotic homogenization of periodic electromagnetic structures: Uncertainty principles," *Physical Review B*, vol. 93, no. 2, p. 024 418, 2016. DOI: 10.1103/PhysRevB.93.024418.

[119] T. Li and J. B. Khurgin, "Hyperbolic metamaterials: Beyond the effective medium theory," *Optica*, vol. 3, no. 12, pp. 1388–1396, 2016. DOI: 10.1364/OPTICA.3.001388.

[120] T. Geng, S. Zhuang, J. Gao, *et al.*, "Nonlocal effective medium approximation for metallic nanorod metamaterials," *Physical Review B*, vol. 91, no. 24, p. 245 128, 2015. DOI: 10.1103/PhysRevB.91.245128.

[121] A. V. Chebykin, M. A. Gorlach, A. A. Gorlach, *et al.*, "Spatial dispersion in metamaterials based on three-dimensional arrays of spheres and disks," *2015 Days on Diffraction*, pp. 1–5, 2015. DOI: 10.1109/DD.2015.7354835.

[122] S. S. Kruk, Z. J. Wong, E. A. Pshenay-Severin, *et al.*, "Magnetic hyperbolic optical metamaterials," *Nature communications*, vol. 7, p. 11 329, 2016. DOI: 10.1038/ncomms11329.

[123] S. I. Maslovski, T. A. Morgado, M. G. Silveirinha, *et al.*, "Generalized additional boundary conditions for wire media," *New Journal of Physics*, vol. 12, no. 11, p. 113 047, 2010. DOI: 10.1088/1367-2630/12/11/113047.

[124] V. Agranovich and V. Yudson, "Boundary conditions in media with spatial dispersion," *Optics Communications*, vol. 7, no. 2, pp. 121–124, 1973. DOI: https://doi.org/10.1016/0030-4018(73)90081-3.

[125] Y. Aharonov and D. Bohm, "Significance of electromagnetic potentials in the quantum theory," *Physical Review*, vol. 115, no. 3, pp. 485–491, 1959. DOI: 10.1103/PhysRev.115.485.

[126] K. Mnasri, A. Khrabustovskyi, M. Plum, *et al.*, "Retrieving effective material parameters of metamaterials characterized by nonlocal constitutive relations," *Physical Review B*, vol. 99, no. 3, p. 035 442, 2019. DOI: 10.1103/PhysRevB.99.035442.

[127] J. Feis, K. Mnasri, A. Khrabustovskyi, *et al.*, "Surface plasmon polaritons sustained at the interface of a nonlocal metamaterial," *Physical Review B*, vol. 98, no. 11, p. 115 409, 2018. DOI: 10.1103/PhysRevB.98.115409.

[128] A. Otto, "Excitation of nonradiative surface plasma waves in silver by the method of frustrated total reflection," *Zeitschrift für Physik A Hadrons and nuclei*, vol. 216, no. 4, pp. 398–410, 1968. DOI: 10.1007/BF01391532.

[129] C. Kittel, P. McEuen, and P. McEuen, *Introduction to solid state physics*. Wiley New York, 1996, vol. 8.

[130] A. Sihvola, "Mixing rules with complex dielectric coefficients," *Subsurface Sensing Technologies and Applications*, vol. 1, no. 4, pp. 393–415, 2000. DOI: 10.1023/A:1026511515005.

[131] J. M. Pitarke, F. J. García-Vidal, and J. B. Pendry, "Effective electronic response of a system of metallic cylinders," *Physical Review B*, vol. 57, no. 24, pp. 15 261–15 266, 1998. DOI: 10.1103/PhysRevB.57.15261.

[132] Y. Wu, J. Li, Z.-Q. Zhang, *et al.*, "Effective medium theory for magnetodielectric composites: Beyond the long-wavelength limit," *Physical Review B*, vol. 74, no. 8, p. 085 111, 2006. DOI: 10.1103/PhysRevB.74.085111.

[133] U. C. Hasar, J. J. Barroso, C. Sabah, *et al.*, "Retrieval of effective electromagnetic parameters of isotropic metamaterials using reference-plane invariant expressions," *Progress In Electromagnetics Research*, vol. 132, pp. 425–441, 2012. DOI: 10.2528/PIER12072412.

[134] A. F. Mota, A. Martins, J. Weiner, *et al.*, "Constitutive parameter retrieval for uniaxial metamaterials with spatial dispersion," *Physical Review B*, vol. 94, no. 11, p. 115 410, 2016. DOI: 10.1103/PhysRevB.94.115410.

[135] E. Martini, G. M. Sardi, and S. Maci, "Homogenization processes and retrieval of equivalent constitutive parameters for multisurface-metamaterials," *IEEE Transactions on Antennas and Propagation*, vol. 62, no. 4, pp. 2081–2092, 2014. DOI: 10.1109/TAP.2014.2300169.

[136] X.-X. Liu and A. Alù, "Generalized retrieval method for metamaterial constitutive parameters based on a physically driven homogenization approach," *Physical Review B*, vol. 87, no. 23, p. 235 136, 2013. DOI: 10.1103/PhysRevB.87.235136.

[137] A. M. Nicolson and G. F. Ross, "Measurement of the intrinsic properties of materials by time-domain techniques," *IEEE Transactions on Instrumentation and Measurement*, vol. 19, no. 4, pp. 377–382, 1970. DOI: 10.1109/TIM.1970.4313932.

[138] W. B. Weir, "Automatic measurement of complex dielectric constant and permeability at microwave frequencies," *Proceedings of the IEEE*, vol. 62, no. 1, pp. 33–36, 1974. DOI: 10.1109/PROC.1974.9382.

[139] C. Menzel, C. Rockstuhl, T. Paul, *et al.*, "Retrieving effective parameters for quasiplanar chiral metamaterials," *Applied Physics Letters*, vol. 93, no. 23, p. 233 106, 2008. DOI: 10.1063/1.3046127.

[140] D. R. Smith, S. Schultz, P. Markos, *et al.*, "Determination of effective permittivity and permeability of metamaterials from reflection and transmission coefficients," *Physical Review B*, vol. 65, no. 19, p. 195 104, 2002. DOI: 10.1103/PhysRevB.65.195104.

[141] C. Menzel, C. Rockstuhl, T. Paul, *et al.*, "Retrieving effective parameters for metamaterials at oblique incidence," *Physical Review B*, vol. 77, no. 19, p. 195 328, 2008. DOI: 10.1103/PhysRevB.77.195328.

[142] E. Noponen and J. Turunen, "Eigenmode method for electromagnetic synthesis of diffractive elements with three-dimensional profiles," *Journal of the Optical Society of America A*, vol. 11, no. 9, pp. 2494–2502, 1994. DOI: 10.1364/JOSAA.11.002494.

[143] M. G. Moharam, D. A. Pommet, E. B. Grann, *et al.*, "Stable implementation of the rigorous coupled-wave analysis for surface-relief gratings: Enhanced transmittance matrix approach," *Journal of the Optical Society of America A*, vol. 12, no. 5, pp. 1077–1086, 1995. DOI: 10.1364/JOSAA.12.001077.

[144] M. G. Moharam, E. B. Grann, D. A. Pommet, *et al.*, "Formulation for stable and efficient implementation of the rigorous coupled-wave analysis of binary gratings," *Journal of the Optical Society of America A*, vol. 12, no. 5, pp. 1068–1076, 1995. DOI: 10.1364/JOSAA.12.001068.

[145] P. Götz, T. Schuster, K. Frenner, *et al.*, "Normal vector method for the rcwa with automated vector field generation," *Optics Express*, vol. 16, no. 22, pp. 17 295–17 301, 2008. DOI: 10.1364/OE.16.017295.

[146] N. Stefanou, V. Yannopapas, and A. Modinos, "Heterostructures of photonic crystals: Frequency bands and transmission coefficients," *Computer Physics Communications*, vol. 113, no. 1, pp. 49–77, 1998. DOI: https://doi.org/10.1016/S0010-4655(98)00060-5.

[147] J. H. Burnett, S. G. Kaplan, E. Stover, *et al.*, "Refractive index measurements of ge," in *Infrared Sensors, Devices, and Applications VI*, International Society for Optics and Photonics, vol. 9974, 2016, p. 99740X. DOI: 10.1117/12.2237978.

[148] N.-H. Shen, T. Koschny, M. Kafesaki, *et al.*, "Optical metamaterials with different metals," *Physical Review B*, vol. 85, no. 7, p. 075 120, 2012. DOI: 10.1103/PhysRevB.85.075120.

[149] B. Kanté, S. N. Burokur, A. Sellier, *et al.*, "Controlling plasmon hybridization for negative refraction metamaterials," *Physical Review B*, vol. 79, no. 7, p. 075 121, 2009. DOI: 10.1103/PhysRevB.79.075121.

[150] H. T. Nguyen, T. S. Bui, S. Yan, *et al.*, "Broadband negative refractive index obtained by plasmonic hybridization in metamaterials," *Applied Physics Letters*, vol. 109, no. 22, p. 221 902, 2016. DOI: 10.1063/1.4968802.

[151] C. Menzel, R. Alaee, E. Pshenay-Severin, *et al.*, "Genuine effectively biaxial left-handed metamaterials due to extreme coupling," *Optics Letters*, vol. 37, no. 4, pp. 596–598, 2012. DOI: 10.1364/OL.37.000596.

[152] Y. Zhou, X. Y. Chen, Y. H. Fu, *et al.*, "Fabrication of large-area 3d optical fishnet metamaterial by laser interference lithography," *Applied Physics Letters*, vol. 103, no. 12, p. 123 116, 2013. DOI: 10.1063/1.4821508.

[153] S. Zhang, W. Fan, N. C. Panoiu, *et al.*, "Experimental demonstration of near-infrared negative-index metamaterials," *Physical Review Letters*, vol. 95, no. 13, p. 137 404, 2005. DOI: 10.1103/PhysRevLett.95.137404.

[154] G. Dolling, C. Enkrich, M. Wegener, *et al.*, "Low-loss negative-index metamaterial at telecommunication wavelengths," *Optics Letters*, vol. 31, no. 12, pp. 1800–1802, 2006. DOI: 10.1364/OL.31.001800.

[155] C. Rockstuhl, T. Paul, F. Lederer, *et al.*, "Transition from thin-film to bulk properties of metamaterials," *Physical Review B*, vol. 77, no. 3, p. 035 126, 2008. DOI: 10.1103/PhysRevB.77.035126.

[156] J. Zhou, T. Koschny, M. Kafesaki, *et al.*, "Size dependence and convergence of the retrieval parameters of metamaterials," *Photonics and Nanostructures - Fundamentals and Applications*, vol. 6, no. 1, pp. 96–101, 2008, The Seventh International Symposium on Photonic and Electromagnetic Crystal Structures. DOI: https://doi.org/10.1016/j.photonics.2007.10.003.

[157] J. Zhou, T. Koschny, M. Kafesaki, *et al.*, "Negative refractive index response of weakly and strongly coupled optical metamaterials," *Physical Review B*, vol. 80, no. 3, p. 035 109, 2009. DOI: 10.1103/PhysRevB.80.035109.

[158] J. Petschulat, C. Menzel, A. Chipouline, *et al.*, "Multipole approach to metamaterials," *Physical Review A*, vol. 78, no. 4, p. 043 811, 2008. DOI: 10.1103/PhysRevA.78.043811.

[159] A. Alù, A. D. Yaghjian, R. A. Shore, *et al.*, "Causality relations in the homogenization of metamaterials," *Physical Review B*, vol. 84, no. 5, p. 054 305, 2011. DOI: 10.1103/PhysRevB.84.054305.

[160] T. Koschny, P. Markos, D. R. Smith, *et al.*, "Resonant and antiresonant frequency dependence of the effective parameters of metamaterials," *Physical Review E*, vol. 68, no. 6, p. 065 602, 2003. DOI: 10.1103/PhysRevE.68.065602.

[161] K. Mnasri, F. Z. Goffi, M. Plum, *et al.*, "Homogenization of wire media with a general purpose nonlocal constitutive relation," *Journal of the Optical Society of America B*, vol. 36, no. 8, F99–F108, 2019. DOI: 10.1364/JOSAB.36.000F99.

[162] R. Zhou, H. Zhang, and H. Xin, "Metallic wire array as low-effective index of refraction medium for directive antenna application," *IEEE Transactions on Antennas and Propagation*, vol. 58, no. 1, pp. 79–87, 2010. DOI: 10.1109/TAP.2009.2036282.

[163] M. G. Silveirinha, P. A. Belov, and C. R. Simovski, "Subwavelength imaging at infrared frequencies using an array of metallic nanorods," *Physical Review B*, vol. 75, no. 3, p. 035 108, 2007. DOI: 10.1103/PhysRevB.75.035108.

[164] P. B. Johnson and R. W. Christy, "Optical constants of the noble metals," *Physical Review B*, vol. 6, no. 12, pp. 4370–4379, 1972. DOI: 10.1103/PhysRevB.6.4370.

[165] S. V. Zhukovsky, A. Andryieuski, O. Takayama, *et al.*, "Experimental demonstration of effective medium approximation breakdown in deeply subwavelength all-dielectric multilayers," *Physical Review Letters*, vol. 115, no. 17, p. 177 402, 2015. DOI: 10.1103/PhysRevLett.115.177402.